Étude structurale et biochimique d'un facteur d'échange atypique d'Arf

Kaheima Aizel

UNIVERSITÉ PARIS-SUD 11

ECOLE DOCTORALE :

INNOVATION THÉRAPEUTIQUE : DU FONDAMENTAL A L'APPLIQUÉ

PÔLE : INGENIERIE DES PROTEINES ET CIBLES THERAPEUTIQUES

DISCIPLINE :
STRUCTURE, FONCTION ET INGÉNIERIE DES PROTÉINES

ANNÉE 2011 - 2012 SÉRIE DOCTORAT 1188

THÈSE DE DOCTORAT
soutenue le 24/09/2012

par

Kaheina AÏZEL

Étude Structurale et Biochimique d'un Facteur d'Échange Atypique d'Arf

Directeur de thèse :	Jacqueline CHERFILS	DR1-CNRS (LEBS, Gif-sur-Yvette)
Co-directeur de thèse :	Mahel ZEGHOUF	CR1-CNRS (LEBS, Gif-sur-Yvette)

Composition du jury :

Président du jury :	Herman VAN TILBEURGH	PR-UPS (IBBMC, Orsay)
Rapporteurs :	Katrin RITTINGER	PhD (MRC, London)
	Michel FRANCO	CR1-CNRS (IPMC, Valbonne)
Examinateur :	Alain EYCHÈNE	DR2-INSERM (Institut Curie, Orsay)

A ma grand-mère Titis,

A mes parents Monique et Kamal

Acknowledgments

I would like to thank my two PhD supervisors, **Jacqueline Cherfils and Mahel Zeghouf**, for their welcome in the lab, for their support all along these four years, for their advice, for the trust they had in me, for all the productive scientific discussions. Thank you Jacqueline for all the congresses and workshops you sent me to. Thank you Mahel for having trained me in the joys of enzymology! Thank you both for having trained me to become a researcher. Many thanks for everything.

I would like to thank **Katrin Rittinger, Michel Franco and Alain Eychène** for giving me the honor to be part of my jury and to evaluate my work.

I want to thank our collaborators: **Jorge Navaza** for the great help with the molecular replacement of my complex structure, **Bob St Onge** who provided us with all the Si inhibitors and **Hans-Christian Kornau** who provided us with the peptide CATY.

Many thanks to all the people who contributed to the structural characterization. My first thanks will go to **Valérie Biou** who trained me in the joys of crystallography and crystallization. Thank you for your help, your patience and for all these nights at the synchrotron! I will remember our music discussions. Next I would like to thank **Valérie Campanacci** who also helped me with some crystallization and crystallography software issues, and with a lot of little tricks in the lab that were really useful in the end. For your good humor all the time and for your patience. Thank you for all the scientific discussions, your advice and your help. I will remember all the jokes, which allowed me to relax a little in stressful times!

I would like to thank all the people from the beam lines for their technical support: **Andrew Thompson, Beatriz Guimaraes** and **Pierre Legrand** on PROXIMA 1 beam line at SOLEIL synchrotron, and **Javier Perez** and **Pierre Roblin** on SWING beamline for their help with the SAXS experiments. Thank you as well to **Gordon Leonard** on ID23-2 beam line at the ESRF synchrotron.

Thank you to all the members of my team present or past! First **Amira**, for your help with many little things in the lab and with the ADIT association. We have known each other for four years now and you became one of my best friends. I always could count on you and that was really nice, thank you for that. I will remember all our nights at the synchrotron both on PROXIMA I and SWING. But I will also remember all our nights in Paris and all the good times we had. It was a real pleasure to get to know you and I hope we will remain friends forever! **Marcia**, when you arrived in the lab as the new young PhD student we became rapidly good friends. I will remember our nights at the synchrotron, where we were both fighting hard to not fall asleep! The nights at SWING were particularly memorable. I will also remember our trip to Warwick for the CCP4 meeting, where we both accumulated the worst bad luck that is! This trip was really memorable. Thank you for reminding me to take coffee breaks! I hope we will remain good friends. My little **Audrey**, thank you for all the purifications of Arf

proteins, for your help, and for the good times we had. It was a pleasure to work with you and hope that we will remain good friends. **Dominique**, the only guy of the team at the time and "The" post-doc. You might have suffered amongst all these girls! Thank you for all your help and advice with difficult kinetics interpretation and experiments. Thank you for the purification of myrArf6 protein. I will also remember all the good scientific discussions we had. I hope we will stay in touch and remain good friends. **Lionel**, its only six months since you arrived in the lab, but you helped me a lot with purifications of my last mutants. So thank you a lot for that and for the purification of myrArf1 protein. I appreciated your kindness and your good humor. **Anne-Gaëlle**, its only five months since you arrived in the lab, but it was a pleasure to work with you. Thank you for your help and for your kindness.
I would like to thank the past members of the team, **Anna**, **Pampa**, **Arnaud** and **Jean-Christophe**. **Anna**, for your help and for the wonderful night at the Opera in Paris. **Pampa**, for all your help and I will remember our music discussions. **Arnaud**, for the purifications of Arf proteins, for your kindness and helpfulness. Thank you for the great tennis matches we played after work. **Jean-Christophe**, and for all your advice. It was a great pleasure to work with you all. I would also like to thank my three trainees **Manon, Amélie and Alice**.

I would like to thank all the members of team 10, **Julie**, **Mélanie**, **Aline**, **Philippe**, **Annélie** and **Paola** our nice neighbors. Thank you for all for your kindness. **Philippe**, we have known each other since the university and it was a pleasure to work with you. **Aline**, it was a real pleasure to get to know you and to work with you and our nights in Paris with the girls were really fun. **Mélanie, Annélie and Paola** it was a pleasure to know you and to work with you. Thank you for your kindness.

Special thanks to **Lydia, José** and **Martine** from team 2. To Lydia, my compatriot, for being you, and for all the good times we had in the lab and during our trips in Paris. Stay as you are. You became one of my best friends and hope we will remain friends forever.

I would also like to thank all my colleagues from the lab, **Jocelyne**, for everything from the time you were responsible for my Master2 degree to now. You were really efficient and that was appreciable. I wish you a good retirement. Annie, **Maud**, **Angélique** and **Jeanne**, from the administrative staff, thank you for everything! You were really efficient, which made it really easier for me to work. That was very appreciable. Many thanks **Corine** and **Tracy**, for all the M9 media you made for me and for all the rest. **Véronique**, for all the BRAG2 constructs and mutants you made for me and for our music discussions. I will remember our trip in Belfort with our respective orchestras, that was fun. **Pascal**, thank you for all your jokes and our tennis discussions. I regret not having had time to play a tennis match with you. **Solange, Sylvie, Manu, Elodie, Louis, Alexis, Christophe** and **Guillaume** for the nice discussions we had.

Not to mention all the students, young engineers and post-docs of the LEBS, with whom we had great times. Firstly, I would like to thank **Chafika** (Kika), my other compatriot of the lab, it was a real pleasure to get to know you and I missed you after your sudden departure from the lab. But I was really happy for your little one.

Armelle, thank you for everything from the time we were in the same team to now, for your great work with the crystallization platform, for all our discussions and of course for your delicious cakes! You are a really good Pastry cook! **Moutsé**, for your help, for our enjoyable discussions and for all our travels in the RER. **Jozsef**, for your kindness and for all the interesting museums we visited with the girls. I hope we will remain good friends. Thank you to **Samantha**, **Lionel**, **Amandine**, **Jérémie**, **Azaria**, **Isaline**, **Andréa**, **Yannick**, **Laura**, **Samira**, **Joachin**, **Sarah**, **José**, **Guillaume**, **Carla** and **Rosa**.

I would like to thank my best friends **Odile** (Didile), **Elodie**, **Claire**, **Lucile B.**, **Lucile Z.** and **Géraldine** for all the good times and laughs we had since the University and the music school (Géraldine) and for your support in difficult times. I hope we will remain best friends for life.

Finally, I would like to warmly thank all my family in Algeria and in France for their support all along. And I would like to thank especially my beloved parents, who sacrificed themselves for giving me the best education possible and without whom I would not be who I am today. I owe them a lot. Thank you for everything! I would like to thank my too brothers **Koceila** and **Méziane** who supported me all along. I would finally thank my grand-mother, **Titis**, who was always there for me. I regret that you could not be here to see me become a Doctor as you always wanted, but I hope you will be proud of me from heaven.

Table des matières

Liste des abréviations

ADRP: Adipose Differentiation-Related Protein or Adipophilin
AGAP2: Arf GAP Protein 2
AMAP1 or PAG2: Paxillin-binding ArfGAP
AMPAR: α-Amino-3-hydroxy-5-Methyl-4-isoxazolePropionic Acid Receptor
AP: Adaptator Protein
Arf: ADP Ribosyl Factor
ArfGAP: GTPase Activating Protein for Arf
ArfGEF: Guanine Exchange Factor for Arfs
Arl: Arf-Like
ARNO: Arf Nucleotide binding Opener
ATGL: Adipose Triglyceride Lipase
BFA: Brefeldine A
BIG: Brefeldin A-Inhibited GEF
BP3K: Binding to products of PI3K
BRAG: Brefeldin-Resistant ArfGEF
CAPS: Calcium-dependent Activator Protein for Secretion
CD: Circular Dichroism
CERT: Ceramide Transfer protein
CHO: Chinese Hamster Ovary
COPI: Coat Protein 1
DCB: Dimerization and Cyclophilin Binding domain
DLS: Dynamic Light Scattering
DTT: Dithiothreitol
EFA6: Exchange Factor for Arf6
ELISA: Enzyme-linked Immunosorbent Assay
ERGIC: Endoplasmic Reticulum-Golgi Intermediate Compartment
ERK: Extracellular-signal-Regulated Kinases
FAPP: Four-Phosphate-Adaptor Protein
FBX8: F-Box only protein 8
GAP: GTPase Activating Protein
GBF: Golgi-specific Brefeldin A-resistance Factor
GCA: Golgicide A
GDI: Guanine Dissociation Inhibitor
GDP: Guanosine DiPhosphate
GEF: Guanine Exchange Factor
GGA: Golgi-localized Gamma adaptin ear-containing Arf-binding
GluA2: Glutamate subunit A2
GMAP210: Golgi Microtubule Associated Protein of 210 kDa
GST: Glutathione S-Transferase
GTP: Guanosine TriPhosphate
HDS: Homology Downstream of Sec7
HEPES: 4-(2-HydroxyEthyl)-1-PiperazineEthaneSulfonic acid
Her2: Human Epidermal growth factor Receptor 2
HUS: Homology Upstream of Sec7
HUVEC: Human Umbilical Vein Endothelial Cells
ID: Intellectual Disability
IgG: Immunoglobulin G

IRSP53: Insulin Receptor tyrosine kinase Substrate p53
LD: Lipid Droplets
LTD: Long Term Depression
MDCK cell: Madin-Darby Canine Kidney cell
mGluR: metabotropic Glutamate Receptor
myrArf: myristoylated Arf
NLS: Nuclear Localization Signal or Sequence
NMT: N-Myristoyl-Transferase
NRK cells: Normal Rat Kidney Epithelial Cells
PC: Phosphatidyl Choline
PDZ: Post synaptic density protein (PSD95)-Drosophila disc large tumor suppressor (Dlg1)-and Zonula occludens-1 protein (zo-1)
PE: Phosphatidyl Ethanolamine
PH: Pleckstrin Homology
PI4P: Phosphatidyl Inositol-4-Phosphate
PIP4K: Phosphatidyl Inositol-4-Kinase
PI4P5K: Phosphatidyl-4-Phosphtate-5-Kinase
PIKE: AGAP2 or centaurin-γ1
$PI4,5P_2$ or PIP_2: Phosphatidyl Inositol-4,5-bisPhosphate
PIP_3: Phosphatidyl Inositol-3,4,5-triPhosphate
PLD: PhosphoLipase D
PMA: Phorbol 12-Myristate 13-Acetate
PS: Phosphatidyl Serine
PSD: Post Synaptic Density
RIBEYE: Ribbon Eye
SAR: Secretion Associated and Ras-related
SAP97: Synapse-Associated Protein 97
SAXS: Small-Angle X-ray Scattering
SEC-MALLS: Size Exclusion Chomatography - Multi-Angle Laser Light Scattering
SOS: Son Of Sevenless
S-SCAM/MAGI2: Synaptic SCAffolding Molecule/Membrane-Associated Guanylate kinase with Inverted organization
SynArfGEF: Synaptic Guanine nucleotide Exchange Factor for Arf
TGN: Trans-Golgi Network
VEGF: Vascular Endothelial Growth Factor
VEGFR: Vascular Endothelial Growth Factor Receptor

RÉSUMÉ

Les petites protéines G de la famille Arf, régulateurs majeurs du trafic membranaire, sont activées par plusieurs familles de facteurs d'échange nucléotidiques (ArfGEFs). Les ArfGEFs jouent un rôle essentiel dans l'intégration des signaux de régulation qui conduisent à l'activation d'Arf au niveau de compartiments cellulaires spécifiques, cependant les mécanismes par lesquels ils ciblent les Arfs activés aux membranes spécifiques et leur coordination avec l'échange de nucléotide reste peu comprise. Nous utilisons ici la cristallographie et la reconstitution des activités ArfGEF sur des membranes artificielles pour analyser ces mécanismes pour un ArfGEF humain atypique, impliqué dans l'endocytose de récepteurs et associé à l'invasion tumorale dans de nombreuses cellules cancéreuses. Les membres de cette famille ont été décrits comme des GEFs spécifique d'Arf6, et comporte un domaine de type PH après leur domaine Sec7. Dans la deuxième partie de ma thèse, nous voulions savoir comment les isoformes Arf1 et Arf6 achevaient leurs fonctions dans la cellule. Arf1 et Arf6 sont très similaires: elles possèdent plus de 60% d'identité de séquence, et des études structurales ont montré que la surface qu'ils utilisent pour interagir avec leurs régulateurs et effecteurs est essentiellement identique en séquence et en structure. Cependant, elles ont des fonctions différentes dans la cellule et des propriétés différentes *in vitro*, pour lesquelles aucune donnée structurale n'a donné d'explications. Nous utilisons ici la cristallographie, le SAXS et la RMN pour comprendre la différence entre ces deux isoformes.

SUMMARY

Small GTPases of the Arf family, which are pivotal regulators of membrane traffic in eukaryotes, are activated by several families of guanine nucleotide exchange factors (ArfGEFs). ArfGEFs play a key role in processing upstream regulatory signals that lead to Arf activation onto specific subcellular compartments, yet the mechanisms by which they target activated Arfs to specific membranes and their coordination with nucleotide exchange remain poorly understood. Here we used X-ray crystallography and reconstitution of ArfGEF activities on artificial membranes to analyze these mechanisms for an atypical human ArfGEF, involved in receptor endocytosis and associated with tumour invasion in various cancer cells. Members of this family have been described as Arf6-specific GEFs, and carry a PH-like domain downstream their Sec7 domain. In a second part of the work we wanted to know how the isoforms Arf1 and Arf6 achieve exquisitely specific functions in cells. Arf1 and Arf6 are highly similar: they have over 60% sequence identity, and structural studies have shown that the surfaces they use to interact with regulators and effectors are essentially identical in sequence and structure. Yet, they have non-overlapping functions in cells. Arf1 is a major regulator of most aspects of vesicular traffic, while Arf6 is restricted to the plasma membrane where it acts at the crossroads of trafficking and cytoskeleton functions (D'Souza-Schorey and Chavrier 2006). Consistent with their cellular specificities, Arf1 and Arf6 also have distinctive biochemical properties *in vitro*, for which no straightforward structural explanation has been put forward. Here we used X-ray crystallography, synchrotron SAXS experiments and NMR to assess the difference between these two isoforms.

INTRODUCTION

Famille	Nombre de membres chez l'homme	Principales fonctions cellulaires	Modifications post-traductionnelles	Modifications co-traductionnelles
Ras	39	Régulation de l'expression des gènes Transduction du signal	-Farnesyl C-terminale - Géranylgéranyl C-terminale	
Rho	22	Organisation du cytosquelette Expression des gènes	-Farnesyl C-terminale - Géranylgéranyl C-terminale	
Rab	65	Trafic cellulaire	Géranylgéranyl C-terminale	
Arf/Sar1	30	Trafic cellulaire		Myristoyl N-terminale
Ran	1	Transport nucléo-cytoplasmique Cycle cellulaire	Aucune	Aucune

Tableau 1 : Classification des petites protéines G

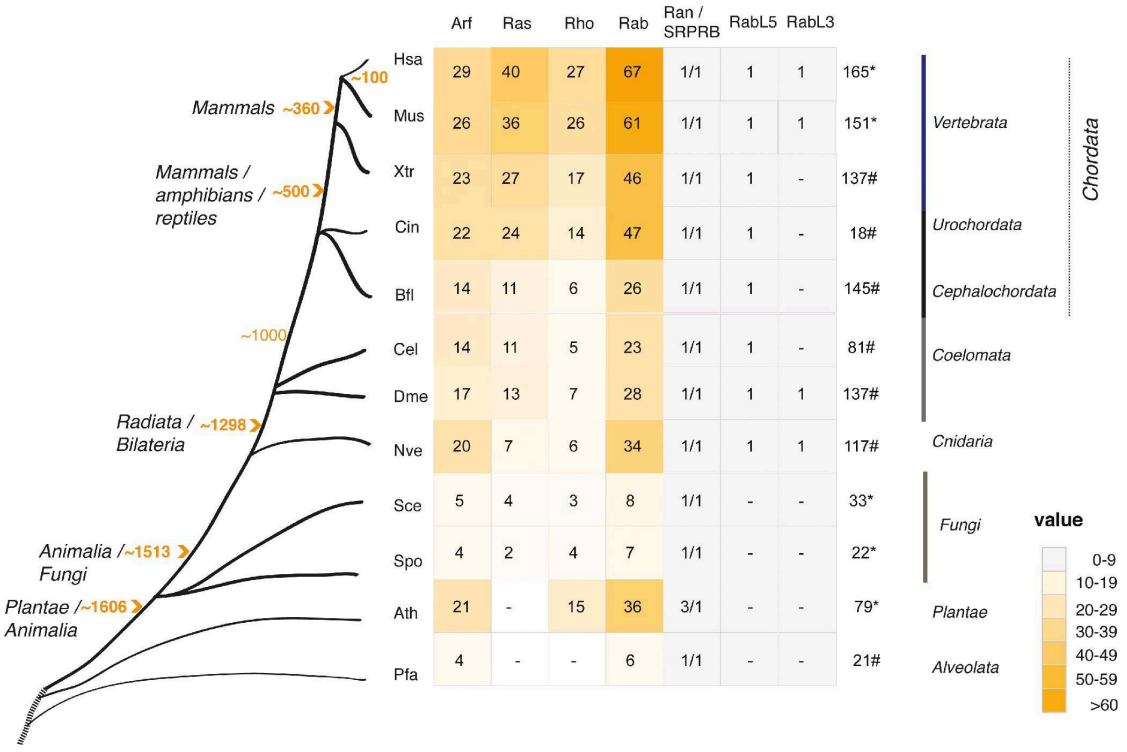

Figure 1 : Orthologues de la superfamille de Ras humain dans 11 protéomes (emprunté à (Rojas et al. 2012))

INTRODUCTION GENERALE

I. Les petites protéines G

Les petites protéines G (pour protéines fixant le GTP) existent dans les trois grandes branches du vivant, avec une forte proportion chez les eucaryotes. Un total de 37767 protéines ont été identifiées parmi 1383 génomes (pour revue (Wittinghofer and Vetter 2011)). La première protéine G découverte a été la protéine Ras, dont les gènes ont été identifiés dans les années 60 comme des oncogènes transformants exprimés par des rétrovirus murins ((Harvey 1964) ; (Kirsten and Mayer 1967)). Dans les années 80, il fut établit que ces protéines virales étaient des protéines monomériques avec une masse moléculaire allant de 20 à 30 kDa, qui fixaient les nucléotides GDP et GTP et qui avaient des fonctions de signalisation médiées par ces nucléotides (Shih et al. 1980). De plus, ces protéines Ras ont été reliées aux protéines G hétérotrimériques, telles que Gs et Gi, ainsi qu'à des protéines G impliquées dans la synthèse protéique tel que le facteur d'élongation Tu (EF-Tu) ((Gibbs et al. 1984) ; (Scolnick et al. 1979) ; (Shih et al. 1980)). Plus tard, ont suivi la découverte d'Arf, qui a été purifié en tant que cofacteur nécessaire à l'ADP-ribosylation de la protéine Gs par la toxine du choléra (Kahn and Gilman 1984) et identifié comme une petite protéine G (Kahn and Gilman 1986). Puis il y a eu la découverte du gène homologue de Ras, Rho, chez l'*Aplysia* en 1985 (Madaule and Axel 1985) et celles de nombreuses autres petites protéines G (pour revue (Takai et al. 2001)).

A ce jour, les petites protéines G sont structuralement et fonctionnellement classées en cinq familles: les familles Ras, Rho, Rab, Sar1/Arf et Ran et constituent une superfamille comportant 167 membres chez l'homme dont 10 sont non classifiés (pour revue (Rojas et al. 2012) **(Tableau 1)**. Il existe également 766 orthologues aux 167 protéines humaines provenant de 11 organismes **(Figure 1)**. Ces familles interviennent dans différents processus cellulaires et sont localisées soit dans le cytosol soit aux membranes grâce, entre autres, à la présence de modifications post-traductionnelles **(Tableau 1)**.

A. Des interrupteurs moléculaires de la signalisation cellulaire

Les petites protéines G sont souvent décrites comme des interrupteurs moléculaires, qui transmettent un signal venant de l'extérieur vers des partenaires cellulaires appelés effecteurs, dans un contexte spatio-temporel donné, pour moduler leur activité et induire une

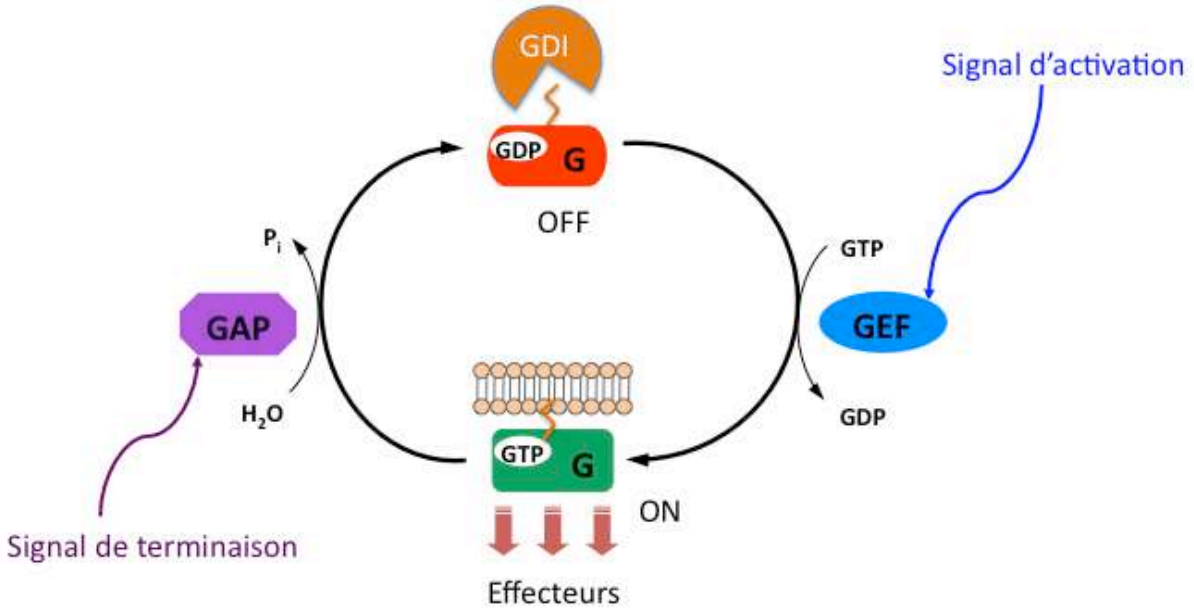

Figure 2 : Cycle général d'activation des petites protéines G

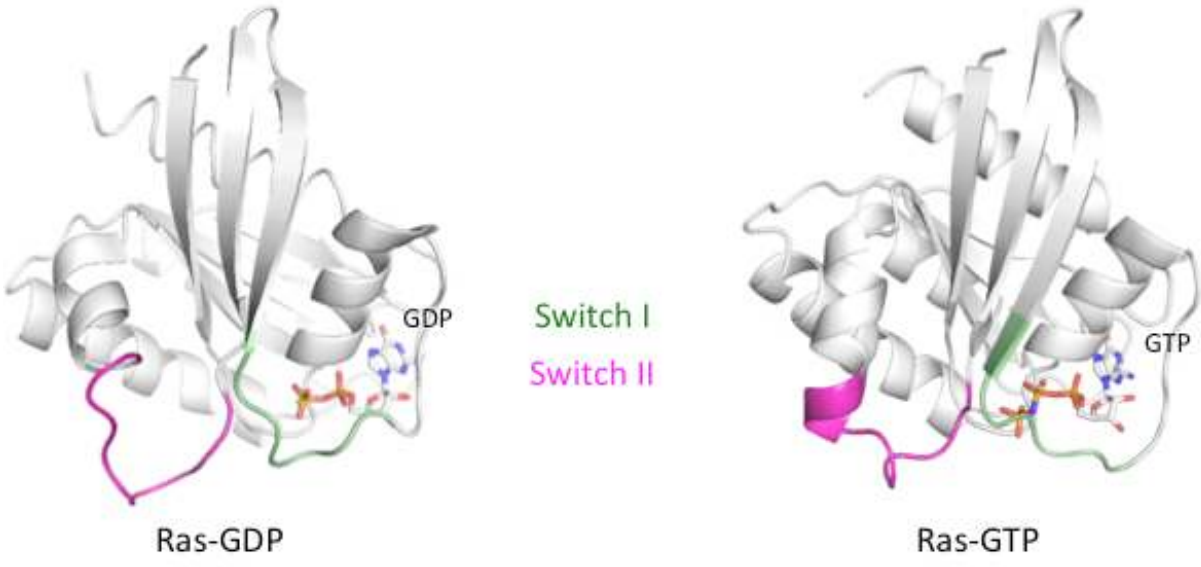

Figure 3 : Les régions mobiles dans l'échange GDP/GTP. Représentation de la protéine Ras sous sa forme GDP (code pdb 4q21, à gauche) (Milburn et al. 1990) et sous sa forme GTP (code pdb 5p21, à droite) (Pai et al. 1990) avec en vert pâle et magenta, les régions switch 1 et 2 mobiles, respectivement. Le GDP et GTP sont représentés en bâtonnets.

réponse cellulaire (pour revue (Vetter and Wittinghofer 2001). Elles cyclent entre un état inactif lorsqu'elles sont liées au GDP et un état actif lorsqu'elles sont liées au GTP. La dissociation du GDP s'effectue à l'aide de régulateurs appelés GEFs (Guanine nucléotide Exchange Factors) car cette dissociation est très lente dans les protéines G, le GDP étant très fortement lié à la protéine. L'hydrolyse du GTP par les petites protéines G, quant à lui, est effectué à l'aide de régulateurs appelés GAP (GTPase-Activating Proteins) qui viennent stimuler l'hydrolyse intrinsèque très lente du GTP **(Figure 2)**. Ce cycle est accompagné d'un changement de conformation de la protéine G au niveau de ses régions Switch (Switch 1 et 2) **(Figure 3)**, qui reconnaissent la nature du nucléotide fixé et sont impliquées dans l'hydrolyse du GTP. L'obtention de nombreuses structures de petites G sous forme GDP ou GTP a permis de caractériser les changements conformationnels des régions Switch au cours de la réaction d'échange (pour revue (Vetter and Wittinghofer 2001)). Les régions Switch 1 et/ou Switch 2 sont engagées dans la plupart, si ce n'est toutes les interactions que les petites protéines G établissent avec leurs partenaires cellulaires. Enfin, une dernière famille de régulateurs, propre à la famille des protéines Rho et Rab, les GDI (Guanine Dissociation Inhibitors) séquestrent la petite protéine G sous forme GDP dans le cytoplasme en masquant leurs modifications post-traductionnelles lipidiques (décrites plus loin, §B.1) ((Seabra and Wasmeier 2004) **(Figure 2)**.

B. Switch structuraux

1. Généralités

Les membres de la famille des protéines G ont en commun un corps central appelé domaine G et des régions variables appelées Switch 1 et 2 **(Figure 3)**. Le domaine G est un domaine globulaire composé d'un feuillet β à 6 brins entouré par 5 hélices α (pour revues (Colicelli 2004) ; (Wennerberg et al. 2005)). Structuralement, ce domaine est une variation autour du domaine classique de fixation et d'hydrolyse d'un nucléotide qui est très conservé parmi les protéines fixant un nucléotide (ATPases, GTPases). Ce domaine est caractérisé par la présence de cinq séquences « G box » conservées **(Figure 4)**, qui contiennent le site de fixation du nucléotide et certaines régions des Switch (pour revues (Dever et al. 1987) ; (Colicelli 2004)). La boite G1 (GxxxxGK(S/T)), aussi connue sous le nom de P-loop, est responsable de la fixation des phosphates du nucléotide. Ainsi, la lysine du site consensus interagit avec les phosphates en β et γ du nucléotide, le groupement NH de la sérine (ou de la thréonine) interagit avec le phosphate β, tandis que l'hydroxyle de sa chaine latérale interagit avec le magnésium (Mg^{2+}) **(Figure 5)**. La boite G3 (DxxG(Q/H/T)) est impliquée dans la

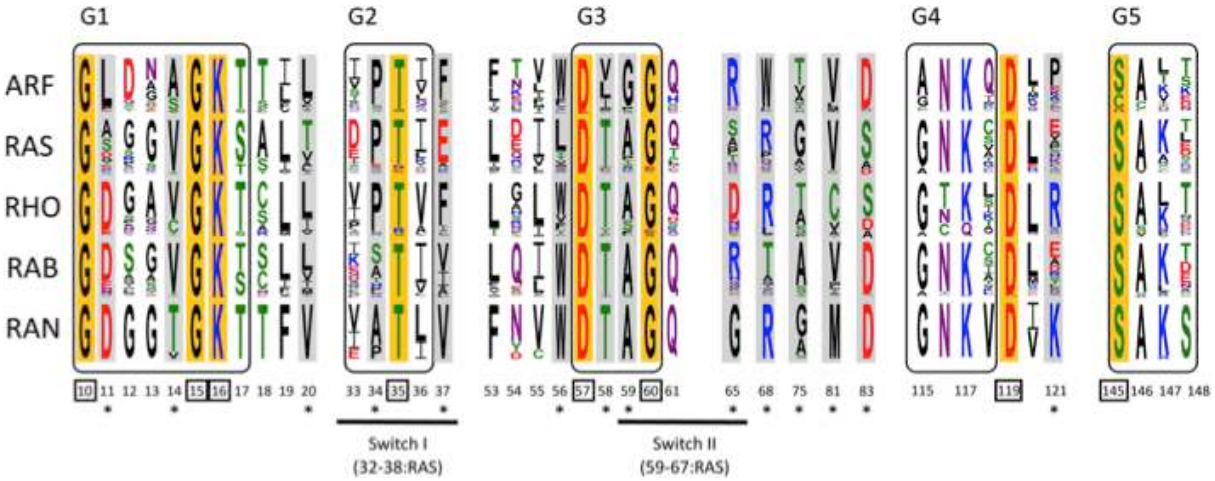

Figure 4 : Séquences « G box » de la superfamille des Ras (emprunté à (Rojas et al. 2012)). La numérotation de la séquence est celle de Ras.

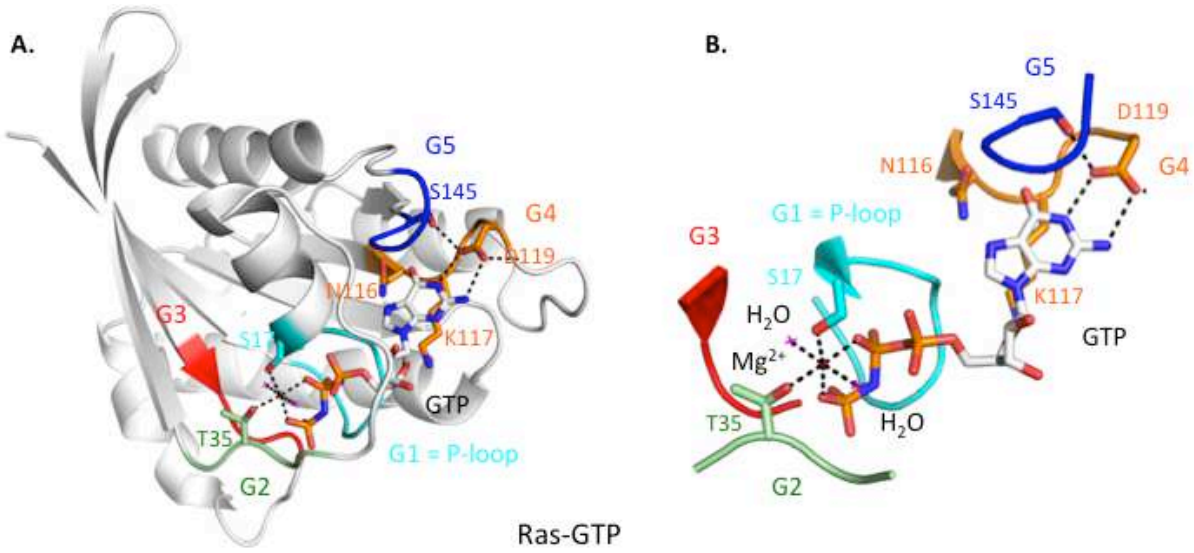

Figure 5 : Structure d'une petite protéine G et de son site de fixation au nucléotide. A. Représentation de la structure de Ras-GTP-Mg^{2+} (code pdb 5p21), avec en couleur la localisation des « G-box », le GTP en bâttonets et les pointillés représentant les interactions ioniques avec le GTP et le magnésium **B.** Élargissement du site de fixation du nucléotide avec les 5 « G-box » représentées en couleur. Deux molécules d'eau (magenta) coordonnent le Mg^{2+} (en rouge).

coordination de l'ion Mg^{2+} et du nucléotide. En effet, l'aspartate lie le Mg^{2+} via une molécule d'eau et la glycine forme une liaison hydrogène avec le phosphate γ du GTP **(Figure 5)**. Les résidus de la boite G4 (NKxD) confèrent la spécificité pour la base du nucléotide et dans le cas des GTPases, établissent des liaisons hydrogènes avec la guanine. Les acides aminés de la boite G5 (C/SAK/L/T) forment des interactions indirectes avec le nucléotide et sont moins conservés. La boite G2 possède une thréonine invariante qui fixe le magnésium (Chardin et al. 1996) **(Figure 5)**. Cette thréonine est située au niveau du Switch 1. Dans la forme GDP et GTP, le magnésium n'est pas coordonné de la même manière. En effet, dans la forme GDP il interagit avec un oxygène du phosphate β, la sérine/thréonine de la P-loop, et quatre molécules d'eau. Dans la forme GTP, il interagit avec l'un des oxygènes des phosphates β et γ, la sérine/thréonine de la P-loop, la thréonine invariante du Switch 1 et deux molécules d'eau **(Figure 5)**. Cependant certaines structures de petites protéines G (Arf6, Arl3 et Arl8) ((Menetrey et al. 2000) ; (Hillig et al. 2000) et code PDB 1YZG non publié) ne possèdent pas de magnésium sous leur forme GDP.

Un autre aspect structural important pour la régulation de la plupart des petites protéines G de la superfamille Ras, est la présence de modifications post-traductionnelles lipidiques **(Tableau 1)**. En effet, la majorité des protéines Ras et Rho ont une séquence tétrapeptidique Caax dans leur extrémité C-terminale (a=acide aminé aliphatique) (pour revues (Cox and Der 2002) ; (Wennerberg et al. 2005)). Le motif Caax est la séquence de reconnaissance de la farnésyl transférase et de la géranyl-géranyl transférase I, qui catalysent l'addition d'un farnésyl ou d'un isoprénoïde gérany-géranyl respectivement, à la cystéine du tétrapeptide. Les séquences des protéines Rab possèdent également sur leur extrémité C-terminale différents motifs contenant des cystéines (CC, CxC, CCx, CCxx ou CCxxx), modifiés par la géranyl-géranyl transférase II, et qui similairement rajoute un groupe géranyl-géranyl sur la cystéine. Certains membres de la famille Arf sont modifiés de façon co-traductionelle à leur extrémité N-terminale par la N-Myristoyl-Transférase (NMT), par un acide gras myristate sur leur deuxième glycine. Certains membres de la famille Ras ne semble pas être modifiés par des lipides, mais s'associent quand même aux membranes (par exemple Rit, RhoBTB, Miro, et Sar1). D'autres comme Ran et Rerg n'ont pas de modification lipidique et ne s'associent pas aux membranes (pour revue (Wennerberg et al. 2005).

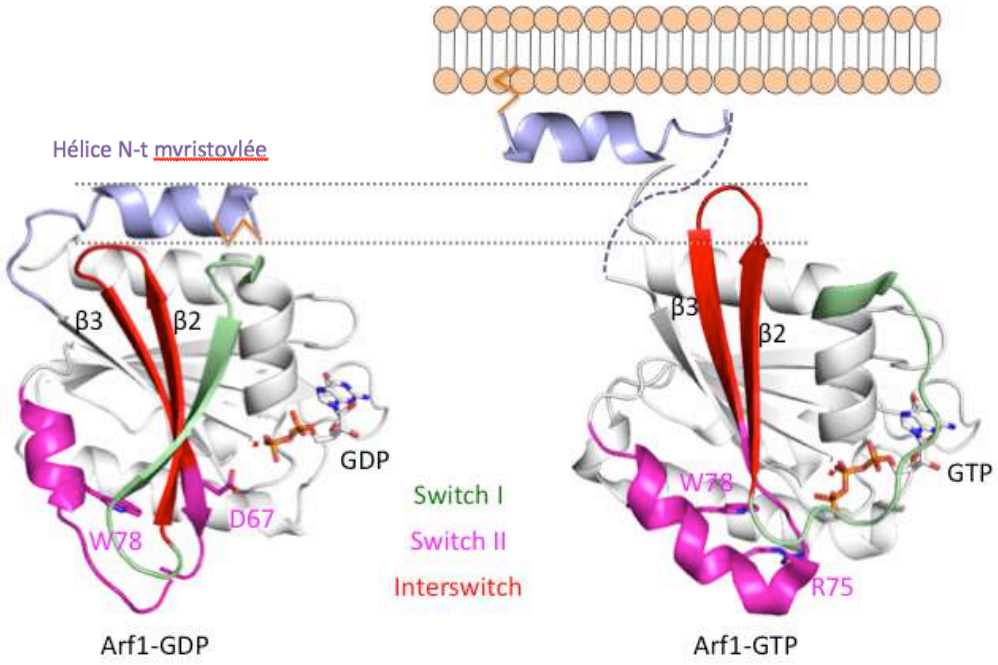

Figure 6 : Le changement de conformation unique des petites protéines G de la famille Arf. Représentation de Arf1-GDP (code pdb 1HUR, à gauche) (Amor et al. 1994) et Δ17Arf1-GTP (code pdb 1O3Y, à droite) (Shiba et al. 2003) dans la même orientation. L'hélice N-Terminale (violet) dans la molécule de droite a été modélisée et les pointillés représentent les résidus reliant l'hélice à la molécule. Les résidus conservés du motif wDvGGqxxxRxxW du Switch 2 sont représentés en magenta. Le GDP et GTP sont représentés en bâtonnets.

2. Particularités structurales des protéines Arfs

Les protéines Arfs se distinguent par la présence d'un interswitch (brins β2-β3) et d'une hélice N-terminale amphipatique. L'interswitch permet de propager l'information d'un bout à l'autre de la protéine (pour revue (Pasqualato et al. 2002)). Le changement de conformation unique chez les Arfs, qui affecte les brins β2-β3 reliant les Switch 1 et 2 ainsi que l'hélice N-terminale, est appelé « interswitch toggle» (pour bascule de l'interswitch) (**Figure 6)** (pour revue (Pasqualato et al. 2002)). Dans la forme Arf-GDP, l'interswitch positionne l'aspartate du motif wDvGGqxxxRxxW (en amont du Switch 2, D67 chez Arf1) de telle sorte à ce qu'il empêche la fixation du GTP. De plus, le tryptophane invariant (W78 chez Arf1) agit comme une cale aromatique pour stabiliser le Switch 2 et l'interswitch dans une conformation incompatible avec la fixation d'un GTP **(Figure 6)**. Dans la forme Arf-GTP, la paire de glycines, le tryptophane et l'arginine (R75 chez Arf1) se réorganisent pour créer un réseau de liaisons hydrogènes qui stabilisent le Switch 2 dans une conformation compatible avec la fixation d'un GTP **(Figure 6)**. De plus, la région des Switch est plus large chez les Arfs que dans les autres familles de petites G **(Figures 3 et 6)** (pour revue (Pasqualato et al. 2002)).

Dans les structures d'Arf1 et d'Arf6 sous forme GDP, l'interswitch est rétracté et forme une poche dans laquelle vient se loger l'hélice N-terminal amphipatique. Cette hélice sert de verrou pour maintenir la conformation inactive de la forme GDP ((Amor et al. 1994) ; (Greasley et al. 1995) ; (Menetrey et al. 2000)) **(Figure 6)**. *In vivo,* en présence de membranes, cette hélice s'ouvre pour laisser apparaître sa face hydrophobe du côté membranaire et permet ainsi la bascule de l'interswitch lors de la réaction d'échange ((Goldberg 1998) ; (Pasqualato et al. 2001)) **(Figure 6)** (Voir plus loin § III.B). Grâce à cette hélice N-terminale, les Arfs n'ont pas besoin de GDI pour les dissocier de la membrane comme chez les Rhos et les Rabs.

Enfin, l'hélice N-terminale est connectée au corps de la protéine G par une courte séquence flexible d'acides aminés, imposant aux protéines de la famille Arf d'être proche de la surface membranaire. Cette proximité avec les membranes leur impose probablement une contrainte d'orientation ainsi qu'à leurs partenaires cellulaires, incluant leurs effecteurs, qui pourraient influencer leur mode de fixation ((Isabet et al. 2009) ; (Liu et al. 2010)). Cette particularité les distingue des familles Rab et Rho dans lesquelles la région de connexion à l'extrimité C-terminale consiste en une longue région flexible qui peut potentiellement s'étendre loin de la surface membranaire (pour revue (Gillingham and Munro 2007).

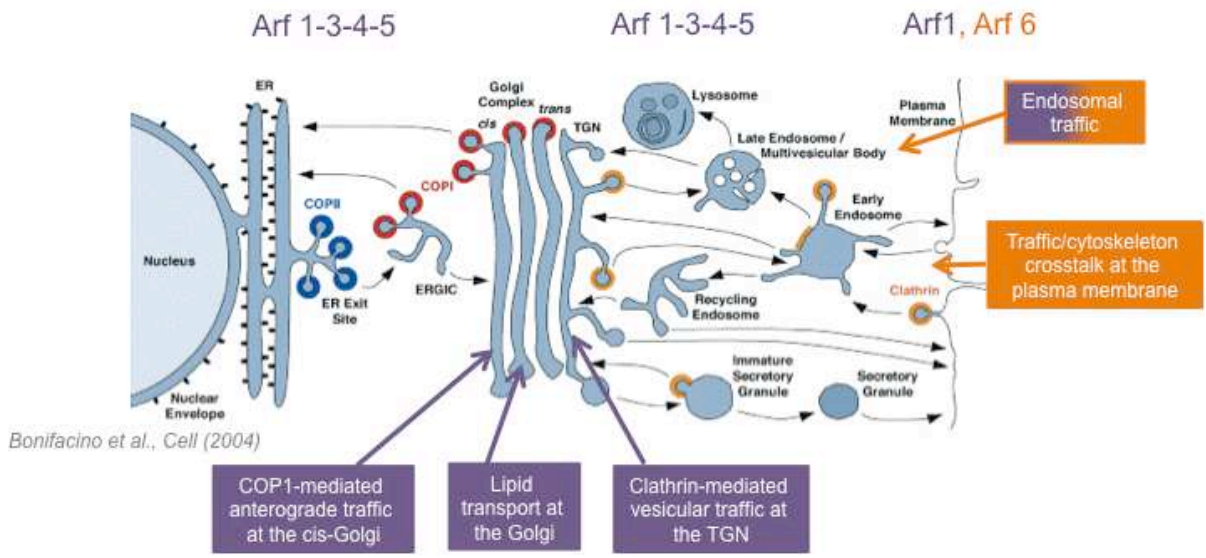

Figure 7 : Localisation cellulaire des différentes classes d'Arf. Les étapes du transport sont indiquées par des flèches. Les couleurs sur les vésicules indiquent les localisations connues ou présumées de COPII (bleu), COPI (rouge) et clathrine (orange). Adapté de (Bonifacino and Glick 2004).

II. Les petites protéines G Arf

A. Les différentes classes et leurs fonctions

Les protéines de la famille Arf sont des protéines de 20 kDa comportant 30 membres chez l'homme, qui peuvent être subdivisés en trois groupes : les Arfs, les Arls (pour « Arf-like ») et les SARs (Kahn et al. 2006). Les Arfs sont présents dans tous les règnes eucaryotes et sont très conservés. En effet, leur identité de séquence est supérieure à 60%. Ils sont composés de six membres chez les mammifères, qui jouent un rôle de régulation dans la formation de vésicules et le trafic cellulaire (pour revue (Donaldson and Jackson 2011)) ainsi que dans la dynamique du cytosquelette (pour revue (Myers and Casanova 2008)).

Les Arfs sont localisés aux membranes dans toute la cellule, incluant la membrane plasmique et les membranes du système sécrétoire, endosomal et lysosomal **(Figure 7)**.

Ces six protéines Arf de mammifère peuvent être classées en trois classes, basées sur leur identité de séquence. La classe I, comprenant les Arf1, Arf2 et Arf3 possède une identité de séquence de plus de 96% entre ses membres. La classe II, comprenant Arf4 et Arf5 ont une identité de séquence de 90% entre eux et de 80% avec la classe I. Enfin, la classe III comprenant uniquement Arf6, possède une identité de séquence avec les autres classes de 64%-69%.

1. Les Arfs de classe I

Arf1 est la protéine la plus caractérisée de cette classe et participe principalement au trafic membranaire et en particulier au bourgeonnement de vésicules depuis le Golgi (pour revue (D'Souza-Schorey and Chavrier 2006)). De ce fait on le trouve principalement fixé aux membranes du Golgi et aux vésicules sécrétoires **(Figure 7)**. Cependant, des études récentes ont montré qu'il pouvait également se trouver aux membranes plasmiques où il régule l'endocytose en couplant son activité avec celle de Cdc42. Arf1 activé recrute à la membrane plasmique la protéine ARHGAP10 via son domaine PH, qui ensuite avec son activité GAP va moduler le recyclage de Cdc42 à la surface cellulaire (Kumari and Mayor 2008).

L'un des rôles d'Arf1 est de recruter le complexe I du manteau cytosolique (COPI) aux membranes du golgi, permettant aux protéines cargo de s'organiser dans des vésicules recouvertes de COPI (pour revue (Beck et al. 2009)). De plus, au niveau du trans-golgi (TGN) il recrute la protéine hétérotétramérique adaptatrice de clathrine 1 (AP1), AP3 et AP4, ainsi que les protéines GGAs (pour revue (Bonifacino and Lippincott-Schwartz 2003). Par ailleurs Arf1 interagit avec des facteurs du cytosquelette, tels que GMAP210 (Cardenas et al. 2009).

De plus, Arf1 est impliqué dans le recrutement et l'activation d'enzymes de modification des lipides telles que la phosphatidyl inositol 4-kinase (PI4K) ou la phospholipase D (PLD) ((Godi et al. 2004) ; pour revue (Santarius et al. 2006)). En effet, Arf1 recrute et stimule l'activité de la PI4K au golgi pour former le PI4P, qui est un lipide membranaire important pour le fonctionnement du golgi (Godi et al. 2004). De plus, il recrute et active la PI-4-phosphate 5-kinase (PI4P5K), une enzyme qui phosphoryle le PI4P en 5' pour générer le PI-4,5-bisphosphate ($PI(4,5)P_2$ ou PIP_2) (pour revue (D'Souza-Schorey and Chavrier 2006). Arf1 se fixe également au domaine PH spécifique du PI4P présent dans une famille de protéines fixant l'oxystérole, impliquées dans l'homéostasie des lipides au golgi (Godi et al. 2004). Des découvertes récentes ont également montré qu'Arf1 régulait les protéines de transfert de lipides dans le golgi et qu'il permettait la formation de gouttelettes lipidiques dans le ERGIC (Endoplasmic Reticulum-Golgi Intermediate Compartment) (Chun et al. 2008). Au niveau du golgi, Arf1 recrute les protéines de transfert de lipides telles que CERT (CERamide Transfer) et FAPP2 via l'interaction avec leur domaine PH, qui peut aussi fixer le PI4P (De Matteis and Godi 2004). CERT régule le transport non vésiculaire de céramide du réticulum endoplasmique au golgi et FAPP2 régule le transfert de glucosyl-céramide depuis le cytosol du golgi précoce jusqu'au TGN (D'Angelo et al. 2007). Cependant, la directionnalité de ce transfert et le rôle d'Arf1 dans ce transfert sont encore peu clairs. De la même manière, il a été montré que FAPP1, qui régule le transport vésiculaire depuis le TGN jusqu'à la membrane plasmique, reconnaissait le phosphatidylisositol-4-phosphate et Arf1 via son domaine PH (He et al. 2011).

La découverte qu'Arf1 s'associait à GBF1 et COPI pendant la formation de gouttelettes lipidiques n'était pas attendue, mais a été identifiée par ARNi chez *D. melanogaster* (Guo et al. 2008) et également apparue dans des analyses protéomiques de gouttelettes lipidiques avec d'autres protéines du trafic cellulaire, ce qui a conduit à l'idée que les gouttelettes lipidiques pouvaient être à l'interface de multiples chemins du trafic membranaire (Bartz et al. 2007). En particulier, la libération de deux protéines, l'ATGL et l'ADRP, à la surface des gouttelettes lipidiques requière Arf1, GBF1 et COPI et probablement la machinerie de COPII dans les cellules de mammifère (Soni et al. 2009). Des résultats similaires ont été observés chez des cellules de *D. melanogaster* (Beller et al. 2008).

Récemment, il a été montré qu'Arf1 régulait l'activation du trypsinogène via le trafic de la pro-catepsine-B et la maturation autophagique dans les pancréatites aigues (Orlichenko et al. 2012).

2. Les Arfs de classe II

La classe II contient deux membres, Arf4 et Arf5, dont la fonction cellulaire reste encore très peu connue. Arf4 est localisé au niveau du ERGIC et du *cis*-golgi où il organise le trafic entre ces compartiments (Ben-Tekaya et al. 2010). De plus, il a été montré qu'Arf4 reconnaissait le motif VxPx cytosolique dans la rhodopsine de la rétine pour faciliter son transport dans le segment extérieur de rod, qui est un cil spécialisé. Le site de fixation de la rhodopsine dans Arf4 est l'hélice α3 (Deretic et al. 2005).

Arf4 et Arf5 peuvent aussi se fixer directement à la protéine CAPS (Calcium-dependent Activator Protein for Secretion), qui régule l'exocytose des corps denses des nerfs terminaux (Sadakata et al. 2010).

3. La classe III : Arf6

Arf6 est le moins conservé des membres de la famille Arf et partage 66% d'identité de séquence avec Arf1, mais contrairement à Arf1, Arf6 n'a aucun effet sur la dynamique des membranes golgiennes. Au contraire, il est localisé à la membrane plasmique et au niveau de compartiments endosomaux, où il régule l'endocytose et le remodelage de l'actine. Arf6 a également comme Arf1 un effet sur le métabolisme des phospholipides. En effet, il a été montré qu'Arf6 activait la PIP5K de type I ((Honda et al. 1999) ; (Krauss et al. 2003)) ainsi que la PLD ((Brown et al. 1993) ; (Cockcroft et al. 1994)) conduisant à la production de messagers secondaires.

Arf6 est nécessaire au recyclage des récepteurs à partir des endosomes. Ce qui a été documenté en premier lieu dans des cellules d'ovaires de hamster chinois (CHO), dans lesquelles l'expression d'un mutant dominant négatif d'Arf6 bloquait le recyclage des ligands endosomaux ((D'Souza-Schorey et al. 1995) ; (D'Souza-Schorey et al. 1998)). De plus, Arf6 est impliqué dans l'internalisation des récepteurs couplés aux protéines G, le récepteur β2-adrénergique (Claing et al. 2001) et le récepteur à l'hormone leutinine (Mukherjee et al. 2000).

En plus de son rôle dans le recyclage des récepteurs à partir des endosomes et dans le métabolisme des phospholipides, Arf6 est également impliqué dans le remodelage de l'actine à la surface cellulaire ainsi que dans des évènements tels que la formation de pseudopodes et de bourgeons membranaires ((Radhakrishna et al. 1996) ; (D'Souza-Schorey et al. 1997)), de queues de comète sur les endosomes (shafer 2000), dans la croissance des neurites (Albertinazzi et al. 2003), la migration cellulaire ((Palacios et al. 2001) ; (Santy and Casanova 2001) ; (Riley et al. 2003)), et la phagocytose ((Zhang et al. 1998) ; (Balana et al. 2005)).

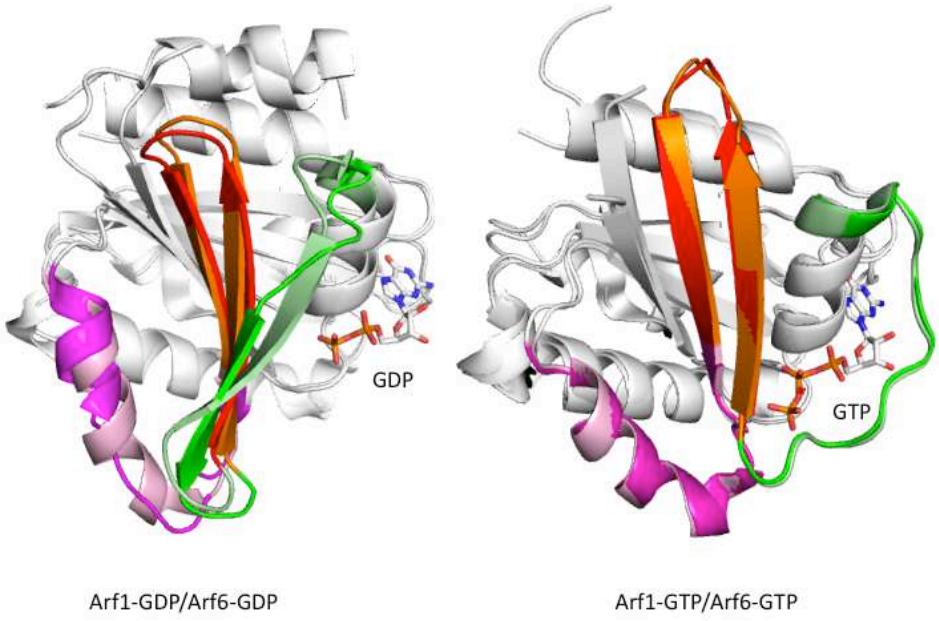

Figure 8 : Comparaison des superpositions des formes GDP de Arf1 et Arf6 et des formes GTP de Arf1 et Arf6. Le Switch 1 est représenté en vert foncé pour Arf6 et vert pâle pour Arf1, l'interswitch en orange pour Arf6 et rouge pour Arf1 et le Switch 2 en rose pâle pour Arf6 et magenta pour Arf1. A gauche, sont superposées les formes GDP entre-elles et à droite les formes GTP entre-elles. Le GDP et GTP sont représentés en bâtonnets. Codes pdb : 1HUR, 1O3Y pour Arf1 et 1E0S, 2J5X pour Arf6.

Le remodelage de la membrane plasmique implique l'internalisation des E-cadherines conduisant au désassemblage des jonctions adhérentes, ceci étant régulé par Arf6 (pour revue (D'Souza-Schorey and Chavrier 2006)). Toutes ces fonctions au niveau de la membrane plasmique et du cytosquelette font qu'Arf6 est impliqué dans un grand nombre de cancers résultant d'une dérégulation des voies de signalisation régulées par Arf6 (pour revue (D'Souza-Schorey and Chavrier 2006)). Par ailleurs, Arf6 est aussi impliqué dans la cytokinèse pendant la division cellulaire, probablement via son effet sur le trafic endosomal (Schweitzer and D'Souza-Schorey 2005) et serait régulé par l'arfophilin et le complexe de l'exocyste (pour revue (D'Souza-Schorey and Chavrier 2006) ; (Fielding et al. 2005)).

Il a été montré récemment qu'Arf6 jouait un rôle dans la régulation de la fonction des ostéoclastes et dans la résorption des os (pour revue (Itzstein et al. 2011)), et aussi qu'il jouait un rôle dans l'autophagie (Moreau et al. 2012). Il a été également proposé un modèle où Arf6 jouerait un rôle dans la désensibilisation des récepteurs β2-adrénergiques (Macia et al. 2012).

B. Arf1 et Arf6 : faux jumeaux ?

Arf1 et Arf6 sont les plus étudiées des 5 isoformes d'Arf humain. Malgré leur forte homologie (plus de 60% d'identité de séquence), Arf1 et Arf6 ont des fonctions distinctes dans la cellule (revues dans (D'Souza-Schorey and Chavrier 2006) ; (Gillingham and Munro 2007) ; (Donaldson and Honda 2005)). Arf1 agit principalement au Golgi alors qu'Arf6 fonctionne principalement à la membrane plasmique. Pour expliquer cette différence de fonctions entre Arf1 et Arf6 dans la cellule, il a été proposé que leurs différentes localisations en étaient probablement la cause. Cependant, des études récentes ont révélés une promiscuité d'Arf1 et d'Arf6 à la membrane plasmique, où elles pourraient agir de concert dans une cascade de signalisation, qui requiert que les deux protéines soient reconnues en fonction de leurs critères structuraux ((Cohen et al. 2007) ; (DiNitto et al. 2007)). En adéquation avec l'hypothèse qu'Arf1 et Arf6 diffèrent par leurs propriétés structurales, des études *in vitro* ont montré que les ArfGEFs (facteurs d'échange spécifiques des Arfs) de la famille de EFA6 (Exchange Factor for Arf6) ont une stricte spécificité pour Arf6 (Macia et al. 2001), et que contrairement à Arf1, Arf6 est résistante à la drogue Brefeldine A (BFA) (Zeeh et al. 2006). De plus, Arf6 échange sont GDP beaucoup plus vite qu'Arf1 ((Macia et al. 2001) ; (Zeeh et al. 2006)). Cependant, les structures d'Arf1-GDP (Amor et al. 1994) et d'Arf6-GDP (Menetrey et al. 2000) sont très semblables, et celles des formes GTP ((Goldberg 1998) ; (Pasqualato et al. 2001)) sont presque indistingables **(Figure 8)**. Par ailleurs, tous les résidus dans Arf1 qui interagissent avec les ArfGEFs ou la BFA dans les structures de

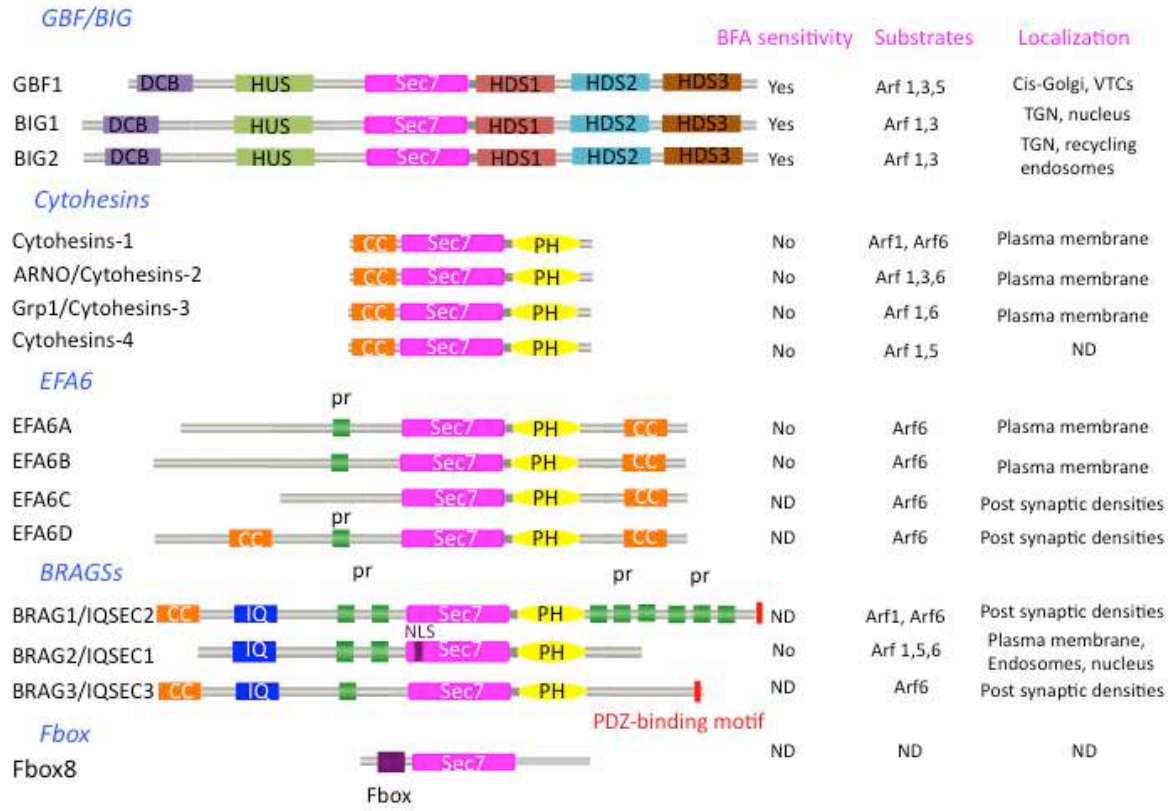

Figure 9 : Les différentes familles d'ArfGEFs

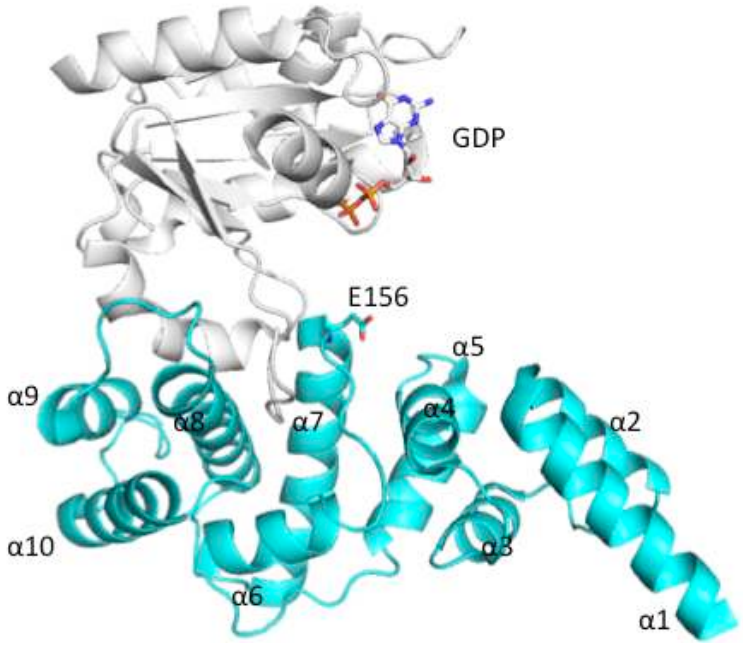

Figure 10 : Structure du domaine Sec7 d'ARNO en complexe avec Arf1-GDP (code pdb 1S9D). Les hélices α sont numérotées de 1 à 10 de l'extremité N- à C-terminale. Le « doigt catalytique » (glutamate 156 chez ARNO) est représenté en bâtonnets.

complexe Arf1/ArfGEF ((Goldberg 1998) ; (Mossessova et al. 2003) ; (Renault et al. 2003)) sont identiques entre Arf1 et Arf6. Par ailleurs, l'obtention d'une structure d'Arf6 avec son effecteur JIP4 (Isabet et al. 2009) a permis de fournir quelques réponses sur la différence de spécificité pour les effecteurs de ces deux isoformes, notamment la présence de différences au niveau de la séquence qui se trouvent au bord des régions Switch et plus précisément à l'extrémité de l'interswitch et du Switch 2 (pour revue (Chavrier and Menetrey 2010). Ceci suggère que des résidus non conservés aux extrémités des régions Switch sont des déterminants structuraux clé pour la spécificité vis à vis des effecteurs.

III. Les ArfGEFs

A. Généralités

Chez les mammifères, il existe 15 ArfGEFS qui peuvent être classés en cinq familles conservées au cours de l'évolution : GBF/BIG (Golgi-specific BFA-resistance Factor 1/BFA-Inhibited GEF), EFA6 (Exchange Factor for Arf6), BRAG (Brefeldin-Resistant ArfGEF) qui fait l'objet de ma thèse et sera discuté dans le chapitre suivant, ARNO (ARf Nucleotide binding Opener)/cytohesine et FBX8 (F-BoX only protein 8) **(Figure 9)**. Alors que la famille GBF/BIG est présente chez tous les eucaryotes, les quatre dernières sont présentes uniquement chez les métazoaires (pour revue (Casanova 2007) ; (Gillingham and Munro 2007)). Chaque ArfGEF fonctionne dans un compartiment cellulaire spécifique et est sujet à différents types de régulation.

Tous les ArfGEFs possèdent en commun un domaine catalytique Sec7 conservé, de 200 résidus environ, dont le nom provient de son homologie avec la protéine Sec7p de levure ((Cox et al. 2004) ; (Chardin et al. 1996) ; (Cherfils et al. 1998)) **(Figure 9)**. Le domaine Sec7 est constitué de 10 hélices α (1-10) organisées en un long cylindre séparé en deux sous-domaines par une poche hydrophobe exposée au solvant, dans sa région centrale (comprenant les hélices 6, 7 et 8) **(Figure 10)**. Cette poche, en association avec la boucle hydrophile entre les hélices 6 et 7, forme le site de fixation d'Arf. De plus, une des caractéristiques clé de ce domaine, est qu'il contient un glutamate invariant qui est critique pour la catalyse et qui est situé face au nucléotide dans la poche de fixation d'Arf. Ce glutamate est nommé « doigt catalytique » (Beraud-Dufour et al. 1998) **(Figure 10)**. Par ailleurs, ce domaine Sec7 est une cible de la toxine fongique Brefeldine A (BFA), une drogue qui inhibe la sécrétion en inhibant l'activation d'Arf1 (Misumi et al. 1986) (voir § III.E.1).

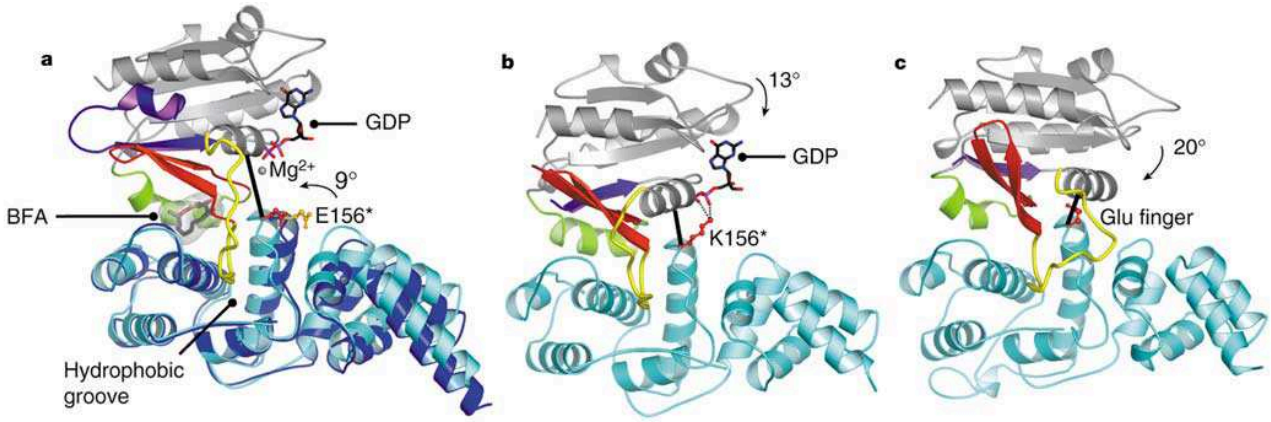

Figure 11 : Etapes de la réaction d'échange reconstituées. A. Inhibition de la bascule de l'interswitch par la BFA dans le complexe Arf1-GDP-Mg^{2+}/BFA/ARNO, avec ARNO non lié en bleu foncé superposé par son extrémité C-terminale. La fermeture de la poche hydrophobe du domaine Sec7 est représentée par une flèche. B. Inhibition de la dissociation du GDP par la mutation du doigt catalytique dans le complexe de pré-dissociation (Δ17)Arf1-GDP/$ARNO^{E156K}$. La rotation de Arf par rapport à l'interface Arf/Sec7 est représentée par une flèche. C. Complexe vide de nucléotide (Δ17)Arf1/Gea2 (Goldberg et al. 1998). La rotation de Arf vers le doigt catalytique est représentée par une flèche. Toutes les structures sont superposées par l'extremité C-terminale de leur domaine Sec7 et représentées dans la même orientation. Arf est en gris, avec l'hélice N-terminal et le brin β1 en violet, le switch 1 est en jaune, l'interswitch est en rouge et le switch 2 est en vert. Le domaine Sec7 est en cyan, avec le doigt catalytique ou la mutation en orange. Les résidus du domaine Sec7 sont notés avec un astérisque. Le GDP et le Mg^{2+} sont représentés en bâtonnets et la BFA est représentée en bâtonnets et en volume. L'approche du GDP vers le doigt catalytique est représentée par des barres noires entre la Lys 30 et la P-loop et le doigt catalytique. Les liaisons hydrogènes sont indiquées par des pointillés. Emprunté à (Renault et al. 2003).

B. Description structurale de la réaction d'échange

En général, le GDP est très fortement associé à la protéine G, d'où la nécessité d'avoir l'aide d'un GEF pour le dissocier (pour revue (Bos et al. 2007) ; (Cherfils and Chardin 1999)). La réaction d'échange, stimulée par les GEFs, est initiée par la formation d'un complexe de faible affinité entre la forme GDP de la protéine G et le GEF, qui se transforme en un complexe vide de nucléotide de haute affinité, après dissociation du GDP. L'entrée du GTP qui est en excès dans la cellule conduit à la dissociation du GEF et à la forme active de la protéine G. Le fait que le déplacement du GDP conduise à la formation d'un complexe stable a été la clé pour la résolution de structures cristallines de complexes protéine G/GEF vides de nucléotide ces dix dernières années. Les structures représentatives de complexes vide protéine G/GEF de la plupart des grandes familles de GEF eucaryotes ont été résolues (pour revue Cherfils and Zeghouf 2012, soumis), nous permettant ainsi de décrire comment les GEFs fonctionnent au niveau atomique.

Dans le cas particulier des ArfGEFs, un film « 3D » de la réaction d'échange a été reconstitué grâce à la résolution de plusieurs complexes Arf/ArfGEF ((Mossessova et al. 2003) ; (Renault et al. 2003) ; (Mossessova et al. 1998) ; pour revue Cherfils et Zeghouf 2012 soumis). De plus des études combinées de biochimie et de cristallographie ont permis d'établir comment les membranes et les ArfGEFs coopèrent pour conduire au changement conformationnel des Arfs (Cherfils and Melancon 2005) discuté plus haut (§ I.B.2). Le domaine Sec7 reconnaît tout d'abord la forme inactive Arf-GDP, favorisant la bascule de l'interswitch qui va déplacer l'hélice amphipatique alors disponible pour les membranes. Puis le « doigt catalytique » du domaine Sec7 va déplacer le GDP par répulsion de charge (Renault et al. 2003), avant de stabiliser le site vide de nucléotide par un pont salin qu'il réalise avec la lysine invariante de la P-loop de la protéine G (Mossessova et al. 1998). Puis finalement, la dissociation du GDP produit le complexe vide Arf/Sec7 (Mossessova et al. 1998) **(Figure 11)**. Ce mécanisme sophistiqué, dans lequel les membranes agissent comme co-facteurs de la réaction d'échange, assure que la forme active Arf-GTP est fortement attachée aux membranes où elle pourra assurer ses fonctions dans le trafic cellulaire.

C. Organisation et fonctions cellulaires des ArfsGEFs

1. La famille ARNO/Cytohésines

Les cytohesines sont probablement les mieux caractérisées des ArfGEFs et la première cytohésine a été identifiée en 1996 par Chardin *et al.* (Chardin et al. 1996). Tous les vertébrés expriment quatre isoformes : cytohesine-1, cytohésine-2/ARNO, cytohésine-3/Grp1/ARNO3 et cytohésine-4 (68% d'identité entre chaque forme chez l'homme).

Les cytohésines sont relativement petites (45-50 kDa) et comportent un court coiled-coil à leur extremité N-terminale, suivi par un domaine Sec7, un domaine PH de fixation aux phosphoinositides et une courte extension C-terminale riche en acides aminés positivement chargés **(Figure 9)** (pour revue (Casanova 2007)).

Les cytohésine-2 et -3 sont exprimées de façon ubiquitaire, la cytohésine-1 est principalement (mais pas exclusivement) trouvée dans les leucocytes et la cytohésine-4 est plus spécifique des leucocytes (Ogasawara et al. 2000).

Les cytohésines sont principalement distribuées à la périphérie cellulaire (Frank et al. 1998) et peuvent être recrutées à la membrane plasmique en réponse à la signalisation de la PI3K qui transforme le PIP_2, abondant à la membrane plasmique de façon constitutive, en PIP_3, fortement régulé ((Klarlund et al. 1997) ; (Venkateswarlu 2003)). En effet, leurs domaines PH est capable de se fixer avec une forte affinité et spécificité au PIP_3 (Klarlund et al. 1997).

Les cytohésines 1, 2 et 3, sont exprimées sous deux isoformes d'épissage qui diffèrent par l'insertion d'une glycine dans le site de fixation des phosphoinositides du domaine PH (Klarlund et al. 2000). Cette unique différence a un large effet sur la fixation des phosphoinositides : la forme diglycine possède une forte affinité pour le PIP_3 par rapport au PIP_2, alors que la forme triglycine perd cette affinité pour le PIP_3 ((Klarlund et al. 2000) ; ((Ogasawara et al. 2000) ; pour revue (Casanova 2007)). Ceci suggère que l'expression préférentielle de l'un des variants d'épissage, peut avoir des conséquences biologiques importantes. On peut noter à ce propos que dans le cerveau, les cytohésine-1 et -2 sont exprimées principalement sous leur forme triglycine, alors que les cytohésine-3 et -4 le sont principalement sous leur forme diglycine (Ogasawara et al. 2000). De plus, une étude récente a montré que les variants de Grp1 ou d'ARNO n'avaient pas la même capacité à internaliser les intégrines β1 (Oh and Santy 2012).

Par ailleurs, les cytohésines telles qu'ARNO et la cytohésine-1 avec leur région polybasique en aval du domaine PH peuvent interagir avec des lipides négativement chargés, tels que la phosphatidyl sérine (PS) ((Nagel et al. 1998) ; (Santy et al. 1999)).

Le recrutement d'ARNO à la membrane plasmique peut être régulé par l'interaction avec Arl4-GTP ou Arf6-GTP via son domaine PH ((Li et al. 2007) ; (Cohen et al. 2007) ; (Hofmann et al. 2007) ; (Stalder et al. 2011)). De plus, une étude récente a montré qu'ARNO pouvait être activé par Arf1-GTP à travers une boucle de rétro-action positive (Stalder et al. 2011), modèle ressemblant à celui de SOS, un RasGEF sans homologie avec ARNO (Margarit et al. 2003)). Le domaine PH des cytohésines est également impliqué dans un mécanisme d'autoihibition de leur domaine Sec7 (DiNitto et al. 2007) (voir plus loin § III.D).

Bien que la signalisation des phosphoinositides soit un composant important pour le recrutement des cytohésines aux membranes, ce n'est pas le seul. En effet, un certains nombre de protéines qui interagissent avec le domaine coiled-coil des cytohésines ont été identifiées (pour revue (Casanova 2007)).

Par ailleurs, *in vitro*, les cytohésines sont bien plus actives sur la classe I des Arfs, ((Chardin et al. 1996) ; (Langille et al. 1999) ; (Ogasawara et al. 2000) ; (Macia et al. 2001)). ARNO possède le domaine Sec7 qui est parmi les plus efficaces *in vitro* (kcat/Km $\approx 10^6$ $M^{-1}s^{-1}$) ((Beraud-Dufour et al. 1998) ; (Renault et al. 2003)). Cependant, *in vivo*, les cytohésines colocalisent préférentiellement avec Arf6 à la périphérie cellulaire et il a été montré qu'ARNO active Arf6 endogène dans les cellules saines ((Santy and Casanova 2001) ; pour revue (Casanova 2007)). Pour expliquer cette divergence, une hypothèse est que la préférence d'ARNO pour Arf1 *versus* Arf6 *in vitro* peut être modulées par d'autres facteurs *in vivo*, notamment par des effets de localisation subcellulaires (pour revues (Casanova 2007) ; (Gillingham and Munro 2007)).

Les fonctions biologiques des cytohésines sont diverses. La cytohésine-1 a été initialement caractérisée comme un activateur de l'adhésion cellulaire via les intégrines β2 (Kolanus et al. 1996) ce qui a été renforcé par l'observation de son rôle important dans l'attachement et la migration des leucocytes, à travers un mécanisme qui requiert à la fois ses fonctions catalytiques et non-catalytiques (Geiger et al. 2000). ARNO est impliqué dans la migration cellulaire (Santy and Casanova 2001), la phagocytose (Beemiller et al. 2006), la macropinocytose (Cohen et al. 2007) et dans les processus de signalisation de l'insuline ((Fuss et al. 2006) ; (Hafner et al. 2006)). De plus, il favorise à la fois la migration des cellules épithéliales et la croissance et le branchement des neurites à travers un mécanisme qui requiert son activité catalytique (Hernandez-Deviez and Wilson 2005) ; (Hernandez-Deviez et

al. 2004) ; (Hernandez-Deviez et al. 2002) ; (Torii et al. 2012)). Dans les deux cas, l'activation d'Arf6 par ARNO conduit à l'activation en aval de Rac1, nécessaire à la fois pour la migration cellulaire et la croissance des neurites. De plus, ARNO est impliqué à différents niveaux du transport vésiculaire. Il intervient dans l'accrochage et la fusion des granules sécrétoires dans les cellules chromaffin adrenale (Caumont et al. 2000) et les cellules neuroendocrines (Liu et al. 2005), dans l'endocytose de certains récepteurs couplés aux protéines G à travers une interaction avec les β-arrestines (Claing et al. 2001), dans la régulation du trafic pos-synaptique via une interaction avec l'ATPase vacuolaire (Hurtado-Lorenzo et al. 2006) et dans la régulation de la dynamique des endosomes dans les neurones (Hernandez-Deviez et al. 2007).

2. La famille GBF/BIG

GBF1 (Golgi-specific Brefeldin A-resistance Factor) et BIG (Brefeldin A-Inhibited GEF) font partie des grands ArfGEFs (>100 kDa) **(Figure 9)**, les seuls ArfGEFs présents chez tous les eucaryotes (métazoaires, levures et plantes) (Mouratou et al. 2005) et sont localisés au niveau du Golgi où ils régulent l'activation des classes I et II d'Arfs, mais semblent fonctionner dans des sous-compartiments Golgiens différents. En effet, GBF1 se trouve principalement au niveau du *cis*-Golgi et du ERGIC alors que les BIGs sont plutôt localisés au niveau du TGN (pour revue (Casanova 2007)).

En plus du domaine Sec7, ils possèdent un domaine DCB (Dimerization and Cyclophilin Binding domain) basé sur le motif du même nom chez l'homologue d'*Arabidopsis*, GNOM ; un domaine HUS (Homology Upstream of Sec7) qui contient un motif très conservé appelé HUS box et trois domaines HDS (Homology Downstream of Sec7) (Mouratou et al. 2005) **(Figure 9)**.

Les fonctions biologiques de GBF1 sont connues. On sait qu'il interagit avec la protéine p115 et qu'il est responsable du recrutement des vésicules recouvertes de COPI sous la dépendance des Arfs ((Garcia-Mata and Sztul 2003) ; pour revue (Casanova 2007)). De plus, récemment il a été montré que GBF1 jouerait un rôle dans l'homéostasie des lipides *via* la voie Arf-COPI-ArfGAP sans pour autant être en contact avec les gouttelettes lipidiques (LDs) ou l'adipose triglycéride lipase (ATGL) (Takashima et al. 2011), alors que d'autres études ont montré un contact avec les LDs ou l'ATGL ((Soni et al. 2009) ; (Ellong et al. 2011)). Récemment, il a été montré que GBF1 était crucial pour le chimiotactisme des neutrophiles et la production de superoxide régulée par les GPCRs. GBF1 semblerait se fixer au PIP_3, via un domaine nouvellement identifié, nommé BP3K (association des domaines

HDS1 et HDS2 et d'une région riche en proline et Alanine) (Mazaki et al. 2012). Par ailleurs, GBF1 agit préférentiellement sur Arf5 *in vitro* mais peut recruter d'autres classes I et II au Golgi lorsqu'il est surexprimé *in vivo* ((Claude et al. 1999) ; (Zhao et al. 2006)).

Chez les mammifères, il existe deux isoformes de BIG, BIG1 et BIG2, qui ont des localisations cellulaires et des fonctions distinctes. BIG2 régule le recrutement des complexes adaptateurs AP-1 et GGA au TGN via l'activation des Arfs. De plus, il semblerait que BIG2 soit impliqué dans le recyclage des récepteurs à la transferrine au niveau des endosomes de recyclage périnucléaires (Shen et al. 2006) et que BIG1 soit nécessaire au bon fonctionnement et à la glycosylation correct des intégrines β1 (Shen et al. 2007). Par ailleurs, il a été montré que BIG1 interagissait avec un membre de la famille des kinésines 21A (KIF21A), lui conférant donc un rôle dans le processus de transport cellulaire (Shen et al. 2008).

3. La famille EFA6

Chez les mammifères, la famille EFA6 comprend quatre protéines résultantes d'épissage alternatif : EFA6A, EFA6B, EFA6C et EFA6D (Derrien et al. 2002). Les membres de cette famille sont caractérisés par une région variable à son extremité N-terminale, un domaine Sec7 central associé à un domaine PH et à un domaine C-terminal contenant un motif coiled-coil **(Figure 9).**

Contrairement aux cytohésines, la famille EFA6 est très sélective pour Arf6, même *in vitro* ((Franco et al. 1999) ; (Macia et al. 2001)). Leur domaine PH interagit sélectivement avec le PIP_2 (Macia et al. 2008). Ceci est en adéquation avec le fait qu'EFA6 est principalement localisé à la membrane plasmique ((Macia et al. 2008) ; (Derrien et al. 2002)).

L'expression des isoformes d'EFA6 est plutôt variée. En effet, EFA6A est principalement exprimé dans le cerveau, avec des plus petits transcrits exprimés dans les tissus intestinaux (Derrien et al. 2002). EFA6C a aussi été détecté dans le cerveau, notamment dans les cellules de Purkinje de souris adultes ((Sakagami et al. 2006) ; (Matsuya et al. 2005)) alors qu'EFA6B est plus largement retrouvé dans le placenta, le pancréas, la moelle épinière et le thymus. EFA6D est quant à lui ubiquitaire (Sakagami et al. 2006). Malgré qu'EFA6A, EFA6C et EFA6D soient tous enrichis dans le cerveau, ils montrent une distribution régionale distincte. En effet EFA6A et EFA6D coprécipitent avec des marqueurs des densités post synaptiques suggérant qu'ils sont concentrés dans les synapses (Sakagami et al. 2006). De plus, EFA6A favorise la formation de colonnes dendritiques de manière dépendante de l'activité d'échange, suggérant que les membres de la famille EFA6 peuvent avoir un rôle dans la formation et la plasticité des synapses (Choi et al. 2006).

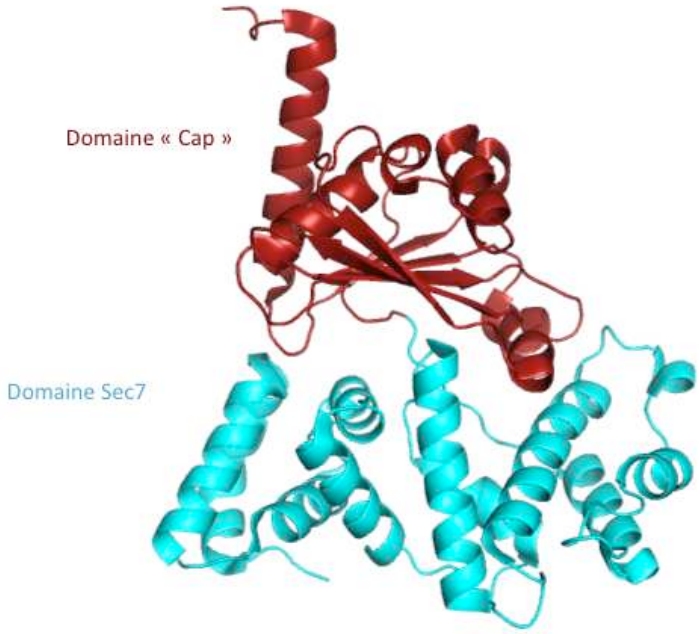

Figure 12 : Structure de RalF (pdb 1XSZ). En cyan, le domaine Sec7 de RalF et en rouge, le domaine « cap ».

Par ailleurs, l'expression des isoformes d'EFA6 favorise la réorganisation de l'actine corticale en des structures ressemblant à des microvilli. Ce mécanisme n'est pas encore bien compris, mais il n'est pas dépendant de l'activité d'échange et requiert au contraire le coiled-coil C-terminal (Derrien et al. 2002). Dans les cellules épithéliales, EFA6A est associé à la membrane plasmique apicale où il joue un rôle dans la formation des jonctions serrées ((Luton et al. 2004) ; (Klein et al. 2008) ; (Theard et al. 2010)).

4. La famille RalF

Les bactéries pathogènes *Legionella pneumophila* et *Rickettsia prowazekii* expriment un ArfGEF appelé RalF, utilisé par ces organismes pour infecter les cellules hôtes. RalF chez *Legionella* a été découverte suite à une recherche dans son génome d'un possible candidat pour le recrutement d'Arf1 qui avait été observé au niveau des vacuoles d'infection ((Kagan and Roy 2002) ; (Nagai et al. 2002)). L'analyse de mutants de RalF de *Legionella* a révélé que la protéine est requise pour le recrutement d'Arf1 au niveau des vacuoles de *Legionella* et des essais biochimiques ont montré que la protéine RalF a une fonction d'ArfGEF sur Arf1 (Nagai et al. 2002). De plus, la structure cristallographique de RalF a été résolue à 1.4 Å de résolution (Amor et al. 2004), révélant la présence de deux domaines : un domaine Sec7 N-terminal et un domaine C-terminal unique en son genre, qui couvre le domaine Sec7 et qui pourrait être impliqué dans la reconnaissance de protéines partenaires et dans la régulation de son activité GEF (voir §III-D plus bas) **(Figure 12).**

D. Régulation des ArfGEFs

1. Auto-inhibition des cytohésines et de RalF bactérien

Ces dix dernières années, il est devenu clair que l'activité d'échange de beaucoup de GEFs est autorégulée à travers des interactions intramoléculaires. L'auto-inhibition émerge en tant que mécanisme critique pour réguler un GEF. L'autoinhibition est régulée par des domaines se trouvant en N- ou C-terminal du domaine catalytique, qui obstruent l'accès au site de fixation de la protéine G, et qui doivent subir de larges déplacements pour permettre au GEF d'être actif. Il apparaît également que les régions linker jouent un rôle actif pour

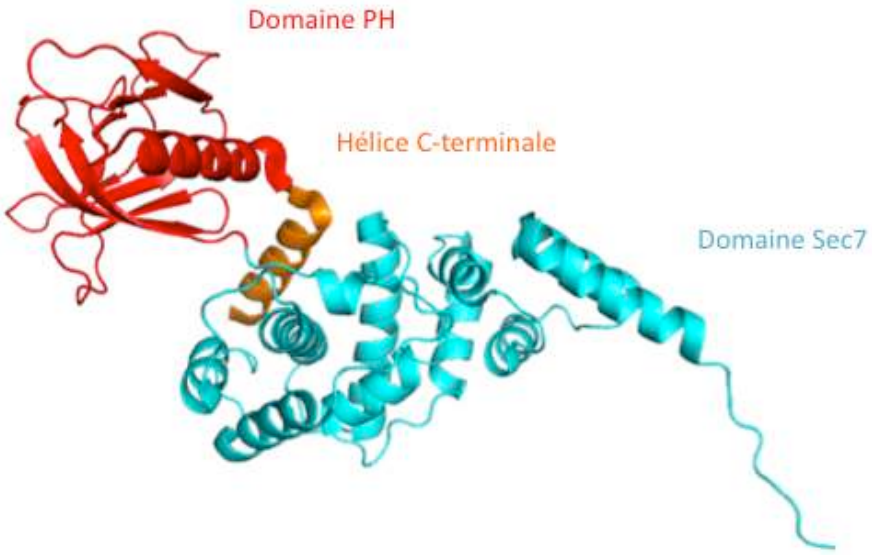

Figure 13 : Structure de Grp1 auto-inhibée (pdb 2R0D).

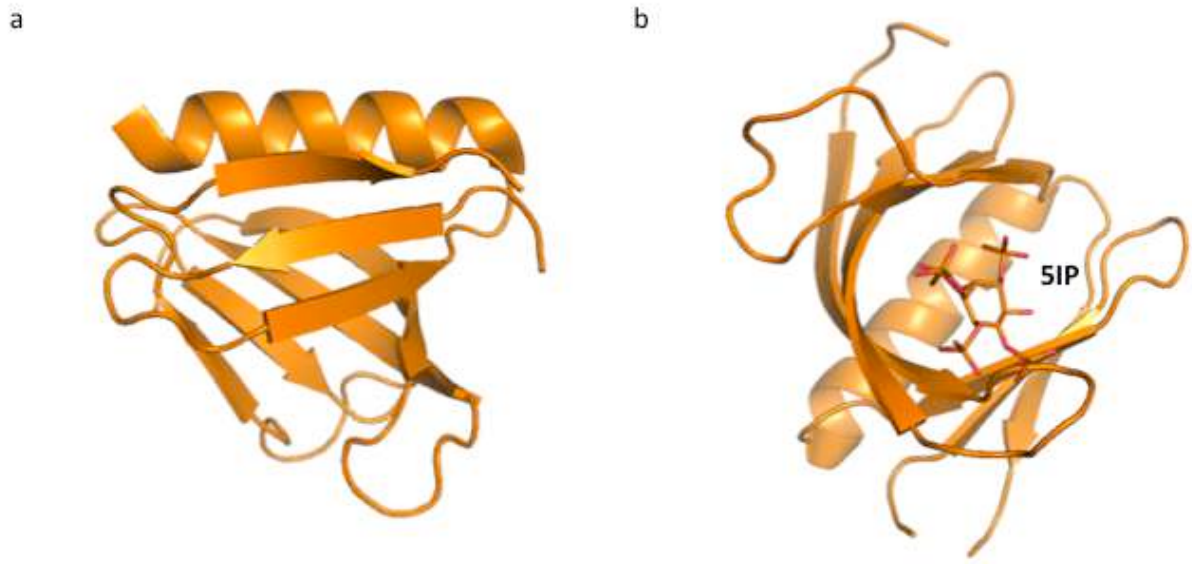

Figure 14 : Structure du domaine PH de la pleckstrin (pdb 2I5F).A. vue de face. B. vue du dessus.

maintenir la conformation auto-inhibée et pour conduire à l'activation (DiNitto et al. 2007). A l'heure actuelle, l'auto-inhibition a été décrite pour la famille des cytohésines chez les ArfGEFs (DiNitto et al. 2007). En effet, la structure de Grp1 auto-inhibé a été décrite, montrant un mécanisme d'auto-inhibition par pseudo-substrat, dans lequel la région polybasique de l'hélice C-terminale amphipatique du domaine PH, bloquent le site de fixation des régions Switch d'Arf (DiNitto et al. 2007) **(Figure 13)**. Par ailleurs, chez la bactérie *Legionella*, RalF semble montrer également un mécanisme d'autorégulation de part son domaine C-terminal « cap » qui en absence de membrane reste fermé sur le domaine Sec7 empêchant ainsi Arf1 de se fixer **(Figure 12)** (Folly-Klan *et al.*, soumis). Ce domaine semble jouer un rôle positif dans l'efficacité catalytique en présence de membrane car l'activité catalytique du domaine Sec7 seul de RalF sur Arf1 en présence de membrane est quasi nulle comparée à celle de la forme entière de RalF (Amor et al. 2004).

2. Régulation par les membranes

La majorité des ArfGEFs possède un domaine PH capable de les recruter à la surface des membranes, à l'exception de la famille GBF/BIG. Dans le cas des BIGs aucune donnée n'est pour l'instant disponible. Les domaines PH sont les plus caractérisés parmi les domaines de fixation des phosphoinositides (pour revue (Lemmon 2008)). On dispose à l'heure actuelle de nombreuses structures de domaines PH décrites (pour revue (Lemmon 2008)). Il comprend environ 120 résidus repliés en tonneau β avec 7 brins couronnés par une hélice α amphipatique à une extrémité, alors que l'extrémité opposée est encadrée par trois boucles variables **(Figure 14)**. Les trois boucles forment la poche de fixation des PIs et leur longueur et séquence primaire définissent la spécificité des domaines PH. Ils possèdent une structure très conservée, malgré une faible similarité de séquence parmi les membres de la famille. La conséquence de cette variabilité de séquence est que les domaines PH ont plusieurs fonctions et interagissent avec de nombreux ligands, incluant des protéines, des phospholipides acides, des inositols phosphates et des phosphoinositides. Une faible proportion de domaine PH (10-20%) fixe spécifiquement et fortement des PIs individuels, qui sont plus communément le $PI(3,4,5)P_3$, le $PI(4,5)P_2$ ainsi que le $PI(3,4)P_2$, l'affinité des domaines PH pour le PI variant significativement du nanomolaire au micromolaire (DiNitto and Lambright 2006). Chez les ArfGEFs, les domaines PH qui sont le mieux caractérisé pour la fixation de PIs sont le domaine PH d'ARNO, de Grp1 et de la cytohésine-1 ((Klarlund et al. 1997) ; (Cronin et al. 2004)).

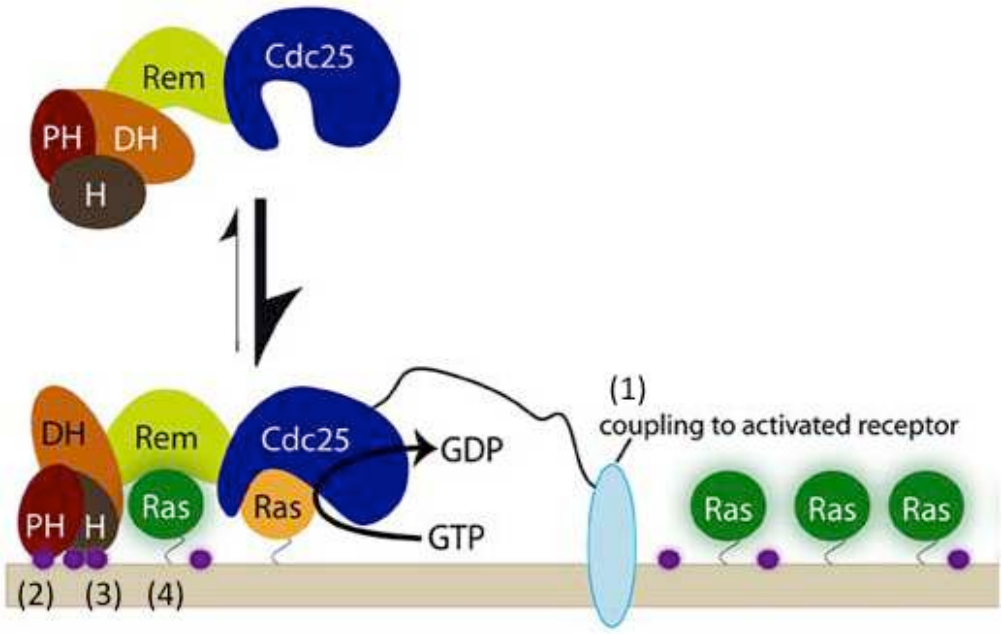

Figure 15 : L'association aux membranes de SOS est améliorée par de multiples interactions à la membrane. Cette association est régulée par (1) le couplage à des récepteurs activés (2) l'interaction du domaine PH avec le PIP_2 (cercles violets) (3) l'interaction électrostatique non spécifique entre la membrane et une surface de fixation aux membranes putative sur le domaine histone de SOS, et (4) l'engagement de Ras au site allostérique de SOS. La combinaison synergique de ces évènements de fixation à la membrane conduisent aux relargage de l'auto-inhibition et facilite la réorientation productive de SOS dans le plan de la membrane, maximisant l'accessibilité des deux sites de fixation de Ras sur SOS à la membrane. Schéma emprunté à (Gureasko et al. 2010).

Le modèle pour le mécanisme moléculaire de l'association des GEFs aux membranes a été bien décrit pour SOS, un facteur d'échange de Ras ((Margarit et al. 2003) ; (Sondermann et al. 2004) ; (Freedman et al. 2006) ; (Gureasko et al. 2008) ; (Gureasko et al. 2010)). En effet, le groupe de Kuriyan a proposé le modèle suivant : 1) à faible densité de Ras-GDP et à faible concentration de PIP_2 à la surface membranaire, la région N-terminale régulatrice de SOS la maintient dans un état inactif en inhibant la localisation de SOS à la membrane. La fixation de Ras aux sites allostériques de SOS lui permet de s'ouvrir et un changement de conformation au niveau du site actif s'opère, permettant ainsi l'engagement du substrat (Freedman et al. 2006). 2) L'activité de SOS autoinhibé est stimulée par une augmentation de la densité de Ras à la membrane, par le remplacement du GDP par du GTP sur Ras et par une augmentation de la concentration de PIP_2 dans la membrane. 3) D'autres accrochages de SOS à la membrane, comme le couplage à des récepteurs activés en combinaison avec une densité élevée de Ras, la génération de Ras-GTP et une forte concentration de PIP_2, résultent en une levée efficace de l'autoinhibition ((Gureasko et al. 2008) ; (Gureasko et al. 2010)) **(Figure 15)**. Actuellement, chez les ArfGEFs, on ne dispose que de la structure d'une forme fermée décrite chez les cytohésines (DiNitto et al. 2007), mais il nous manque les informations concernant la façon dont les ArfGEFs s'ouvrent à la membrane. On pourrait imaginer que cela se passe de la même manière que pour SOS. Des premiers éléments on été fournis par une combinaison d'analyses structurales et biochimiques. Il a été proposé un modèle commençant par la fixation d'un Arf-GTP (Arf1 ou Arf6) au niveau d'une région du domaine PH correspondant à une zone comprenant les brins β3-β4 et la boucle β6-β7 du domaine PH et résultant en une perturbation des contacts inhibiteurs entre le domaine Sec7 et le domaine polybasique C-terminal. Puis, s'en suit la fixation au PIP_2 qui est effectuée par l'intermédiaire de la poche de fixation du domaine PH. Une fois le PH fixé à la membrane, il s'en suit un déplacement de la région auto-inhibitrice (Stalder et al. 2011).

3. Régulation par des boucles de rétroaction

Le concept que l'activation des protéines G peut être régulée par des boucles de rétroactions dans lesquelles le produit de la réaction d'échange (forme liée au GTP de la protéine G) se fixe au GEF et modifie sa constante d'échange, a été récemment mis en avant par des analyses structurales et biomimétiques réalisées sur le RasGEF SOS (Margarit et al. 2003) et les ArfGEFs cytohésines ((Cohen et al. 2007); (Stalder et al. 2011)). Le fait que l'autoinhibition des cytohésines soit levée par le recrutement d'ARNO à la membrane via

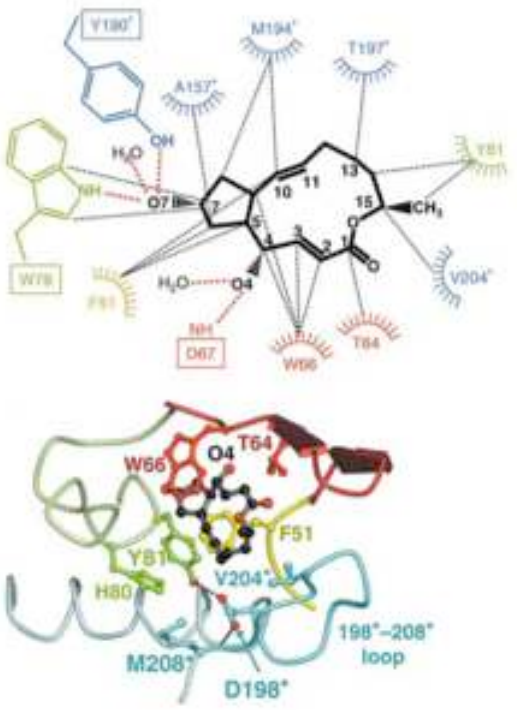

Figure 16 : Site de fixation de la BFA au niveau de l'interface Arf–Sec7. En bleu, Sec7 du GEF; en rouge interswitch d'Arf ; en vert Switch 2 d'Arf et en jaune Switch 1 d'Arf. Les liaisons hydrogène sont indiquées par des pointillés rouges; les contacts de van der Waals (cutoff de 4A°) par des pointillés noirs. Emprunté à (Renault et al. 2003)

l'interaction de son domaine PH avec Arf6-GTP (Cohen et al. 2007), a soulevé la possibilité d'un mécanisme de boucle de rétroaction. En effet, l'étude réalisée par Stalder et ses collaborateurs, a montré que non seulement Arf6 mais également Arf1 est efficace pour établir une boucle de rétroaction positive (Stalder et al. 2011). Cela a conduit les auteurs à proposer que les cytohésines recruteraient une quantité initiale d'Arf6-GTP qui déclencherait l'activation d'Arf1-GTP, qui à son tour maintiendrait sa propre activation. De plus, des mutations dans la région du domaine PH qui affectent la boucle de rétroaction (Stalder et al. 2011) suggèrent que le site de fixation d'Arf-GTP n'empiète pas sur les surfaces de l'autoinhibition (DiNitto et al. 2007) ou de la fixation des phosphoinositides (Cronin et al. 2004). Un mécanisme alternatif pourrait être qu'Arf-GTP se fixe au domaine PH des cytohésines de la même manière qu'Arf1-GTP se fixe au domaine PH d'ARHGAP21 (le seul domaine PH à ce jour dont la structure en complexe avec une protéine Arf a été résolue (Menetrey et al. 2007)), puisque ce mode de fixation est compatible avec l'effet des mutants décrits dans le papier de Stalder *et al.* (Stalder et al. 2011).

E. Inhibiteurs des ArfGEFs

Actuellement, un nombre croissant de petites molécules capables d'inhiber l'activation d'Arf est décrit dans la littérature. Bien caractérisés, ces inhibiteurs pourraient être des outils puissants pour l'étude des fonctions spécifiques des ArfGEFs dans la cellule. Ils pourraient également cibler des ArfGEFs dans des voies dérégulées par des pathologies et conduire à de nouveaux agents thérapeutiques.

1. Le cas de la BFA

La BFA est une toxine fongique qui bloque la sécrétion en empêchant l'assemblage des composants protéiques du manteau sur les membranes donneuses (Misumi et al. 1986). La BFA est le seul inhibiteur à ce jour dont la structure fixée à un complexe Arf/GEF est connu **(Figure 11)** ((Renault et al. 2003) ; (Mossessova et al. 2003)). La BFA est un inhibiteur remarquable en ce sens où il ne se fixe pas uniquement au domaine Sec7 du GEF, mais se fixe avec une double spécificité à un complexe Arf-GDP/Sec7 (Zeeh et al. 2006) **(Figure 16)**, séquestrant le GEF dans un intermédiaire réactionnel abortif (Peyroche et al. 1999) et ceci selon un mode d'inhibition incompétitif (Beraud-Dufour et al. 1999). Cela à conduit au concept d'« inhibition interfaciale » ((Renault et al. 2003) ; (Pommier and Cherfils 2005)). Seuls certains ArfGEFs sont sensibles à la BFA **(Figure 9)** et de même si les classes I et II des Arfs sont sensibles à la BFA, Arf6 est résistant à la toxine (Zeeh et al. 2006).

2. Autres inhibiteurs d'ArfGEFs

Récemment, un certain nombre d'inhibiteurs d'ArfGEFs ont été identifiés. Parmi ceux-ci, il existe le composé LM11, qui a été identifié par criblage *in silico* basé sur la structure et qui inhibe l'activité catalytique à la fois des ArfGEFs sensibles et résistants à la BFA par un mécanisme d'inhibition non compétitif (Viaud et al. 2007). Cette molécule se fixe dans une poche près de l'interface ARNO/Arf1 et comme la BFA, empêche le changement de conformation nécessaire à l'activité d'échange. De plus, des essais fonctionnels suggèrent que le LM11 inhibe l'activation des classes I et II des Arfs, mais pas d'Arf6 (Viaud et al. 2007).

D'autres inhibiteurs, découverts par criblage phénotypique (Exo2, GolgicideA et LG186) ont été testés initialement sur les grands ArfGEFs mais également sur ARNO et BRAG2 (Boal et al. 2010). Dans cette étude, les auteurs ont montré qu'Exo2, un inhibiteur de la voie sécrétoire précoce qui perturbe le trafic des toxines ((Feng et al. 2004) ; (Spooner et al. 2008)), inhibe la fonction de GBF1 dans les cellules humaines et inhibe légèrement l'activité de BIG1 *in vitro*. Il n'a cependant pas d'effet significatif sur ARNO *in vitro* et il a un faible effet d'inhibition sur BRAG2. La Golgicide A (GCA), un composé reporté comme étant un inhibiteur sélectif de GBF1 et dont le site de fixation chevaucherait celui de la BFA (Saenz et al. 2009), a un léger effet sur BIG1 *in vitro*, n'a pas d'activité significative sur ARNO et a un faible effet sur BRAG2 (Boal et al. 2010). LG186, un dérivé d'Exo2, qui possède un anneau cyclooctenyl plus large comparé à l'anneau cyclohexenyl d'Exo2, semble inhiber la fonction de GBF1 *in vitro* et dans les cellules MDCK, cellules modèles de la polarisation apico-basale, dans lesquelles Exo2 et la BFA n'ont pas d'activité. Il a un léger effet sur l'activité de BIG1 *in vitro*, alors qu'il n'a pas d'effet significatif sur ARNO et un faible effet sur BRAG2 (Boal et al. 2010). Par ailleurs, Exo2 et LG186 sont des inhibiteurs réversibles comme la BFA, mais leurs mécanismes d'inhibition ne sont pas connus (Boal et al. 2010).

Pour finir, une petite molécule antagoniste des cytohésines a été identifiée par criblage de déplacement d'aptamère: la Secin H3 (Hafner et al. 2006). Cette molécule se fixe au domaine Sec7 des cytohésines et inhibe l'échange GDP/GTP (Hafner et al. 2006).

A ce jour la BFA reste encore un inhibiteur inégalé tant par sa spécificité que par son efficacité. Ces inhibiteurs sont encore peu spécifiques et certains ArfGEFs, comme BRAG2 n'ont pas encore pu être inhibés.

The BRAG Family : an overview

Kaheina Aizel[1], Jacqueline Cherfils[1 *] and Mahel Zeghouf[1*]

[1] Laboratoire d'Enzymologie et Biochimie Structurales, CNRS, Gif-sur-Yvette, France

* Corresponding authors:

Jacqueline Cherfils, cherfils@lebs.cnrs-gif.fr

Mahel Zeghouf, zeghouf@lebs.cnrs-gif.fr

This is a preliminary version of the review that will be submitted by the end of 2012.

A. Description of the family

The first member of this family, BRAG2, was discovered and cloned by Someya and collaborators (Someya et al. 2001) and given the name **B**refeldin **R**esistant **A**rf**G**EFs after preliminary experiments which were interpreted. These experiments were made with Arf6 as substrate, and we know now that Arf6 is not inhibited by BFA. However, it has been shown when Arf1 was the substrate that BRAG2 seemed to be resistant to BFA *in vitro* (Boal et al. 2010).

This family has been found in many species going from mammals to insects through aves, fish, nematodes, reptiles, ciona and maybe more **(Annex 1)** (for review (Casanova 2007)). Mammals contain 3 genes in this family, which still remain poorly characterized: BRAG1 (IQSEC2 or IQ-ArfGEF), BRAG2 (IQSEC1 or ArfGEP100) and BRAG3 (IQSEC3 or SynArfGEF, for synaptic guanine nucleotide exchange factor for Arf). *C. elegans* and insects each seem to have only one BRAG gene (for review (Casanova 2007)). Human BRAG2 is ubiquitously expressed in at least two splice isoforms (called BRAG2a and BRAG2b) with an N-terminal extension of 122 amino acids for the b form (Dunphy et al. 2006). BRAG2a is also called ArfGEP100 or IQSEC1 and is a 95-kDa protein composed of 841 amino acids. It is also the most characterized between the two isoforms. BRAG1 and BRAG3 have at least two splice isoforms ((Murphy et al. 2006); (Fukaya et al. 2011)).

These proteins are characterized by the presence of a conserved catalytic Sec7 domain **(Figure 9)**. Some predictions associated an IQ motif, a putative PH domain and some proline rich regions (for review (Casanova 2007)). IQ motif was first discovered as calmodulin binding domain (Alexander et al. 1988) and contain the [I,L,V]QxxxRxxxx[R,K] motif (for review (Bahler and Rhoads 2002)), although in BRAG2 no clear evidence of calmodulin binding was detected (Someya et al. 2001). PH domains are generally known to recognize membrane phospholipids and may bind to proteins (for review (Lemmon 2008) and (DiNitto and Lambright 2006)). In BRAG1 there is an additive predicted coiled coil domain in N-terminus, which is involved in protein-protein interactions (for review (Casanova 2007)). In BRAG2 and BRAG3, some predictions found one coiled coil in C-terminus (for review (Casanova 2007)) and for BRAG2, nuclear localization signals (NLS) motifs have been predicted as well (Dunphy et al. 2006). In BRAG1 and BRAG3, an addition type I PDZ-binding motif (consensus, -T/SxV) has been predicted at their carboxyl terminus ((Murphy et al. 2006); (Inaba et al. 2004)).

B. BRAGs are ArfGEFs

It has been shown *in vitro* with GST-Sec7 fusion protein that rat BRAG1 could promote binding of (^{35}S)GTPγS to Arf1 (Murphy et al. 2006). I*n vivo,* by Arf pull down assay with GST-GGA1 fusion protein (known to interact specifically with GTP-bound Arfs (Santy and Casanova 2001)), it has been shown that transfected mouse BRAG1 activated Arf6 more potently than Arf1 in the same conditions (Sakagami et al. 2008).

Transfected BRAG3 selectively activates Arf6 i*n vivo,* using Arf pull down assay with GST-GGA1 fusion protein (Fukaya et al. 2011). On the contrary, Hattori *et al.* (Hattori et al. 2007) had previously shown *in vivo* using an Arf pull down assay with GST-GGA1, that human BRAG3 exhibits GEF activity toward Arf1 but not Arf6. The reasons for this difference are unknown but could be due to the fact that in Hattori *et al.* study, they used a partial protein and that maybe the full-length protein is necessary for the GEF activity toward Arf6.

BRAG2a has been shown to preferentially activate Arf6, compared to Arf1 and Arf5, *in vitro* by GTPγS-binding assay with recombinant proteins, although their purity and characterization was not clear (Someya et al. 2001). Two other groups also described a BRAG2 Arf6 GEF activity *in vivo* using Arf pull down assay with GST-GGA3 ((Dunphy et al. 2006); (Sakurai et al. 2011)). Dunphy and collaborators showed that exogenous expression of BRAG2a or BRAG2b resulted in increased levels of Arf6-GTP (Dunphy et al. 2006). Recently, Jian and collaborators observed as well that recombinant BRAG2a and constructions of BRAG2a, comprising the Sec7 and PH domains, could activate Arf1 and Arf6 *in vitro* by fixed time point assay, fluorescence spectroscopy and stopped flow, although no evidence of purity of the proteins was shown (Jian et al. 2012)

A *Drosophila* ortholog of BRAGs, Loner, has also been shown to specifically activate dArf6 (an Arf6 ortholog, which shares 97% identity) *in vitro* by GDP release assays, using GST fusion proteins containing dArf6 and GST fusion proteins containing the Sec7 domain of Loner (Chen et al. 2003).

All these findings suggest that BRAGs are ArfGEFs, but the substrate specificity remain unclear.

C. Localization of BRAGs

BRAG1 was identified in postsynaptic density (PSD) fractions in rat brain, with the use of mass spectrometry (Murphy et al. 2006). In this study they showed by immunocytochemistry that endogenous BRAG1 forms clusters at excitatory synapses at sites

that also label for PSD-95, a component of PSD. PSD represents an electron-dense thickening of the postsynaptic membrane, where glutamate receptors form huge macromolecular complexes with scaffold proteins and various signaling molecules (for review (Boeckers 2006)). Another group also found endogenous BRAG1 in the PSD of excitatory synapses of mouse brain by immunohistochemistry (Sakagami et al. 2008). The same group also found endogenous BRAG1 associated with synaptic ribbons in the mouse retina by immunohistochemistry, using light and electron microscopy to examine this localization (Katsumata et al. 2009).

BRAG3 has been originally identified by screening for mRNA species associated with the post-synaptic density fraction in rat brain (Tian et al. 1999). Inaba and collaborators confirmed the localization of the protein BRAG3 in PSD fraction prepared from the rat forebrain, by western blot using a BRAG3 specific antibody (Inaba et al. 2004). The same group found endogenous BRAG3 at post-synaptic specializations of inhibitory synapses in mouse brain by immunohistochemistry (Fukaya et al. 2011).

BRAG2 was also shown to be concentrated in synaptic vesicle and PSD fraction of mouse brain by cell fractionation (Scholz et al. 2010). It has been shown by confocal immunofluorescence microscopy using a rabbit BRAG2 antibody, that endogenous BRAG2 in T98G glioblastoma cells was mostly distributed in punctate patterns throughout the cytoplasm, that remain to be identified and has apparent colocalization with Arf6 in the cell periphery. They showed as well by cell fractionation and western blotting that endogenous BRAG2 was detected only in cytosol and not in crude membrane fraction (Someya et al. 2001). The same group observed by confocal microscopy the same distribution in punctate patterns in HepG2 liver carcinoma cells, with concentration in the perinuclear region (Hiroi et al. 2006). Another group observed by immunofluorescence microscopy these punctate collections of BRAG2 in the cytoplasm and perinuclear region, in PMA-differentiated human macrophage-monocyte-like U937 cells (Someya et al. 2010). Transfected BRAG2a and BRAG2b have been shown to accumulate in the nucleus of HeLa and MDCK cells, although BRAG2b had a more cytoplasmic distribution than BRAG2a. They also found by cell fractionation, that a fraction of endogenous BRAG2 also associates with nucleus (Dunphy et al. 2006). The same group found that ectopic co-expression of the nuclear GTPase PIKE/AGAP2 and BRAG2 in HeLa cells, causes both BRAG2 and the Cajal bodies marker coilin to accumulate in nucleoli (Dunphy et al. 2007).

All these experiments suggest that the BRAG family is localized near membranes and in vesicular structures. The fact that all the members of the family are localized in PSD of synapses suggests a role of the entire BRAG family in synaptic membrane turnover.

Considering that BRAGs have a PH-like domain, they could possibly interact with membranes and phosphoinositides. Few groups have studied the role of BRAGs PH domain in membrane binding or PI binding. It has been shown by *in vitro* lipid binding assay that a recombinant construction of BRAG2a containing the Sec7 and PH domains, showed high affinity for liposomes containing $PI(4,5)P_2$ and PIP_3. By titrating each PI into the binding reaction they found a Kd of 0.97 μM for $PI(4,5)P_2$ and 1.53 μM for PIP_3 (Sakurai et al. 2011). They also tested the effect of PIs on the GEF activity of BRAG2 by GTPγS binding assay using liposomes containing different compositions of PIs, although it was reported with GTPγS binding assay using soluble PIs, that PIs did not affect this activity (Someya et al. 2001). The difference between the two observations is probably due to the fact that in Sakurai experiments they used liposomes containing PIs and that Someya used soluble PIs. Sakurai and collaborators found that the activity of BRAG2 was significantly enhanced by the addition of $PI(4,5)P_2$ and PIP_3. Indeed, the activity of BRAG2 was increased in a PI-concentration-dependant manner (Sakurai et al. 2011). Another recent study showed that PIP_2 binding to the PH domain of BRAG2 seems to modify BRAG2 activity (Jian et al. 2012). However, in this study, no estimation of the purity of the proteins was shown so their kinetics results could be biased. The group of Sabe has shown by pull-down assays, that BRAG2 PH domain associates with phosphorylated receptors ((Menju et al. 2011); (Hashimoto et al. 2011); (Morishige et al. 2008)). Scholz and collaborators showed by yeast two-hybrid analyses that fragment encompassing the Sec7 and PH domains of BRAG2 could bind to the dephosphorylated GluA2 subunit of the AMPA receptor (Scholz et al. 2010). This could imply a recruitment of BRAG2 by its PH domain to membranes. Up to date, no experiments have been done to characterize BRAG1 ad BRAG3 PH domains.

D. Cellular functions of BRAGs

1. Functions in endocytosis

Several biological functions for BRAG2 have been reported in endocytosis. In HeLa cells, knockdown of BRAG2 increased amounts of β1 integrins at the cell surface, and increased cell spreading on fibronectin-coated substrates, suggesting that BRAG2 regulates cell adhesion through endocytosis of β1 integrins (Dunphy et al. 2006). In a liver carcinoma

cell line, it has been found that BRAG2 interacted with α-catenin in a yeast two-hybrid screen and that BRAG2 accelerated the GTPγS binding to Arf6 in the presence of α-catenin. They also found that BRAG2 depleted by siRNA in HepG2 cells led to an increase in E-cadherin content and that overexpression of BRAG2-GFP decreased amounts of F-actin seen microscopically in NRK cells. All these experiments suggest that BRAG2 regulates actin cytoskeleton remodeling and cell adhesion *via* internalization of E-cadherin and *via* α-catenin, through the activation of Arf6 (Hiroi et al. 2006).

Transfected and endogenous BRAG2 has been shown to interact directly with a subunit of AMPAR in synapses, by yeast two hybrid experiments, GST pull down assays and immunoprecipitation (Scholz et al. 2010). In this study they showed by GTPγS binding assay and mutations on tyrosines of the 3Y motif of GluA2 subunit of AMPAR, that the dephosphorylation of one tyrosine triggered BRAG2 activation. They showed as well, in neuronal cultures using anti-pY to monitor the tyrosines phosphorylation level in an mGluR-dependent manner, that this tyrosin was involved in Schaffer collateral long term depression (LTD) (Scholz et al. 2010). It is known that expression of mGluR-LTD relies on regulated endocytosis, resulting in decrease of surface AMPARs (Carroll et al. 2001), so they showed that BRAG2 was involved in endocytosis of AMPAR, with a cell surface ELISA assay and that this endocytosis was mediated by the activation of Arf6, using GTPγS binding assay (Scholz et al. 2010).

A role of BRAG2 in phagocytosis has also been found. Indeed, BRAG2-depleted U937 cells expressing BRAG2-shRNA plasmids were used to examine a potential role for BRAG2 in phagocytosis of opsonized zymosan or IgG beads, which were bound predominantly to complement and Fcγ receptors, respectively. They showed that the uptake of opsonized zymosan or IgG beads was significantly less in BRAG2-depteted cells than the control cells, consistent with a role for BRAG2 in both complement receptor-and Fcγ receptor-mediated phagocytosis. They also showed by immunofluorescence microscopy that endogenous BRAG2 and overexpressed Arf6 were partially co-localized during phagocytosis around phagocytosed particles and that knockdown of Arf6 in BRAG2-depteted U937 cells decreased phagocytosis of opsonized zymosan or IgG beads. So these experiment suggest that BRAG2 is a regulator of Arf6 activation in the signaling cascade involved in complement receptor-and Fcγ receptor-mediated phagocytosis (Someya et al. 2010).

All these experiment taken together suggest a role for BRAG2 in different types of endocytosis, including endocytosis of receptors and phagocytosis.

2. Functions in Fusion

In myoblasts and macrophages, it has been shown by interference RNA in cultured mammalian cells that myotubes failed to form when BRAG2 was depleted. These results suggest that BRAG2 is involved in cell-cell fusion. They showed as well by GGA3-GST pull down assays that this cell-cell fusion was mediated by the activation of Arf6 in BRAG2-depleted cells (Pajcini et al. 2008).

In *Drosophila*, it has been shown that Loner, an homolog of BRAG2, was required for myoblast fusion using Loner mutant embryos and that this fusion was mediated by the activation of dArf6 by Loner in transgenic flies carrying a dominant-negative form of dArf6 (dArf6 T27N) (Chen et al. 2003).

Recently, another group found that Schizo/Loner, regulates N-cadherin to induce fusion competence of myoblasts. Yeast two-hybrid experiments showed that the N-terminal region of Schizo/Loner interact with N-cadherin and that in Schizo/Loner mutant cells, regulation of N-cadherin from the myoblast membrane is important for the fusion process (Dottermusch-Heidel et al. 2012).

3. Functions in Neurons

Immunoprecipitation and *in vitro* binding experiments revealed that BRAG1 forms a protein complex with NMDA-type glutamate receptors in PSD of excitatory synapses, through the interaction of BRAG1 with the PDZ domains 1 and 2 of PSD-95 (a PDZ domain-containing synaptic protein ((Dosemeci et al. 2007)); (Sakagami et al. 2008)). Endogenous and overexpressed BRAG1 has been shown to interact as well with insulin receptor tyrosine kinase substrate p53 (IRSp53) in PSD of excitatory synapses, by yeast two-hybrid screening, GST pull down assays and immunoprecipitation assays. The interaction was mediated by the binding of the proline rich C-terminus of BRAG1 to regions of IRSP53 comprising the SH3 domain (Sanda et al. 2009). Transfected and endogenous BRAG1 has been shown to form, by immunoprecipitation experiments, a protein complex with RIBEYE (a major protein component of the synaptic ribbons (for review (Schmitz et al. 2000))), in synaptic ribbons in the mouse retina (Katsumata et al. 2009).

Using pull down assays with the C-terminus PDZ-binding motif of BRAG3, the synaptic localization of BRAG3 was confirmed by its interaction with PSD scaffold proteins such as PSD-95, SAP97 and Homer/VesII/PSD-Zip45 (Inaba et al. 2004). The same group showed by yeast two-hybrid and pull down assays, that BRAG3 interacts with the scaffolding

proteins utrophin/dystrophin and S-SCAM/MAGI-2 of inhibitory synapses (Fukaya et al. 2011).

All these findings strongly suggest a role of BRAG1 and 3 in neurons and specifically in the functioning of synapses. The role of BRAG2 in LTD (Scholz et al. 2010) also lead to the same conclusion.

4. Other functions

Overexpression of exogenous BRAG2 in monocytic phagocytes showed the induction of apoptosis, which was induced by the N-terminal region containing IQ motif and C-terminal region of BRAG2. This was shown by overexpression of different deletion mutants of BRAG2. So this suggested that the apoptotic function of BRAG2 was independent of its GEF activity (Someya et al. 2006).

Recently, a role of BRAG2 has been shown in Angiogenesis. Indeed, the group of Sabe showed in Human umbilical vein endothelial cells (HUVECs) that endogenous BRAG2 co-precipitates with VEGFR2 when cells were stimulated by VEGF (Vascular Endothelial Growth Factor). They showed as well that knockdown of BRAG2 in HUVECs by siRNA abolished the VEGF-induced activation of Arf6, suggesting that BRAG2 is primarily responsible for the VEGF-induced activation of Arf6 in HUVECs. They also showed that *in vitro*, the knockdown of BRAG2 and AMAP1 each significantly affected VEGF-induced tubular formation, one of the hallmark processes necessary for angiogenesis. They found as well by immunoprecipitation that cortactin forms a complex with AMAP1 in HUVECs and that this complex formation increased when cells were cultured with VEGF. All these experiments together suggest that BRAG2-Arf6-AMAP1-cortactin pathway is activated by VEGFR2 to promote angiogenesis (Hashimoto et al. 2011).

E. BRAGs and Pathologies

Up until now, BRAG2 has been reported to be involved in four types of cancer (breast cancer, lung adenocarcinoma, pancreatic cancer and possibly hepatic cancer). Indeed, recent studies showed that BRAG2 played an important role in tumor invasion. BRAG2 links EGF receptor signaling to Arf6 activation to induce breast cancer (Morishige et al. 2008) and lung cancer invasion (Menju et al. 2011). The group of Sabe has shown by Matrigel invasion assay and by invadopodia formation assay using siRNA of BRAG2, that BRAG2 was responsible for the invasive activities of breast cancer cell lines, where it has been found to be overexpressed by RT-PCR. They also showed by *in vitro* pull-down assays, that BRAG2

associates through its PH domain with two phosphotyrosines of EGFR (Epidermal Growth Factor Receptor) to activate Arf6 in breast cancer invasion (Morishige et al. 2008). The same group found that in the same way, that BRAG2 associates through its PH domain to two phosphotyrosines of Her2 receptor (Human Epidermal Growth Factor Receptor-2, a member of the EGFR-family). They also found an endogenous binding of BRAG2 with Her2 overexpressed in lung adenocarcinoma cells, by immunoprecipitation of cell lysates. They showed by Matrigel invasion assays coupled with immunoblotting that Arf6 and AMAP1 siRNAs were effective in suppressing these protein expressions and inhibited the matrigel invasion of lung cancer cells. They concluded that overexpressed Her2 activates Arf6 *via* its association with BRAG2, and induces lung cancer cell invasion (Menju et al. 2011). BRAG2 plays also a pivotal role in pancreatic cancer cell invasion. It has been shown that down-regulation of BRAG2 in a pancreatic cancer cell line significantly decreased invasive activity by Matrigel invasion assay *in vitro*. *In vivo* study showed that liver metastasis was significantly decreased in the pancreatic cancer cell line with BRAG2 stably knocked-down. Immunofluorescence study showed that expression of E-cadherin protein was increased by 2-3 folds accompanied by its redistribution to the cell-cell contacts. So they showed that down-regulation of BRAG2 causes increase in E-cadherin levels and inhibits the invasive abilities of pancreatic cancer cells (Xie et al. 2012). Recently, it has been shown that BRAG2, through the activation of Arf6, stimulate cell migration in human hepatoma HepG2 cells via ERK/Rac1 signaling stimulated by EGF (Hu et al. 2012). The authors showed that EGF dose-dependently stimulated the migration of human hepatoma cells HepG2 by wound closure assay. Additionally, EGF increased Arf6 activity in transfected cells by pull down assays, and ectopic expression of Arf6 T27N, a dominant negative Arf6 mutant, abolish EGF-induced cell migration by transwell migration assay. Blocking BRAG2 with BRAG2 siRNA or BRAG2-ΔPH, blocked EGF-induced Arf6 activity and cell migration. Ectopic expression of BRAG2 siRNA, BRAG2-ΔPH, or Arf6-T27N suppressed EGF-induced ERK and Rac1 activity, using pull down assay and cell migration assays. Taken together, this study highlights the function of the PH domain of BRAG2 and its regulated Arf6/ERK/Rac1 signaling cascade in EGF-induced hepatoma cell migration (Hu et al. 2012).

Recently, another pathology involving the BRAG family has been found. Indeed, mutations in the Sec7 domain of BRAG1 have recently been shown to cause non-syndromic X-linked intellectual disability (ID) in three families with this syndrome, which is characterized by substantial limitations in intellectual functioning and in the adaptive

behavior. This discovery was made possible by systematic and unbiased X chromosome exome resequencing. They also showed that these mutations significantly diminished GTP binding to Arf6 as compared to wild type, using GTP binding assay *in vitro* (Shoubridge et al. 2010).

All these observations suggest that BRAG2 could be considered as a new target for developing therapeutics to prevent cancer. Indeed, cancer is one of the most important causes of mortality in the world (OMS report 2012), so finding new targets to prevent cell invasion is a major public health issue.

OBJECTIVES

In this context, the objective of my thesis was to determine the substrate specificity of BRAG2, to characterize the structure and document its regulation by membranes and to characterize potential inhibitors of BRAG2, which could serve as precursor for future anti-cancer inhibitors. In order to give an explanation for the differences observed between the two isoforms Arf1 and Arf6, I also performed a structural analysis of Arf6. For that, we used molecular biology methods to clone different constructions of BRAG2 and to produce the mutants. The cloning of the constructions was performed by Kevin Contrepois and the mutagenesis was performed by the cloning platform of the laboratory (Véronique Henriot), except for the catalytic mutant, which I mutated myself. I used biochemical methods (chromatography, SEC-MALLS, complex reconstitution) to purify different constructions and mutant of BRAG2, as well as the complexes. SEC-MALLS experiments were done by Valérie Campanacci in the team. I also used structural methods (crystallization, crystallography, SAXS) to obtain the structure of Arf1/BRAG2^{E498K} complex and of the unfolded conformation of Arf6. Biophysical methods were used to characterize BRAG2 and Arf6 (CD, DLS), and study the regulation *in vitro* of BRAG2, (fluorescence spectroscopy). Molecular replacement with the software AMORE of Arf1/BRAG2^{E498K} complex was done by Jorge Navaza. Valérie Biou trained me in the techniques of crystallization and crystallography during my thesis. Flotation assays and membranes specificity fluorescence assays were done by Mahel Zeghouf. Cloning and purification of all the Arf constructs were performed by Bernard Guibert, Arnaud Guillien, Audrey Labarde and Lionel Duarte in the team.

RESULTS

Structure and regulation of BRAG2, an endosomal ArfGEF involved in tumour invasion (publication n°1)

Kaheina Aizel, Valérie Biou, Jorge Navaza, Valérie Campanacci, Jacqueline Cherfils and Mahel Zeghouf

Version préliminaire pour soumission en août 2012. ***Considérez comme confidentiel***

I. Résumé

BRAG2, un GEF reporté pour activer Arf6, possède plusieurs fonctions dans la cellule. Il joue un rôle dans la régulation de l'adhésion cellulaire, dans le remodelage du cytosquelette d'actine, dans la migration cellulaire, dans la fusion entre cellules, dans la régulation de l'architecture nucléolaire, dans la phagocytose, dans l'apoptose et dans l'angiogénèse. Si plusieurs groupes ont montré l'importance du domaine PH de BRAG2 dans ses fonctions, très peu d'études biochimiques et aucune donnée structurale ne sont disponibles à l'heure actuelle sur la régulation de BRAG2. De plus, son implication dans de nombreux cancers via l'activation d'Arf6 en fait une cible thérapeutique de choix.

Dans ce papier, nous combinons des études structurales, biochimiques et biophysiques pour étudier *in vitro* la spécificité de BRAG2 vis-à-vis de ses substrats, sa structure et ses mécanismes de régulation. Pour cela, nous avons utilisé différentes constructions de BRAG2 : $BRAG2^{Sec7}$ (domaine Sec7 isolé), $BRAG2^{Sec7\text{-}PH}$ (domaine Sec7 combiné au PH) et $BRAG2^{\Delta 30}$ (domaine Sec7 combiné au PH et sans les 30 derniers acides aminés) ainsi que le mutant $BRAG2^{E498K}$. Nous avons tout d'abord étudié la spécificité de BRAG2 vis-à-vis de Δ13Arf6 et Δ17Arf1 (mutants solubles dépourvus de leur hélice N-terminale) *in vitro* en solution et montré que $BRAG2^{Sec7\text{-}PH}$ est un GEF spécifique d'Arf1 et d'Arf6 avec une efficacité catalytique 5 fois supérieure pour Arf1 que pour Arf6. Pour tester la possible auto-inhibition de BRAG2 en solution, nous avons comparé l'activité d'échange de $BRAG2^{Sec7\text{-}PH}$ et de $BRAG2^{Sec7}$. A notre surprise, l'efficacité catalytique de $BRAG2^{Sec7\text{-}PH}$ obtenue avec Δ17Arf1 comme substrat était 10-fois supérieure à celle de $BRAG2^{Sec7}$. Ces résultats suggèrent fortement que $BRAG2^{Sec7\text{-}PH}$ n'est pas auto-inhibé en solution et suggère un mécanisme catalytique assisté par le domaine PH. Des essais en présence de membranes *in*

vitro ont révélé une efficacité catalytique pour BRAG2$^{Sec7\text{-}PH}$ 650 fois plus élevée que celle de BRAG2^{Sec7}, suggérant que le domaine PH aurait un rôle important dans la fixation aux membranes. Des expériences de flottaison sur membranes confirment cette hypothèse. De plus nous avons montré que l'activité de BRAG2$^{Sec7\text{-}PH}$ sur myrArf1 était plus importante sur des membranes chargées négativement, comprenant soit du PS ou du PIP_2 mais pas du PIP_3 ou du PIP_4. Pour comprendre le mécanisme moléculaire de la régulation de BRAG2, nous avons entrepris des études structurales de complexes Arf/BRAG2 et obtenu deux formes cristallines du complexe Δ17Arf1/BRAG2^{E498K} à 3.2 et 3.3 Å de résolution. Cette structure nous a révélé une conformation étendue de BRAG2, avec un domaine PH qui présente une structure similaire à celle d'autres domaines PH connus malgré une très faible identité de séquence, une région linker entre le domaine Sec7 et le domaine PH, qui interagit avec Arf1 et le domaine PH et la présence des éléments retrouvés dans les cytohésines auto-inhibées mais dans une orientation complètement différente. Nous avons également pu, grâce à cette structure, avoir une photo d'un nouvel intermédiaire de la réaction d'échange. Des expériences de SAXS ont montré que la conformation de BRAG2 dans le cristal est comparable à sa structure non liée à Arf en solution. Toutes ces expériences montrent donc que BRAG2 active à la fois Arf1 et Arf6, que cette activité est potentialisée par les membranes et que le domaine PH de BRAG2, outre son rôle essentiel dans la régulation par les membranes, pourrait participer à la catalyse de la réaction d'échange.

Structure and regulation of BRAG2, an endosomal ArfGEF involved in tumor invasion

Kaheina Aizel[1], Valérie Biou[1], Jorge Navaza[2,3], Valérie Campanacci[1], Jacqueline Cherfils[1 *] and Mahel Zeghouf[1*]

[1] Laboratoire d'Enzymologie et Biochimie Structurales, CNRS, Gif-sur-Yvette, France

[2] Institut de Biologie Structurale, CNRS/CEA/Université Joseph Fourier, Grenoble, France

[3] Unidad de Biofísica CSIC-UPV/EHU, Leioa, Bizkaia, Spain.

* Corresponding authors:

Jacqueline Cherfils, cherfils@lebs.cnrs-gif.fr

Mahel Zeghouf, zeghouf@lebs.cnrs-gif.fr

This is a preliminary version of the article that will be submitted by the end of October 2012. ***Please consider confidential***

Abstract

Small GTPases of the Arf family are pivotal regulators of membrane traffic in eukaryotes. They are activated by several families of guanine nucleotide exchange factors (ArfGEFs), which play a key role in processing upstream regulatory signals that lead to Arf activation onto specific subcellular compartments. However, the mechanisms by which ArfGEFs coordinate nucleotide exchange to membrane targeting remain poorly understood. Here we used X-ray crystallography and reconstitution of nucleotide exchange on artificial membranes to analyze these mechanisms for human BRAG2/GEP100, a member of the BRAG/IQSEC family of ArfGEFs involved in receptor endocytosis and associated with tumor invasion in various cancer cells. Members of this family have been described as Arf6-specific GEFs, and carry a PH-like domain downstream their Sec7 domain. We find that BRAG2 has in fact a dual specificity for Arf1 and Arf6 similar to ArfGEFs of the cytohesin family, but, unlike cytohesins, it is not intrinsically auto-inhibited nor regulated by a feedback loop. However, its exchange activity is potentiated by membranes that contain phosphatidylserine (PS) or PI(4,5)P_2, and is inhibited by neutral membranes or by the presence of PI(3)P or PI(4)P. The crystal structure of Arf1 in complex with the Sec7/linker/PH–like domains of BRAG2 reveals an unprecedented close-packed interface between these domains, which explains the synergy between nucleotide exchange by the Sec7 domain and membrane recruitment by the linker/PH-like tandem. These data are consistent with a restriction of BRAG ArfGEfs localization and activity to PS-enriched and PIP2-containing membranes, where it can activates both Arf1 and Arf6 in early endosomal pathways.

Introduction

Small GTPases of the Arf family are major regulators of most aspects of vesicular traffic (reviewed in (D'Souza-Schorey and Chavrier 2006)). Arf1, the most abundant isoform, has many roles in vesicular maturation and transport, notably the assembly of COP1 and clathrin coats at the Golgi, the recruitment of membrane-modifying enzymes and the targeting of vesicular carriers. The functions of Arf6 are more restricted to the cell periphery, where it coordinates membrane traffic and actin dynamics. Arf1 was long thought to have non-overlapping localization with Arf6, until recent studies showed that it is activated at the plasma membrane (Cohen et al. 2007), possibly in an exquisitely regulated cascade with Arf6 (DiNitto et al. 2007; Stalder et al. 2011). The many roles of Arf1 and Arf6 are orchestrated by their guanine nucleotide exchange factors (ArfGEFs). There are 5 major families of ArfGEFs in higher eukaryotes, which share a highly conserved catalytic Sec7 domain that stimulates GDP/GTP nucleotide exchange. ArfGEFs have a more narrow subcellular localization than their Arf substrates, suggesting that they determine on which endomembranes Arf proteins are activated and possibly which effectors they recruit. However, the underlying molecular mechanisms remain poorly characterized.

The BRAG group (also called IQSEC), which is present only in higher organisms, is one of the least characterized ArfGEF group. Members of this family carry a conserved region in N-terminus with a motif resembling a calmodulin-binding IQ signature, and a Sec7 nucleotide exchange domain followed by a domain with remote relationship with pleckstrin homology (PH) domains in their C-terminus (reviewed in (Casanova 2007)). They are considered Arf6-specific GEFs based on *in vitro* nucleotide exchange assays (Someya et al. 2001) and cellular transfection and depletion assays (Dunphy et al. 2006) (Sakurai et al. 2011) (Morishige et al. 2008). A general function of BRAG proteins is currently emerging in the regulation of receptor endocytosis. BRAG2 (also called GEP100), the most studied of the three human members, promotes the endocytosis of β1 integrins in HeLa (Dunphy et al. 2006) and endothelial (Sakurai et al. 2011) cells and of the AMPA receptor endocytosis in neurons (Scholz et al. 2010), while its depletion results in increased E-cadherin expression at the cell surface, possibly in relationship with internalization defects (Xie et al. 2012). In neurons, BRAG2-mediated AMPA receptor endocytosis required a direct interaction with a non-phosphorylated peptide of the receptor, which weakly stimulated Arf6 nucleotide exchange *in vitro* (Scholz et al. 2010). Direct interactions between the PH-like domain of BRAG2 and phosphorylated

tyrosines of epidermal growth factor receptors (EGFR) were also described, which resulted in Arf6 activation in cells (Morishige et al. 2008; Menju et al. 2011). Overexpression of BRAG2 was associated with detrimental invasion phenotypes in breast cancer tumors (Morishige et al. 2008) and in primary lung adenocarcinomas (Menju et al. 2011), while its depletion in human pancreatic cancer cell lines decreased invasive phenotypes (Xie et al. 2012). Other roles of BRAG ArfGEFs have been related to myoblast fusion, an important process in muscle formation, first shown in the insect homolog Schizo/Loner where it required the GEF activity and the PH-like region (Chen et al. 2003). This effect may be related to the regulation of N-cadherin endocytosis to induce a protein-free fusion zone (Dottermusch-Heidel et al. 2012).

Accumulating evidence indicates that ArfGEFs establish an intimate partnership with membranes. Membranes play an active role in regulating the core nucleotide exchange reaction (Pasqualato et al. 2002; Renault et al. 2003), and were recently shown to relieve auto-inhibition of the cytohesins family by their PH domain (DiNitto et al. 2007; Stalder et al. 2011). Although BRAG2 was initially proposed to be insensitive to phosphoinositides (Someya et al. 2001), a link between BRAG2, Arf6 and $PI(4,5)P_2$ (PIP2 hereafter) was recently established. BRAG2 bound to $PI(4,5)P_2$–containing liposomes, which increased $[^{35}S]GTP\gamma S$ loading onto Arf6 as assessed by single time point measurements (Sakurai et al. 2011). Consistently, Arf6-mediated attachment to the extracellular matrix and migration was reduced upon depletion of PIP5 kinase (Sakurai et al. 2011). A stimulating effect of PIP2 on BRAG2 exchange activity towards Arf1 was also shown recently, which was dependent on the presence of the PH-like domain (Jian et al. 2012).

In this work, we combined X-ray crystallography with carefully reconstituted nucleotide exchange activity on artificial membranes to investigate the GTPase and membrane specificity of human BRAG2, and the coordination between its recruitment to membranes and its nucleotide exchange efficiency. This allowed us to revisit the specificity of BRAG2 toward the two major Arf isoforms and to propose a simple model for the localization and regulation of BRAG2 on membranes of the early endosomal pathway.

Results

BRAG2 is an efficient exchange factor for Arf1 and Arf6

In order to establish the specificity of human BRAG2 *in vitro*, we expressed the Sec7 domain alone (residues 390-594, numbering according to short isoform also called BRAG2a (Dunphy et al. 2006), BRAG2^{Sec7} hereafter) and constructs comprising the Sec7, PH-like and predicted coiled-coil domains without (residues 390-763, BRAG2$^{Sec7\text{-}PH}$) or with (residues 390-811, BRAG2$^{\Delta 30}$) the proximal residues, the latter construct lacking only the 30 last residues. All proteins were purified to homogeneity to ensure accurate enzymatic analysis (**Figure 1A**). The exchange activity of BRAG2 was monitored by tryptophan fluorescence kinetics, using Arf constructs truncated of their N-terminus helix, which allows to by-pass their requirement for membranes to be fully activated (reviewed in (Pasqualato et al. 2004)). Both Δ17Arf1 (**Figure 2A**) and Δ13Arf6 (**Figure 2B**) were efficiently activated, and had k_{cat}/K_m in the same range (respectively 0.2 x 10^5 $M^{-1}s^{-1}$ and 0.1 x 10^5 $M^{-1}s^{-1}$, **Table 1**). To confirm that BRAG2 is able to use Arf1 as a substrate, we analyzed whether Arf1 could form exchange intermediates with BRAG2$^{Sec7\text{-}PH}$. We either used a BRAG2 mutant in which the catalytic glutamate is replaced by a lysine (BRAG2$^{Sec7\text{-}PH/E498K}$), which allows to trap an early Arf-GDP-ArfGEF intermediate (Beraud-Dufour et al. 1998; Renault et al. 2003), or removed the nucleotide to form the nucleotide-free Arf/ArfGEF intermediate (Goldberg 1998). As shown in **Figures 1B** and **1C**, both complexes were readily formed. It should be noted that we could not reconstitute the equivalent complexes with Arf6 under these conditions, for which we have no ready explanation. These data suggest that Arf1 and Arf6 are equally good substrates for BRAG2, although possibly with mechanistic differences in the detail.

The crystal structure of the Arf1-BRAG2$^{Sec7\text{-}PH}$ complex uncovers a novel role for the PH domain

The ability to reconstitute nucleotide exchange intermediates with Arf1 allowed us to solve the crystal structure of BRAG2$^{Sec7\text{-}PH}$ carrying the E498K mutation in complex with Δ17Arf1-GDP (**Figure 3A**, **Table 2**). Taken individually, the Sec7 and PH-like domain resemble previously described Sec7 domains (Cherfils et al. 1998; Goldberg 1998; Renault et al. 2003) and PH domains of known structures (reviewed in (Lemmon

2008)). Notably, the PH-like domain has the classical PH domain fold despite its remote sequence relationship and will be referred to as BRAG2^{PH} hereafter (**Figure 3B**). The linker that bridges the Sec7 and PH domain forms a small domain, which interacts with both domains, rather than forms an unstructured tether. It packs against β-strands β1, β2 and β3 of the PH domain and stabilizes an ordered conformation of loop β3-β4. Remarkably, residues that form the interface between the linker and PH domains are among the most conserved in this region (**Figures 3C and S1**). Members of the BRAG2/IQSEC1 group feature extra residues in the linker (**Figure S1**), which are disordered in our structures (**Figure 3A**). The PH domain interacts with the N-terminus of the Sec7 domain by its C-terminal helix, and does not impinge on the Arf-binding site. The helix and elements immediately downstream were predicted to form a coiled-coil (Dunphy et al. 2006). We do not observed dimerization in the crystal, and the monomeric structure of BRAG2 was confirmed in solution by SEC-MALS and gel filtration analysis (**Figure 1B**).

The Sec7 and PH domains have a relative position that is completely different from that seen in auto-inhibited cytohesins ((DiNitto et al. 2007), **Figure 3D**), which allows Arf to bind to the Sec7 active site. Arf1-GDP recapitulates the interactions with the Sec7 domain previously seen in the ARNO$^{Sec7\text{-}E156K}$/Arf1-GDP complex (Renault et al. 2003). Notably, the central β-strands (the interswitch) have undergone the two-residue shift that primes Arf-GDP for nucleotide dissociation and binding of GTP. The position of Arf1 relative to the Sec7 domain is midway between those in ARNO^{E156K}/Arf1-GDP (Renault et al. 2003) and in nucleotide-free Arf1/Gea2 (Goldberg 1998), suggesting that it is slightly more advanced towards nucleotide dissociation (**Figure S2**). The linker domain is located in the immediate vicinity of the switch 1 region of Arf-GDP, although whether direct interactions are formed cannot be sorted out because the linker appears partially disordered at the resolution of our structures.

These edge contacts are reminiscent of those between Rho GTPases and the PH domains of DBS and related DH-PH containing RhoGEFs (**Figure 3D**), which suffice to assist in the exchange reaction (Rossman et al. 2002). In order to investigate whether the PH domain of BRAG2 has a similar role, we compared the nucleotide exchange efficiencies of BRAG2^{Sec7} and BRAG2$^{Sec7\text{-}PH}$ towards Δ17Arf1 and Δ13Arf6. BRAG2$^{Sec7\text{-}PH}$ was more active than BRAG2^{Sec7} by one order of magnitude towards Δ17Arf1 (**Figure 2A, Table 1**), and 4-fold more active towards Δ13Arf6 (**Figure 2B, Table 1**), in agreement with a contribution of the PH domain in the exchange reaction. Finally, we analyzed the small-angle X-ray scattering (SAXS) curve of unbound BRAG2 in order to analyze whether it undergoes a conformational change to reach the structure seen in the crystal. The SAXS

curve calculated from the structure of BRAG2 $^{Sec7\text{-}PH}$ extracted from the crystalline complex agreed well with the experimental SAXS curve of unbound BRAG2 in solution (**Figure S3**), consistent with the observation that its exchange activity is not auto-inhibited. Altogether, these results suggest that the PH-like domain of BRAG2 is not auto-inhibitory and may assist in the exchange reaction.

Membranes potentiate BRAG2 efficiency.

Since BRAG2$^{Sec7\text{-}PH}$ is an efficient ArfGEF in solution, this raised the question of whether membranes further affect its catalytic efficiency. We measured the catalytic efficiency of BRAG2$^{Sec7\text{-}PH}$ towards myristoylated Arf proteins in the presence of liposomes that mimic the plasma membrane (PM-like liposomes). The exchange efficiency towards ^{myr}Arf1 was 390 x 10^5 $M^{-1}s^{-1}$, corresponding to an increase of more than 2 orders of magnitude compared to its efficiency towards Δ17Arf1 in solution (**Figure 2C, Table 1**). The contribution of the PH domain was critical, as the exchange efficiency of BRAG2^{Sec7} remained in the same range regardless of the presence of liposomes (**Table 1**). BRAG2$^{Sec7\text{-}PH}$ also strongly activated ^{myr}Arf6, although with unusual kinetics whether using tryptophan fluorescence, which measures Arf conformational change upon nucleotide exchange (**Figure 2D, Figure S4A**) or mantGTP fluorescence (data not shown), which measures nucleotide exchange directly. This behavior has been seen with other Arf6-GEFs ((Macia et al. 2001), our unpublished results), but was not observed with BRAG2^{Sec7} in the presence of liposomes or with BRAG2$^{Sec7–PH}$ in solution (data not shown), and was not due to undesirable liposome aggregation (**Figure S4B**). It was also independent of the concentration of ^{myr}Arf6 used in the assay, thus ruling out a saturation effect (data not shown). We surmise that it is due to the fact that a significant fraction of ^{myr}Arf6-GDP is bound to membranes ((Macia et al. 2004), our unpublished data) where it undergoes fast activation, unlike ^{myr}Arf1-GDP, which does not bind to liposomes, whatever their composition (**Figure S5**). Analysis of kinetics curves by single exponential fit was however precluded, and was done instead from initial velocities. Vi values were linear as a function of BRAG2 concentration and were in the same range as those found for Arf1 (**Figure S4C)**, suggesting that membranes also potentiate the efficiency of BRAG2 towards Arf6**.**

Several membrane-located GEFs, including the plasma membrane ArfGEFs cytohesins (Stalder et al. 2011) and Golgi ArfGEF BIG (Richardson et al. 2012) have been described to undergo a positive regulatory feedback loop on membranes mediated by freshly produced Arf-GTP. Such loops can be highlighted by an increase of the exchange rates as

membranes are pre-loaded with increasing amounts of active ^{myr}Arf-GTP. Alternatively, a decrease in the exchange rate could indicate a negative feedback loop. The exchange rates towards ^{myr}Arf1 were unaffected when increasing amounts of ^{myr}Arf6-GTP were pre-loaded on membranes, thus ruling out both feedback effects (**Figure 4**). We conclude that membranes potentiate the exchange efficiency of BRAG2 for both Arf1 and Arf6, and that this depends on the atypical PH domain but does not involve a feedback loop.

Brag2 exchange activity is regulated by its interaction with negatively charged lipids.

The structure shows that BRAG2^{PH} features the classical pocket located at the bottom of the β-sandwich, which binds phosphoinositides in other PH domains, and that the pocket is surrounded by numerous positively charged residues contributed by flanking loops (**Figures 3B and S6**). Besides, the pocket is located on the same side as the myristoylated N-terminus of Arf, such that both could interact with membranes in tandem. However, BRAG2^{PH} lacks one of the most conserved PH domain residue, a lysine located at the bottom of the pocket which interacts with a phosphate of the lipid head group in all known structures, which is replaced by a glutamate in all BRAG members (Glu 639 in BRAG2) (**Figure 3B and S6**). As this strategic negative charge may compromise the ability of BRAG2 to recognize negatively charged membranes, we analyzed the recruitment of BRAG2$^{Sec7\text{-}PH}$ to liposomes of various compositions using a flotation assay. This assay was preferred over liposome sedimentation for its ability to accurately separate liposome-bound proteins from aggregated proteins. BRAG2$^{Sec7\text{-}PH}$ did not bind to liposomes devoid of negative charges (**Figure 5A, lane 1**). It partially bound to liposomes that contained 30 % phosphatidylserine (**Figure 5A, lane 2**) or 2% PIP_2 (**Figure 5A, lane 3**), while near complete binding was achieved when both PS and PIP_2 were present **(Figure 5A, lane 4**). BRAG2$^{Sec7\text{-}PH}$ was also recruited to liposomes PM-like liposomes, which contain cholesterol in addition to PS and PIP_2 so as to more closely mimic the composition of the plasma membrane **(Figure 5A, lane 5**). BRAG2^{Sec7} was unable to bind these liposomes, indicating that recruitment was dependent on the PH domain (**Figure 5B**).

Next, we analyzed the dependency of BRAG2 exchange efficiency on the lipid composition under fixed protein conditions (**Figures 5C and S7**). The activity of BRAG2$^{Sec7\text{-}PH}$ towards ^{myr}Arf1 in the presence of neutral liposomes was weak and similar to that of BRAG2^{Sec7}, consistent with its negligible binding in the flotation experiments. Liposomes containing 30% PS, 2% PIP_2 or both with or without cholesterol, strongly

stimulated nucleotide exchange. In contrast, liposomes containing 2% PI(3)P or PI(4)P were inefficient at stimulating BRAG2. We noticed a decrease of the fluorescence plateau when PIP_2 was added in the presence of low to moderate amounts of PS, for which have no ready explanation (**Figure S7**). We conclude that the PH domain of BRAG2 recognizes both PIP_2 and PS, and is activated by these phospholipids alone or in combination, in a way that excludes PI(3)P and PI(4)P. *We are currently completing the analysis of mutations of the atypical glutamate in the PH domain to assess its role in the observed lipid specificity pattern.*

Discussion

Understanding the molecular mechanisms by which GEFs are regulated has become a major issue in small GTPases biology (reviewed in (Bos et al. 2007)). Recent studies highlighted regulation by auto-inhibition and membrane recruitment provided by domains associated in tandem with the exchange domains (DiNitto et al. 2007; Gureasko et al. 2010), and by feedback loops (Margarit et al. 2003; Stalder et al. 2011; Richardson et al. 2012). In this study, we analyzed the structure and regulatory mechanisms of BRAG2, previously described as an Arf6-specific GEF, which is involved in endocytotic pathways and associated with tumor invasion.

We found that BRAG2 is in fact a dual specificity GEF, which is equally active on Arf1 and Arf6 *in vitro*. Its exchange efficiency towards both Arf isoforms was similar to that of cytohesins, which are themselves among the most active ArfGEFs (Zeeh et al. 2006). Earlier *in vitro* studies using Arf1 did not meet the requirements for efficient exchange, explaining why this dual specificity escaped prior identification and was subsequently not investigated in cells. A dual specificity for Arf1 and Arf6 was previously observed *in vitro* for cytohesins ArfGEFs (Chardin et al. 1996), and was reconciled with functional models only recently with the observation that Arf1 was not excluded from the plasma membrane and had an active role in coordination with Arf6 (Cohen et al. 2007), possibly as part of an intricate feedback loop (Stalder et al. 2011). The strong activity of BRAG2 towards Arf1 and Arf6 *in vitro* suggests that both isoforms may play a role in BRAG2 functions in the endocytosis pathway. This may explain earlier observation that depletion of BRAG2 impaired endocytosis of β1 integrins, whereas depletion of Arf6 lead to intracellular accumulation of β1 integrins (Dunphy et al. 2006). Our crystal structure of the Arf1/BRAG2 complex and the availability of Arf and ArfGEF-specific chemical inhibitors (Viaud et al. 2007; Boal et al. 2010), our unpublished results) should be valuable for documenting these issues in cells.

Auto-inhibition is currently emerging as a general regulatory mechanism of GEFs (reviewed in (Bos et al. 2007)). In cytohesins, the PH domain located immediately in C-terminus of the Sec7 domain is auto-inhibitory by blocking access to the Arf-binding site (DiNitto et al. 2007), and is also necessary for full activation by recognizing specific phosphoinositides (Cronin et al. 2004) and supporting a positive feedback loop (Stalder et al. 2011). Our kinetics and structural analysis show that BRAG2, despite a similar domain organization, has a completely different regulatory mechanism. Its PH domain is not auto-inhibitory, but associates with a small liaison domain to slightly assist in the exchange reaction in the absence of membranes. Its nucleotide exchange efficiency is strongly potentiated by membranes that contain PIP_2 and/or PS but not by membranes that contain only neutral lipids, which correlates with its ability to bind to these membranes *in vitro*. This ensemble of data suggests that membranes activate BRAG2 mostly by accretion of Arf and BRAG. The difference between cytohesins and BRAGs is further emphasized by our crystal structure of an exchange intermediate containing Arf1-GDP and BRAG2$^{Sec7\text{-}PH}$, which reveals that the PH domain of BRAG2 packs onto the N-terminus of the Sec7 domain. The same surface in the Sec7 domain was previously involved in auto-inhibition of the bacterial ArfGEF RalF by its capping domain (Amor et al. 2005), and mutations in this region in large Golgi ArfGEFs in plants resulted in impaired functions, suggesting that it may serve a general role as a scaffold for various regulatory interactions. SAXS analysis of unbound BRAG2 in solution is consistent, although not discriminative, with the structure seen in the complex, suggesting that BRAG2$^{Sec7\text{-}PH}$ probably does not require a major conformational change to activate Arf protein on membranes.

How similar the active form of cytohesins is to the structure of BRAG2 in the complex remains to be established. The PH domains of BRAG2 and GRP1 feature an unusually long C-terminal helix, which is straight and interacts with the N-terminus of the Sec7 domain in BRAG2, and is kinked and auto-inhibitory in GRP1 (**Figure 3C**). The kinked helix of GRP1 could not form the proper interface with the N-terminus of the Sec7 domain, nor could the straight helix in BRAG2 be accommodated into the Sec7 active site. The kink occurs near a proline residue in cytohesins (Pro383 in GRP1), which is not present in BRAG ArfGEFs and possibly favors a regulatory alternation between a kinked, autoinhibitory and a straight, active conformation. BRAGs and cytohesins also differ by their Sec7-PH linker region, which is very short in ARNO while it forms a small domain that interacts with the Sec7 and PH domains in the vicinity of the Arf GTPase in BRAG2. Residues of the PH domain of cytohesins that are involved in the positive feedback loop (Stalder et al. 2011) or are in contact with Arl4-GTP (Hofmann et al. 2007) or Arf6-GTP

(Cohen et al. 2007) (I303, Y290), correspond to residues of BRAG2^{PH} (S683, V664) that are shielded by this linker and are thus unavailable for other interactions. Thus, it cannot be excluded that active cytohesins have a different conformation that allows them to bind to Arf-GTP.

Our data establish that the PH domain of BRAG2 has a remarkable pattern of recognition of PIP_2 and PS which excludes PI(3)P and PI(4)P. Phosphatidylserine, which constitutes the predominant anionic lipid at the plasma membrane in association with a minor fraction of PIP_2 and PIP_3, was recently shown to be also a major lipid enriched in endosomal membranes, where it contributes to target or maintain proteins (Yeung et al. 2008). In contrast, PI(3)P and PI(4)P are preferentially found on late endosomes and at the Golgi, respectively, where PIP_2 and PIP_3 are absent and PS is little abundant (van Meer et al. 2008). Thus, the PH domain of BRAG2 may drive it to the plasma membrane and retain it on early endosomal membranes, while excluding its interaction with Golgi and late endosomal membranes. This would be consistent with its function in the endocytosis of receptors, and its localization as observed in transfection assays. This pattern of membrane preference could also allow BRAG2 to switch substrates from Arf6 to Arf1 as it proceeds along the early endocytic pathways.

Structural recognition of lipids by PH domains has mostly been described for analogs of PIP_2 and PIP_3, with the recent exception of phosphatidylserine-binding evectin-2 in complex with phosphoserine (Uchida et al. 2011). Although the lipid-binding site has the same location in all structures, there is considerable variability in the residues that recognize the phosphates (**Figure S7**), except for an invariant lysine located on strand β1 (**Figures 3B and S7**). Mutation of this residue to alanine in cytohesins (K268A) completely abolished its exchange activity (Stalder et al. 2011). In all members of the BRAG group, this residue is replaced by a glutamate, which should repel phosphates negative charge. *We are currently investigating mutants of this residue into Ala and Lys to determine whether it recognizes PS or has another role.* It should also be noted that the β3-β4 loop, which carries several conserved lysines, is stabilized away from the classical phospholipid-binding site by the linker domain, which may allow the PH domain to probe a larger surface of endosomal membranes for the presence of negatively charged lipids.

In conclusion, we propose a model in which BRAG2 is a dual specificity ArfGEF, which, unlike cytohesins, is not auto-inhibited by its PH domain nor is under a feedback regulatory mechanism, probably because its PH domain is firmly positioned by the liaison domain between the Sec7 and PH domains. Instead, its activity is strongly

enhanced by its recruitment to membranes carrying PIP_2 or PS lipids, an effect that seems to depend mostly on the accretion of the GEF and its Arf substrate. The role of the N-terminal part, and whether it adds another level of regulation, remains to be established.

Materials and methods

Protein expression and purification.

PCR products encoding residues 390-594 of human BRAG2 (BRAG2^{Sec7}), residues 390-763 (BRAG2$^{Sec7\text{-}PH}$) and residues 390-811 (BRAG2$^{\Delta 30}$) were cloned between the *Eco*RI and *Hind*III sites into the pProEX-HTb vector (Invitrogen) as a fusion with a N-terminal 6-His tag followed by a tobacco etch virus (TEV) protease cleavage site. The BRAG2$^{Sec7\text{-}PH/E498K}$ mutant was generated with BRAG2$^{Sec7\text{-}PH}$ as a matrix using the QuikChange II XL kit (Stratagene). All constructs were confirmed by sequencing. BRAG2 constructs were expressed in *E. coli* BL21 Gold strain at 37˚C with 3h of induction with IPTG (0.5 mM). Seleno-methionine (SeMet)-incorporated BRAG2$^{Sec7\text{-}PH/E498K}$ was expressed in *E. coli* BL21 Gold strain grown at 37°C in L-SeMet-enriched media as described in (Doublie 1997). Cells were disrupted by sonication in buffer A (20 mM phosphate buffer pH7.4, 10 mM imidazole, 500 mM NaCl and 5 mM β-mercaptoethanol) completed with 0.5 mg/ml of lysozyme and a protease inhibitor cocktail (1 mg/ml aprotinin, leupeptin, pepstatin, antipain, and 1 mM Pefabloc and benzamidine). Lysates were cleared by centrifugation at 110,000 x *g* for 1h then purified by nickel-nitrilotriacetic acid (Ni-NTA) affinity chromatography (HisTrap FF, GE Healthcare) equilibrated with buffer A. After elution with a 10-500 mM linear imidazole gradient, BRAG2-containing fractions were desalted and, when indicated, subjected to TEV protease cleavage (1:10 w/w) overnight at 4˚C and reloaded on a HisTrap column. For BRAG2$^{Sec7\text{-}PH/E498K}$, an additional step of ion exchange chromatography was performed on a MonoS column (GE Healthcare). Purification of all BRAG2 constructs was polished by gel filtration on a Superdex 75 XK 16/90 (GE Healthcare) equilibrated with 20 mM HEPES pH 7.4, 5 mM β-mercaptoethanol and 100-500 mM NaCl. All Arf constructs are a gift from M. Franco and B. Antonny (CNRS, Sophia-Antipolis, France). Human Δ17Arf1 and Δ13Arf6 were expressed and purified as described in (Beraud-Dufour et al. 1998) and (Chavrier and Franco 2001), and loaded with GDP prior to kinetics experiments. Nucleotide content was assessed by thermal denaturation followed by ion exchange chromatography. Myristoylation of full-length Arf1 was done by co-expression with yeast N-myristoyl transferase and purified by ammonium sulfate precipitation, DEAE and MonoS ion

exchange chromatographies as described in (Franco et al. 1995). Myristoylation of full-length Arf6 carrying a C-terminal 6-His tag was done by *in vitro* myristoylation with recombinant human N-myristoyltransferase (our unpublished results).

Preparation of Arf1/BRAG2 complexes

The complex between Δ17Arf1-GDP and BRAG2$^{Sec7\text{-}PH/E498K}$ was prepared by incubation (2:1 ratio) for 10 min at room temperature in 20 mM HEPES pH 7.4, 100 mM NaCl, 1 mM $MgCl_2$, 5 mM β-mercaptoethanol and 2 mM EDTA. The nucleotide-free complex was obtained by incubating Δ17Arf1-GDP and BRAG2$^{Sec7\text{-}PH}$ (2:1 ratio) with 1U/mg of alkaline phosphatase (Sigma) in 20 mM HEPES pH 7.4, 150 mM NaCl, 4 mM β-mercaptoethanol overnight at 4˚C. Both complexes were purified by size exclusion chromatography at 4˚C on a Superdex75 10/300 column (GE Healthcare) equilibrated with the corresponding incubation buffer, containing 5 mM EDTA for the nucleotide-free complex. The BRAG2$^{Sec7\text{-}PH/E498K}$/Δ17Arf1-GDP complex was concentrated to a maximum of 1.3-1.7 mg/ml for crystallization. The oligomerization state and size of BRAG2$^{Sec7\text{-}PH/E498K}$, Δ17Arf1-GDP and the BRAG2$^{Sec7\text{-}PH/E498K}$/Δ17Arf1-GDP complex were analyzed by MALS/QELS/RI coupled on-line with an analytical SEC column, as described in (Biou et al. 2010) in a buffer containing 20 mM Hepes pH 7.4, 150 mM NaCl and either 30 μM BRAG2$^{Sec7\text{-}PH/E498K}$, 30 μM Δ17Arf1 or 20 μM BRAG2$^{Sec7\text{-}PH/E498K}$/Δ17Arf1-GDP complex.

Liposome preparation and flotation assay.

Soya phosphatidylcholine (PC), liver phosphatidylethanolamine (PE), brain phosphatidylserine (PS), ovine wool cholesterol, brain phosphatidylinositol-4,5-bisphosphate (PIP_2), brain phosphatidylinositol-4-phosphate (PI(4)P) and 18:1 phosphatidylinositol-3-phosphate (PI(3)P) were from Aventi Polar Lipids, NBD-PE was from Invitrogen. Liposomes were prepared as described (Stalder et al. 2011) in 50 mM HEPES pH7.4, 120 mM potassium acetate buffer and freshly extruded through a 0.2 μm filter (Whatman). Flotation assay was performed as described in (Bigay et al. 2005). Briefly, 1μM of protein was incubated with liposomes (1 mM total lipids) for 5 min at room temperature in 50 mM HEPES pH7.4 buffer containing 120 mM potassium acetate, 1 mM $MgCl_2$ and 1 mM DTT (HKM buffer). The solution was brought to 30% sucrose, overlaid with two layers of HKM containing 25% and no sucrose then submitted to centrifugation at 240 000 *g* in a TLS55 swing rotor (Beckman) for 1h at 20˚C. Liposome-bound proteins (top fraction) and unbound proteins (bottom fraction) were collected manually and analyzed by SDS-PAGE after SYPRO Orange (Invitrogen) staining using a Fuji LAS-3000 fluorescence imaging system.

Nucleotide exchange assay

Nucleotide exchange kinetics were monitored by tryptophan fluorescence with excitation and emission wavelengths of 292 nm and 340 nm on a Cary Eclipse fluorimeter (Varian) equipped with a stirring instrument. All experiments were carried out at 37°C by the successive addition of Arf, BRAG2 and finally 100 µM GTP to initiate nucleotide exchange. Exchange assays without liposomes were performed in 50 mM HEPES pH 7.4, 50 mM NaCl, 2 mM $MgCl_2$, 2 mM β-mercaptoethanol, using 1 µM Arf and BRAG2 constructs (0-0.4 µM range) for k_{cat}/K_m determinations. Exchange assays with liposomes were done with 100 µM pre-warmed liposomes in 50 mM HEPES pH 7.4, 120 mM potassium acetate, 1 mM $MgCl_2$, 1 mM DTT with 0.4 µM ^{myr}Arf and BRAG2 constructs (0-1 nM range) for k_{cat}/K_m determinations, or a fixed concentration of 1 nM for k_{app} determination. Except for ^{myr}Arf6 activation, which was analyzed using initial velocities (see results), pseudo-first order reaction rate constants (k_{app}) were determined from a monoexponential fit taking into account the linear drift of fluorescence due to photobleaching. Catalytic efficiencies were obtained as described in (Beraud-Dufour et al. 1998) from

$$k_{app} = \left(\frac{k_{cat}}{K_m}\right)[GEF] + k_{spont}$$

where k_{spont} is the spontaneous nucleotide exchange rate constant.

Feedback loop experiment.

Increasing amounts of ^{myr}Arf6 previously loaded with GTP (0, 0.2, 0.4, 0.9 and 1.5 µM) were pre-loaded at the surface of PM-like liposomes (150 µM), before 1nM BRAG2$^{\Delta 30}$, 100 µM GTP and 0.4 µM ^{myr}Arf1-GDP were added in sequence. The apparent activation rate constant of ^{myr}Arf1 (k_{app}) was determined by fitting the fluorescence change to a single exponential.

Crystallization and data collection

Crystals of the Δ17Arf1-GDP/BRAG2$^{Sec7\text{-}PH/E498K}$ complex were obtained with either Se-Met derived BRAG2 from which the 6-His tag had been removed, or from native BRAG2 carrying the tag, which yielded crystals belonging to P2 and C2 groups, respectively. Small crystals obtained under several conditions of the crystallization screens were optimized in hanging drops containing 0.15 M ammonium sulfate, 0.1 M

NaH_2PO_4/Na_2HPO_4 pH 6, and 13% PEG 4000 for the native complex, and in 0.15 M ammonium sulfate, 0.1 M MES pH 6 and 16% PEG 4000 for the SeMet-substituted complex. Crystals were transferred to a cryoprotectant solution containing the reservoir solution adjusted at 17% PEG 4000 plus 20% PEG 400 and flash frozen in liquid nitrogen. Diffraction data were collected at beamline PROXIMA1 (SOLEIL Synchrotron, Gif-sur-Yvette, France) at 0.98 Å for the native crystals, and at the f ' maximum and f " minimum of the selenium edge and at a high energy remote wavelength (0.98 Å) for the Se-Met crystals. The native crystals belong to space group C2, with a = 90.98 Å, b = 65.78 Å, c = 196.86 Å, α=90°, β=108.19°, γ=90° and contain 2 complexes related by non-crystallographic translation in the asymmetric unit. The Se-Met-substituted crystal belong to space group P2 with a = 210.7 Å, b = 66.2 Å, c = 91 Å, α=90°, β=96,13°, γ=90° and contain 4 complexes related by non-crystallographic translations in the asymmetric unit. Intensities were integrated and scaled with the program XDS (Kabsch 2010) for the P2 crystal and integrated with imosflm and scaled with scala for the C2 crystal.

Structure determination and refinement

Selenium sites were searched with ShelXD (Sheldrick 2010) but did not allow SAD phasing. The structure of the C2 crystal was solved by molecular replacement with the program AMORE (Trapani and Navaza 2008), using Δ17Arf1-GDP from the Δ17Arf1-GDP/ARNO complex (PDB entry 1R8S, (Renault et al. 2003)), the Sec7 domain from the Δ17Arf1-GDP/ARNO (PDB entry 1R8S) from which sequence differences were modeled as alanines, and $BRAG2^{PH}$ (unpublished PDB entry 3QWM) as search models. The solution was found using translational NCS with data between 15 and 4.5 Å. The similar strategy using NCS and data between 45 and 3.5 Å was used to solve the P2 form, in which one of the four Δ17Arf1-GDP molecules was subsequently repositioned with Phaser (McCoy et al. 2007). Refinement was carried out with the programs Phenix (Adams et al. 2010) and autoBUSTER (Blanc et al. 2004), alternatively with graphical building using Coot (Emsley et al. 2010). Crystallographic statistics are given in **Table 2**. Coordinates will be deposited with the Protein Data Bank.

Small angle X-ray scattering.

SAXS experiments were conducted on beamline SWING (SOLEIL Synchrotron, Gif-sur-Yvette, France) essentially as described in (Biou et al. 2010). The histidine tag of $BRAG2^{Sec7\text{-}PH}$ was cleaved for SAXS data collection, as unstructured tags add noise to SAXS experiments. The protein sample was centrifuged at 16,100 g for 30 min before the SAXS experiment, and were injected into a size-exclusion column and eluted directly

into the SAXS flow-through capillary cell. Fifty frames of 2 s each were collected, normalized to the transmitted intensity, and averaged using the image analysis software Foxtrot (SOLEIL software group and SWING beamline). Subsequent data analysis was done with the ATSAS software suite (EMBL, Hamburg, www.embl-hamburg.de/biosaxs/software.html). Scattered intensity curves were calculated from the atomic coordinates of the crystallographic structure using CRYSOL. The fit of the calculated intensity to the experimental intensity was assessed as described in (Biou et al. 2010).

Dynamic light scattering experiments

DLS experiments were performed at 37°C in a DynaPro NanoStar™ apparatus (Wyatt technology) in HKM buffer in a disposable cuvette (Eppendorf). Sets 10 autocorrelation curves (one autocorrelation curve every 5 seconds) were acquired for the buffer alone, then after each sequential addition of extruded liposomes (100 μM total lipids), ^{myr}Arf6-GDP (0.4 μM), BRAG2$^{Sec7\text{-}PH}$ (1 nM) and finally 100 μM GTP to start the exchange reaction. Data were analyzed using the software DYNAMICS® (Wyatt Technology) assuming that the size distribution is a simple Gaussian function to yield the mean radius and polydispersity.

Acknowledgements

This work was supported by grants from the Association pour la Recherche Contre le Cancer (ARC) and from the Agence Nationale de la Recherche (ANR) to J.C, by grants from ARC and from the Cancéropôle to K.A and a grant from the IKERBASQUE foundation to J.N. We are grateful to Audrey Labarde and Lionel Duarte (LEBS) for their expert assistance with protein productions, and to Dominique Padovani (LEBS) for his help with preparing myristoylated Arf6. We thank Véronique Henriot (LEBS/IMAGIF/IFR115) for her help with mutagenesis, Armelle Vigouroux (LEBS/IMAGIF/IFR115) for making the crystallization platform available to us, and the staff of the SOLEIL synchrotron (Gif-sur-Yvette, France) for making the X-ray crystallography PROXIMA1 beamline and the SAXS SWING beamline available to us.

References

Adams, P. D., P. V. Afonine, G. Bunkoczi, V. B. Chen, I. W. Davis, N. Echols, J. J. Headd, L. W. Hung, G. J. Kapral, R. W. Grosse-Kunstleve, A. J. McCoy, N. W. Moriarty, R. Oeffner, R. J. Read, D. C. Richardson, J. S. Richardson, T. C. Terwilliger and P. H. Zwart (2010). "PHENIX: a comprehensive Python-based system for macromolecular structure solution." Acta Crystallogr D Biol Crystallogr **66**(Pt 2): 213-221.

Amor, J. C., J. Swails, X. Zhu, C. R. Roy, H. Nagai, A. Ingmundson, X. Cheng and R. A. Kahn (2005). "The structure of RalF, an ADP-ribosylation factor guanine nucleotide exchange factor from Legionella pneumophila, reveals the presence of a cap over the active site." J Biol Chem **280**(2): 1392-1400.

Beraud-Dufour, S., S. Robineau, P. Chardin, S. Paris, M. Chabre, J. Cherfils and B. Antonny (1998). "A glutamic finger in the guanine nucleotide exchange factor ARNO displaces Mg2+ and the beta-phosphate to destabilize GDP on ARF1." EMBO J **17**(13): 3651-3659.

Bigay, J., J. F. Casella, G. Drin, B. Mesmin and B. Antonny (2005). "ArfGAP1 responds to membrane curvature through the folding of a lipid packing sensor motif." Embo J.

Biou, V., K. Aizel, P. Roblin, A. Thureau, E. Jacquet, S. Hansson, B. Guibert, E. Guittet, C. van Heijenoort, M. Zeghouf, J. Perez and J. Cherfils (2010). "SAXS and X-ray crystallography suggest an unfolding model for the GDP/GTP conformational switch of the small GTPase Arf6." J Mol Biol **402**(4): 696-707.

Blanc, E., P. Roversi, C. Vonrhein, C. Flensburg, S. M. Lea and G. Bricogne (2004). "Refinement of severely incomplete structures with maximum likelihood in BUSTER-TNT." Acta Crystallogr D Biol Crystallogr **60**(Pt 12 Pt 1): 2210-2221.

Boal, F., L. Guetzoyan, R. B. Sessions, M. Zeghouf, R. A. Spooner, J. M. Lord, J. Cherfils, G. J. Clarkson, L. M. Roberts and D. J. Stephens (2010). "LG186: An inhibitor of GBF1 function that causes Golgi disassembly in human and canine cells." Traffic **11**(12): 1537-1551.

Bos, J. L., H. Rehmann and A. Wittinghofer (2007). "GEFs and GAPs: critical elements in the control of small G proteins." Cell **129**(5): 865-877.

Casanova, J. E. (2007). "Regulation of arf activation: the sec7 family of Guanine nucleotide exchange factors." Traffic **8**(11): 1476-1485.

Chardin, P., S. Paris, B. Antonny, S. Robineau, S. Beraud-Dufour, C. L. Jackson and M. Chabre (1996). "A human exchange factor for ARF contains Sec7- and pleckstrin-homology domains." Nature **384**(6608): 481-484.

Chavrier, P. and M. Franco (2001). "Expression, purification, and biochemical properties of EFA6, a Sec7 domain-containing guanine exchange factor for ADP-ribosylation factor 6 (ARF6)." Methods Enzymol **329**: 272-279.

Chen, E. H., B. A. Pryce, J. A. Tzeng, G. A. Gonzalez and E. N. Olson (2003). "Control of myoblast fusion by a guanine nucleotide exchange factor, loner, and its effector ARF6." Cell **114**(6): 751-762.

Cherfils, J., J. Menetrey, M. Mathieu, G. Le Bras, S. Robineau, S. Beraud-Dufour, B. Antonny and P. Chardin (1998). "Structure of the Sec7 domain of the Arf exchange factor ARNO." Nature **392**(6671): 101-105.

Cohen, L. A., A. Honda, P. Varnai, F. D. Brown, T. Balla and J. G. Donaldson (2007). "Active Arf6 recruits ARNO/cytohesin GEFs to the PM by binding their PH domains." Mol Biol Cell **18**(6): 2244-2253.

Cronin, T. C., J. P. DiNitto, M. P. Czech and D. G. Lambright (2004). "Structural determinants of phosphoinositide selectivity in splice variants of Grp1 family PH domains." Embo J **23**(19): 3711-3720.

D'Souza-Schorey, C. and P. Chavrier (2006). "ARF proteins: roles in membrane traffic and beyond." Nat Rev Mol Cell Biol **7**(5): 347-358.

DiNitto, J. P., A. Delprato, M. T. Gabe Lee, T. C. Cronin, S. Huang, A. Guilherme, M. P. Czech and D. G. Lambright (2007). "Structural basis and mechanism of autoregulation in 3-phosphoinositide-dependent Grp1 family Arf GTPase exchange factors." Mol Cell **28**(4): 569-583.

Dottermusch-Heidel, C., V. Groth, L. Beck and S. F. Onel (2012). "The Arf-GEF Schizo/Loner regulates N-cadherin to induce fusion competence of Drosophila myoblasts." Dev Biol **368**(1): 18-27.

Doublie, S. (1997). "Preparation of selenomethionyl proteins for phase determination." Methods Enzymol **276**: 523-530.

Dunphy, J. L., R. Moravec, K. Ly, T. K. Lasell, P. Melancon and J. E. Casanova (2006). "The Arf6 GEF GEP100/BRAG2 regulates cell adhesion by controlling endocytosis of beta1 integrins." Curr Biol **16**(3): 315-320.

Emsley, P., B. Lohkamp, W. G. Scott and K. Cowtan (2010). "Features and development of Coot." Acta Crystallogr D Biol Crystallogr **66**(Pt 4): 486-501.

Franco, M., P. Chardin, M. Chabre and S. Paris (1995). "Myristoylation of ADP-ribosylation factor 1 facilitates nucleotide exchange at physiological Mg2+ levels." J Biol Chem **270**(3): 1337-1341.

Goldberg, J. (1998). "Structural basis for activation of ARF GTPase: mechanisms of guanine nucleotide exchange and GTP-myristoyl switching." Cell **95**(2): 237-248.

Gureasko, J., O. Kuchment, D. L. Makino, H. Sondermann, D. Bar-Sagi and J. Kuriyan (2010). "Role of the histone domain in the autoinhibition and activation of the Ras activator Son of Sevenless." Proc Natl Acad Sci U S A **107**(8): 3430-3435.

Hofmann, I., A. Thompson, C. M. Sanderson and S. Munro (2007). "The Arl4 family of small G proteins can recruit the cytohesin Arf6 exchange factors to the plasma membrane." Curr Biol **17**(8): 711-716.

Jian, X., J. M. Gruschus, E. Sztul and P. A. Randazzo (2012). "The PH domain of the Arf exchange factor Brag2 is an allosteric binding site." J Biol Chem.

Kabsch, W. (2010). "Xds." Acta Crystallogr D Biol Crystallogr **66**(Pt 2): 125-132.

Lemmon, M. A. (2008). "Membrane recognition by phospholipid-binding domains." Nat Rev Mol Cell Biol **9**(2): 99-111.

Macia, E., M. Chabre and M. Franco (2001). "Specificities for the small G proteins ARF1 and ARF6 of the guanine nucleotide exchange factors ARNO and EFA6." J Biol Chem **276**(27): 24925-24930.

Macia, E., F. Luton, M. Partisani, J. Cherfils, P. Chardin and M. Franco (2004). "The GDP-bound form of Arf6 is located at the plasma membrane." J Cell Sci **117**(Pt 11): 2389-2398.

Margarit, S. M., H. Sondermann, B. E. Hall, B. Nagar, A. Hoelz, M. Pirruccello, D. Bar-Sagi and J. Kuriyan (2003). "Structural evidence for feedback activation by Ras.GTP of the Ras-specific nucleotide exchange factor SOS." Cell **112**(5): 685-695.

McCoy, A. J., R. W. Grosse-Kunstleve, P. D. Adams, M. D. Winn, L. C. Storoni and R. J. Read (2007). "Phaser crystallographic software." J Appl Crystallogr **40**(Pt 4): 658-674.

Menju, T., S. Hashimoto, A. Hashimoto, Y. Otsuka, H. Handa, E. Ogawa, Y. Toda, H. Wada, H. Date and H. Sabe (2011). "Engagement of overexpressed Her2 with GEP100 induces autonomous invasive activities and provides a biomarker for metastases of lung adenocarcinoma." PLoS One **6**(9): e25301.

Morishige, M., S. Hashimoto, E. Ogawa, Y. Toda, H. Kotani, M. Hirose, S. Wei, A. Hashimoto, A. Yamada, H. Yano, Y. Mazaki, H. Kodama, Y. Nio, T. Manabe, H. Wada, H. Kobayashi and H. Sabe (2008). "GEP100 links epidermal growth factor receptor signalling to Arf6 activation to induce breast cancer invasion." Nat Cell Biol **10**(1): 85-92.

Pasqualato, S., L. Renault and J. Cherfils (2002). "Arf, Arl, Arp and Sar proteins: a family of GTP-binding proteins with a structural device for 'front-back' communication." EMBO Rep **3**(11): 1035-1041.

Pasqualato, S., L. Renault and J. Cherfils (2004). The GDP/GTP cycle of Arf proteins. Structural and biochemical aspects., Kluwer Academic Publishers.

Renault, L., B. Guibert and J. Cherfils (2003). "Structural snapshots of the mechanism and inhibition of a guanine nucleotide exchange factor." Nature **426**(6966): 525-530.

Richardson, B. C., C. M. McDonold and J. C. Fromme (2012). "The Sec7 Arf-GEF is recruited to the trans-Golgi network by positive feedback." Dev Cell **22**(4): 799-810.

Rossman, K. L., D. K. Worthylake, J. T. Snyder, D. P. Siderovski, S. L. Campbell and J. Sondek (2002). "A crystallographic view of interactions between Dbs and Cdc42: PH domain-assisted guanine nucleotide exchange." EMBO J **21**(6): 1315-1326.

Sakurai, A., X. Jian, C. J. Lee, Y. Manavski, E. Chavakis, J. Donaldson, P. A. Randazzo and J. S. Gutkind (2011). "Phosphatidylinositol-4-phosphate 5-kinase and GEP100/Brag2 protein mediate antiangiogenic signaling by semaphorin 3E-plexin-D1 through Arf6 protein." J Biol Chem **286**(39): 34335-34345.

Scholz, R., S. Berberich, L. Rathgeber, A. Kolleker, G. Kohr and H. C. Kornau (2010). "AMPA receptor signaling through BRAG2 and Arf6 critical for long-term synaptic depression." Neuron **66**(5): 768-780.

Sheldrick, G. M. (2010). "Experimental phasing with SHELXC/D/E: combining chain tracing with density modification." Acta Crystallogr D Biol Crystallogr **66**(Pt 4): 479-485.

Someya, A., M. Sata, K. Takeda, G. Pacheco-Rodriguez, V. J. Ferrans, J. Moss and M. Vaughan (2001). "ARF-GEP(100), a guanine nucleotide-exchange protein for ADP-ribosylation factor 6." Proc Natl Acad Sci U S A **98**(5): 2413-2418.

Stalder, D., H. Barelli, R. Gautier, E. Macia, C. L. Jackson and B. Antonny (2011). "Kinetic studies of the Arf activator Arno on model membranes in the presence of Arf effectors suggest control by a positive feedback loop." J Biol Chem **286**(5): 3873-3883.

Trapani, S. and J. Navaza (2008). "AMoRe: classical and modern." Acta Crystallogr D Biol Crystallogr **64**(Pt 1): 11-16.

Uchida, Y., J. Hasegawa, D. Chinnapen, T. Inoue, S. Okazaki, R. Kato, S. Wakatsuki, R. Misaki, M. Koike, Y. Uchiyama, S. Iemura, T. Natsume, R. Kuwahara, T. Nakagawa, K. Nishikawa, K. Mukai, E. Miyoshi, N. Taniguchi, D. Sheff, W. I. Lencer, T. Taguchi and H. Arai (2011). "Intracellular phosphatidylserine is essential for retrograde membrane traffic through endosomes." Proc Natl Acad Sci U S A **108**(38): 15846-15851.

van Meer, G., D. R. Voelker and G. W. Feigenson (2008). "Membrane lipids: where they are and how they behave." Nat Rev Mol Cell Biol **9**(2): 112-124.

Viaud, J., M. Zeghouf, H. Barelli, J. C. Zeeh, A. Padilla, B. Guibert, P. Chardin, C. A. Royer, J. Cherfils and A. Chavanieu (2007). "Structure-based discovery of an inhibitor of Arf activation by Sec7 domains through targeting of protein-protein complexes." Proc Natl Acad Sci U S A **104**(25): 10370-10375.

Xie, C. G., S. M. Wei, J. M. Chen, X. F. Xu, J. T. Cai, Q. Y. Chen and L. T. Jia (2012). "Down-Regulation of GEP100 Causes Increase in E-Cadherin Levels and Inhibits Pancreatic Cancer Cell Invasion." PLoS One **7**(5): e37854.

Yeung, T., G. E. Gilbert, J. Shi, J. Silvius, A. Kapus and S. Grinstein (2008). "Membrane phosphatidylserine regulates surface charge and protein localization." Science **319**(5860): 210-213.

Zeeh, J. C., M. Zeghouf, C. Grauffel, B. Guibert, E. Martin, A. Dejaegere and J. Cherfils (2006). "Dual specificity of the interfacial inhibitor brefeldin a for arf proteins and sec7 domains." J Biol Chem **281**(17): 11805-11814.

Figure legends

Figure 1: Characterization of BRAG2 constructs used in this study

A. Schematic representation of BRAG2 constructs and their SDS-PAGE analysis. The linker domain is shown in yellow. **B.** SEC-MALS analysis of the Δ17Arf1-GDP/BRAG2$^{Sec7\text{-}PH/E498K}$ complex. The molecular masses are 50.6 ±0.5 kDa for BRAG2$^{Sec7\text{-}PH/E498K}$, 20.6 ± 0.04 for Δ17Arf1-GDP and 64.2 ± 1.3 kDa for the complex. **C.** Gel filtration analysis of the nucleotide-free Δ17Arf1/BRAG2 $^{Sec7\text{-}PH}$ complex obtained by elimination of GDP.

Figure 2: **BRAG2 is a dual Arf1 and Arf6 GEF that is not auto-inhibited in solution and is potentiated by membranes**.

Representative tryptophan fluorescence kinetics used to determine k_{cat}/K_m given in **Table 1**. Exchange reactions in **A** and **B** were done in the absence of liposomes with 1 μM truncated Arf proteins. Exchange reactions in **C** and **D** were done with 100 μM PM-like liposomes (34.3% PC, 14% PE, 21% PS, 0,7%PIP_2, 30% cholesterol) with 0.4 μM ^{myr}Arf proteins.

Figure 3. The crystal structure of the Δ17Arf1-GDP/ BRAG2$^{Sec7\text{-}PH/E498K}$ complex.

A. Overall view of the complex. Arf1 is in grey, the domains of BRAG2 are color-coded as indicated. The bound nucleotide is GDP-3'P, a GDP analog produced by *E.coli* under stress conditions. **B.** Superposition of the PH domains of BRAG2 (cyan) and auto-inhibited GRP1 (brown), seen from the top of the phosphoinositide-binding pocket. Note the kink of the C-terminal helix in GRP1. Positively charged residues in the vicinity of the pocket are shown in yellow. (Below) Close-up view of BRAG2^{PH} superposed to the PH domain of pleckstrin bound to IP3. Note the conserved lysine on strand β1, which is replaced by a glutamate in BRAG proteins. **C.** Surface view of BRAG2, showing the compact structure formed by the Sec7, PH and linker domains. Conserved residues in the linker/PH interface are highlighted in red. **D.** Comparison of the BRAG2$^{Sec7\text{-}PH/E498K}$ /ΔArf1-GDP complex (center) to auto-inhibited GRP1$^{Sec7\text{-}PH}$ (left, Sec7 domains in the same orientation) and to the DBS$^{DH\text{-}PH}$/RhoA complex (right, GTPases in the same orientation (Rossman et al. 2002)). Note that the DBS^{PH} is close to the switch 2 of Rho, whereas BRAG2^{PH} is close to the switch 1 of Arf, resulting in opposite orientations.

Figure 4: **BRAG2 is not regulated by a feedback loop.**

Activation of ^{myr}Arf1 by BRAG2$^{\Delta 30}$ was analyzed by tryptophan fluorescence kinetics with PM-like liposomes pre-incubated with increasing amounts of ^{myr}Arf6-GTP as indicated. The right panel shows the kinetics associated to the formation of ^{myr}Arf1-GTP corrected for the intrinsic fluorescence of ^{myr}Arf6-GTP.

Figure 5: **Selective binding and activation of BRAG2 by negatively charged lipids.**

A. BRAG2$^{\Delta 30}$ (1 µM) was submitted to flotation assays using liposomes of the indicated composition (1 mM of total lipids). The 100% lane corresponds to the complete recovery of the protein in the fraction. **B.** Comparison of BRAG2$^{\Delta 30}$ and BRAG2^{Sec7} binding to PM-like liposomes using the flotation assay. **C.** Nucleotide exchange activity of BRAG2$^{\Delta 30}$ (1nM) towards ^{myr}Arf1-GDP (0.4 µM) using 100 µM of liposomes of indicated compositions. Reactions were initiated by addition of 100µM GTP. k_{app} values are mean of at least three experiments and are given ± S.D.

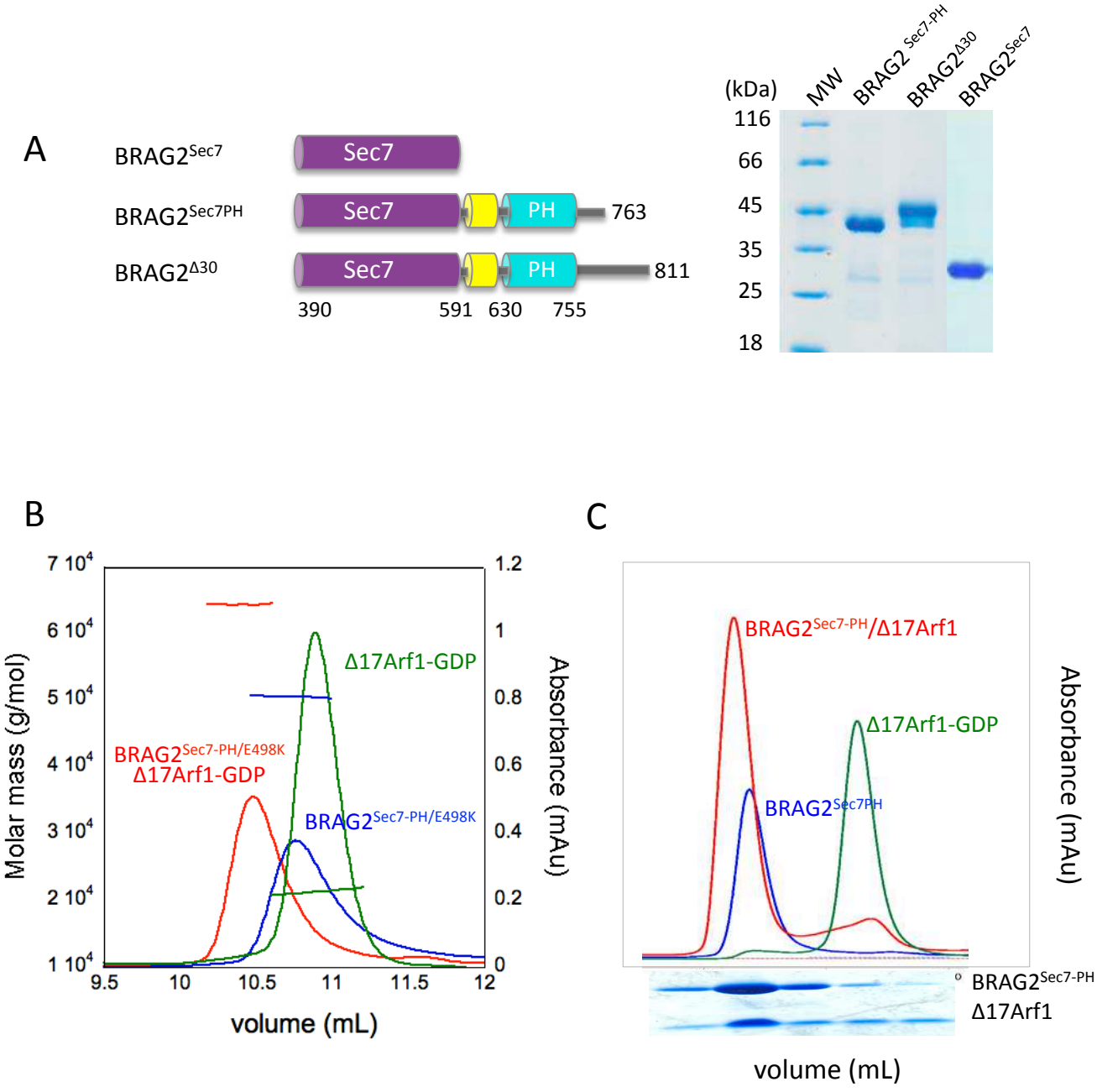
A
BRAG2Sec7
BRAG2Sec7PH
BRAG2Δ30
Sec7
PH
763
811
390
591
630
755
(kDa)
MW
BRAG2 Sec7-PH
BRAG2Δ30
BRAG2Sec7
116
66
45
35
25
18
B
Molar mass (g/mol)
Absorbance (mAu)
volume (mL)
Δ17Arf1-GDP
BRAG2Sec7-PH/E498K
Δ17Arf1-GDP
BRAG2Sec7-PH/E498K
C
BRAG2Sec7-PH/Δ17Arf1
Δ17Arf1-GDP
BRAG2Sec7PH
Absorbance (mAu)
BRAG2Sec7-PH
Δ17Arf1
volume (mL)

Figure 1

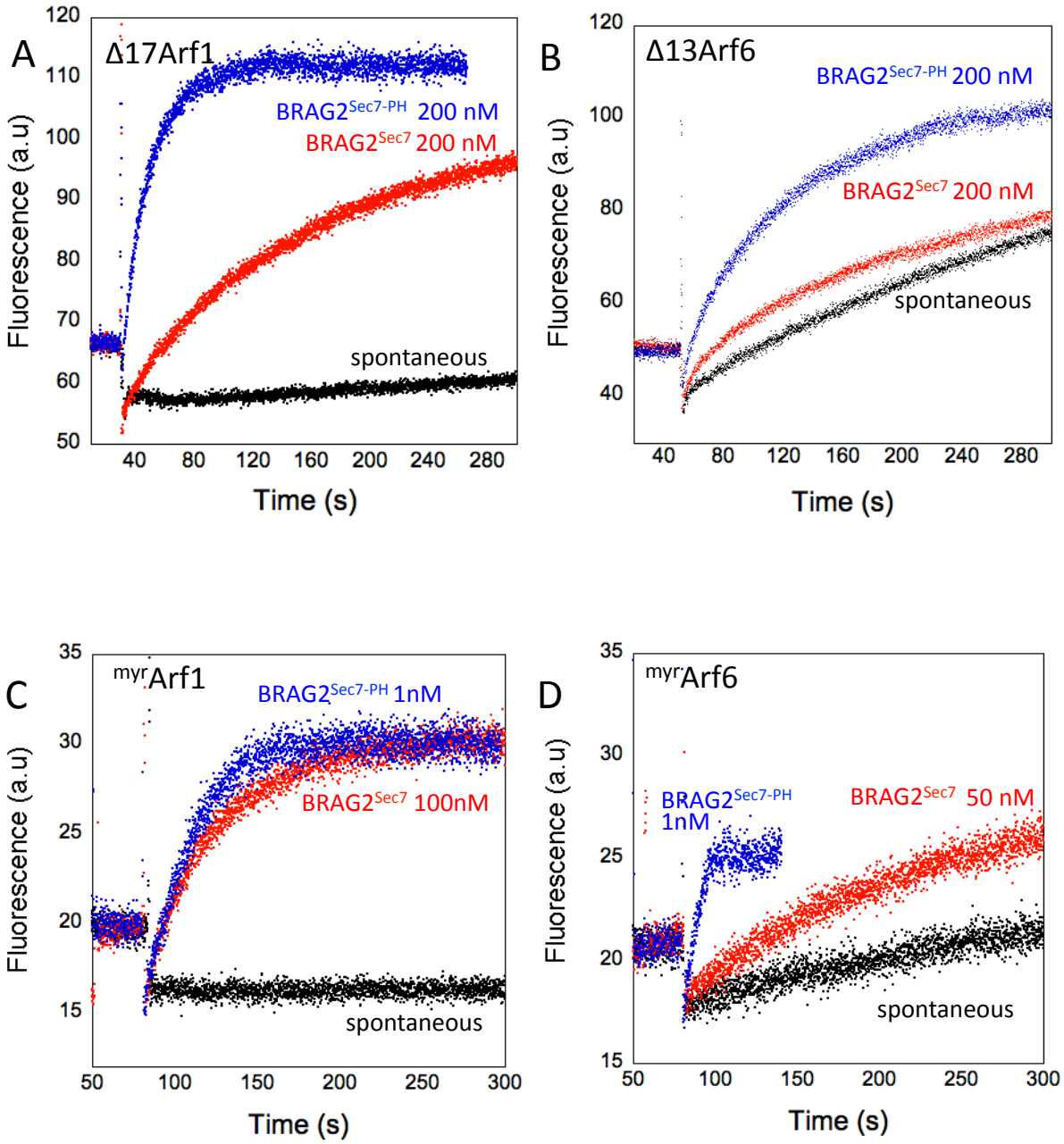
A
Δ17Arf1
BRAG2Sec7-PH 200 nM
BRAG2Sec7 200 nM
spontaneous
Fluorescence (a.u)
Time (s)
B
Δ13Arf6
BRAG2Sec7-PH 200 nM
BRAG2Sec7 200 nM
spontaneous
Fluorescence (a.u)
Time (s)
C
myrArf1
BRAG2Sec7-PH 1nM
BRAG2Sec7 100nM
spontaneous
Fluorescence (a.u)
Time (s)
D
myrArf6
BRAG2Sec7-PH 1nM
BRAG2Sec7 50 nM
spontaneous
Fluorescence (a.u)
Time (s)

Figure 2

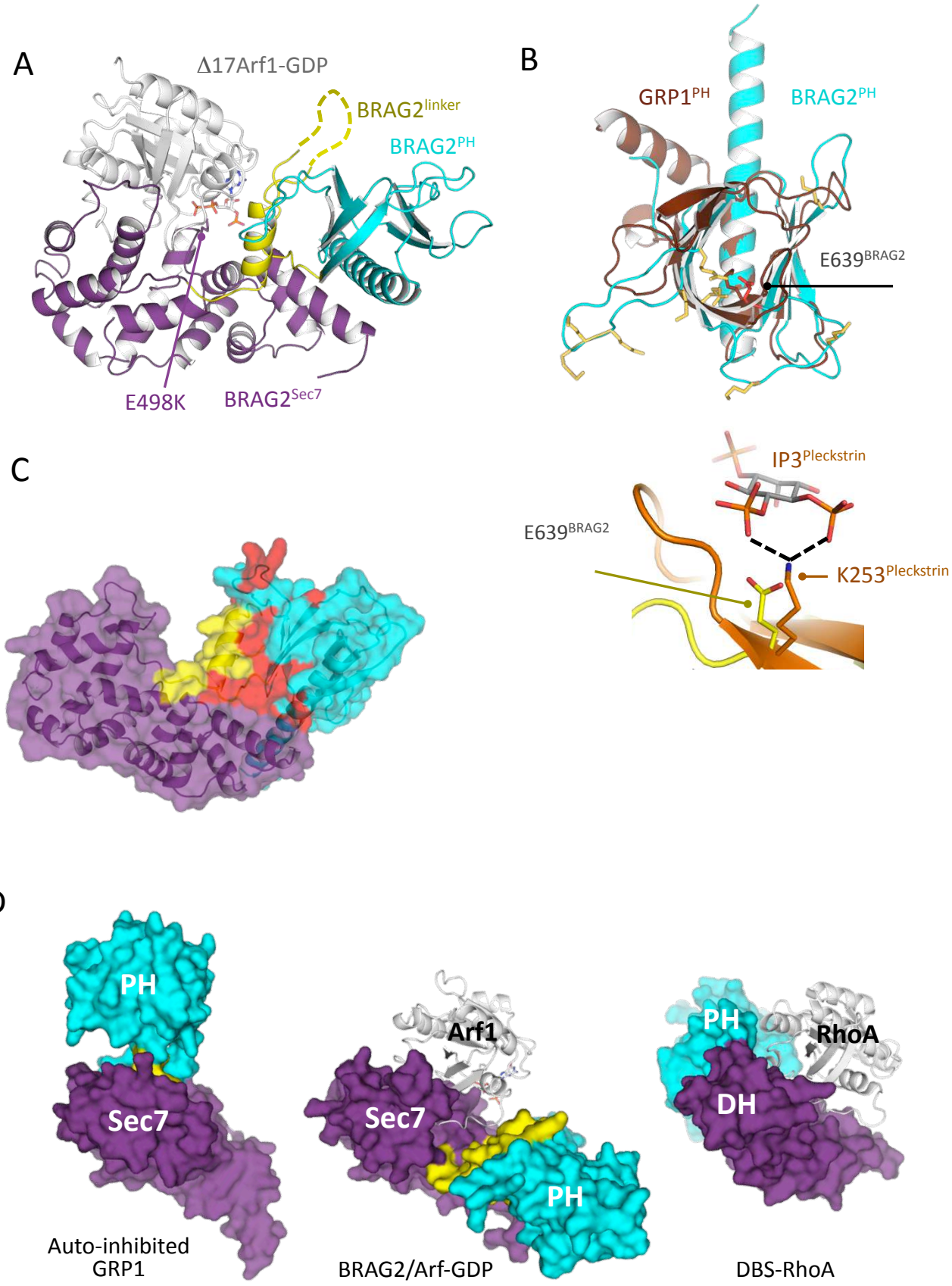
A
Δ17Arf1-GDP
BRAG2linker
BRAG2PH
E498K
BRAG2Sec7
B
GRP1PH
BRAG2PH
E639BRAG2
C
IP3Pleckstrin
E639BRAG2
K253Pleckstrin
D
PH
Sec7
Auto-inhibited
GRP1
Arf1
Sec7
PH
BRAG2/Arf-GDP
PH
RhoA
DH
DBS-RhoA

Figure 3

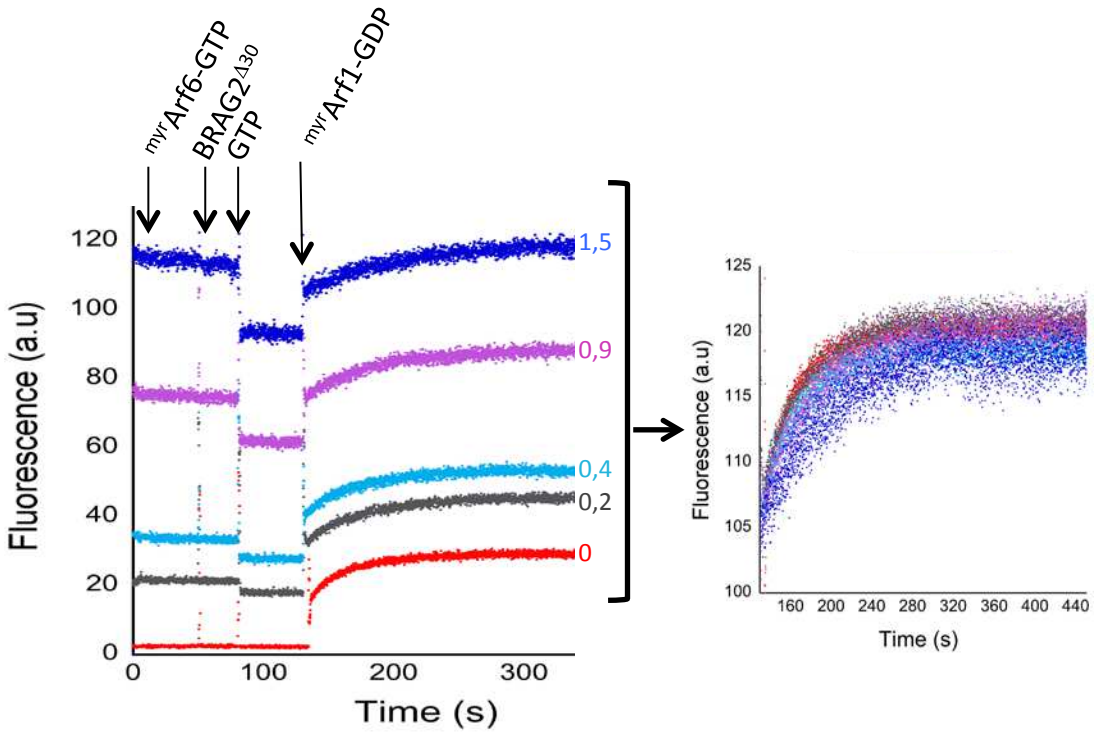
myrArf6-GTP
BRAG2Δ30
GTP
myrArf1-GDP
Fluorescence (a.u)
Time (s)
1,5
0,9
0,4
0,2
0
Fluorescence (a.u)
Time (s)

Figure 4

A

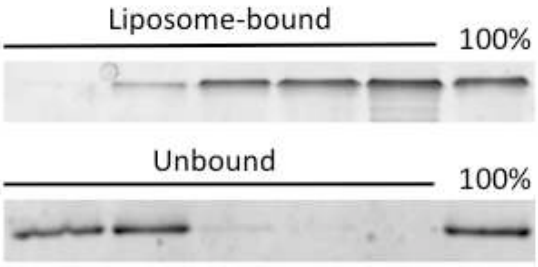

PC	80	50	78	48	34.3
PE	20	20	20	20	14
PS	0	30	0	30	21
PIP_2	0	0	2	2	0.7
Chol	0	0	0	0	30

B

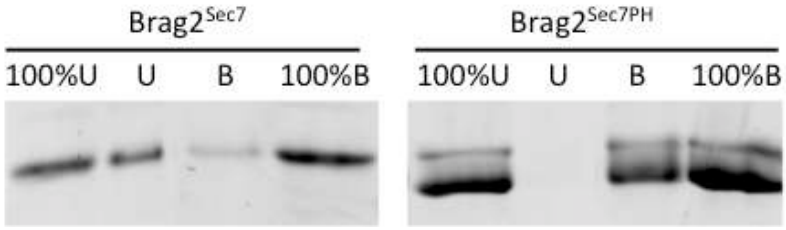

C

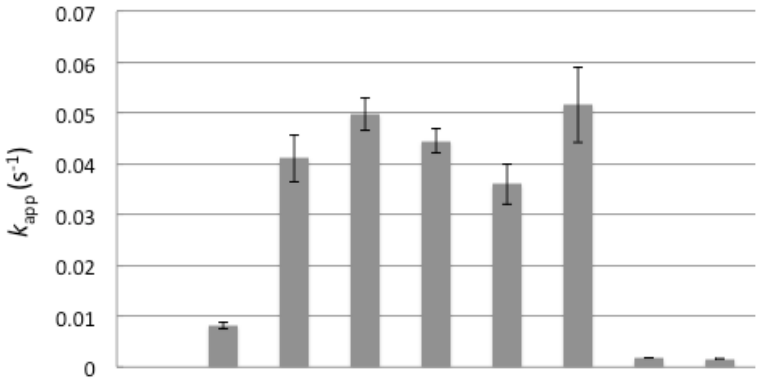

PC	80	68	50	78	68	48	34.3	78	78
PE	20	20	20	20	20	20	14	20	20
PS	0	10	30	0	10	30	21	0	0
PIP_2	0	0	0	2	2	2	0.7	0	0
Chol	0	0	0	0	0	0	30	0	0
PI3P	0	0	0	0	0	0	0	2	0
PI4P	0	0	0	0	0	0	0	0	2

Figure 5

Table 1: Catalytic efficiency of BRAG2 constructs in solution (truncated Arf proteins) and in the presence of PM-like liposomes (myristoylated Arf proteins). (*) Kinetics for ^{myr}Arf6 activation by BRAG2 constructs could not be fitted by a single exponential and were analyzed from initial velocities instead (see text and **Figure S4)**

k_{cat}/K_M (10^5 $M^{-1}s^{-1}$)	Δ17Arf1	Δ13Arf6	^{myr}Arf1	^{myr}Arf6
BRAG2^{Sec7}	0.2 ± 0.02	0.1 ± 0.04	0.6 ± 0.04	0.5 ± 0.09
BRAG2$^{Sec7\text{-}PH}$	2.4 ± 0.1	0.5 ± 0.1	390 ± 31	*
BRAG2$^{\Delta 30}$	2.5 ± 0.06	0.5 ± 0.1	346 ± 46	*

Table 2. Data collection and refinement statistics

	Δ17Arf1-GDP/ BRAG2$^{SEC7\text{-}PH/E498K}$ (native with His-tag)	Δ17Arf1-GDP/ BRAG2$^{SEC7\text{-}PH/E498K}$ (Se-Met, His-tag cleaved)
Data collection		
Wavelength	0.98	0.98
Space group	*C2*	*P2*
Cell dimensions		
a, *b*, *c* (Å)	210.72, 66.22, 91.06	90.98, 65.78, 196.86
α, β, γ (°)	90.00, 108.19, 90.00	90.00, 96.13, 90.00
Resolution (Å)	49.48 – 3.2 (3.69 – 3.2) *	42.84 – 3.3 (3.4 – 3.3)
R_{merge}	22.8 (42.4)	20.1 (73.5)
I / σI	3.1 (1.9)	6.8 (1.94)
Completeness (%)	95.8 (97.7)	99 (95.6)
Redundancy	3.5 (2.5)	3.24 (3.16)
Refinement		
Resolution (Å)	49.48 – 3.2 (3.37 – 3.2)	42.84 – 3.3 (3.4 – 3.3)
No. reflections	19,487	35,125
R_{work} / R_{free}	24.78 / 30.79	21.6 / 25.26
No. atoms		
Protein	8,421	16,804
Ligand/ion	6	8
B-factors		
Protein	66.16	61.36
R.m.s. deviations		
Bond lengths (Å)	0.008	0.009
Bond angles (°)	1.16	1.22

*Values in parentheses are for highest-resolution shell.

Supplementary Figures

Figure S1: Sequence alignment of the linker and PH domains of BRAG proteins from selected species.

Invariant residues are in red. Secondary structures observed in the BRAG2$^{Sec7\text{-}PH/E498K}$ crystal structure are indicated. Invariant residues in the linker-PH interface are indicated by a red arrowhead. The invariant glutamate in strand β1 is indicated by a black arrowhead.

Figure S2: **Snapshots of Arf captured along the exchange reaction.**

Arf/ArfGEF complexes (color-coded as indicated) were superposed based on their Sec7 domain. Only Arf is shown for clarity. The BFA-inhibited Arf-GDP-ARNO complex (in brown, (Renault et al. 2003)) represents an early step before the toggle of the interswitch. Arf from the Arf-GDP-BRAG2$^{Sec7\text{-}PH/E698K}$ complex (in yellow) has undergone the interswitch toggle and is mid-way between the Arf-GDP-ARNOSec7/E156K complex ((Renault et al. 2003), in magenta) and the nucleotide-free Arf-Gea2 complex ((Goldberg 1998), in grey).

Figure S3. **Synchrotron radiation SAXS analysis of BRAG2$^{Sec7\text{-}PH}$**.

Fit of the experimental SAXS data from unbound BRAG2$^{Sec7\text{-}PH}$ (red) with the scattering curve calculated from the crystal structure of BRAG2 $^{Sec7\text{-}PH}$ extracted from the complex (blue). The logarithm of intensity is displayed as a function of the momentum transfer Q. The χ^2 value is given.

Figure S4. Analysis of ^{myr}Arf6 activation.

A. Representative tryptophane fluorescence kinetics of ^{myr}Arf6 (0,4μM) activation by BRAG2$^{Sec7\text{-}PH}$ (0-1nM range). Note the shape of the curves, which cannot be fitted by a single exponential. **B.** Analysis of liposome polydispersity and radius by dynamic light scattering (DLS) along the exchange reaction. PM-like liposomes were mixed sequentially with ^{myr}Arf6 (0.4 μM), BRAG2 (1 nM) and GTP (100 μM). Polydispersity and average radius were 29% and 100 Å for liposomes alone, 37% and 110 nm after addition of myrArf6-GDP, 33% and 114 nm after addition of BRAG2, and 27% and 111 nm after addition of GTP and completion of nucleotide exchange, ruling out that liposome aggregation occurs during the exchange reaction. **C.** Analysis of initial velocities as a function of BRAG2 concentration, done with BRAG2$^{Sec7\text{-}PH}$ and the longer

BRAG2$^{\Delta 30}$ constructs for both ^{myr}Arf1 and ^{myr}ARF6. The curves were linear in all analysis, and was similar for both BRAG2 constructs and in the same range for Arf1 and Arf6.

Figure S5. Binding of ^{myr}ARF1 to liposomes depends on the bound nucleotide and is independent of liposome composition

Flotation assays were performed using liposomes of indicated compositions. Prior to centrifugation, 1 μM of ^{myr}Arf1 was incubated with 100 μM of either GDP or GTP during 15 min at 37˚C in the presence of 1 mM liposomes and 2 mM EDTA. The reaction was stop by addition of 1 mM $MgCl_2$. ^{myr}Arf1-GDP did not bind to liposomes. ^{myr}ARF1-GTP was fully recruited to liposomes, independently of the liposome composition.

Figure S6. Structure-based sequence alignment of BRAG2 with phospholipid-bound PH domains.

Structures that can be structurally aligned are in normal characters, structures that are non-superposable are in italics. Residues involved in binding lipid analogs were identified from the crystal structures using LIGPLOT and are indicated in bold characters (black). The glutamate in strand β1 of BRAG proteins that replaces the invariant lysine in other PH domains is indicated in red. Positively charged residues of BRAGs located in the vicinity of the classical lipid-binding pocket are indicated in cyan (see also **Figure 3B**). BRAG sequences are from human. The crystals structures are: GRP1-IP4 (PDB code 2R0D), DAPP1-IP4 (PDB code 1FAO), Pleckstrin-IP5 (PDB code 2I5F), PEPP1-IP4 (PDB code 1UPR), AKT-PKB-IP4 (PDB code 1UNQ), PLC-IP3 (PDB code 1MAI), PDK1-IP4 (PDB code 1W1D) and Evectin-2-phosphoserine (PDB code 3AJ4).

Figure S7: **Fluorescence kinetics analysis of Brag2 sensitivity to liposome composition**

Representative fluorescence kinetics curves for nucleotide exchange of ^{myr}Arf1-GDP (0.4 μM) catalyzed by BRAG2$^{\Delta 30}$ (1 nM) in the presence of liposomes (100 μM) of indicated composition. Reactions were started by 100 μM GTP. Pseudo-first order reaction rate constants (k_{app}) were determined from a mono-exponential fit and used to prepare Figure 5C. Note the change in the plateau for 2% PIP_2 and 10% PS/2% PIP_2 liposomes, for which we have no ready explanation.

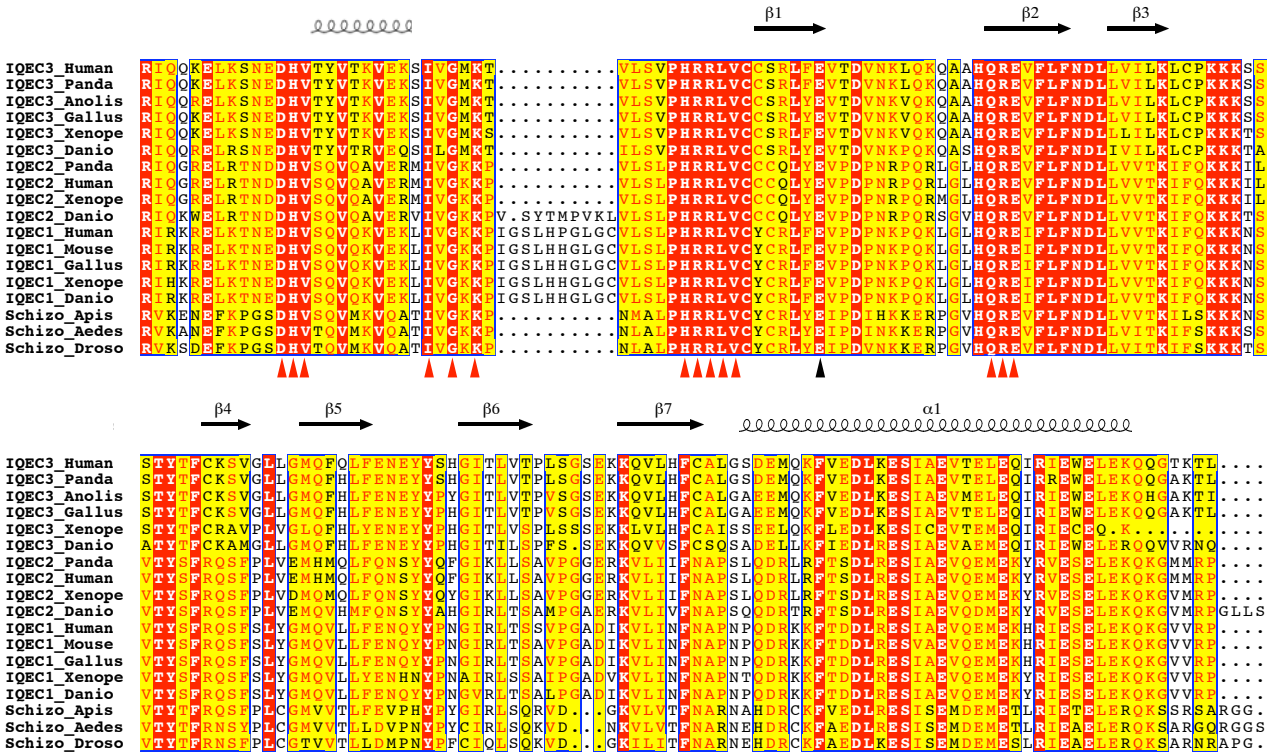
β1
β2
β3
β4
β5
β6
β7
α1
IQEC3_Human
IQEC3_Panda
IQEC3_Anolis
IQEC3_Gallus
IQEC3_Xenope
IQEC3_Danio
IQEC2_Panda
IQEC2_Human
IQEC2_Xenope
IQEC2_Danio
IQEC1_Human
IQEC1_Mouse
IQEC1_Gallus
IQEC1_Xenope
IQEC1_Danio
Schizo_Apis
Schizo_Aedes
Schizo_Droso

Figure S1

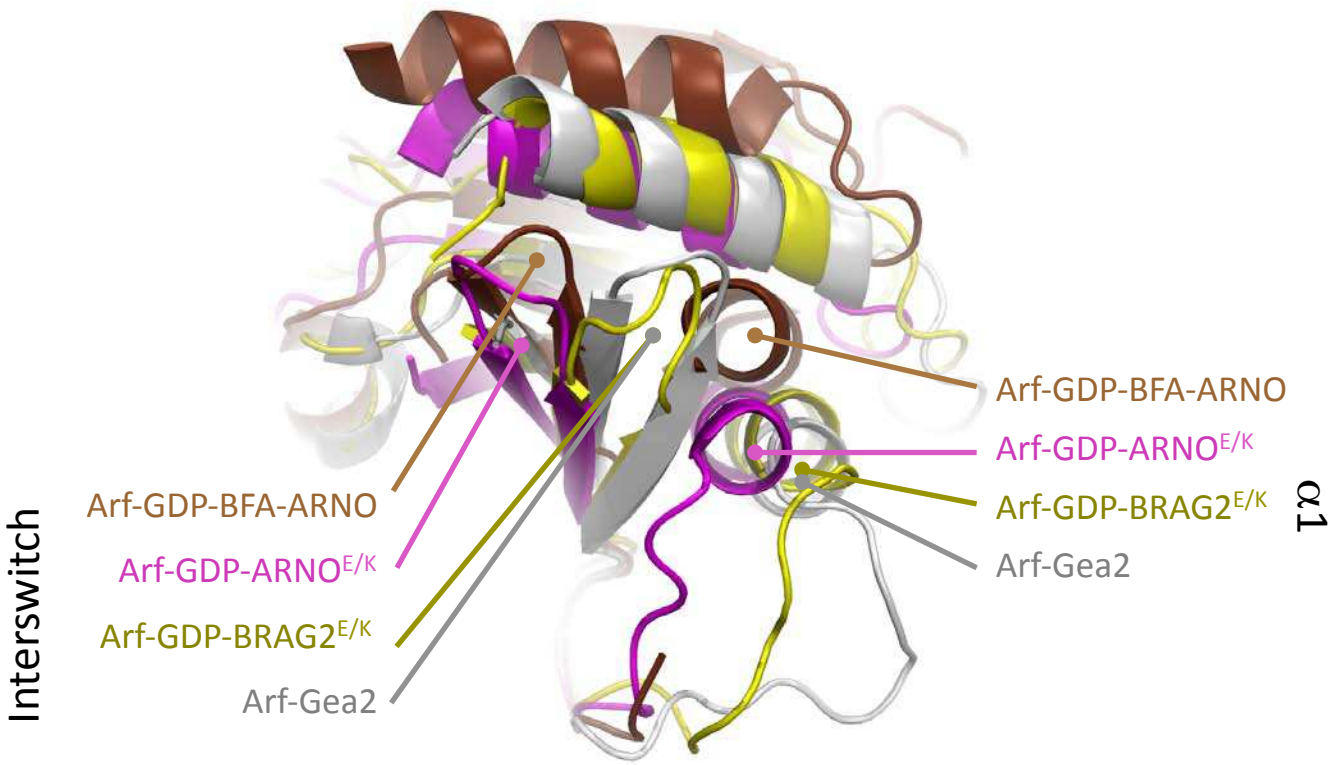
Interswitch
Arf-GDP-BFA-ARNO
Arf-GDP-ARNO$^{E/K}$
Arf-GDP-BRAG2$^{E/K}$
Arf-Gea2
Arf-GDP-BFA-ARNO
Arf-GDP-ARNO$^{E/K}$
Arf-GDP-BRAG2$^{E/K}$
Arf-Gea2
α1

Figure S2

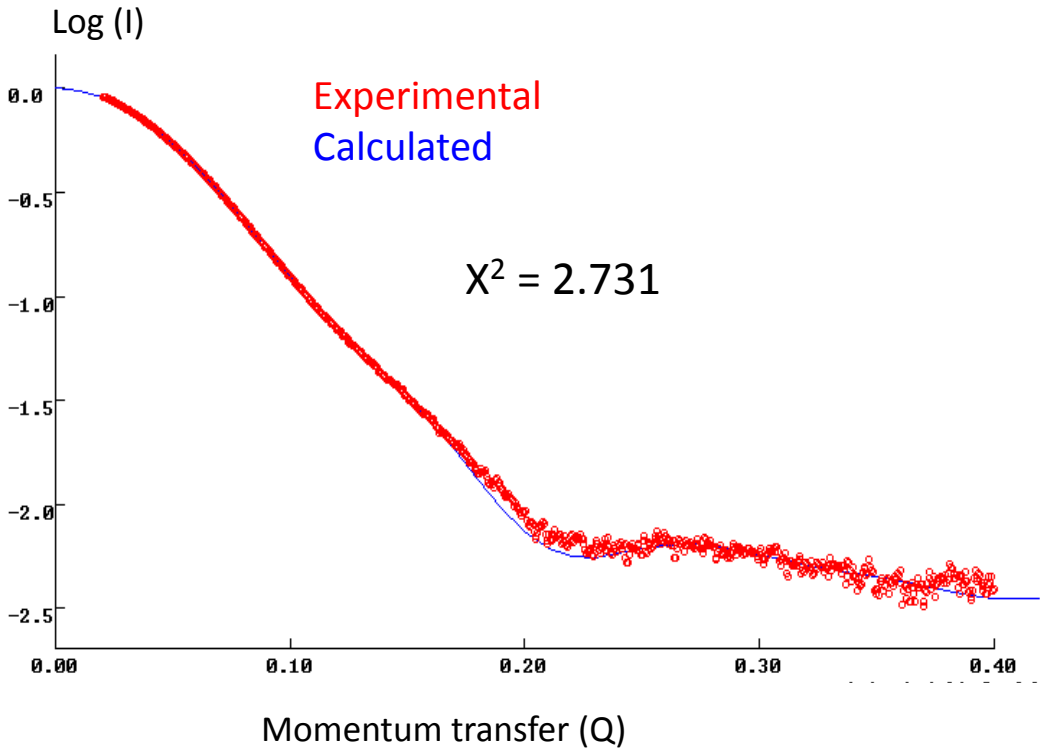
Log (I)
Experimental
Calculated
X^2 = 2.731
0.0
-0.5
-1.0
-1.5
-2.0
-2.5
0.00
0.10
0.20
0.30
0.40
Momentum transfer (Q)

Figure S3

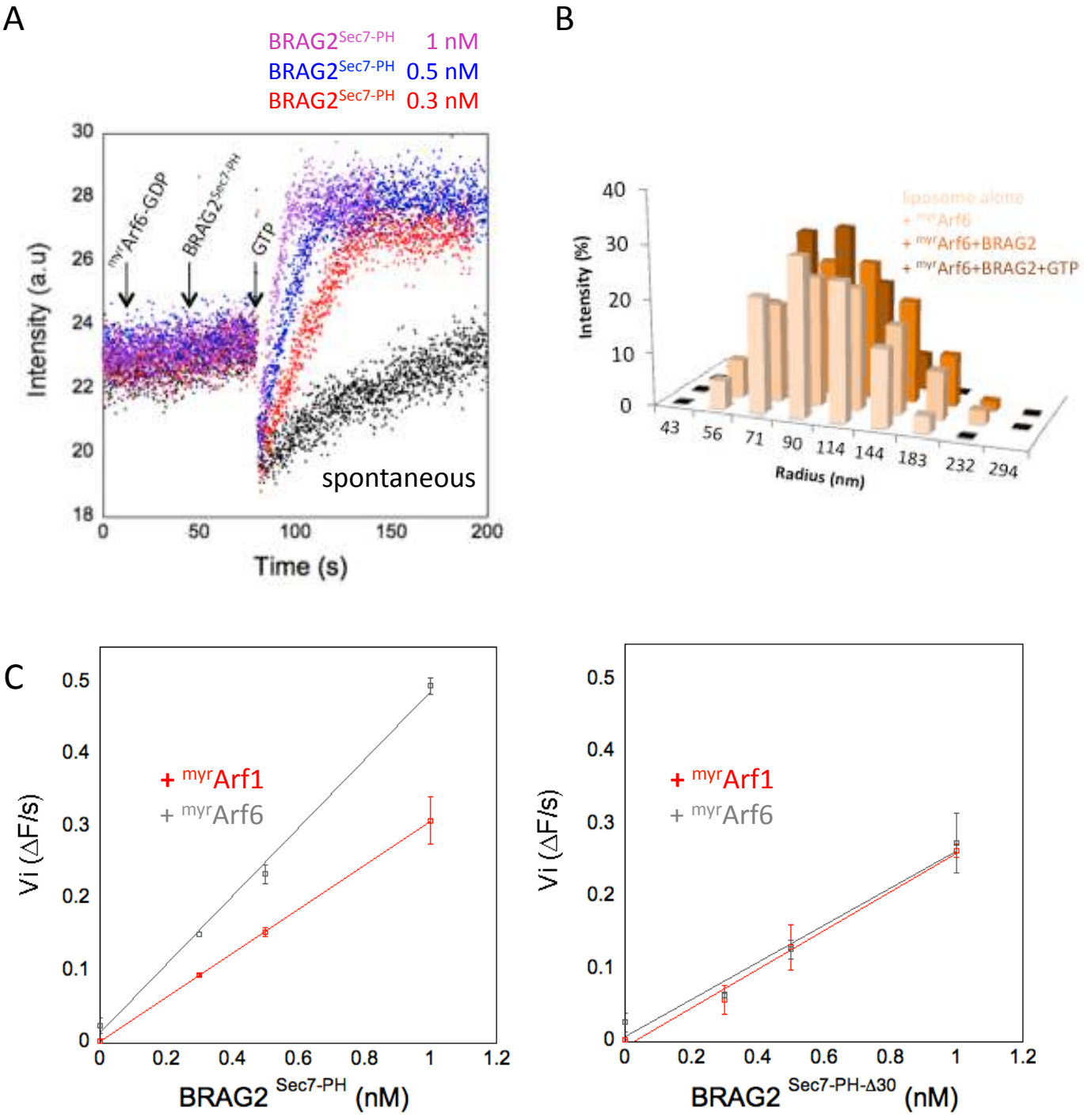
A
BRAG2Sec7-PH 1 nM
BRAG2Sec7-PH 0.5 nM
BRAG2Sec7-PH 0.3 nM
mycArf6-GDP
BRAG2Sec7-PH
GTP
spontaneous
Intensity (a.u)
Time (s)
B
liposome alone
+ mycArf6
+ mycArf6+BRAG2
+ mycArf6+BRAG2+GTP
Intensity (%)
Radius (nm)
C
+ mycArf1
+ mycArf6
Vi (ΔF/s)
BRAG2 Sec7-PH (nM)
BRAG2 Sec7-PH-Δ30 (nM)

Figure S4

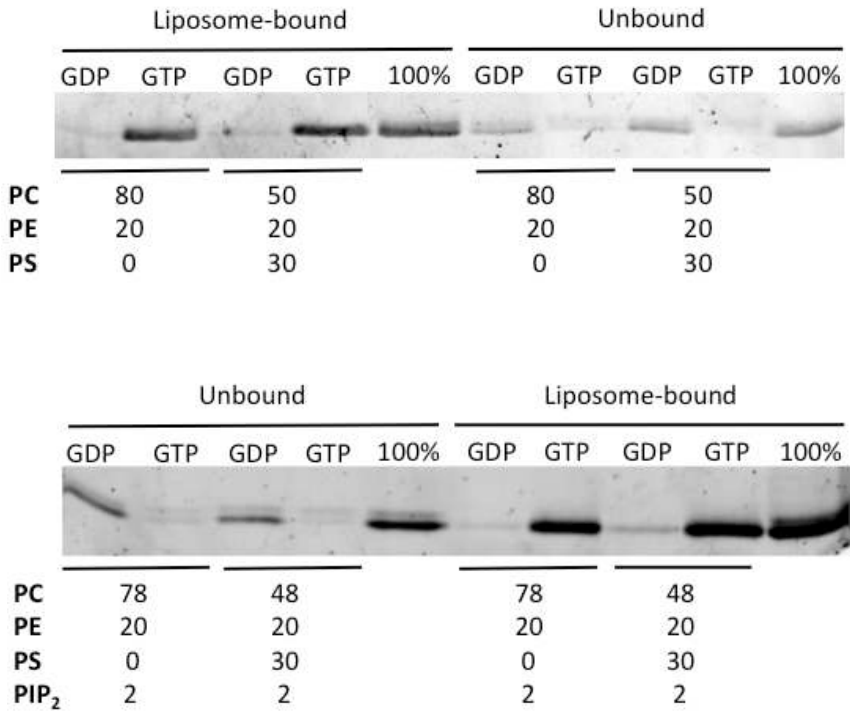
Liposome-bound
Unbound
GDP GTP GDP GTP 100% GDP GTP GDP GTP 100%
PC 80 50 80 50
PE 20 20 20 20
PS 0 30 0 30
Unbound
Liposome-bound
GDP GTP GDP GTP 100% GDP GTP GDP GTP 100%
PC 78 48 78 48
PE 20 20 20 20
PS 0 30 0 30
PIP2 2 2 2 2

Figure S5

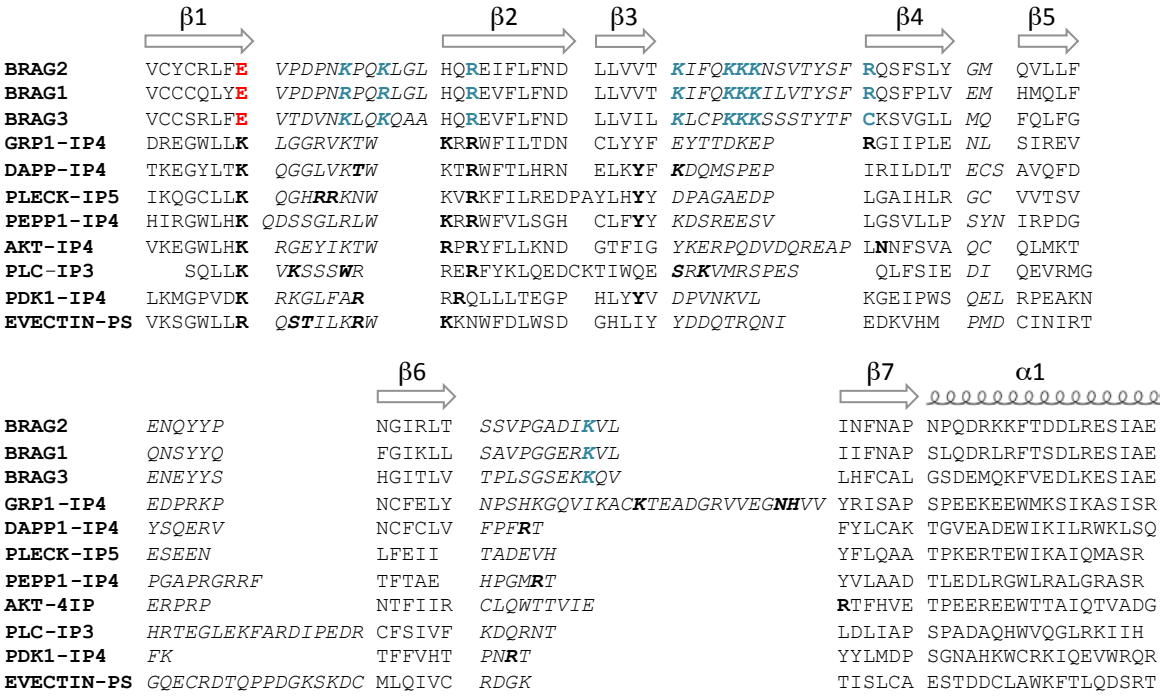
β1 β2 β3 β4 β5
BRAG2 VCYCRLFE VPDPNKPQKLGL HQREIFLFND LLVVT KIFQKKKNSVTYSF RQSFSLY GM QVLLF
BRAG1 VCCCQLYE VPDPNRPQRLGL HQREVFLFND LLVVT KIFQKKKILVTYSF RQSFPLV EM HMQLF
BRAG3 VCCSRLFE VTDVNKLQKQAA HQREVFLFND LLVIL KLCPKKKSSSTYTF CKSVGLL MQ FQLFG
GRP1-IP4 DREGWLLK LGGRVKTW KRRWFILTDN CLYYF EYTTDKEP RGIIPLE NL SIREV
DAPP-IP4 TKEGYLTK QGGLVKTW KTRWFTLHRN ELKYF KDQMSPEP IRILDLT ECS AVQFD
PLECK-IP5 IKQGCLLK QGHRRKNW KVRKFILREDPAYLHYY DPAGAEDP LGAIHLR GC VVTSV
PEPP1-IP4 HIRGWLHK QDSSGLRLW KRRWFVLSGH CLFYY KDSREESV LGSVLLP SYN IRPDG
AKT-IP4 VKEGWLHK RGEYIKTW RPRYFLLKND GTFIG YKERPQDVDQREAP LNNFSVA QC QLMKT
PLC-IP3 SQLLK VKSSSWR RERFYKLQEDCKTIWQE SRKVMRSPES QLFSIE DI QEVRMG
PDK1-IP4 LKMGPVDK RKGLFAR RRQLLLTEGP HLYYV DPVNKVL KGEIPWS QEL RPEAKN
EVECTIN-PS VKSGWLLR QSTILKRW KKNWFDLWSD GHLIY YDDQTRQNI EDKVHM PMD CINIRT
β6 β7 α1
BRAG2 ENQYYP NGIRLT SSVPGADIKVL INFNAP NPQDRKKFTDDLRESIAE
BRAG1 QNSYYQ FGIKLL SAVPGGERKVL IIFNAP SLQDRLRFTSDLRESIAE
BRAG3 ENEYYS HGITLV TPLSGSEKKQV LHFCAL GSDEMQKFVEDLKESIAE
GRP1-IP4 EDPRKP NCFELY NPSHKGQVIKACKTEADGRVVEGNHVV YRISAP SPEEKEEWMKSIKASISR
DAPP1-IP4 YSQERV NCFCLV FPFRT FYLCAK TGVEADEWIKILRWKLSQ
PLECK-IP5 ESEEN LFEII TADEVH YFLQAA TPKERTEWIKAIQMASR
PEPP1-IP4 PGAPRGRRF TFTAE HPGMRT YVLAAD TLEDLRGWLRALGRASR
AKT-4IP ERPRP NTFIIR CLQWTTVIE RTFHVE TPEEREEWTTAIQTVADG
PLC-IP3 HRTEGLEKFARDIPEDR CFSIVF KDQRNT LDLIAP SPADAQHWVQGLRKIIH
PDK1-IP4 FK TFFVHT PNRT YYLMDP SGNAHKWCRKIQEVWRQR
EVECTIN-PS GQECRDTQPPDGKSKDC MLQIVC RDGK TISLCA ESTDDCLAWKFTLQDSRT

Figure S6

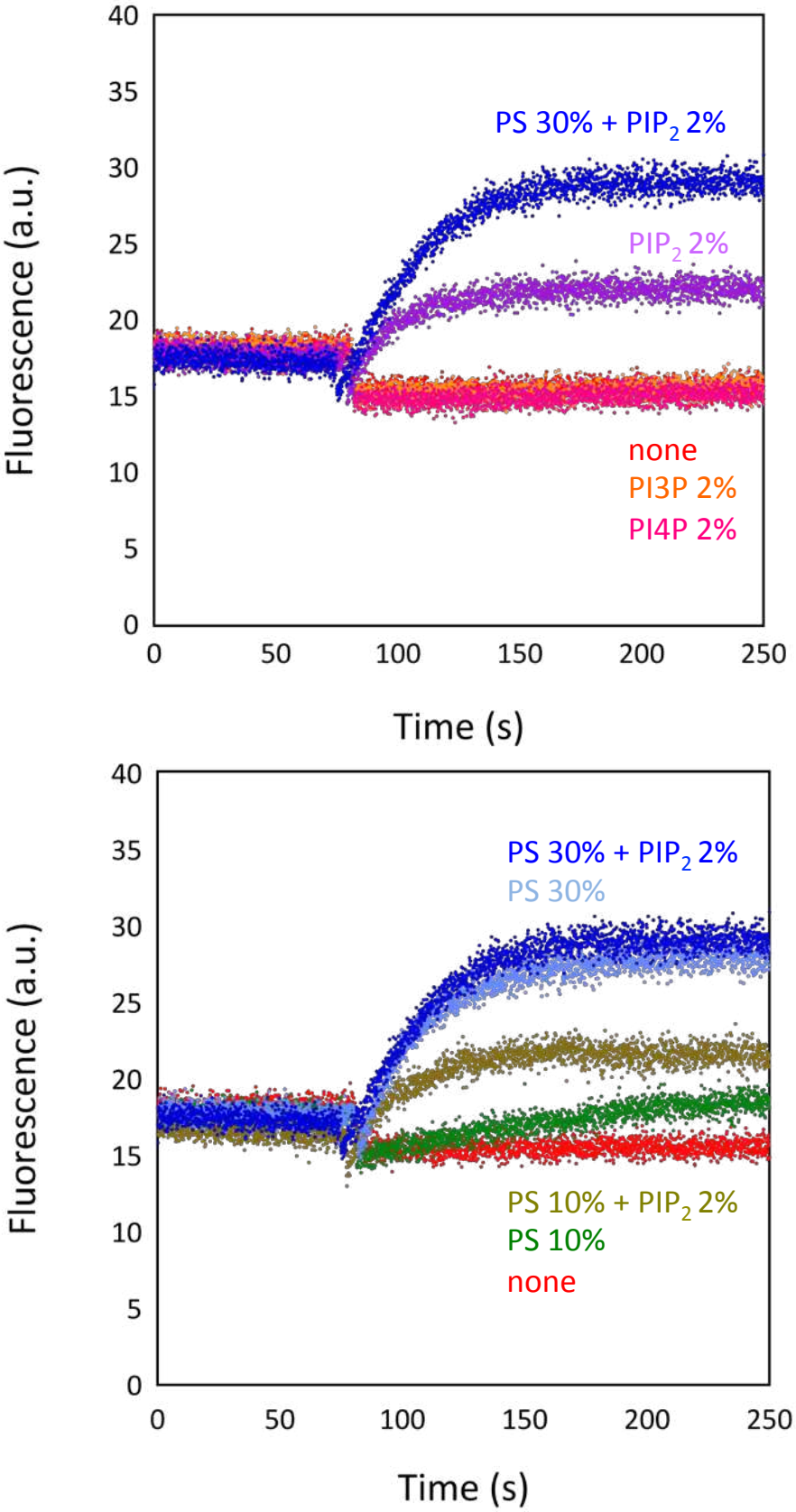
Fluorescence (a.u.)
Time (s)
PS 30% + PIP2 2%
PIP2 2%
none
PI3P 2%
PI4P 2%
PS 30% + PIP2 2%
PS 30%
PS 10% + PIP2 2%
PS 10%
none

Figure S7

SUPPLEMENTAL RESULTS

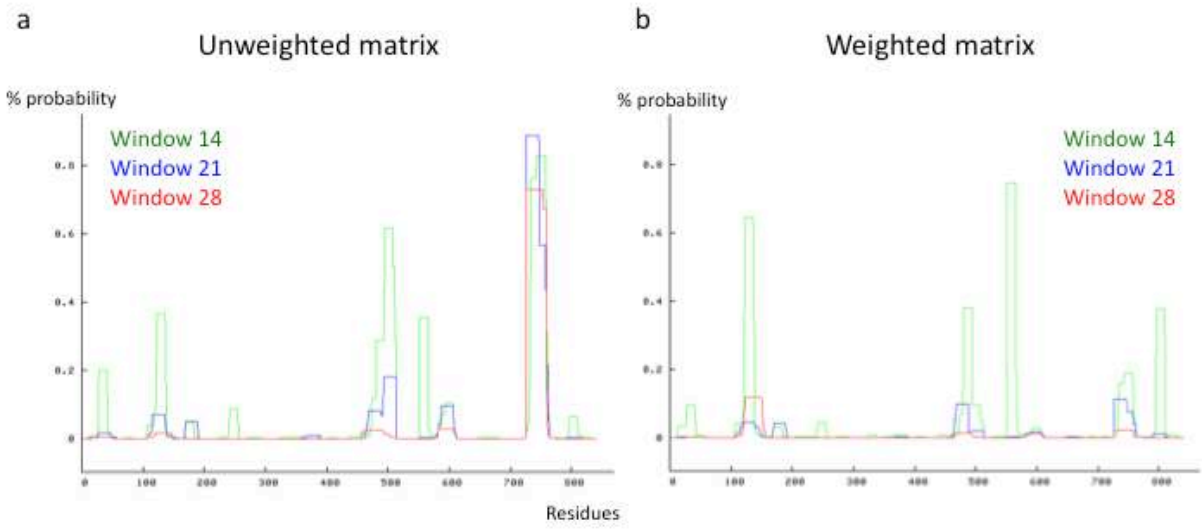

Figure 17: Coiled-coil prediction with COIL (Lupas *et al.*, Science 1991). A. Results obtained using the unweighted matrix. B. Results obtained using the weighted matrix. The 28-residue window in red was used here.

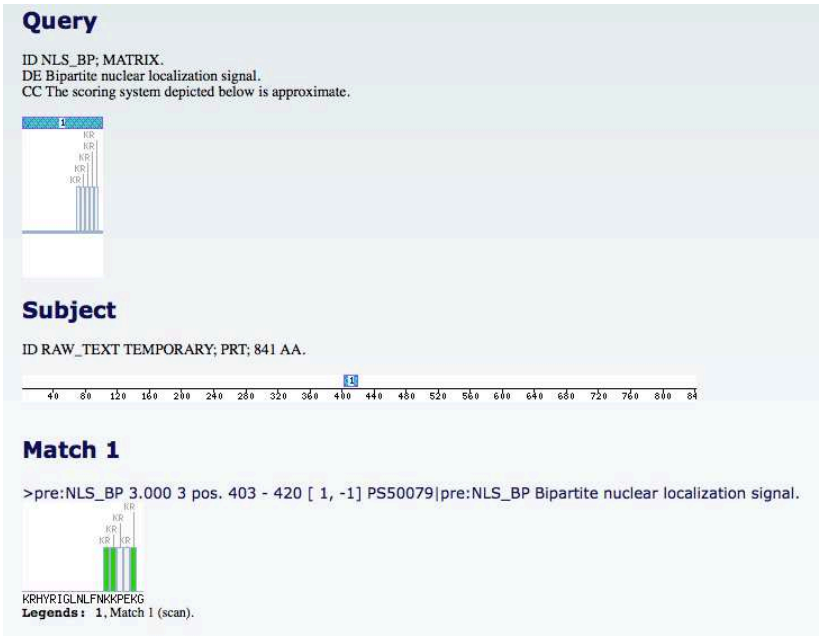

Figure 18: NLS prediction with the software « Pattern search » of « myHits » (http://myhits.isb-sib.ch/cgi-bin/pattern_search)

I. Bioinformatic study of BRAG2

In order to identify the different domains of BRAG2, a bioinformatic study was performed. First of all, the different domains present in the sequence were assessed using PROSITE and only a Sec7 domain and an IQ motif was identified. Then the SMART software (Schultz et al. 1998) was used to identify a PH domain **(Figure 1 of paper n°1)**. Other predictions showed that BRAG2 had a coiled coil motif (for review (Casanova 2007)). COILS software (Lupas *et al.*, Science 1991), was used to look for coiled-coil motifs. It predicted a coiled-coil at 70% probability (window 28) with an unweighted matrix **(Figure 17a)** and at 5% with a weighted matrix **(Figure 17b)**, which suggest that a coiled-coil structure is unlikely. The elevated score (70%) could be mainly due to the high incidence of charged residues. This observation is in agreement with the results showing neither dimerization in solution, nor in the crystal. Other predictions indicated the presence of NLS sequences in the Sec7 domain (Dunphy et al. 2006), however using the software « Pattern search » on the server « myHits », I could only find one NLS sequence in the Sec7 domain, amino acids 403 to 420 **(Figure 18 and 19)**.

An analysis of BRAG2 folding with the software FoldIndex was performed (**Figure 20)**. It showed that BRAG2 is well folded in the Sec7 domain, the PH domain and the linker regions **(Figure 20)**, which is in good agreement with the complex structure **(Figure 19)**. A secondary structure analysis of BRAG2 was performed with the software PSIPRED **(Annex 2)**. It is interesting to highlight that the helices of the Sec7 domain (residues 390 to 591) are approximately well predicted compared to the crystal structure, excepted for helix 8 (residues 518 to 524), which was not predicted **(Figure 19, Annex 2)**. The linker (residues 592 to 629) has also been predicted as a helix for the most part, which is coherent with what I observe in the structure (for residues 596 to 606) **(Figure 19, Annex 2)**. On the contrary, the PH domain prediction differs from the crystal structure. Indeed, two β strands of my structure are predicted as helices (residues 632-635 and 662-664 of **Annex 2**).

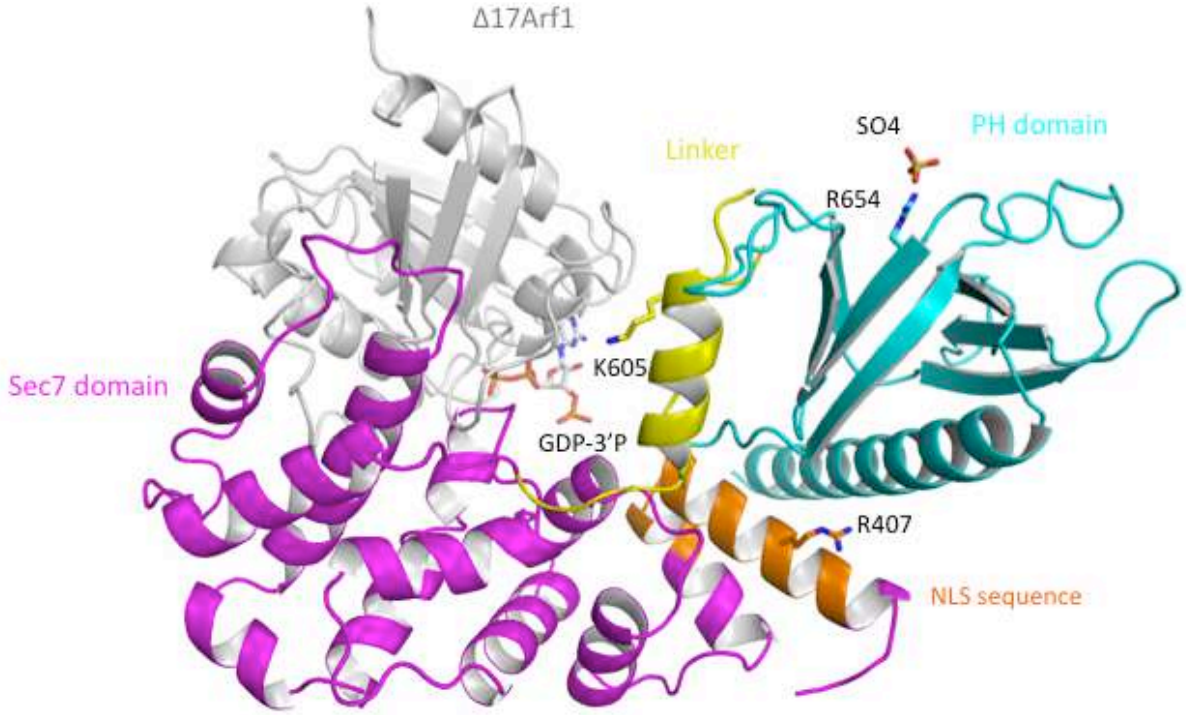

Figure 19: Structure of Δ17Arf1/BRAG2^{E498K} complex. The Sec7 domain is represented in magenta, the PH domain in cyan, the linker in yellow, the predicted NLS sequence in orange and Δ17Arf1 in grey. The three residues that were mutated are represented in sticks (R407 in orange, K605 in yellow and R654 in blue).

A

Summary:
Number Disordered Regions: 12
Longest Disordered Region: 179
Number Disordered Residues: 474
Predicted disorder segment: [1]-[60] length: 60 score: -0.16 ± 0.07
Predicted disorder segment: [111]-[115] length: 5 score: -0.02 ± 0.02
Predicted disorder segment: [117]-[122] length: 6 score: -0.04 ± 0.02
Predicted disorder segment: [130]-[233] length:104 score: -0.11 ± 0.05
Predicted disorder segment: [235]-[413] length:179 score: -0.22 ± 0.09
Predicted disorder segment: [419]-[427] length: 9 score: -0.04 ± 0.03
Predicted disorder segment: [435]-[440] length: 6 score: -0.04 ± 0.03
Predicted disorder segment: [562]-[589] length: 28 score: -0.09 ± 0.04
Predicted disorder segment: [603]-[608] length: 6 score: -0.03 ± 0.02
Predicted disorder segment: [718]-[723] length: 6 score: -0.03 ± 0.01
Predicted disorder segment: [725]-[773] length: 49 score: -0.10 ± 0.05
Predicted disorder segment: [786]-[801] length: 16 score: -0.06 ± 0.04

```
   1 MLERRYGGNL VTKHAARTIQ TAFRQYQMNK NFERLRSSMS EKNMSNRIVL
  51 SNMRMQFSFE GPEKVESSIF EGKQVSVIMD GSQLGALVSP ECGDLSEPTT
 101 LKSPAPSSDF ADAITELEDA FSRQVKSLAE SIDDALNCRS LHTEEAPALD
 151 AARARDTEPQ TALSGMDHNK LDEMTASYSD VTLYIDEEEL SPPLPLSQAG
 201 DRPSSTESDL RLNAGGAAPD YWALARKEDK ADTDTSCRST PSLERQEQKL
 251 RVEMLPLLTI EPPSDSSVDL SDRSERGSLK RQSAYERSLG GQQGSPKSGP
 301 HSGAPKSLPR EEPELRPRPP RPLDSHLAIN GSANRQSKSE SDYSDGDNDS
 351 INSTSNSNDT INCSSESSSR DSLREQTLSK QTYHKEANNS WDSPAFSNDV
 401 IRKRHYRIGL NLFNKKPEKG VQYLIERGFV PDTPVGVAHF LLQRKGLSRQ
 451 MIGEFLGNRQ KQFNRDVLDC VVDEMDFSTM ELDEALRKFQ ARIRVQGEAQ
 501 KVEKLIEAFS QRYCICRPGV VRQFRNPDTI FILAFAIILL NTDMYSPNVK
 551 PEKKMKLEDF IKNLRGVDDG EDIPREMLNG IYERIRKREL KTNEDHVSQV
 601 QKVEKLIVGK KPIGSLRPGL GCVLSLPERR LVCICRLFEV PDPNKPQKLG
 651 LRQREIFLFN DLLVVTKIFQ KKKNSVTYSF RQGFSLYGMQ VLLFENQYYP
 701 NGIRLTSSVP GADIKVLINF NAPNPQDRKK FTDDLRESIA EVQEMEKNRI
 751 ESELEKQKGV VRPSMSQCSS LEKESGNGTL SNACLDDSYA SGEGLKRSAL
 801 SSSLRDLSEA GKRGRRSSAG SLESNVEFQP FEPLQPSVLC S

( Predicted disordered segment )
```

B

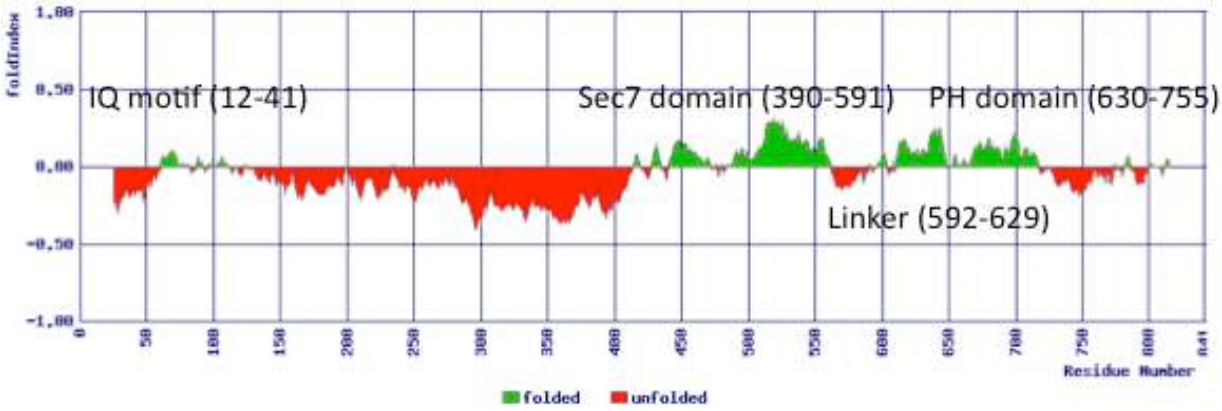

Figure 20: Folding prediction of BRAG2 with FoldIndex (http://bip.weizmann.ac.il/fldbin/findex/). In red are represented the unfolded regions and in green the folded regions. B. The numbers in brackets represent the residue numbers forming the domains.

II. Characterization of BRAG2 mutants

A. The case of BRAG2^{E498K} mutant

The mutation of the catalytic glutamate has been shown to abolish the activity of ARNO on Arf1 in solution and to trap an abortive Arf1-GDP/ARNO^{E156K} complex (Beraud-Dufour et al. 1998). We wanted to use the same strategy to trap the equivalent Arf/BRAG2 complex.

In order to characterize BRAG2^{E498K} mutant, circular dichroism experiments were performed to assess its secondary structure. The experiment was done at 20°C with 2 µM of mutant in 200 µl of buffer 50 mM $NaHPO_4/NaH_2PO_4$ and 50 mM NaF. The result showed that BRAG2^{E498K} was folded with well-defined pics at 220 and 210 nm, which is characteristic of a protein with a majority of helices **(Figure 21a)**. A denaturing test was performed between 4°C and 70°C and showed that the mutant was relatively stable with a Tm of 54°C **(Figure 21a inset)**, similar to the wild type forms **(Figure 21b and c insets)**.

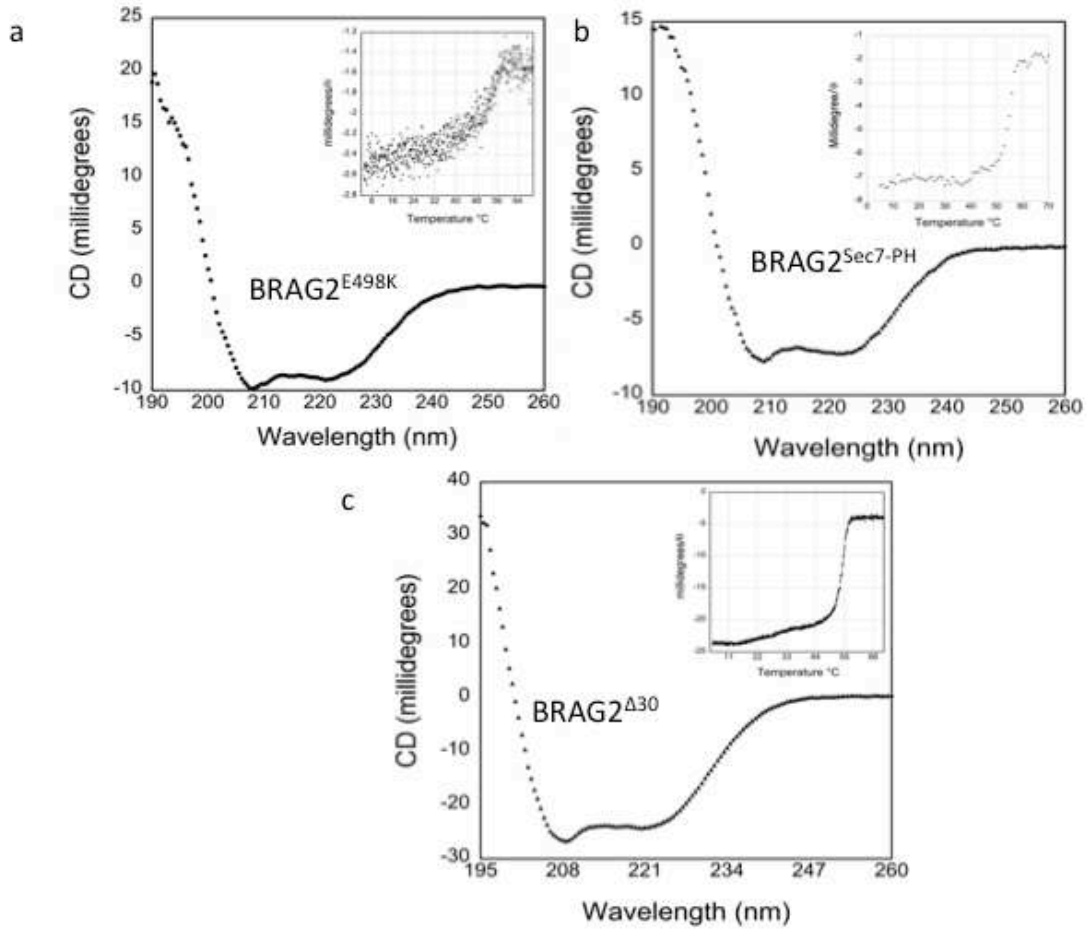

Figure 21: BRAG2^{E498K} is well folded and stable. CD experiments of A. BRAG2^{E498K} B. BRAG2$^{Sec7\text{-}PH}$ C. BRAG2$^{\Delta 30}$. Insets represent denaturing tests.

In order to assess the activity of BRAG2^{E498K}, kinetic experiments were performed by fluorescence spectroscopy as described in **Annex 3**. The experiments were done in duplicate at 37°C with 1 µM of Δ17Arf1, 0.1 µM of BRAG2^{E498K}, 0.1 µM of BRAG2$^{Sec7\text{-}PH}$ as a control and 100 µM of GTP in 800 µl of a prewarmed buffer (50 mM HEPES pH 7.4, 300 mM NaCl, 2 mM β-mercaptoethanol, 2 mM $MgCl_2$). The proteins were added sequentially as described in **Figure 22**. We observed that the mutation abolished the activity of BRAG2, with a rate about 7-fold lower than the wild type and similar to the one of the spontaneous exchange.

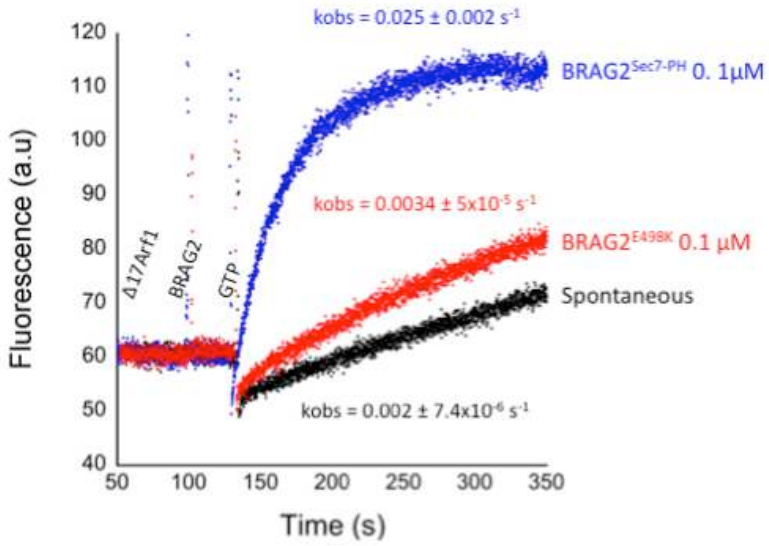

Figure 22: E498K mutation abolishes BRAG2 exchange activity in solution

In order to see if the BRAG2^{E498K} had a competitive effect on the activity of BRAG2$^{Sec7\text{-}PH}$, the same experiment was performed except that 0.1 µM of BRAG2$^{Sec7\text{-}PH}$ was added before the addition of either 1 µM of BRAG2^{E498K} or buffer as a control. The experiment was done only once. The results show that it seems to be a slight positive effect of BRAG2^{E498K} mutant on the rate constant of BRAG2$^{Sec7\text{-}PH}$ in solution **(Figure 23)**. Under those conditions, there is no competitive effect of BRAG2^{E498K}.

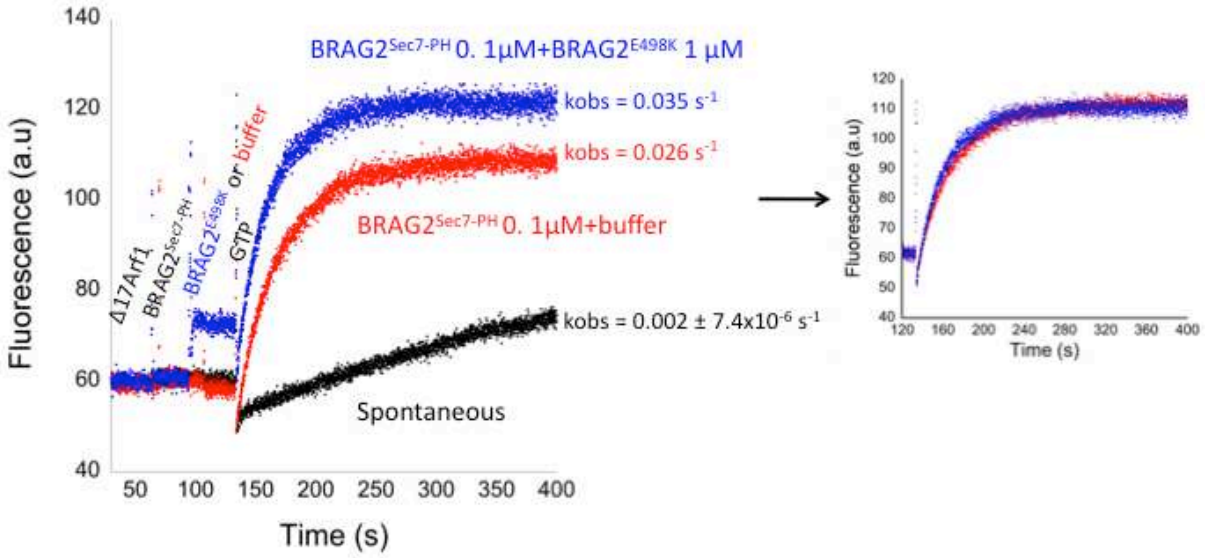

Figure 23: No competitive effect of BRAG2^{E498K} on the activity of BRAG2$^{Sec7\text{-}PH}$ in solution. The rate constants (kobs) of each reaction are represented in blue, red and black. The inset represents the superposition of the curves with BRAG2$^{Sec7\text{-}PH}$ and BRAG2^{E498K} (in blue), and BRAG2$^{Sec7\text{-}PH}$ and buffer (in red).

The same experiments were done in the presence of liposomes to see if membranes had an effect on the behavior of BRAG2^{E498K}. The experiments were done in duplicate at 37°C with 0.4 µM of myrArf1, 0.4 µM of BRAG2^{E498K}, 1 nM of BRAG2$^{Sec7\text{-}PH}$ as a control, 100 µM of GTP and 100 µM of plasma membrane-like liposomes extruded at 0.2 µm (see paper n°1 for composition) in 800 µl of a prewarmed buffer (50 mM HEPES pH 7.4, 120 mM K-acetate, 1 mM DTT, 1 mM $MgCl_2$). The proteins were added sequentially as described in **Figure 24**. **Figure 24** shows that the addition of BRAG2^{E498K} not only killed the exchange activity in the presence of liposomes but also leads to a decrease of the fluorescence. The appearance of the curve could be due in these conditions, either to some aggregation, which has to be verified with DLS, or to the fact that BRAG2^{E498K} sequestrate myrArf1-GDP in an alternative state, as seen in the structure of (Renault et al. 2003). The fact that this decrease of fluorescence is not visible in solution could be due to the difference of substrates (Δ17Arf1, myrArf1) or to the presence of membranes.

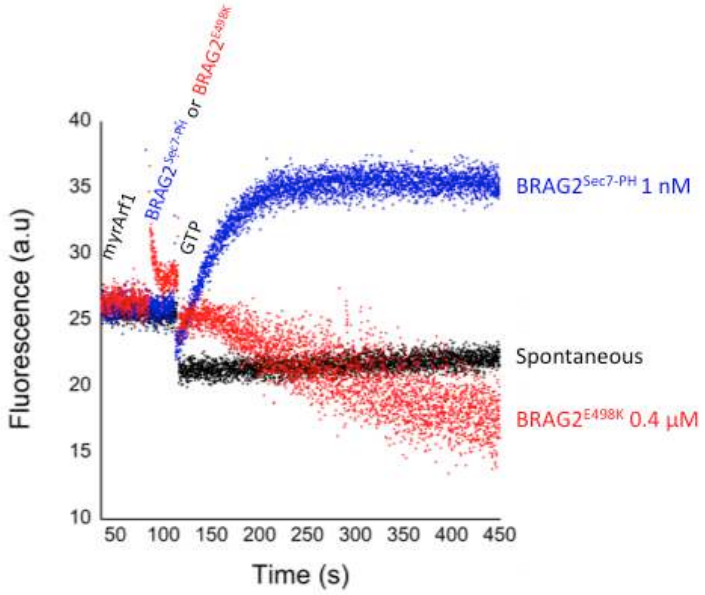

Figure 24: E498K abolishes BRAG2 exchange activity on membranes

To go further in the characterization of BRAG2^{E498K}, and see if there was a competition between BRAG2$^{Sec7\text{-}PH}$ and BRAG2^{E498K} in the presence of membranes, the same experiment was performed except that after the addition of 1 nM of BRAG2$^{Sec7\text{-}PH}$, 0.4 µM of BRAG2^{E498K} or of buffer was added. This experiment was only done once **(Figure 25)**. The same decrease of fluorescence induced by BRAG2^{E498K} was observed in the presence of BRAG2$^{Sec7\text{-}PH}$.

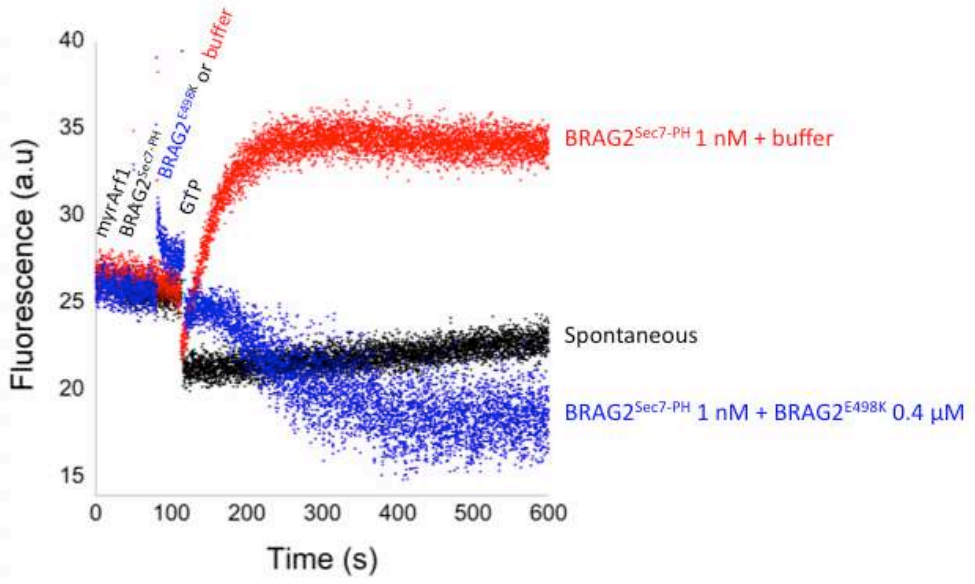

Figure 25: Competition of BRAG2^{E498K} on the activity of BRAG2$^{Sec7\text{-}PH}$ on membranes

Finally, to assess if BRAG2^{E498K} had an effect on myrArf1-GTP, myrArf1-GTP was formed at the membrane as above, before the addition of 0.4 µM of BRAG2^{E498K}. Figure 26 shows that addition of BRAG2^{E498K} induced a fast decrease of the fluorescence, which return to the basal state in less than 10 seconds. This was really surprising and difficult to reconcile with a mechanism where BRAG2^{E498K} will bind to myrArf1-GTP, expel the nucleotide and somehow favor the binding of the GDP. We cannot exclude that BRAG2^{E498K} sequestrates myrArf1-GTP in an alternative conformation, but aggregation also appears as a very likely scenario.

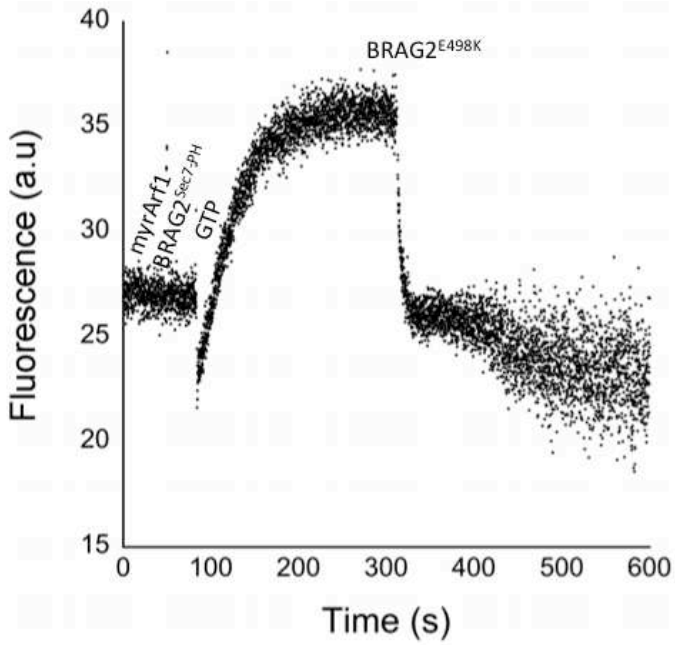

Figure 26: Competition between BRAG2^{E498K} and BRAG2$^{Sec7\text{-}PH}$ for the binding of myrArf1-GTP on membranes. The experiment was only done once.

B. Effects of BRAG2^{R407E}, BRAG2^{K605E} and BRAG2^{R654E} mutants

After the resolution of the Δ17Arf1/BRAG2^{E498K} complex structure, the following questions arose: does the linker region contribute to Arf1 binding? Is the PIP_2 essential for the activity of BRAG2 and is the Sec7/PH interaction essential for the stability and activity of BRAG2? To answer these questions we proposed three mutations: R407E, which is located in the interface between the C-terminal helix of the PH domain, K605E, which belongs to the linker and could interact with Arf1 and play a role in the exchange activity, and R654E, which is in the PIP-binding site **(Figure 19)**. These mutations were done using BRAG2$^{Sec7\text{-}PH}$ as template. We could not express the BRAG2^{R407E} mutant, suggesting that the protein with a glutamate in position 407 is probably not correctly folded. We expressed and purified

BRAG2^{K605E} and BRAG2^{R654E} with a good yield and we determined their kcat/Km as described in paper n°1. Both mutants had a catalytic efficiency on both Arfs similar to the wild type in solution **(Figure 27 a and b)**. Furthermore, mutant K605E increased the activity of about 1.3 fold on membranes with Arf1 and mutant R654E decreased this activity of about 1.5 fold **(Figure 27 a and b)**, which is not significant. Activation rate constants for myrArf6 could not be measured because of the atypic fluorescence change profile (see figure S4-A of paper n°1), we then represented the initial velocities as a function of BRAG2 concentration. As the wild type, the curves were linear, but with a lower slope **(Figure 27 c)**. This suggests that these mutants have a lower activity on myrArf6 in the presence of membranes, which was not observed with myrArf1 (data not shown).

a

kcat/Km (10^5 $M^{-1}s^{-1}$)	Δ17Arf1	Δ13Arf6	myrArf1
BRAG2$^{Sec7-PH}$	2.4 ± 0.1	0.47 ± 0.13	**390 ± 31**
BRAG2^{K605E}	2 ± 0.03	0.35 ± 0.05	517 ± 3.1
BRAG2^{R654E}	2.55 ± 0.014	0.36 ± 0.02	265 ± 20

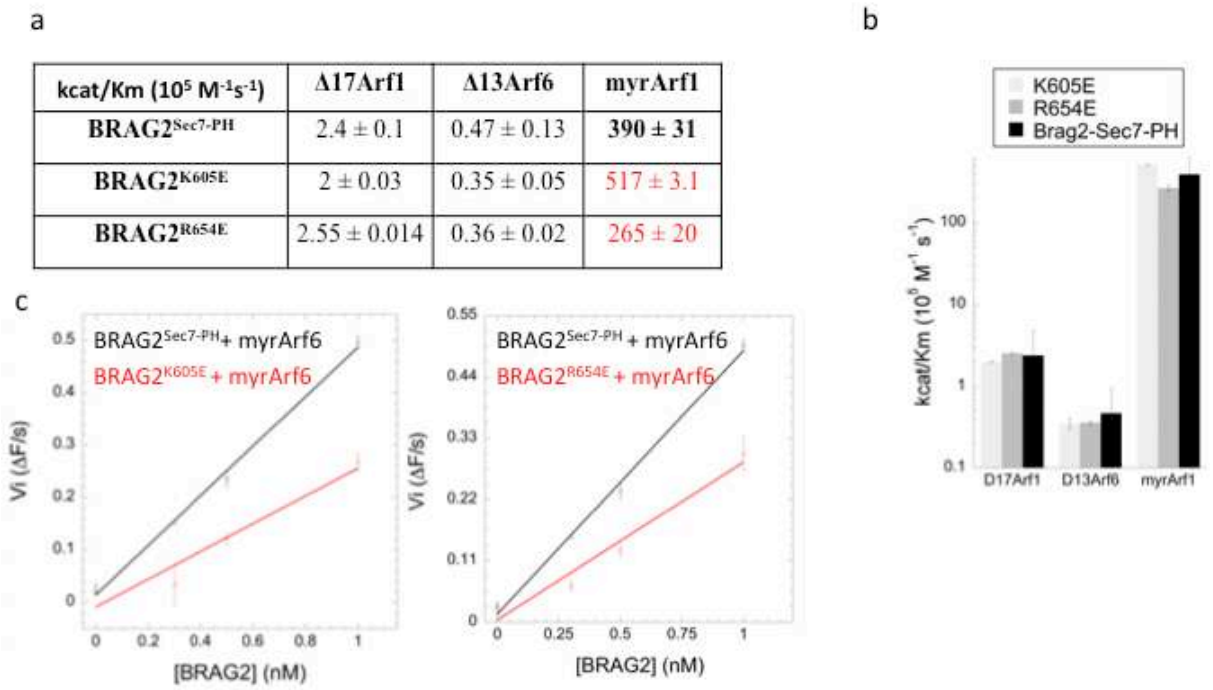

Figure 27: A single mutant in the linker region or in the PIP-binding site did not allow to perturb the exchange activity. A. Measure of the kcat/Km of both mutants in solution with Δ17Arf1 and Δ13Arf6 and in presence of liposomes with myrArf1. B. kcat/Km values represented in bars. C. Mutants and wild type BRAG2 initial velocities as a function of the concentrations of BRAG2.

III. Crystallization assays of BRAG2

Several screens were performed in order to crystallize BRAG2 alone. PEG screens, $AmSO_4$ screens, $JCSG^+$ screens from Qiagen were tested, which only led to small and thin needle-like crystals **(Figure 28 a)**. They were optimized with salt concentration gradients, protein concentration gradients, PH gradients, agarose, glycerol, different temperatures (4°C, 18°C), seeding, additives and proteolysis. These needles were tested on Synchrotron and diffracted as protein. $BRAG2^{E498K}$ was also tested for crystallization, and gave needle-like crystals even after optimization. These needles were also tested on Synchrotron and diffracted as protein but the low resolution prevented further analysis **(Figure 28 b)**.

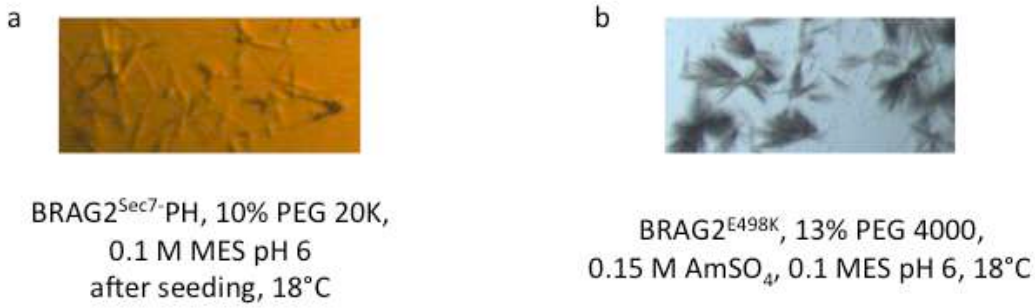

Figure 28: Needle-like crystals obtained for $BRAG2^{Sec7\text{-}PH}$ and $BRAG2^{E498K}$. A. Needle-like crystals of $BRAG2^{Sec7\text{-}PH}$ obtained after seeding at 18°C in 10% PEG 20K and 0.1 M MES PH 6. B. Needle-like crystals of $BRAG2^{E498K}$ obtained after optimization at 18°C in 13% PEG 4000, 0.15 M $AmSO_4$ and 0.1 M MES pH 6.

Crystallization assays with the nucleotide free complex Δ17Arf1-$BRAG2^{Sec7\text{-}PH}$ were performed as well. The proplex screen of Qiagen was used, followed by optimization with salt concentration gradients, protein concentration gradients, PH gradients and seeding, but only urchin-like crystals were obtained. They were tested on Synchrotron and diffracted as protein but the low resolution prevented further analysis **(Figure 29)**.

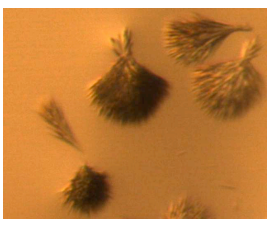

Figure 29: Urchin-like crystals obtained for nucleotide free complex Δ17Arf1-$BRAG2^{Sec7\text{-}PH}$. Obtained with proplex screen (Qiagen) in condition 0.1 M KCl, 0.1 M Tris pH 8, 15% PEG 2000 MME.

IV. Preparation of Arf6/BRAG2 complexes

The Δ13Arf6/BRAG2 complexes were prepared as described in paper n°1 for the Δ17Arf1/BRAG2 complexes, namely either with alkaline phosphatase to form the stable nucleotide free complex **(Figure 30 a)** or with BRAG2^{E498K} to form a stable ternary complex **(Figure 30 b)**. BRAG2 was not able to form a tight complex with Δ13Arf6 under these conditions. One could notice that the putative complex in both cases is eluted after BRAG2 alone and before Δ13Arf6-GDP alone **(Figure 30)**, which is not what we observe with the Δ17Arf1/BRAG2 complexes **(see Figure 1 paper n°1)**.

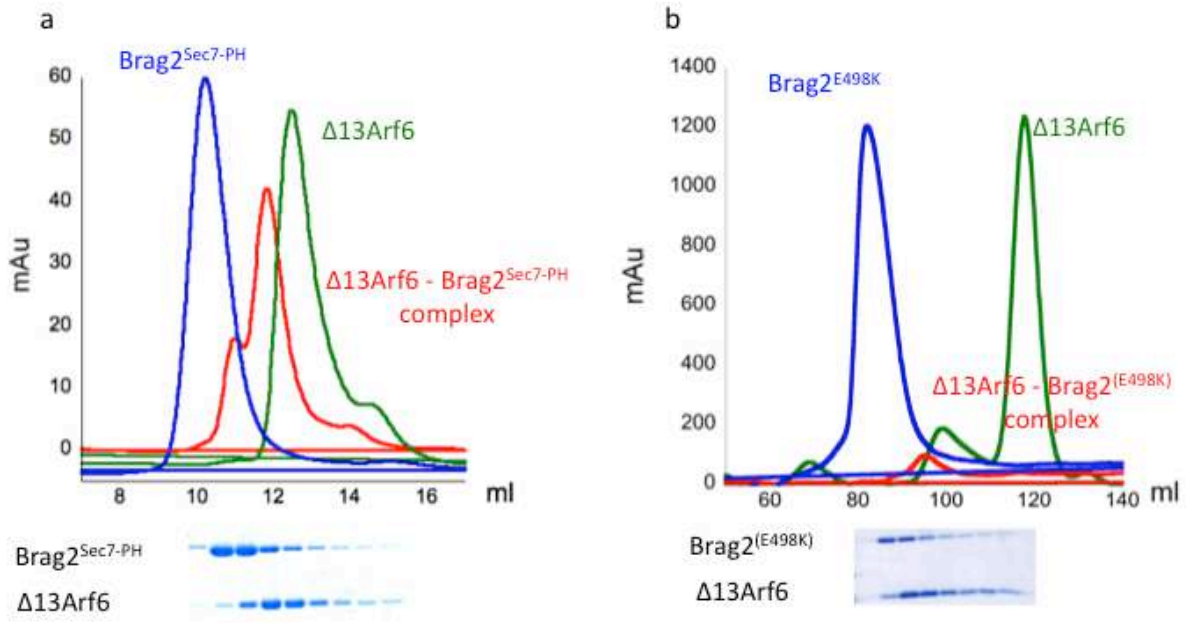

Figure 30: Reconstitution of the Δ13Arf6/Brag2 complexes. A. Gel filtration analysis of Δ13Arf6 (in green), Brag2$^{Sec7-PH}$ (in blue) and Δ13Arf6-Brag2$^{Sec7-PH}$ complex (in red), after formation of the complex in a ratio 2:1 (Arf:BRAG2) by elimination of GDP with alkaline phosphatase. Elution buffers are as follows: 20 mM HEPES pH 7.4, 150 mM NaCl; 4 mM BME, 5 mM EDTA for Brag2$^{Sec7-PH}$ alone and for the complex, and 20 mM HEPES pH 7.4, 100 mM NaCl; 5 mM BME for Δ13Arf6 alone. B. Gel filtration analysis of Δ13Arf6 (in green), Brag2^{E498K} (in blue) and Δ13Arf6-Brag2^{E498K} complex (in red) in a ratio 2:1. Elution buffers are as follows: 20 mM HEPES pH 7.4, 100 mM NaCl; 2 mM BME, 200 µM GDP for the complex, 20 mM HEPES pH 7.4, 100 mM NaCl; 5 mM BME for Brag2^{E498K} and 20 mM HEPES pH 7.4, 100 mM NaCl; 5 mM BME for Δ13Arf6 alone.

Crystallization assays were also performed, but they led to the formation of Δ13Arf6-GDP crystals, which were used to resolve the structure of the unfolded conformation of Δ13Arf6-GDP (see paper n°2). This unfolded conformation of Δ13Arf6 could explain its atypical behavior of elution. Indeed, Δ13Arf6 in this conformation is elongated so could be eluted in complex with BRAG2 at a lower molecular weight.

V. Preliminary studies of inhibitors

In collaboration with Bob St-Onge in Stanford, we tested inhibitors initially found from chemogenomic screen. Our collaborators found one compound, Si1, and designed analogs, Si2 to Si9, that could be of interest. Six of them were tested for their effect on the rate constants (kobs) of the exchange reaction between BRAG2$^{\Delta 30}$ and myrArf1 in presence of membrane-like liposomes. The experiment was done at 37°C in 800 µl of a buffer containing 50 mM HEPES pH 7.4; 120 mM K acetate; 1 mM $MgCl_2$ and 1 mM DTT. The final concentration of the inhibitors was 200 µM. BRAG2$^{\Delta 30}$ was used at a final concentration of 1 nM, myrArf1 at 0.4 µM, the liposomes were extruded at 0.2 µm and used at 100 µM, and the reaction was started with 100 µM GTP. First buffer containing myrArf1, liposomes and inhibitors (or DMSO) were incubated 2 minutes and the acquisition was started. Then BRAG2 was added for 30 seconds and the reaction was activated with GTP. The experiment was done only once **(Figure 31)**. It seems that Si1, Si3, Si5 and Si9 are efficient inhibitors of BRAG2$^{\Delta 30}$ activity in presence of membrane.

Inhibitors	kobs
DMSO	0,041
Si1	0,0055892
Si2	0,026899
Si3	0,0054358
Si4	0,03309
Si5	0,010792
Si9	0,00025366

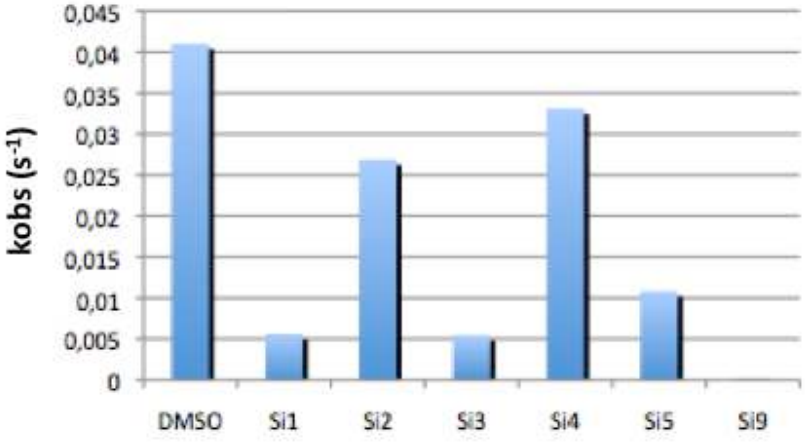

Figure 31: Characterization of BRAG2 inhibitors

First attempts of BRAG2$^{Sec7\text{-}PH}$ and Si1 (1 mM) co-crystallization assays in PEG, JCSG^{+}, and classic screens from Qiagen were also performed. Under these conditions no crystals appeared. The next step could be to co-crystallize Si1 and the Arf1-GDP/BRAG2 complex or to soak Arf1-GDP/BRAG2 crystals with an Si1 solution.

VI. Preliminary studies of CATY peptide from AMPA receptor

We started a collaboration with Hans-Christian Kornau, who recently showed that AMPA receptors directly interact via the GluA2 subunit with the synaptic protein BRAG2 and that BRAG2-mediated catalysis, controlled by ligand binding and tyrosine phosphorylation of GluA2, activates Arf6 to internalize synaptic AMPA receptors upon LTD induction. The interaction of regions encompassing the Sec7 and PH domains of BRAG2 with a 11 amino acid motif comprising 3 tyrosine residues of the GluA2 subunit was shown by yeast two-hybrid (Scholz et al. 2010). Kornau's group have shown using synthetic peptides encompassing the 3Y motif with either tyrosine or phosphotyrosine at position 876, that the unphosphorylated peptide increased the BRAG2 exchange rate, whereas the phosphorylated peptide did not. In this context we carried out crystallization trials of BRAG2 in presence of a peptide comprising these 11 amino acids with an additive cystein in N-terminus (**CATY**KEGYNVYG). This cystein can be used to mark the peptide. This peptide was named CATY. Kornau's group studied the regulation of BRAG2 activity in presence of membrane *in vitro* and we carried out its study in solution for crystallization purpose.

The first experiments were done in solution, at 37°C in 800 µl of buffer containing 50 mM Hepes pH 7.4; 50 mM NaCl; 2 mM $MgCl_2$; 2 mM BME and with 0.1 µM of $BRAG2^{\Delta 30}$ or $BRAG2^{Sec7}$, 1 µM of Δ13Arf6, 10 µM or 100 µM of CATY and the reaction was started with 100 µM of GTP. The buffer was prewarmed at 37°C, then the components of the reaction were added sequentially in the order described in **Figure 32**. As a control, one point was also done with Δ13Arf6 and CATY (10 µM) without BRAG2 **(Figure 32a last line)**. These preliminary results did not show a significative effect of CATY on BRAG2 activity in solution, but we still performed first attempts of $BRAG2^{E498K}$ and CATY peptide (1 mM) co-crystallization assays in PEG screen. $BRAG2^{E498K}$ was used in these experiments because alone, the mutant crystallized better than the wild type. But no crystals appeared in the screen. This could be because of the mutation of BRAG2, so crystallization assays with BRAG2 wild type or with a complex Arf/BRAG2 would be the next step.

a

kobs (10^{-3} s^{-1})	$BRAG2^{Sec7\text{-}PH\text{-}S30}$	$BRAG2^{Sec7}$
Spontaneous Δ13Arf6	3	3
Δ13Arf6 + BRAG2	6.6	6
Δ13Arf6 + BRAG2 + CATY 10 µM	7.2	4.9
Δ13Arf6 + CATY 10 µM + BRAG2	8.2	5.2
Δ13Arf6 + CATY 100 µM + BRAG2	7.7	ND

Δ13Arf6 + CATY 10 µM without BRAG2	3.6

b

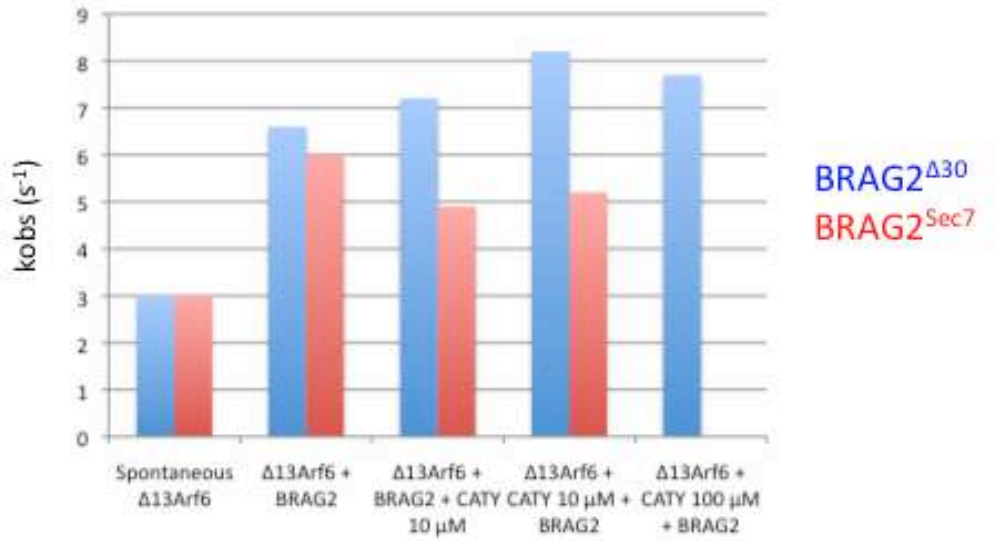

Figure 32: CATY peptide does not have an effect on BRAG2 activity in solution. A. The experiments are described in the first column with the order in which the components of the reactions were added. The additional line represents the control experiment with Δ13Arf6 and CATY without BRAG2. B. The values of the table are represented by a histogram. The experiments were done only once.

SAXS and X-ray crystallography suggest an unfolding model for the GDP/GTP conformational Switch of the Small GTPase Arf6 (publication n°2)

Valérie Biou, Kaheina Aizel, Pierre Roblin, Aurélien Thureau, Eric Jacquet, Sebastian Hansson, Bernard Guibert, Eric Guittet, Carine van Heijenoort, Mahel Zeghouf, Javier Perez and Jacqueline Cherfils

I. Résumé

Comment des isoformes de protéines très homologues peuvent-elles arborer des fonctions si différentes dans la cellule ? Arf1 et Arf6 sont très similaires: elles partagent plus de 60% d'identité de séquence et des études structurales ont montrées que les surfaces qu'elles utilisent pour interagir avec leurs régulateurs et leurs effecteurs sont essentiellement identique en structure et en séquence. Cependant, elles possèdent des fonctions différentes dans la cellule. Arf1 est un régulateur majeur de la plupart des aspects du trafic vésiculaire, alors qu'Arf6 est restreint à la membrane plasmique où il agit sur le trafic endosomal et le remodelage du cytosquelette (D'Souza-Schorey and Chavrier 2006). De façon consistante avec leur spécificité cellulaire, Arf1 et Arf6 ont des propriétés biochimiques différentes *in vitro* (Zeeh et al. 2006), pour lesquelles aucune explication structurale n'est à l'heure actuelle disponible.

L'activation des protéines Arf se fait en plusieurs étapes qui impliquent le recrutement d'Arf-GDP depuis le cytoplasme aux membranes, suivi par l'échange GDP/GTP. Nous montrons dans ce papier, qu'un mutant d'Arf6 tronqué de son extrémité N-terminale, mimant un état lié à la membrane, est partiellement déplié dans le cristal comparé à la forme entière cytosolique d'Arf6. Des expériences de SAXS, ont montré que cette conformation inhabituelle d'Arf6-GDP est l'espèce majoritaire en solution. Par ailleurs, des expériences de RMN ont montré que le mutant équivalent d'Arf1 est essentiellement identique à la forme entière cytosolique d'Arf1-GDP (Buosi et al. 2010). Ces expériences suggèrent donc que le chemin structural de l'activation d'Arf1 et d'Arf6 diverge au moment où Arf-GDP est recruté à la membrane, avant la réaction d'échange. Ces différences pourraient expliquer en partie les différences biochimiques entre Arf1 et Arf6 et pourraient en partie conduire à leur spécificité fonctionnelle.

doi:10.1016/j.jmb.2010.08.002 J. Mol. Biol. (2010) 402, 696–707

Contents lists available at www.sciencedirect.com

Journal of Molecular Biology

journal homepage: http://ees.elsevier.com.jmb

SAXS and X-ray Crystallography Suggest an Unfolding Model for the GDP/GTP Conformational Switch of the Small GTPase Arf6

Valérie Biou[1]*, Kaheina Aizel[1], Pierre Roblin[2], Aurélien Thureau[3], Eric Jacquet[3,4], Sebastian Hansson[1], Bernard Guibert[1], Eric Guittet[3], Carine van Heijenoort[3], Mahel Zeghouf[1], Javier Perez[2] and Jacqueline Cherfils[1]*

[1]*Laboratoire d'Enzymologie et Biochimie Structurales, Centre de Recherche CNRS de Gif-Sur-Yvette, Gif-sur-Yvette, France*
[2]*SOLEIL Synchrotron, L'Orme des Merisiers Saint-Aubin, Gif-sur-Yvette, France*
[3]*Institut de Chimie des Substances Naturelles, Centre de Recherche CNRS de Gif-Sur-Yvette, Gif-sur-Yvette, France*
[4]*IMAGIF, Centre de Recherche de Gif, CNRS, Gif-sur-Yvette Cedex, France*

Received 22 June 2010; received in revised form 29 July 2010; accepted 2 August 2010
Available online 13 August 2010

Edited by K. Morikawa

Keywords:
Small GTPases;
Arf;
Crystal structure;
SAXS;
NMR

The small GTPases Arf1 and Arf6 have nonoverlapping functions in cellular traffic despite their very high sequence and structural resemblance. Notably, the exquisite isoform specificity of their guanine nucleotide exchange factors and their distinctive sensitivity to the drug brefeldin A cannot be explained by any straightforward structural model. Here we integrated structural and spectroscopic methods to address this issue using Δ13Arf6-GDP, a truncated mutant that mimics membrane-bound Arf6-GDP. The crystal structure of Δ13Arf6-GDP reveals an unprecedented unfolding of the GTPase core β-strands, which is fully accounted for by small-angle X-ray scattering data in solution and by *ab initio* three-dimensional envelope calculation. NMR chemical shifts identify this structural disorder in Δ13Arf6-GDP, but not in the closely related Δ17Arf1-GDP, which is consistent with their comparative thermodynamic and hydrodynamic analyses. Taken together, these experiments suggest an unfolding model for the nucleotide switch of Arf6 and shed new light on its biochemical differences with Arf1.

Introduction

Small GTP-binding proteins of the Arf family are essential to most aspects of intracellular traffic (reviewed by D'Souza-Schorey and Chavrier[1]). Arf1 and Arf6 are the most studied of the five human Arf isoforms. Despite their high sequence homology (>60% identity), Arf1 and Arf6 have nonoverlapping functions in cells (reviewed by D'Souza-Schorey and Chavrier,[1] Gillingham and Munro,[2] and Donaldson and Honda[3]). Arf1 acts mostly at the Golgi, where it promotes the

*Corresponding authors. E-mail addresses: biou@lebs.cnrs-gif.fr; cherfils@lebs.cnrs-gif.fr.

Abbreviations used: ArfGEF, Arf-specific guanine nucleotide exchange factor; BFA, brefeldin A; GEF, guanine nucleotide exchange factor; Arf6-GDP^{FL}, full-length Arf6-GDP; HSQC, heteronuclear single quantum coherence; SAXS, small-angle X-ray scattering; SEC-MALS, size-exclusion chromatography–multiangle light scattering; 3D, three-dimensional; EDTA, ethylenediaminetetraacetic acid; PDB, Protein Data Bank.

0022-2836/$ - see front matter © 2010 Elsevier Ltd. All rights reserved.

recruitment of vesicular coats, while Arf6 functions at the plasma membrane, at the crossroads between trafficking and cytoskeleton processes. The separated localizations of Arf1 and Arf6 were thought for some time to account for their distinct functions in cells. However, recent studies revealed a previously overlooked promiscuity of Arf1 and Arf6 at the plasma membrane, where they may act in a signalling cascade in which both proteins require to be discriminated upon structural criteria.[4,5] In support of the hypothesis that Arf1 and Arf6 differ in their structural properties, *in vitro* studies have shown that Arf-specific guanine nucleotide exchange factors (ArfGEFs) of the EFA6 (exchange factor for *Arf6*) group have a strict specificity for Arf6,[6] and that while Arf1 is sensitive to the fungal drug brefeldin A (BFA), Arf6 is resistant to the drug.[7] Yet, the structures of Arf1-GDP[8] and Arf6-GDP[9] are highly similar, and those of Arf1-GTP[10] and Arf6-GTP[11] are almost indistinguishable. Furthermore, all residues in Arf1 that contact the ArfGEFs or BFA in the crystal structures of Arf1/ArfGEF complexes[10,12,13] are identical between Arf1 and Arf6. No straightforward physicochemical or structural model has been put forward to account for these exquisite specificities.

Dynamics is a more elusive aspect of protein structural "personalities," whose functional importance is increasingly being recognized (reviewed by Henzler-Wildman and Kern[14]). Structural dynamics is central to the conversion of Arf proteins from their inactive GDP-bound conformation to their active GTP-bound conformation. Their GDP/GTP switch involves a considerable conformational change, which has been proposed to ensure the allosteric propagation of information between their membrane-facing side and their nucleotide-binding site (reviewed by Pasqualato *et al.*[15]). A consistent structural model for Arf activation was established from biochemical and crystallographic analyses of spontaneous and guanine nucleotide exchange factor (GEF)-stimulated nucleotide exchange.[8–11,13,15–17] In this model, the myristoylated N-terminal α-helix locks strands β2–β3, which are part of the central β-sheet (the interswitch), in a retracted conformation in Arf-GDP, thereby maintaining Arf-GDP in a cytosolic form that cannot be activated by ArfGEFs. The first event of Arf activation is the binding of Arf-GDP to membranes by its N-terminal α-helix, which requires that the helix be displaced from the GTPase core. This movement unlocks the interswitch, thereby turning membrane-attached Arf-GDP into a substrate for ArfGEFs. ArfGEFs then promote a two-residue register shift of the interswitch, which recovers a conformation that can bind GTP, eventually allowing the replacement of GDP by GTP.

In this work, we sought out structural differences between Arf1 and Arf6 by analyzing the structural and spectroscopic properties of an Arf6 mutant that lacks the N-terminal α-helix, and by comparing them to those of the equivalent Arf1 truncation mutant. The truncated Arf1 mutant has been instrumental in deciphering the mechanism of the nucleotide switch (reviewed by Pasqualato *et al.*[18]). As the truncation of the helix mimics its displacement by membranes, nucleotide exchange can be monitored in solution with exchange kinetics close to those of myristoylated full-length Arf1 in the presence of membranes. It therefore provides a tractable model to study the transient steps of the Arf nucleotide switch that take place as Arf-GDP becomes membrane associated prior to its activation by ArfGEFs. Our analysis reveals the existence of an unexpected structural intermediate that is unique to Arf6 and may account for its unresolved functional specificities.

Results

Δ13Arf6-GDP is partially unfolded in the crystal

We solved the crystal structure of human Δ13Arf6-GDP at 1.8 Å resolution (Table 1). The asymmetric unit comprises two Arf6 subunits related by a pseudo-2-fold axis. Both subunits feature an unexpected rearrangement compared to full-length Arf6-GDP (Arf6-GDP^{FL})[9] (Fig. 1; representative electron density shown in Fig. S1 in Supplementary Data). Residues affected by structural changes extend from Lys34 in strand β1′, which corresponds to switch 1 in Arf-GDP structures, to Asn56 after strand β2 (interswitch) in the central β-sheet. The β1′–β2 region is essentially disordered in one Δ13Arf6-GDP subunit of the

Table 1. Crystallographic statistics

	Arf6-GDP
Data collection	
Space group	$P2_12_12_1$
Unit cell parameters *a*, *b*, *c* (Å)	38.47, 49.72, 143.07
Wavelength (Å)	0.98
Resolution range (inner shell) (Å)	41.0–1.82 (1.93–1.82)
Number of unique reflections	25,041 (3966)
Redundancy	5.3 (5.2)
Completeness (%)	97.7 (97.6)
R_{merge} (%)	7.0 (58.7)
$I/\sigma(I)$	14.5 (2.7)
Refinement statistics	
Resolution range (Å)	40.83–1.82
R/R_{free} (%)	17.05/19.54
Protein atoms	2500
Water molecules	172
Ligand	GDP
RMSD	
Bond length (Å)	0.010
Bond angle (°)	1.08

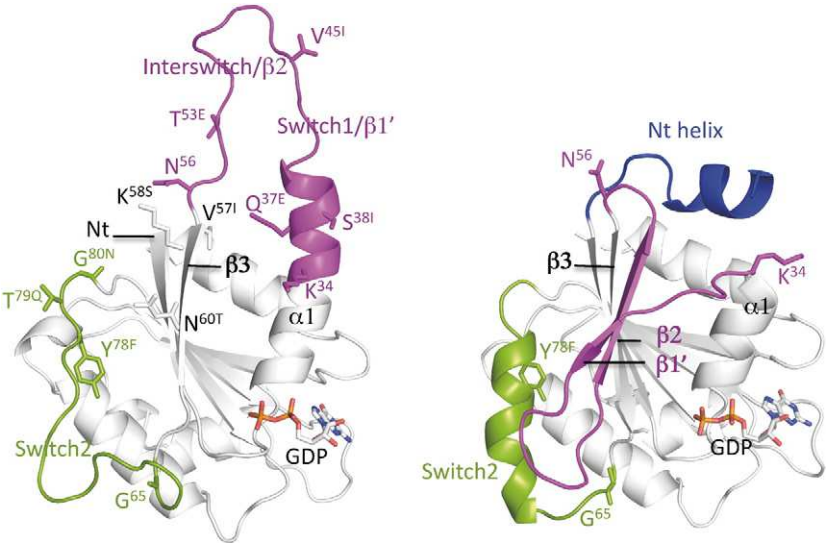

Fig. 1. Crystal structures of human Δ13Arf6-GDP (left) and Arf6-GDP^{FL} (right). The β1′–β2 strands are shown in magenta, switch 2 is shown in green, and the N-terminal helix in Arf6-GDP^{FL} is shown in blue. The sequence differences between Arf1 and Arf6 in the unfolded regions are indicated, with the Arf1 sequence in superscript. The volume occupied by the flexible region is compatible with membrane association. Coordinates of Arf6-GDP^{FL} are from PDB entry 1EOS.[9] All structures were drawn with PyMOL (The PyMOL Molecular Graphics System, Schrödinger, LLC).

asymmetric unit, while in the other subunit, β1′–β2 strands are converted into three helical turns extending from helix α1 followed by a long narrow loop that is loosely maintained by crystal contacts. This structural change brings residue Phe47 in switch 1 about 47 Å away from its position in Arf6-GDP^{FL}. It also triggers a distortion of the neighboring switch 2 and the α2–β4 loop (Gly65-Tyr78) by up to 8 Å. The rest of the structure is otherwise highly similar to Arf6-GDP^{FL}, including the GDP-binding site that lacks an associated Mg^{2+}, as seen in Arf6-GDP^{FL}.[9] Notably, strand β3 of the interswitch has not undergone the register shift needed to acquire the active Arf6-GTP conformation.[11] Interestingly, the pseudo-dimer buries a large surface area (4580 Å^2), which involves the newly exposed β3 strand and switch 2 (Fig. S2 in Supplementary Data), raising the possibility that the protein may exist as a functional dimer. Altogether, this is one of the largest conformational departures from the classical fold of a small GTPase. In order to establish whether the partially unfolded conformation and/or the pseudo-dimer of Δ13Arf6-GDP reflects its actual conformation in solution rather than crystalline artifacts, we analyzed next the structural disorder, shape, and spectroscopic properties of the protein in solution.

Δ13Arf6-GDP has the characteristics of a partially unstructured protein in solution

NMR chemical shifts provide a powerful means of detecting local disorder in proteins. The ^1H–^{15}N heteronuclear single quantum coherence (HSQC) spectrum of Δ13Arf6-GDP is shown in red in Fig. 2. It features a significant number of peaks that are too broad to be resolved individually, and a paucity of peaks in the ranges 8.5–10 ppm (^1H) and 123–133 ppm (^{15}N), which generally correspond to β-sheet structures. While these characteristics precluded the assignment of backbone chemical shifts, they are fully consistent with the unfolding of β-strands and with the enrichment in flexible structures, as seen in the Δ13Arf6-GDP crystal. Δ13Arf6-GDP retains, however, the characteristics of an essentially folded protein, as shown by its circular dichroism (CD) spectrum at room temperature and its unfolding upon heating (melting temperature T_m=51 °C) (Fig. S3 in Supplementary Data).

In contrast, the ^1H–^{15}N HSQC spectrum of Δ13Arf6-GTP is very well defined and is representative of a well-ordered conformation (Fig. 2, blue). This indicates that the local disorder in Δ13Arf6-GDP is not an intrinsic property of Δ13Arf6, but is specific for its GDP-bound form. These high-quality HSQC data allowed us to assign 93% of ^1H–^{15}N backbone correlations (Table S1 in Supplementary Data). R_1, R_2, and heteronuclear nuclear Overhauser

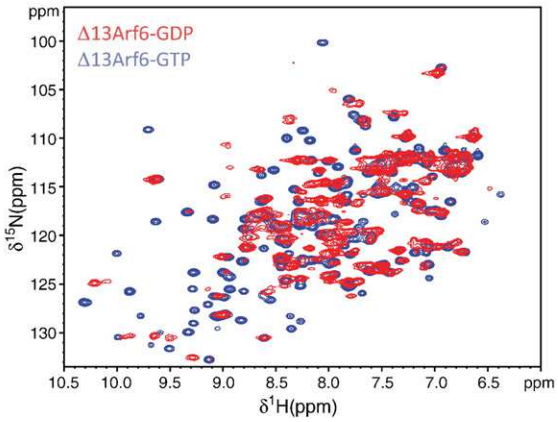

Fig. 2. Spectroscopic analysis of local disorder in Δ13Arf6-GDP. Comparison of the ^1H–^{15}N HSQC spectra of Δ13Arf6-GDP (red) and Δ13Arf6-GTP (blue).

effect $^{1}H–^{15}N$ experiments are also consistent with a Δ13Arf6-GTP structure that is essentially devoid of flexible region (data not shown). Secondary structures predicted from the chemical shifts using the TALOS software[19] are in full agreement with the X-ray structure of Arf6-GTP^{FL}, in which the N-terminal helix is not visible.[11] Altogether, this ensemble of experiments indicates that the partially unfolded structure of Δ13Arf6-GDP seen in the crystal structure is likely to exist in solution.

Δ13Arf6-GDP conformation in solution is consistent with the structure of the crystalline monomer

Small-angle X-ray scattering (SAXS) has emerged as an efficient method to discriminate between alternative structural models in solution (reviewed by Koch *et al.*,[20] Rambo and Tainer,[21] and Putnam *et al.*[22]). Synchrotron radiation SAXS data were measured for Δ13Arf6-GDP and Arf6-GDP^{FL}. At low resolution, these data give direct access to the radius of gyration calculated from Guinier's plot. This radius was 16.57 Å for Δ13Arf6-GDP, which is much closer to the value calculated from the crystalline monomer (16.2 Å) than to the value calculated from the crystalline dimer (20.1 Å). This rules out that Δ13Arf6-GDP is a dimer in solution, which we also confirmed by size-exclusion chromatography–multiangle light scattering (SEC-MALS) analysis (see the text below).

In order to establish which crystallographic structures agree best with the SAXS data, we fitted the scattering curves calculated from atomic coordinates to the experimental SAXS curves using CRYSOL. Curves calculated from the coordinates of Arf6-GDP^{FL}, Arf6-GDP^{FL} deleted of the N-terminal helix (Arf6-GDP$^{FL-\Delta 13}$), and our partially unfolded Δ13Arf6-GDP crystal structure are clearly different (Fig. 3a, red, green, and blue, respectively). The calculated Arf6-GDP^{FL} curve fitted nicely to the SAXS Arf6-GDP^{FL} curve ($\chi^2=1.94$; Fig. 3a, red), while the calculated Δ13Arf6-GDP curve gave a very poor fit to the experimental curve ($\chi^2=9.78$; Fig. 3a, blue). Conversely, the best fit for the Δ13Arf6-GDP SAXS curve was obtained with the calculated Δ13Arf6-GDP curve ($\chi^2=1.98$; Fig. 3b, blue), while a poor fit was obtained with the calculated Arf6-GDP^{FL} curve ($\chi^2=2.92$; Fig. 3b, red). Deletion of the N-terminal helix from the Arf6-GDP^{FL} crystal structure did not improve the fit ($\chi^2=3.01$; Fig. 3b, green), indicating that the differences between the SAXS data are best accounted for by a conformational change between Arf6-GDP^{FL} and Δ13Arf6-GDP, rather than by the sole deletion of the N-terminal amino acids.

We also derived *ab initio* three-dimensional (3D) envelopes from the experimental SAXS data without any constraint from an atomic model, using the DAMMIF suite.[23] The *ab initio* envelopes and crystallographic structures were superimposed with SUPCOMB,[24] a method used to optimize the alignment of 3D objects. The SAXS envelope of Arf6-GDP^{FL} was essentially globular and superimposed very well with the crystal structure of Arf6-GDP^{FL} (Fig. 3c). In contrast, the Δ13Arf6-GDP SAXS envelope displayed a large protrusion (Fig. 3d). Remarkably, the protrusion readily accommodated the partially unfolded β1′–β2 strands from the Δ13Arf6-GDP crystal structure (Fig. 3d), suggesting that a similar unfolding takes place in solution.

Altogether, the SAXS data of Arf6-GDP^{FL} and Δ13Arf6-GDP fit well and selectively with their respective crystal structures and strongly suggest that the β1′–β2 strands in Δ13Arf6-GDP have the same shape in solution and in the crystal.

Δ13Arf6-GDP and Δ17Arf1-GDP have distinctive structural, thermodynamic, and hydrodynamic properties

No straightforward structural or thermodynamic model has been put forward to explain the specificity of GEFs and inhibitors for Arf1 and Arf6, although the crystal structure of Arf6-GDP^{FL} displayed subtle differences from that of Arf1-GDP^{FL}, which were proposed to play a role in ArfGEF specificity.[9] NMR chemical shift analysis of Δ17Arf1-GDP and its extensive cross-validation with crystallographic data have been reported (Buosi *et al.*, unpublished). Unlike the Δ13Arf6-GDP spectrum (this work), the $^{1}H–^{15}N$ HSQC spectrum of Δ17Arf1-GDP is well defined and fully consistent with the well-ordered, fully folded crystal structure of Arf1-GDP^{FL} (Fig. 4a). Thus, the partially unfolded β1′–β2 structure seems specific for truncated Arf6 and is not identified as a major species in truncated Arf1.

To get further insight into the differences between Arf1 and Arf6, we analyzed their thermodynamic and hydrodynamic parameters. The thermal stabilities of Δ17Arf1 and Δ13Arf6 were assessed using a fluorescence-based thermal shift assay, a fast and protein-saving method in which thermal unfolding is monitored by a fluorescent dye that binds to hydrophobic sites on unfolded proteins.[25,26] The melting temperatures (T_m) of Δ13Arf6 and Δ17Arf1 were obtained under a series of conditions, including stoichiometric GDP concentration, excess GDP, excess GDP in the absence of Mg^{2+}, and GTP. T_m values were consistently lower for Δ13Arf6-GDP than for Δ17Arf1-GDP (Fig. 4b). Chelation of Mg^{2+} by ethylenediaminetetraacetic acid (EDTA) had no effect on Δ13Arf6-GDP, in agreement with its absence in the crystal structures of Δ13Arf6-GDP (this work) and Arf6-GDP^{FL}.[9] In contrast, Δ17Arf1-GTP and Δ13Arf6-GTP had very similar T_m values and were significantly more stable (68 and 70 °C,

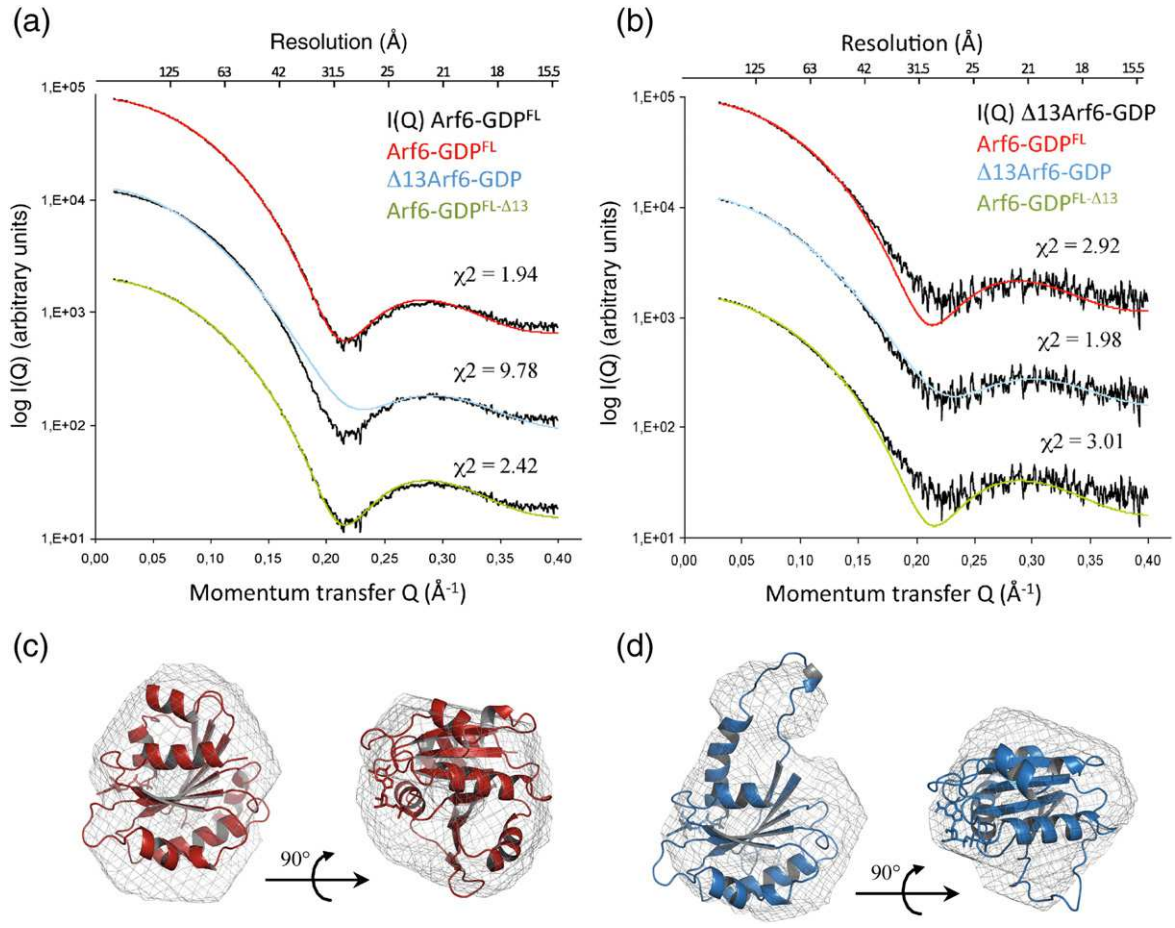

Fig. 3. Synchrotron radiation SAXS analysis of Arf6-GDP^{FL} and Δ13Arf6-GDP. (a) Fit of the experimental SAXS data from Arf6-GDP^{FL} (black) with the scattering curves calculated from either the crystal structure of Arf6-GDP^{FL} (red), the crystal structure of Δ13Arf6-GDP (blue), or Arf6-GDP^{FL} lacking the N-terminal helix (Arf6-GDP$^{FL\text{-}\Delta13}$; green). (b) Fit of the experimental SAXS data from Δ13Arf6-GDP (black) with the scattering curves calculated from the same structural models as in (a). For each scattering curve, the logarithm of intensity is displayed as a function of the momentum transfer Q. For each fit, the corresponding χ^2 is given. The 3 curves are shifted by 1 logarithmic unit for clarity. (c and d) Three-dimensional envelopes (gray) calculated *ab initio* from the SAXS recordings with DAMMIF[23] at $Q = 0.3$ Å^{-1} for Arf6-GDP^{FL} (c; red) and Δ13Arf6-GDP (d; blue). The corresponding crystallographic structures fitted to the *ab initio* envelopes with SUPCOMB are shown in two orientations.

respectively), consistent with their well-ordered conformations depicted by NMR HSQC analysis (this work; Buosi *et al.*, unpublished). We also studied a point mutant, Δ13Arf6^{S38I}, which is discussed below.

Finally, we compared Δ13Arf6-GDP and Δ17Arf1-GDP using SEC-MALS (Fig. 4c). The hydrodynamic radius (21.4 Å) and apparent molecular weight (21,844) of Δ13Arf6-GDP were significantly larger than those of Δ17Arf1-GDP (19.7 Å and 18,992). This is consistent with the higher solvation of the unfolded structure of Δ13Arf6-GDP, which exposes the entire β1′–β2 region to the solvent, compared to that of the more closely packed Δ17Arf1-GDP. For both proteins, the apparent molecular weight is also consistent with a monomer, confirming that the crystalline pseudo-dimer does not form in solution. Altogether, this ensemble of differences between Δ13Arf6-GDP and Δ17Arf1-GDP accounts well for the well-ordered conformation of Δ17Arf1-GDP and the partially disordered and less stable structure of Δ13Arf6-GDP.

Discussion

Δ13Arf6-GDP is partially unfolded

In this study, we combined structural, spectroscopic, and thermodynamic methods to determine the conformation of Δ13Arf6-GDP and its level of

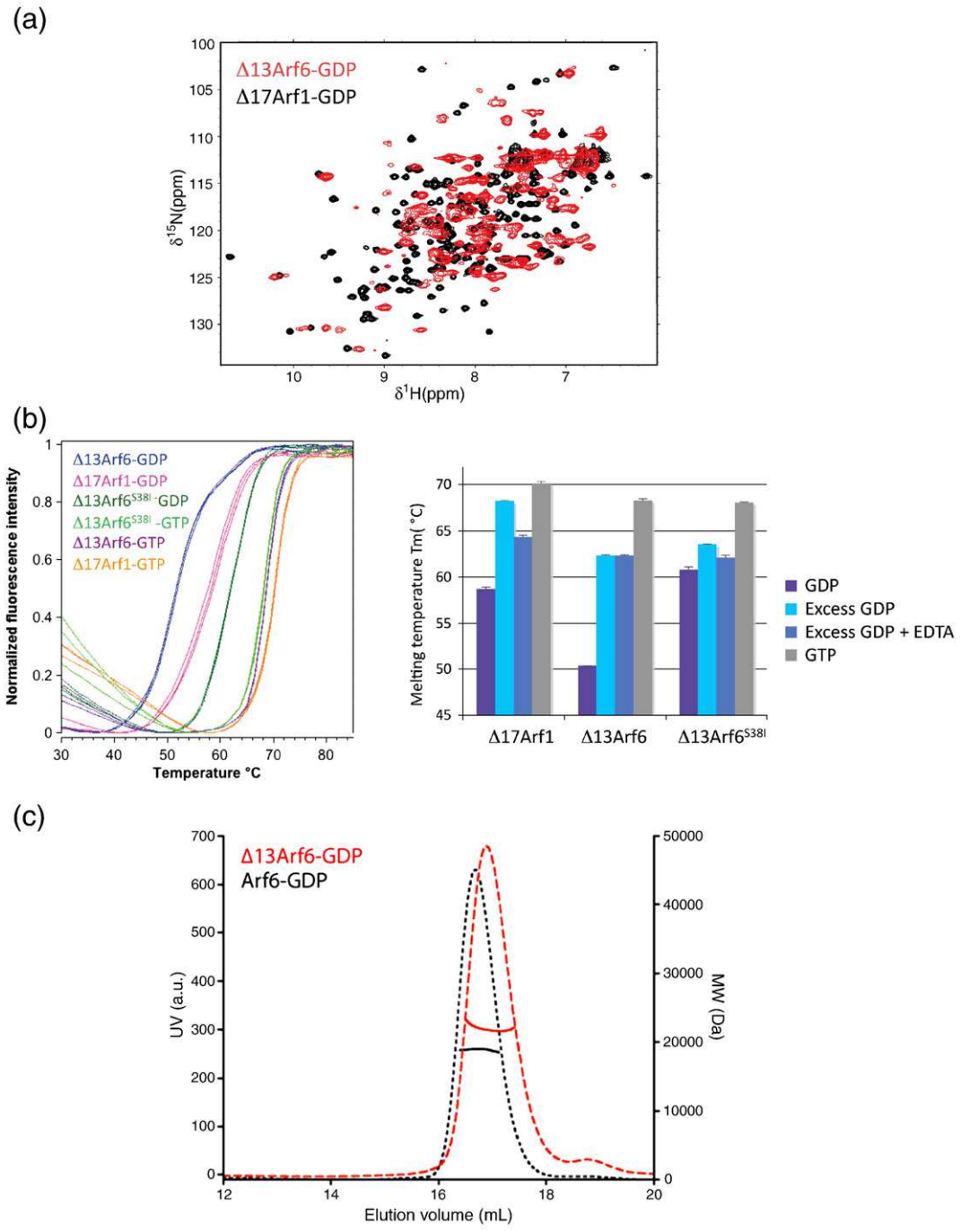

Fig. 4. Spectroscopic, thermodynamic, and hydrodynamic comparisons of Δ13Arf6 and Δ17Arf1. (a) Comparison of the ^{1}H–^{15}N HSQC spectra of Δ13Arf6-GDP (red) and Δ17Arf1-GDP (black; Buosi *et al.*, unpublished). (b) Fluorescence thermal shift assays. Experimental conditions and proteins are color coded as indicated. Left: Fluorescence intensities are recorded in triplicate as a function of temperature. Right: Melting temperatures. (c) SEC-MALS analysis. The size-exclusion chromatography profiles and the estimated molecular weights are shown for Δ13Arf6-GDP (red) and Δ17Arf1-GDP (black).

structural disorder. The 1.8-Å crystal structure shows that strands β1′ and β2, which form switch 1 and part of the interswitch in Arf6-GDP^{FL}, are relocated as far as 47 Å away from their original positions, yielding a flexible loop that protrudes from the small GTPase core. We find this flexible structure to be fully consistent with the SAXS profiles in solution, and the extended loop to be

readily fitted into a protrusion predicted by the *ab initio* SAXS envelope. In combination, NMR spectroscopy data, thermofluorescence and CD thermodynamic data, and SEC-MALS hydrodynamic data fully support the existence of a local disorder of Δ13Arf6-GDP in solution. These experiments also identify that monomeric Δ13Arf6-GDP, rather than the putative dimer observed in the crystal, is the major species in solution. Altogether, our data strongly suggest that Δ13Arf6-GDP is partially unfolded compared to Arf6-GDP^{FL}. This is one of the largest departures from the classical small GTPase fold. It is reminiscent of the structure of Rab27b-GDP,[27] a small GTPase involved in regulated exocytosis in eukaryotic cells. In this structure, the entire switch 1 and the interswitch (strands β2 and β3) are unfolded compared to average Rab protein structures (Fig. 5a). This partially unfolded Rab27b structure formed a dimer in the crystal, which was not detected in solution, as is the case for the Δ13Arf6-GDP pseudo-dimer. However, SAXS data were compatible with the elongated shape of the unfolded monomer, which may thus exist in solution, although this was not investigated further. As for Arf1 and Arf6, Rab27 proteins exist as closely related isoforms endowed with distinct functions in exosome secretion,[28] in which a differential metastability of their central β-sheet core may be involved.

Comparison of Δ13Arf6-GDP and Δ17Arf1-GDP suggests an unfolding model for the GDP/GTP structural shift unique to Arf6

The activations of Arf1 and Arf6 differ in several biochemical aspects. Notably, Arf6 exchanges GDP much faster than Arf1,[6,7] it possesses a group of exchange factors that are strictly specific,[6] and it is insensitive to the interfacial inhibitor BFA regardless of the sensitivity of ArfGEF to the drug.[7] The fact that all residues of Arf1 in contact with ArfGEFs or BFA[10,12,13] are strictly conserved in Arf6 suggests that these residues may not have the same conformation and/or dynamics in the two proteins. Our new data identify the partially unfolded conformation of Δ13Arf6-GDP as the major species in solution, in contrast to Δ17Arf1-GDP, whose major species in solution has the same conformation as the fully folded Arf1-GDP^{FL} structure (Buosi *et al.*, unpublished). Thus, the local unfolding of Δ13Arf6-GDP, together with its distorted switch 2 conformation, is the most significant structural difference identified so far between these two closely related Arf isoforms. Since the truncated mutants mimic membrane-associated Arf-GDP at the initiation of the exchange reaction, structural differences between Δ13Arf6-GDP and Δ17Arf1-GDP are likely to convey specificity determinants relevant to the nucleotide switch, which we will discuss below.

The fast nucleotide exchange of Arf6 has been previously ascribed to a single-residue difference between Arf6 and Arf1, Ser38 in Arf6 corresponding to Ile42 in Arf1,[9] which is located in the unfolded region in Δ13Arf6-GDP. Permutation of these residues between Δ17Arf1 and Δ13Arf6 was sufficient to slow the GDP exchange rate of Δ13Arf6 down to that of Arf1, and to increase the rate of Δ17Arf1 to almost that of Δ13Arf6.[9] The sequence permutation also resulted in a permutation of their respective affinities for Mg^{2+}. Our thermofluorescence assay shows that Δ13Arf6^{S38I} has a higher T_m than Δ13Arf6 and is sensitive to Mg^{2+} chelation by EDTA, indicating that the mutant has a more stable structure and confirming that it recovers the ability to bind Mg^{2+} (Fig. 4b). The Δ13Arf6^{S38I} mutant is also less sensitive to the Arf6-specific ArfGEF EFA6 (our unpublished results). Thus, Ser38 is likely to contribute, to some extent, to the local structural disorder in Δ13Arf6-GDP. However, the Ser/Ile permutation is not sufficient to yield a full Arf6/Arf1 permutation. Notably, Δ17Arf1^{I42S} cannot be activated by EFA6,[6] nor does Δ13Arf6^{S38I} become fully insensitive to this ArfGEF (our unpublished results). Similarly, the Ser/Ile mutation does not make Δ13Arf6 sensitive to BFA.[7] It is thus likely that the unfolding propensity of the β1′–β2 region in Δ13Arf6-GDP requires other, if not most, sequence differences between Arf1 and Arf6 along switch 1/interswitch (Fig. 1, left).

The strict specificity of EFA6 for Arf6 and the insensitivity of Arf6 to BFA can also be revisited in the light of our new structural data. Interestingly, the EFA6 group of ArfGEFs features a conserved arginine downstream of the catalytic glutamate, which is replaced by large hydrophobic residues in all other ArfGEFs (Fig. 5b). This arginine might clash with Phe51, which is located in switch 1 of Arf1 and clamps Arf1 onto the ArfGEF active site throughout the exchange reaction (Fig. 5c).[13] We surmise that the disorder propensity of the β1′–β2 region in Arf6-GDP may facilitate the accommodation of its switch 1 by the EFA6 arginine and may contribute to the strict specificity of this group of ArfGEFs for Arf6. Likewise, Phe51 in Arf1 packs against BFA in the BFA-inhibited Arf1-GDP/BFA/ArfGEF complexes (Fig. 5d). Local unfolding of the β1′–β2 region in Arf6 would displace the equivalent Phe47 residue, thus impairing the BFA-binding site and contributing to the insensitivity of Arf6 to BFA.

Altogether, our results suggest that the GDP/GTP structural switch of Arf6 may follow a structural route different from that of Arf1. The interswitch toggle of Arf6 may proceed through a local unfolding of the interswitch, possibly via a GEF-bound intermediate in which Arf6 resembles the Δ13Arf6-GDP structure (Fig. 5d). Available data for Arf1, in contrast, rather favor a model in which the interswitch inches its way to the active conformation

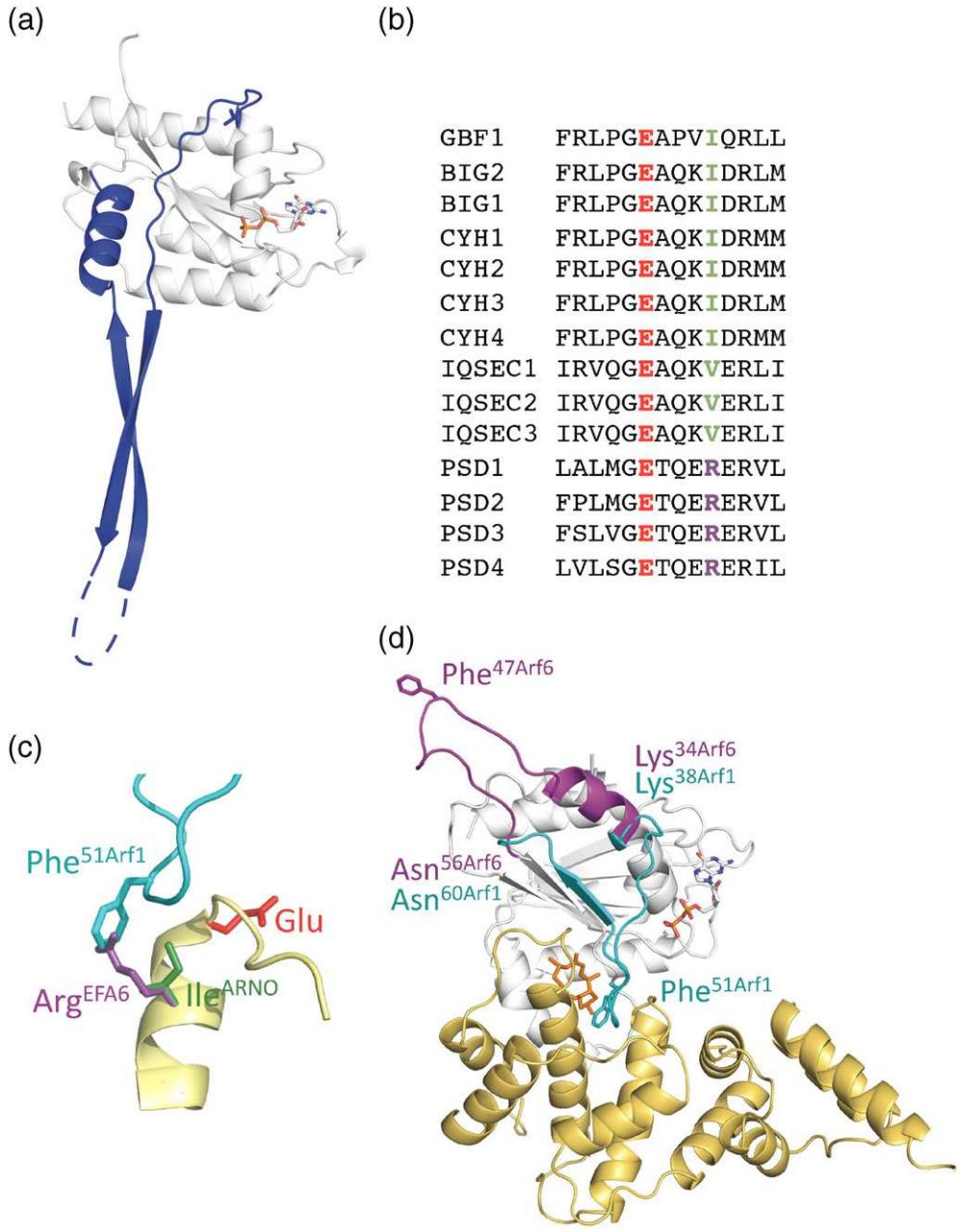

Fig. 5. An unfolding model for the GDP/GTP switch of Arf6. (a) β-Strand metastability in the Rab27b-GDP crystal structure (PDD entry 2EIZ).[27] Rab27b is shown with the same orientation as Arf6 in Fig. 1. Regions shown in blue depart from the average Rab structures. Disordered regions are depicted in dotted lines. (b) Sequence alignment of human ArfGEFs in the vicinity of the catalytic glutamate (red). Names follow the Human Genome Organization nomenclature: CYH, cytohesin; IQSEC, BRAG; PSD, EFA6. The conserved arginine in the EFA6 group is shown in magenta, the equivalent hydrophobic residue in other ArfGEFs is shown in green, and the catalytic glutamate is shown in red. (c) Model of the conserved EFA6 arginine superimposed on the Arf1-GDP/BFA/ARNO complex (PDF entry 1S9D[13]). Arf1 is shown in cyan, and ARNO is shown in yellow. Color coding of the residues as in (b). (d) Superposition of the unfolded β1′–β2 strands from the Δ13Arf6-GDP structure (magenta) onto the Arf1-GDP/BFA/ARNO complex. β1′–β2 strands in Arf1 are shown in cyan.

by using internal motions (Buosi *et al.*, unpublished). While this unfolding model for the GDP/GTP switch of Arf6 would account for the unresolved differences between Arf1 and Arf6, we cannot formally exclude that some unfolding of Arf1 takes place at a later stage of the exchange reaction.

Crystalline snapshots of Arf1/ArfGEF and Arf6/EFA6 short-lived intermediates are still needed to fully clarify this issue.

Experimental Procedures

Protein purification and nucleotide exchange

pET3a-Arf6 and pET11a-Δ13Arf6 were gifts from M. Franco (IPMC, CNRS, France). Arf6-GTP^{FL} and Δ13Arf6-GTP were expressed and purified essentially as previously described by Chavrier and Franco.[29] As judged by SDS-PAGE analysis, proteins were at least 90% pure. All proteins were concentrated to at least 10 mg ml^{-1} on a Vivaspin concentrator (molecular weight cutoff of 5000; Vivascience AG) and stored at −80 °C. Arf6^{FL} or Δ13Arf6 was loaded with GDP by incubation with 5 mM GDP and 5 mM EDTA at 37 °C for 40 min. The reaction was stopped by addition of 20 mM $MgCl_2$. Protein solutions were then centrifuged at 4 °C for 30 min at 15,700***g*** prior to being purified on a Superdex 75 10/300 GL column equilibrated with buffer A [50 mM Tris–HCl (pH 8), 150 mM NaCl, 2 mM $MgCl_2$, and 2 mM β-mercaptoethanol]. The nucleotide content of all proteins was assessed by tryptophan fluorescent assay, as described by Zeeh *et al.*[7]

For NMR spectroscopy analysis, uniformly $^{13}C/^{15}N$ and ^{15}N isotopically enriched Δ13Arf6 were prepared by growing bacteria in minimal medium, which contains $^{15}NH_4Cl$ and either [$^{13}C_6$]glucose or unlabeled glucose. ^{15}N-labeled and $^{15}N/^{13}C$-labeled Δ13Arf6 were purified and loaded with nucleotides using the same protocol as for unlabeled Δ13Arf6.

Crystallization, diffraction data collection, crystal structure determination, structural analysis

Crystals appeared under many conditions ranging from pH 6.5 to pH 8.5, and polyethylene glycols with molecular weights from 400 to 8000. The crystals used for diffraction were obtained in a hanging drop containing equal volumes of Δ13Arf6-GDP (15.3 mg ml^{-1}) and a reservoir solution containing 0.2 M NaCl and 20% polyethylene glycol 3350. Diffraction data were collected at beamline PROXIMA1 (SOLEIL Synchrotron, Gif-sur-Yvette, France) equipped with an ADSC Q315r charge-coupled device detector using a wavelength of 0.98 Å. The intensities were integrated and scaled with the program XDS[30] and were usable up to 1.8 Å resolution. The crystal belonged to space group $P2_12_12_1$. Crystallographic statistics are listed in Table 1. The structure was solved by molecular replacement with the program Phaser,[31] using Arf6-GDP^{FL}[9] [Protein Data Bank (PDB) entry 1E0S] as search model. A solution with Arf6-GDP^{FL} deleted of residues 34–77 (switch 1–interswitch–switch 2) was found. Model building was carried out manually with Coot.[32] Refinement was carried out with the program autoBUSTER,[33] alternately with graphical building using Coot. The final model contained two Arf6 molecules, both in complex with GDP. Statistics are given in Table 1. Accessible surface area calculations were made using the program AREAIMOL from the CCP4 package. Gyration radii were calculated as the RMSD of distances between each atom and the molecule center of mass. Hydrodynamic radii were calculated using the program HYDROPRO.[34] The structure of the Sec7 domain of EFA6 was modelled onto the ARNO structure (PDB entry 1R8S) using the Phyre server.[35]

Synchrotron radiation SAXS analysis

SAXS experiments were conducted on beamline SWING at SOLEIL Synchrotron. The beam wavelength was set to λ = 1.033 Å. The 17 cm × 17 cm low-noise Aviex charge-coupled device detector was positioned at a distance of 2107 mm from the sample, with the direct beam off-centered. The corresponding Q-range was 0.02–0.4 Å^{-1}, where the momentum transfer $Q = 4\pi\sin\theta/\lambda$, and 2θ is the scattering angle. All solutions were circulated in a thermostated quartz capillary with a diameter of 1.5 mm and a wall thickness of 10 μm, positioned within a vacuum chamber. The transmitted intensity was permanently measured using a diode embedded in the beam stop, with an accuracy of 0.1%.

All samples were ultracentrifuged at 100,000***g*** in a TLA45 Beckman rotor for 30 min before the SAXS experiments. Three concentrations were used for Arf6-GDP^{FL} (1.6, 3.2, and 6.4 mg ml^{-1}). Fifty microliters of each sample, separated from the pushing liquid (water) by two air volumes 6 μl each, was circulated into the flow-through capillary cell at 40 μl min^{-1}, as described by David and Perez.[36] Fifty frames of 2 s each were collected, normalized to the transmitted intensity, and subsequently averaged using the image analysis software Foxtrot (SOLEIL software group and SWING beamline, unpublished). The same protocol was applied to buffer scattering. After buffer subtraction, the resulting curves were normalized to mass concentration. A small intensity increase at low angles was observed as a function of concentration, showing concentration-dependent aggregation. The three curves remained, however, superimposable for a Q-range of 0.1–0.4 Å^{-1}. A composite curve was calculated from the low-concentration data (Q-range: 0.02–0.15 Å^{-1}) and the high concentration data (Q-range: 0.07–0.4 Å^{-1}) for subsequent analysis.

For Δ13Arf6-GDP, a concentrated sample (15 mg ml^{-1}) was injected into a size-exclusion column (SHODEX KW402.5) using an Agilent© High Performance Liquid Chromatography system and eluted directly into the SAXS flow-through capillary cell at a flow rate of 150 μl min^{-1}. SAXS data were collected online throughout the whole elution time, with a frame duration of 2 s and a dead time between frames of 0.5 s. Selected frames corresponding to the main elution peak were averaged in accordance with the procedure described by David and Perez.[36] For these frames, the average protein concentration was estimated to be 2.5 mg ml^{-1} from UV absorption at 280 nm using a spectrometer located immediately upstream of the SAXS cell. A large number of frames were collected during the first minutes of the elution flow and averaged to account for buffer scattering, which was subsequently subtracted from the protein signal. Thirty-five frames were averaged to produce a curve with the same Q-range as for Arf6-GDP^{FL}, with no attractive interactions at low angle but with more noise at high Q due to a lower protein concentration.

All subsequent data processing, analysis, and modelling steps were carried out with PRIMUS and other programs of the ATSAS suite.[37] The radius of gyration R_g was evaluated using Guinier approximation,[38] assuming that, at very small angles ($Q<1/3R_g$), intensities can be represented as $I(Q)=I(0)\exp(-(QR_g)^2/3)$. The same parameter was also calculated from the entire scattering pattern using the indirect transform package GNOM,[39] which provides the distance distribution function $p(r)$ of the particle. Scattered intensity curves were calculated from the atomic coordinates of the crystallographic structures using CRYSOL.[40] The fit of the calculated intensity to the experimental intensity was assessed with Eq. (1) below, in which the excluded volume, the averaged atomic radius, and the contrast of the hydration layer surrounding the particle in solution are adjusted to minimize discrepancy:

$$\chi^2 = \frac{1}{N-1}\sum_j \left[\frac{I_{\exp}(Q_j) - cI_{\mathrm{calc}}(Q_j)}{\sigma(Q_j)}\right]^2 \quad (1)$$

where N is the number of experimental points; $I_{\exp}(Q_j)$, $I_{\mathrm{calc}}(Q_j)$, and $\sigma(Q_j)$ are the experimental intensity, calculated intensity, and experimental error at the momentum transfer Q_j, respectively; and c is a scaling factor. The experimental errors $\sigma(Q)$ were evaluated for each frame from the scattered number of photons $N(Q)$ as $\sigma(Q)=\sqrt{N(Q)}$ and adequately propagated.

Three-dimensional envelopes of Arf6-GDP^{FL} and Δ13Arf6-GDP were calculated *ab initio* from the SAXS data, using the dummy atom model method as implemented in the program DAMMIF,[23] which uses simulated annealing to generate a compact model that fits the experimental data to minimize the discrepancy in Eq. (1), where I_{calc} is now calculated using the dummy atom model. Crystallographic models were rigid-body fitted into the envelopes using SUPCOMB.[41]

NMR analysis

NMR samples contained 600 μl of protein at ~800 μM concentration in buffer A with 5% D_2O. All NMR spectra were acquired at 298 K using a 700-MHz spectrometer with cryoprobe. Sequential backbone assignments were carried out using ^{15}N-labeled and ^{13}C-labeled Δ13Arf6-GTP with HNCO, HNCA, HNCACB, and HN(CO)CACB BEST 3D experiments.[42] R_1 was recorded by using 11 delay values: 10, 20 (three times), 40, 80, 160, 500, 1000, 2000, and 3000 ms. R_2 was recorded by using 11 delay values: 4, 8 (two times), 12, 16 (two times), 32 64, 128, 256, and 384 ms. The steady-state ^{15}N–^{1}H nuclear Overhauser effect was measured with and without ^{1}H saturation. The softwares Topspin,[43] NMRPipe,[44] and SPARKY[45] were used for spectral analysis and resonance assignments.

Circular dichroism

Far-UV CD spectra and thermal unfolding profiles were recorded on a Jasco J-810 spectropolarimeter equipped with a Pelletier temperature-controlled single-cell holder (Jasco, Inc.). Measurements were performed in a 0.1-cm path length quartz cell with 2 μM Δ13Arf6-GDP in 50 mM Na-phosphate (pH 7.4) and 50 mM NaF. Spectra are the average of five measurements from 260 to 185 nm at 20 °C. Thermal unfolding profiles were recorded at 222 nm from 4 to 90 °C, at a ramping rate of 1 °C min^{-1}. The CD signal (mdeg) was converted into mean residue ellipticity ([θ]; deg cm^2 dmol^{-1}) using $[\theta]=[\theta]_{\mathrm{obs}}(10lCN)^{-1}$, where $[\theta]_{\mathrm{obs}}$ (mdeg) is the experimental ellipticity, C (mol dm^{-3}) is the protein concentration, l (cm) is the cell path length, and N is the number of residues in the protein.

Fluorescence-based thermal shift assay

Protein samples were diluted at 8 μM in buffer A in the presence of 6.25× SYPRO Orange (Invitrogen), which becomes highly fluorescent when bound to protein hydrophobic sites that accessible upon thermal unfolding.[25] Reactions were carried out in triplicate in a 96-well fast PCR plate at a final volume of 20 μl. Guanine nucleotides (0.5 mM) or EDTA (5 mM) was added to the reaction mixture, as indicated. The temperature gradient was performed in the range of 25–95 °C at 3 °C min^{-1} on an Applied Biosystems 7900HT Fast Real-Time PCR system.[46] Fluorescence was recorded as a function of temperature in real time (excitation wavelength, 488 nm; emission spectrum, 500–660 nm), and the melting temperature T_m was calculated with the ABI SDS2.4 software as the maximum of the derivative of the resulting denaturation curves. For graphic representation, the raw fluorescence intensity was normalized using a second-order polynomial fit corresponding to the observed temperature-dependent decrease in the fluorescence yield of SYPRO Orange.

SEC-MALS analysis

Experiments were carried out with a Viskotek TDAmax system (Malvern) comprising UV, refractive index, differential viscometer, and light scattering detectors. One hundred microliters of Δ17Arf1-GDP and 50 μl of Δ13Arf6-GDP (3 and 10 mg ml^{-1}, respectively) were injected into a Superdex 200 10/300 size-exclusion column (GE Healthcare) equilibrated with buffer containing 50 mM Tris–HCl (pH 8.0), 150 mM NaCl, 2 mM $MgCl_2$, and 2 mM β-mercaptoethanol, and run at 0.4 ml min^{-1}. Δ13Arf6-GDP elutes at a slightly larger volume than Δ17Arf1-GDP, an observation for which we have no straightforward explanation. Molecular weight (M_r) and hydrodynamic radius (R_h) calculations were performed with OmniSEC software (Malvern) using a specific refractive index increment dn/dc value of 0.185 ml g^{-1} (n is the refractive index, and c is the molecular concentration).

Accession code

Coordinates and structures factors have been deposited in the PDB with entry code 3N5C.

Acknowledgements

This work was supported by grants from the Human Frontiers in Science Program and the

Physique-Chimie de Vivant program of the Agence Nationale de la Recherche to J.C.; by a grant from the Association pour la Recherche contre le Cancer to J.C. and M.Z.; and by an ATIP-CNRS grant to V.B. K.A. was supported by a grant from the Cancéropôle/Conseil Général Ile-de-France, and A. T. was supported by a grant from the Institut de Chimie des Substrances Naturelles, CNRS. We thank Lina Ji, Amélie Tora, and Dominique Padovani (Laboratoire d'Enzymologie et Biochimie Structurales, CNRS) for their help with sample preparation; Beatriz Guimaraez, Andrew Thompson, and Pierre Legrand (SOLEIL Synchrotron) for access to beamline PROXIMA 1; Naïma Nhiri (Institut de Chimie des Substrances Naturelles and IMAGIF) for her invaluable help with the thermofluorescence experiments; Bruno Collinet and Herman van Tilbeurgh (Institut de Biochimie et Biophysique Moléculaire et Cellulaire, CNRS/Université Paris-Sud) for their help with the SEC-MALS experiments; and Valérie Campanacci (Laboratoire d'Enzymologie et Biochimie Structurales) for her help with analysis of the SEC-MALS data.

Supplementary Data

Supplementary data to this article can be found online at doi:10.1016/j.jmb.2010.08.002

References

1. D'Souza-Schorey, C. & Chavrier, P. (2006). ARF proteins: roles in membrane traffic and beyond. *Nat. Rev. Mol. Cell Biol.* **7**, 347–358.
2. Gillingham, A. K. & Munro, S. (2007). The small G proteins of the Arf family and their regulators. *Annu. Rev. Cell Dev. Biol.* **23**, 579–611.
3. Donaldson, J. G. & Honda, A. (2005). Localization and function of Arf family GTPases. *Biochem. Soc. Trans.* **33**, 639–642.
4. DiNitto, J. P., Delprato, A., Gabe Lee, M. T., Cronin, T. C., Huang, S., Guilherme, A. *et al.* (2007). Structural basis and mechanism of autoregulation in 3-phosphoinositide-dependent Grp1 family Arf GTPase exchange factors. *Mol. Cell*, **28**, 569–583.
5. Cohen, L. A., Honda, A., Varnai, P., Brown, F. D., Balla, T. & Donaldson, J. G. (2007). Active Arf6 recruits ARNO/cytohesin GEFs to the PM by binding their PH domains. *Mol. Biol. Cell*, **18**, 2244–2253.
6. Macia, E., Chabre, M. & Franco, M. (2001). Specificities for the small G proteins ARF1 and ARF6 of the guanine nucleotide exchange factors ARNO and EFA6. *J. Biol. Chem.* **276**, 24925–24930.
7. Zeeh, J. C., Zeghouf, M., Grauffel, C., Guibert, B., Martin, E., Dejaegere, A. & Cherfils, J. (2006). Dual specificity of the interfacial inhibitor brefeldin A for Arf proteins and Sec7 domains. *J. Biol. Chem.* **281**, 11805–11814.
8. Amor, J. C., Harrison, D. H., Kahn, R. A. & Ringe, D. (1994). Structure of the human ADP-ribosylation factor 1 complexed with GDP. *Nature*, **372**, 704–708.
9. Menetrey, J., Macia, E., Pasqualato, S., Franco, M. & Cherfils, J. (2000). Structure of Arf6-GDP suggests a basis for guanine nucleotide exchange factors specificity. *Nat. Struct. Biol.* **7**, 466–469.
10. Goldberg, J. (1998). Structural basis for activation of ARF GTPase: mechanisms of guanine nucleotide exchange and GTP-myristoyl switching. *Cell*, **95**, 237–248.
11. Pasqualato, S., Menetrey, J., Franco, M. & Cherfils, J. (2001). The structural GDP/GTP cycle of human Arf6. *EMBO Rep.* **2**, 234–238.
12. Mossessova, E., Corpina, R. A. & Goldberg, J. (2003). Crystal structure of ARF1∗Sec7 complexed with brefeldin A and its implications for the guanine nucleotide exchange mechanism. *Mol. Cell*, **12**, 1403–1411.
13. Renault, L., Guibert, B. & Cherfils, J. (2003). Structural snapshots of the mechanism and inhibition of a guanine nucleotide exchange factor. *Nature*, **426**, 525–530.
14. Henzler-Wildman, K. & Kern, D. (2007). Dynamic personalities of proteins. *Nature*, **450**, 964–972.
15. Pasqualato, S., Renault, L. & Cherfils, J. (2002). Arf, Arl, Arp and Sar proteins: a family of GTP-binding proteins with a structural device for 'front–back' communication. *EMBO Rep.* **3**, 1035–1041.
16. Peyroche, A., Antonny, B., Robineau, S., Acker, J., Cherfils, J. & Jackson, C. L. (1999). Brefeldin A acts to stabilize an abortive ARF–GDP–Sec7 domain protein complex: involvement of specific residues of the Sec7 domain. *Mol. Cell*, **3**, 275–285.
17. Antonny, B., Beraud-Dufour, S., Chardin, P. & Chabre, M. (1997). N-terminal hydrophobic residues of the G-protein ADP-ribosylation factor-1 insert into membrane phospholipids upon GDP to GTP exchange. *Biochemistry*, **36**, 4675–4684.
18. Pasqualato, S., Renault, L. & Cherfils, J. (2004). The GDP/GTP cycle of Arf proteins. Structural and biochemical aspects. In *The ARF Book* (Kahn, R. A., ed.), Kluwer Academic Publishers, Boston, MA.
19. Cornilescu, G., Delaglio, F. & Bax, A. (1999). Protein backbone angle restraints from searching a database for chemical shift and sequence homology. *J. Biomol. NMR*, **13**, 289–302.
20. Koch, M. H., Vachette, P. & Svergun, D. I. (2003). Small-angle scattering: a view on the properties, structures and structural changes of biological macromolecules in solution. *Q. Rev. Biophys.* **36**, 147–227.
21. Rambo, R. P. & Tainer, J. A. (2010). Bridging the solution divide: comprehensive structural analyses of dynamic RNA, DNA, and protein assemblies by small-angle X-ray scattering. *Curr. Opin. Struct. Biol.* **20**, 128–137.
22. Putnam, C. D., Hammel, M., Hura, G. L. & Tainer, J. A. (2007). X-ray solution scattering (SAXS) combined with crystallography and computation: defining accurate macromolecular structures, conformations and assemblies in solution. *Q. Rev. Biophys.* **40**, 191–285.
23. Franke, D. & Svergun, D. I. (2009). DAMMIF, a program for rapid ab-initio shape determination in small-angle scattering. *J. Appl. Crystallogr.* **42**, 342–346.
24. Kozin, M. B. & Svergun, D. I. (2000). Automated matching of high- and low-resolution structural models. *J. Appl. Crystallogr.* **34**, 33–41.

25. Ericsson, U. B., Hallberg, B. M., Detitta, G. T., Dekker, N. & Nordlund, P. (2006). Thermofluor-based high-throughput stability optimization of proteins for structural studies. *Anal. Biochem.* **357**, 289–298.
26. Pantoliano, M. W., Petrella, E. C., Kwasnoski, J. D., Lobanov, V. S., Myslik, J., Graf, E. *et al.* (2001). High-density miniaturized thermal shift assays as a general strategy for drug discovery. *J. Biomol. Screen.* **6**, 429–440.
27. Chavas, L. M. G., Torii, S., Kamikubo, H., Kawasaki, M., Ihara, K., Kato, R. *et al.* (2007). Structure of the small GTPase Rab27b shows an unexpected swapped dimer. *Acta Crystallogr. Sect. D*, **63**, 769–779.
28. Ostrowski, M., Carmo, N. B., Krumeich, S., Fanget, I., Raposo, G., Savina, A. *et al.* (2010). Rab27a and Rab27b control different steps of the exosome secretion pathway. *Nat. Cell Biol.* **12**, *19–30.*
29. Chavrier, P. & Franco, M. (2001). Expression, purification, and biochemical properties of EFA6, a Sec7 domain-containing guanine exchange factor for ADP-ribosylation factor 6 (ARF6). *Methods Enzymol.* **329**, 272–279.
30. Kabsch, W. (2010). XDS. *Acta Crystallogr. Sect. D*, **66**, 125–132.
31. McCoy, A. J., Grosse-Kunstleve, R. W., Adams, P. D., Winn, M. D., Storoni, L. C. & Read, R. J. (2007). Phaser crystallographic software. *J. Appl. Crystallogr.* **40**, 658–674.
32. Emsley, P. & Cowtan, K. (2004). Coot: model-building tools for molecular graphics. *Acta Crystallogr. Sect. D*, **60**, 2126–2132.
33. Blanc, E., Roversi, P., Vonrhein, C., Flensburg, C., Lea, S. M. & Bricogne, G. (2004). Refinement of severely incomplete structures with maximum likelihood in BUSTER-TNT. *Acta Crystallogr. Sect. D*, **60**, 2210–2221.
34. Garcia De La Torre, J., Huertas, M. L. & Carrasco, B. (2000). Calculation of hydrodynamic properties of globular proteins from their atomic-level structure. *Biophys. J.* **78**, 719–730.
35. Kelley, L. A. & Sternberg, M. J. (2009). Protein structure prediction on the Web: a case study using the Phyre server. *Nat. Protoc.* **4**, 363–371.
36. David, G. & Perez, J. (2009). Combined sampler robot and high-performance liquid chromatography: a fully automated system for biological small-angle X-ray scattering experiments at the Synchrotron SOLEIL SWING beamline. *J. Appl. Crystallogr.* **42**, 892–900.
37. Konarev, P. V., Volkov, V. V., Petoukhov, M. V. & Svergun, D. I. (2006). ATSAS 2.1, a program package for small-angle scattering data analysis. *J. Appl. Crystallogr.* **39**, 277–286.
38. Guinier, A. (1939). La diffraction des rayons X aux très petits angles: application à l'étude de phénomènes ultramicroscopiques. *Ann.de Phys. (Paris)*, **12**, 161–237.
39. Svergun, D. I. (1992). Determination of the regularization parameter in indirect-transform methods using perceptual criteria. *J. Appl. Crystallogr.* **25**, 495–503.
40. Svergun, D. I., Barberato, C. & Koch, M. H. J. (1995). CRYSOL, a program to evaluate X-ray solution scattering of biological macromolecules from atomic coordinates. *J. Appl. Crystallogr.* **28**, 768–773.
41. Kozin, M. B. & Svergun, D. I. (2001). Automated matching of high- and low-resolution structural models. *J. Appl. Crystallogr.* **34**, 33–41.
42. Lescop, E., Schanda, P. & Brutscher, B. (2007). A set of BEST triple-resonance experiments for time-optimized protein resonance assignment. *J. Magn. Reson.* **187**, 163–169.
43. Zur, Y. (2004). An algorithm to calculate the NMR signal of a multi spin-echo sequence with relaxation and spin-diffusion. *J. Magn. Reson.* **171**, 97–106.
44. Delaglio, F., Grzesiek, S., Vuister, G. W., Zhu, G., Pfeifer, J. & Bax, A. (1995). NMRPipe: a multidimensional spectral processing system based on UNIX pipes. *J. Biomol. NMR*, **6**, 277–293.
45. Lee, W., Westler, W. M., Bahrami, A., Eghbalnia, H. R. & Markley, J. L. (2009). PINE-SPARKY: graphical interface for evaluating automated probabilistic peak assignments in protein NMR spectroscopy. *Bioinformatics*, **25**, 2085–2087.
46. Charveriat, M., Reboul, M., Wang, Q., Picoli, C., Lenuzza, N., Montagnac, A. *et al.* (2009). New inhibitors of prion replication that target the amyloid precursor. *J. Gen. Virol.* **90**, 1294–1301.

Supplementary Figures and Tables

Supplementary Figure S1. 2Fo-Fc electron density drawn at 1 rms of the unfolded β1'-β2 strands (in magenta) in Δ13Arf6-GDP (B subunit). The structure is rotated by 180° rotation with respect to the orientation in Figure 1A.

Supplementary Figure S2: The crystalline Δ13Arf6-GDP asymmetric unit showing the pseudo-dimer. The regions that unfold or rearrange their conformation are in magenta. Disordered regions are depicted in dotted line.

Supplementary Figure S3: Circular dichroism spectrum and thermal unfolding analysis (inset) of Δ13Arf6-GDP.

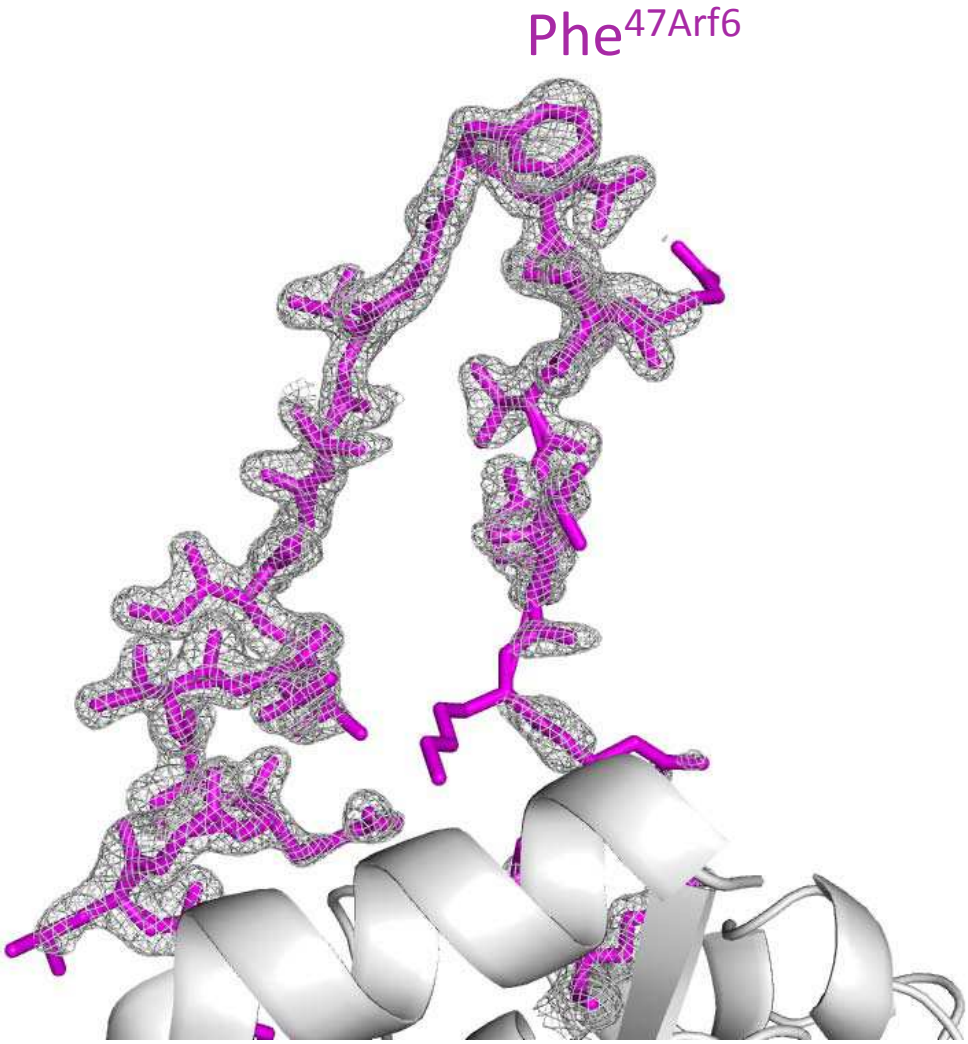

Supplementary Figure S1

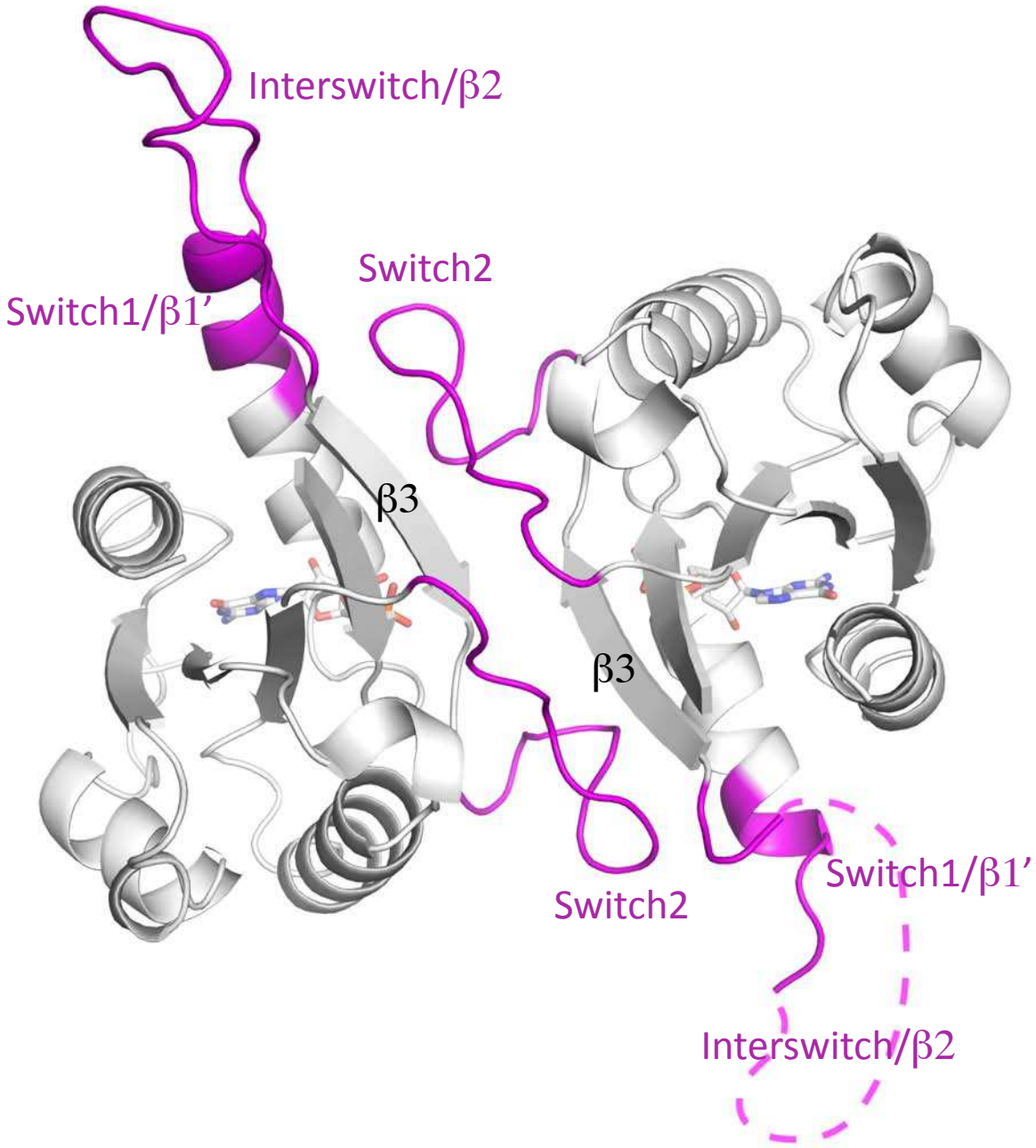

Supplementary Figure S2

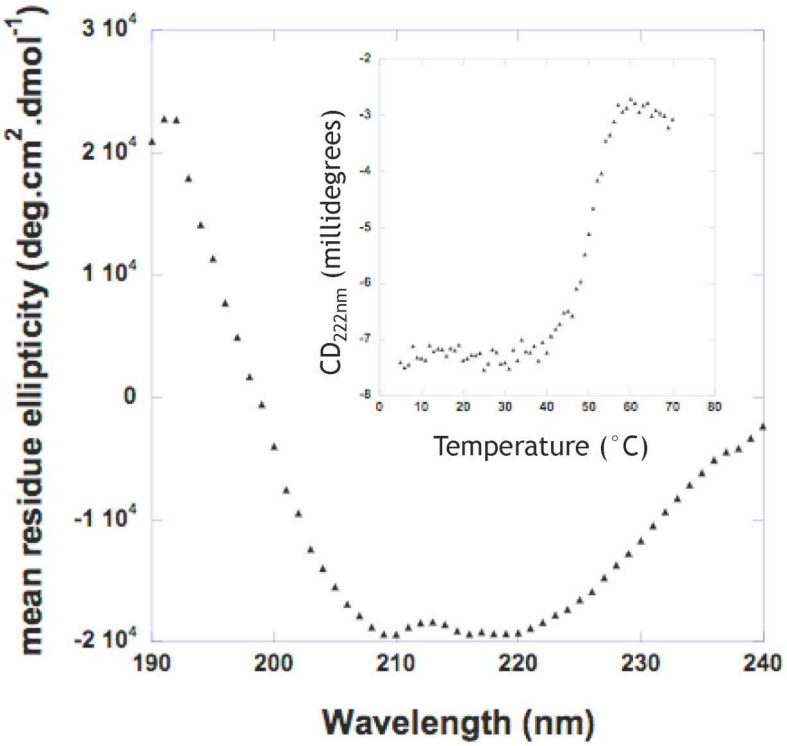

Supplementary figure S3

GENERAL CONCLUSION

During this work we found that BRAG2 was not autoinhibited in solution and in presence of membranes as the cytohesin family even if the components of inhibitory components form of Grp1 (DiNitto et al. 2007) were all present as seen in the Arf1-GDP/BRAG2 complex structure. Nevertheless, inhibition could be achieved through intramolecular interactions with other parts of BRAG2, for instance the N-terminal region or maybe the last 30 amino acids of BRAG2, which are not present in our constructs. Inhibition could also be achieved through intermolecular inhibition with other partners in the cell, either through the IQ motif or the proline rich regions of BRAG2. For example, IQ motif has been described to bind calmodulin and a possible scenario would be that calmodulin regulates BRAG2 activity. We could imagine that in an autoinhibited form, the IQ motif masks the Arf binding site and that the binding of calmodulin induces conformational changes that lead to the active conformation of the GEF. On another hand, we could suppose that the binding of calmodulin somehow inhibits the activation of BRAG2, which could be regulated by calcium signaling. This was tested by Someya and collaborators, who did not find a significant effect of calcium and calmodulin on BRAG2 activity, though this observation remains to be confirmed due to the unknown quality of the recombinant protein they used (Someya et al. 2001). Proline rich regions are generally known to bind proteins with SH3 domains, suggesting that other partners in the cell might interact with BRAG2 and inhibit its activation. The next challenge will be to produce and crystallize a full-length construct of BRAG2 and a new expression system would probably be necessary. The characterization of BRAG2 full-length exchange activity coupled to the resolution of its structure will be highly valuable to answer these issues.

We showed that BRAG2 is equally efficient on Arf1 and Arf6 *in vitro*, which raised questions about its specificity *in vivo*. Our crystal structure of the Arf1-GDP/BRAG2 complex and the availability of Arf and ArfGEF-specific chemical inhibitors (Viaud et al. 2007; Boal et al. 2010), our unpublished results) should be valuable for documenting these issues in cells. We could not form the Arf6/BRAG2 complex and the observation of an unfolded conformation of Arf6 in solution might explain the difficulty to form this complex. This illustrates the different structural routes taken by Arf1 and Arf6 during their activation. To better understand these structural routes we still need crystalline snapshots of Arf1/ArfGEF and Arf6/EFA6 short-lived intermediates, EFA6 being the only GEF highly specific for Arf6 known so far (Macia et al. 2001).

Our data establish that the PH domain of BRAG2 recognizes PIP_2 and PS but not PI(3)P and PI(4)P. Structural recognition of lipids by PH domains has mostly been described

for analogs of PIP_2 and PIP_3, with the recent exception of phosphatidylserine-binding evectin-2 in complex with phosphoserine (Uchida et al. 2011). Although the lipid-binding site has the same location in all structures, there is considerable variability in the residues that recognize the phosphates (**Figure S6 of paper n°1**), except for an invariant lysine located on strand β1 (**Figures 3B and S6 of paper n°1**). Mutation of this residue to alanine in cytohesins (K268A) completely abolished its exchange activity (Stalder et al. 2011). In all members of the BRAG group, this residue is replaced by a glutamate, which should repel phosphates negative charge. We are currently investigating mutants of this residue into Ala and Lys to determine whether it recognizes PS or has another role. Our preliminary results show that this glutamate has a role in the preference of BRAG2 PH domain for charged membranes containing monophosphates phosphoinositides, which could suggest a possible role of BRAG2 PH domain in selecting specific endomembranes.

The resolution of the Arf1-GDP/BRAG2 complex structure allowed us to see that the linker region comprise a well-folded helix packed between Arf1 and the PH domain of BRAG2, conferring a stable area for the anchorage of Arf1. In the autoinhibited form of Grp1 this helix is not present **(Figure 13)**. We could hypothesize that this helix unfold in the autoinhibited form, seat on the Arf binding site and fold back leading to the PH domain 90°C shift, which totally reveals the binding site, becoming thus accessible to Arf and/or membranes for example. Unfortunately SAXS experiments could not discriminate between a closed and an open active conformation in solution. Another region of the linker, which is unfolded and not visible in the crystal structure, is not present in all BRAG species, although it is present in all BRAG2 **(Annex 1)**. This region could have a specific role in BRAG2 activity, which remains to be identified. A construction of BRAG2 comprising the Sec7 domain and the linker could help us identify the role of this region in the regulation of BRAG2.

It has been described in the literature that BRAG2, through its PH domain, binds to cytoplasmic extremities of tyrosine phosphorylated receptors ((Morishige et al. 2008); (Menju et al. 2011); (Hashimoto et al. 2011)) or to unphosphorylated receptors (Scholz et al. 2010). Combining all our results with what we observed in the literature, we could propose a model in which in response to cell signals, an inactive form of BRAG2 will be activated, as a result of a conformational change, which will allow its recruitment to the membrane through the PH domain. This activation will enable BRAG2 to interact with Arf and membrane receptors. From the structure, one side of the PH domain is involved in interactions with the linker and one free side remains exposed, a side that could interact with the receptors. This side contains

several positively charged residues that could indeed interact with phosphotyrosines (pY) of receptors **(Figure 33)**. Reverse charged mutations of the residues K730, R736 and K747 would allow assessing their role in the binding of the PH domain to phosphorylated receptors in cells. To probe our hypothesis, activity of these BRAG2 mutants should be determined *in vitro* on reconstituted membranes in the presence of the cytoplasmic extremity of phosphorylated receptors.

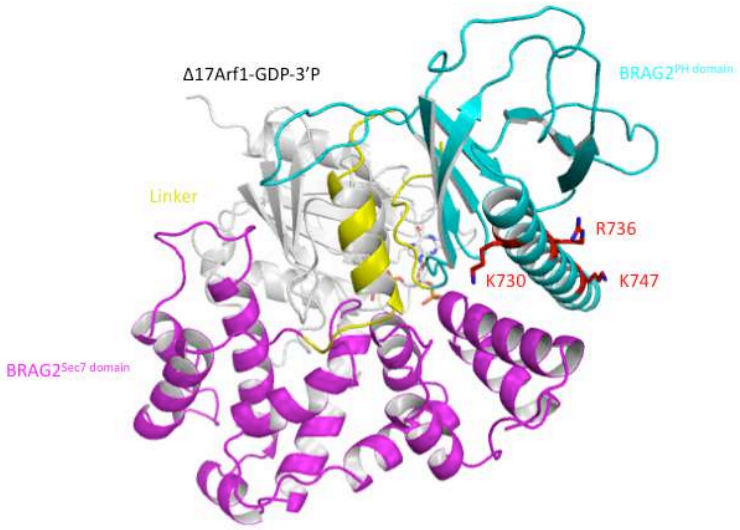

Figure 33: One side of BRAG2 PH domain is accessible to receptors. The color code is as indicated. Residues that could interact with pY in receptors and could be mutated are shown as red sticks.

We also characterized small molecules that inhibit BRAG2 activity, but their specificity remains to be determined. Even though, it might be interesting to test the invasion capacity of cancer cells expressing BRAG2 or metastasis development in an animal model in the presence of those inhibitors. The next challenge will be to crystallize these inhibitors in complex with BRAG2 and/or Arf. An alternative could be to perform docking analysis on our crystal structure and look for a possible binding site, a possible start for an *in silico* screen of novel interfacial inhibitors as previously reported for the Arf1-GDP/ARNO^{E156K} complex (Viaud et al. 2007). These molecules could be valuable tools for describing functions of BRAG2 in the cell and should open new therapeutic perspectives.

REFERENCES

Albertinazzi, C., L. Za, S. Paris and I. de Curtis (2003). "ADP-ribosylation factor 6 and a functional PIX/p95-APP1 complex are required for Rac1B-mediated neurite outgrowth." Mol Biol Cell **14**(4): 1295-1307.

Alexander, K. A., B. T. Wakim, G. S. Doyle, K. A. Walsh and D. R. Storm (1988). "Identification and characterization of the calmodulin-binding domain of neuromodulin, a neurospecific calmodulin-binding protein." J Biol Chem **263**(16): 7544-7549.

Amor, J. C., D. H. Harrison, R. A. Kahn and D. Ringe (1994). "Structure of the human ADP-ribosylation factor 1 complexed with GDP." Nature **372**(6507): 704-708.

Amor, J. C., J. Swails, C. R. Roy, H. Nagai, A. Ingmundson, X. Cheng and R. A. Kahn (2004). "The structure of RalF, an Arf guanine nucleotide exchangefactor from Legionella pneumophila, reveals the presence ofa cap over the active site." J. Biol. Chem.: M410820200.

Bahler, M. and A. Rhoads (2002). "Calmodulin signaling via the IQ motif." FEBS Lett **513**(1): 107-113.

Balana, M. E., F. Niedergang, A. Subtil, A. Alcover, P. Chavrier and A. Dautry-Varsat (2005). "ARF6 GTPase controls bacterial invasion by actin remodelling." J Cell Sci **118**(Pt 10): 2201-2210.

Bartz, R., J. K. Zehmer, M. Zhu, Y. Chen, G. Serrero, Y. Zhao and P. Liu (2007). "Dynamic activity of lipid droplets: protein phosphorylation and GTP-mediated protein translocation." J Proteome Res **6**(8): 3256-3265.

Beck, R., M. Rawet, F. T. Wieland and D. Cassel (2009). "The COPI system: molecular mechanisms and function." FEBS Lett **583**(17): 2701-2709.

Beemiller, P., A. D. Hoppe and J. A. Swanson (2006). "A phosphatidylinositol-3-kinase-dependent signal transition regulates ARF1 and ARF6 during Fcgamma receptor-mediated phagocytosis." PLoS Biol **4**(6): e162.

Beller, M., C. Sztalryd, N. Southall, M. Bell, H. Jackle, D. S. Auld and B. Oliver (2008). "COPI complex is a regulator of lipid homeostasis." PLoS Biol **6**(11): e292.

Ben-Tekaya, H., R. A. Kahn and H. P. Hauri (2010). "ADP ribosylation factors 1 and 4 and group VIA phospholipase A(2) regulate morphology and intraorganellar traffic in the endoplasmic reticulum-Golgi intermediate compartment." Mol Biol Cell **21**(23): 4130-4140.

Beraud-Dufour, S., S. Paris, M. Chabre and B. Antonny (1999). "Dual interaction of ADP ribosylation factor 1 with Sec7 domain and with lipid membranes during catalysis of guanine nucleotide exchange." J Biol Chem **274**(53): 37629-37636.

Beraud-Dufour, S., S. Robineau, P. Chardin, S. Paris, M. Chabre, J. Cherfils and B. Antonny (1998). "A glutamic finger in the guanine nucleotide exchange factor ARNO displaces Mg2+ and the beta-phosphate to destabilize GDP on ARF1." EMBO J **17. 17**(13. 13): 3651-3659, 3651-3659.

Boal, F., L. Guetzoyan, R. B. Sessions, M. Zeghouf, R. A. Spooner, J. M. Lord, J. Cherfils, G. J. Clarkson, L. M. Roberts and D. J. Stephens (2010). "LG186: An inhibitor of GBF1 function that causes Golgi disassembly in human and canine cells." Traffic **11**(12): 1537-1551.

Boeckers, T. M. (2006). "The postsynaptic density." Cell Tissue Res **326**(2): 409-422.

Bonifacino, J. S. and B. S. Glick (2004). "The Mechanisms of Vesicle Budding and Fusion." Cell **116**(2): 153-166.

Bonifacino, J. S. and J. Lippincott-Schwartz (2003). "Coat proteins: shaping membrane transport." Nat Rev Mol Cell Biol **4**(5): 409-414.

Bos, J. L., H. Rehmann and A. Wittinghofer (2007). "GEFs and GAPs: Critical Elements in the Control of Small G Proteins." Cell **129**(5): 865-877.

Brown, H. A., S. Gutowski, C. R. Moomaw, C. Slaughter and P. C. Sternweis (1993). "ADP-ribosylation factor, a small GTP-dependent regulatory protein, stimulates phospholipase D activity." Cell **75**(6): 1137-1144.

Buosi, V., J. P. Placial, J. L. Leroy, J. Cherfils, E. Guittet and C. van Heijenoort (2010). "Insight into the role of dynamics in the conformational switch of the small GTP-binding protein Arf1." J Biol Chem **285**(49): 37987-37994.

Cardenas, J., S. Rivero, B. Goud, M. Bornens and R. M. Rios (2009). "Golgi localisation of GMAP210 requires two distinct cis-membrane binding mechanisms." BMC Biol **7**: 56.

Carroll, R. C., E. C. Beattie, M. von Zastrow and R. C. Malenka (2001). "Role of AMPA receptor endocytosis in synaptic plasticity." Nat Rev Neurosci **2**(5): 315-324.

Casanova, J. E. (2007). "Regulation of Arf activation: the Sec7 family of guanine nucleotide exchange factors." Traffic **8**(11): 1476-1485.

Caumont, A. S., N. Vitale, M. Gensse, M. C. Galas, J. E. Casanova and M. F. Bader (2000). "Identification of a plasma membrane-associated guanine nucleotide exchange factor for ARF6 in chromaffin cells. Possible role in the regulated exocytotic pathway." J Biol Chem **275**(21): 15637-15644.

Chardin, P., S. Paris, B. Antonny, S. Robineau, S. Beraud-Dufour, C. L. Jackson and M. Chabre (1996). "A human exchange factor for ARF contains Sec7- and pleckstrin-homology domains." Nature **384. 384**(6608. 6608): 481-484, 481-484.

Chavrier, P. and J. Menetrey (2010). "Toward a structural understanding of arf family:effector specificity." Structure **18**(12): 1552-1558.

Chen, E. H., B. A. Pryce, J. A. Tzeng, G. A. Gonzalez and E. N. Olson (2003). "Control of myoblast fusion by a guanine nucleotide exchange factor, loner, and its effector ARF6." Cell **114**(6): 751-762.

Cherfils, J. and P. Chardin (1999). "GEFs: structural basis for their activation of small GTP-binding proteins." Trends Biochem Sci **24**(8): 306-311.

Cherfils, J. and P. Melancon (2005). "On the action of Brefeldin A on Sec7-stimulated membrane-recruitment and GDP/GTP exchange of Arf proteins." Biochem Soc Trans **33**(Pt 4): 635-638.

Cherfils, J., J. Menetrey, M. Mathieu, G. Le Bras, S. Robineau, S. Beraud-Dufour, B. Antonny and P. Chardin (1998). "Structure of the Sec7 domain of the Arf exchange factor ARNO." Nature **392. 392**(6671. 6671): 101-105, 101-105.

Choi, S., J. Ko, J. R. Lee, H. W. Lee, K. Kim, H. S. Chung, H. Kim and E. Kim (2006). "ARF6 and EFA6A regulate the development and maintenance of dendritic spines." J Neurosci **26**(18): 4811-4819.

Chun, J., Z. Shapovalova, S. Y. Dejgaard, J. F. Presley and P. Melancon (2008). "Characterization of class I and II ADP-ribosylation factors (Arfs) in live cells: GDP-bound class II Arfs associate with the ER-Golgi intermediate compartment independently of GBF1." Mol Biol Cell **19**(8): 3488-3500.

Claing, A., W. Chen, W. E. Miller, N. Vitale, J. Moss, R. T. Premont and R. J. Lefkowitz (2001). "beta-Arrestin-mediated ADP-ribosylation factor 6 activation and beta 2-adrenergic receptor endocytosis." J Biol Chem **276**(45): 42509-42513.

Claude, A., B. P. Zhao, C. E. Kuziemsky, S. Dahan, S. J. Berger, J. P. Yan, A. D. Armold, E. M. Sullivan and P. Melancon (1999). "GBF1: A novel Golgi-associated BFA-resistant guanine nucleotide exchange factor that displays specificity for ADP-ribosylation factor 5." J Cell Biol **146**(1): 71-84.

Cockcroft, S., G. M. Thomas, A. Fensome, B. Geny, E. Cunningham, I. Gout, I. Hiles, N. F. Totty, O. Truong and J. J. Hsuan (1994). "Phospholipase D: a downstream effector of ARF in granulocytes." Science **263**(5146): 523-526.

Cohen, L. A., A. Honda, P. Varnai, F. D. Brown, T. Balla and J. G. Donaldson (2007). "Active Arf6 recruits ARNO/cytohesin GEFs to the PM by binding their PH domains." Mol Biol Cell **18**(6): 2244-2253.

Colicelli, J. (2004). "Human RAS superfamily proteins and related GTPases." Sci STKE **2004**(250): RE13.

Cox, A. D. and C. J. Der (2002). "Farnesyltransferase inhibitors: promises and realities." Curr Opin Pharmacol **2**(4): 388-393.

Cox, R., R. J. Mason-Gamer, C. L. Jackson and N. Segev (2004). "Phylogenetic analysis of Sec7-domain-containing Arf nucleotide exchangers." Mol Biol Cell **15**(4): 1487-1505.

Cronin, T. C., J. P. DiNitto, M. P. Czech and D. G. Lambright (2004). "Structural determinants of phosphoinositide selectivity in splice variants of Grp1 family PH domains." EMBO J **23**(19): 3711-3720.

D'Angelo, G., E. Polishchuk, G. Di Tullio, M. Santoro, A. Di Campli, A. Godi, G. West, J. Bielawski, C. C. Chuang, A. C. van der Spoel, F. M. Platt, Y. A. Hannun, R. Polishchuk, P. Mattjus and M. A. De Matteis (2007). "Glycosphingolipid synthesis requires FAPP2 transfer of glucosylceramide." Nature **449**(7158): 62-67.

D'Souza-Schorey, C., R. L. Boshans, M. McDonough, P. D. Stahl and L. Van Aelst (1997). "A role for POR1, a Rac1-interacting protein, in ARF6-mediated cytoskeletal rearrangements." EMBO J **16**(17): 5445-5454.

D'Souza-Schorey, C. and P. Chavrier (2006). "ARF proteins: roles in membrane traffic and beyond." Nat Rev Mol Cell Biol **7**(5): 347-358.

D'Souza-Schorey, C., G. Li, M. I. Colombo and P. D. Stahl (1995). "A regulatory role for ARF6 in receptor-mediated endocytosis." Science **267**(5201): 1175-1178.

D'Souza-Schorey, C., E. van Donselaar, V. W. Hsu, C. Yang, P. D. Stahl and P. J. Peters (1998). "ARF6 targets recycling vesicles to the plasma membrane: insights from an ultrastructural investigation." J Cell Biol **140**(3): 603-616.

De Matteis, M. A. and A. Godi (2004). "Protein-lipid interactions in membrane trafficking at the Golgi complex." Biochim Biophys Acta **1666**(1-2): 264-274.

Deretic, D., A. H. Williams, N. Ransom, V. Morel, P. A. Hargrave and A. Arendt (2005). "Rhodopsin C terminus, the site of mutations causing retinal disease, regulates trafficking by binding to ADP-ribosylation factor 4 (ARF4)." Proc Natl Acad Sci U S A **102**(9): 3301-3306.

Derrien, V., C. Couillault, M. Franco, S. Martineau, P. Montcourrier, R. Houlgatte and P. Chavrier (2002). "A conserved C-terminal domain of EFA6-family ARF6-guanine nucleotide exchange factors induces lengthening of microvilli-like membrane protrusions." J Cell Sci **115. 115**(Pt 14. Pt 14): 2867-2879, 2867-2879.

Dever, T. E., M. J. Glynias and W. C. Merrick (1987). "GTP-binding domain: three consensus sequence elements with distinct spacing." Proc Natl Acad Sci U S A **84**(7): 1814-1818.

DiNitto, J. P., A. Delprato, M. T. Gabe Lee, T. C. Cronin, S. Huang, A. Guilherme, M. P. Czech and D. G. Lambright (2007). "Structural basis and mechanism of autoregulation in 3-phosphoinositide-dependent Grp1 family Arf GTPase exchange factors." Mol Cell **28**(4): 569-583.

DiNitto, J. P. and D. G. Lambright (2006). "Membrane and juxtamembrane targeting by PH and PTB domains." Biochim Biophys Acta **1761**(8): 850-867.

Donaldson, J. G. and A. Honda (2005). "Localization and function of Arf family GTPases." Biochem Soc Trans **33**(Pt 4): 639-642.

Donaldson, J. G. and C. L. Jackson (2011). "ARF family G proteins and their regulators: roles in membrane transport, development and disease." Nat Rev Mol Cell Biol **12**(6): 362-375.

Dosemeci, A., A. J. Makusky, E. Jankowska-Stephens, X. Yang, D. J. Slotta and S. P. Markey (2007). "Composition of the synaptic PSD-95 complex." Mol Cell Proteomics **6**(10): 1749-1760.

Dottermusch-Heidel, C., V. Groth, L. Beck and S. F. Onel (2012). "The Arf-GEF Schizo/Loner regulates N-cadherin to induce fusion competence of Drosophila myoblasts." Dev Biol **368**(1): 18-27.

Dunphy, J. L., R. Moravec, K. Ly, T. K. Lasell, P. Melancon and J. E. Casanova (2006). "The Arf6 GEF GEP100/BRAG2 Regulates Cell Adhesion by Controlling Endocytosis of [beta]1 Integrins." Current Biology **16**(3): 315-320.

Dunphy, J. L., K. Ye and J. E. Casanova (2007). "Nuclear functions of the Arf guanine nucleotide exchange factor BRAG2." Traffic **8**(6): 661-672.

Ellong, E. N., K. G. Soni, Q. T. Bui, R. Sougrat, M. P. Golinelli-Cohen and C. L. Jackson (2011). "Interaction between the triglyceride lipase ATGL and the Arf1 activator GBF1." PLoS One **6**(7): e21889.

Feng, Y., A. P. Jadhav, C. Rodighiero, Y. Fujinaga, T. Kirchhausen and W. I. Lencer (2004). "Retrograde transport of cholera toxin from the plasma membrane to the endoplasmic reticulum requires the trans-Golgi network but not the Golgi apparatus in Exo2-treated cells." EMBO Rep **5**(6): 596-601.

Fielding, A. B., E. Schonteich, J. Matheson, G. Wilson, X. Yu, G. R. Hickson, S. Srivastava, S. A. Baldwin, R. Prekeris and G. W. Gould (2005). "Rab11-FIP3 and FIP4 interact with Arf6 and the exocyst to control membrane traffic in cytokinesis." EMBO J **24**(19): 3389-3399.

Franco, M., P. J. Peters, J. Boretto, E. van Donselaar, A. Neri, C. D'Souza-Schorey and P. Chavrier (1999). "EFA6, a sec7 domain-containing exchange factor for ARF6, coordinates membrane recycling and actin cytoskeleton organization." Embo J **18**(6): 1480-1491.

Frank, S., S. Upender, S. H. Hansen and J. E. Casanova (1998). "ARNO is a guanine nucleotide exchange factor for ADP-ribosylation factor 6." J Biol Chem **273**(1): 23-27.

Freedman, T. S., H. Sondermann, G. D. Friedland, T. Kortemme, D. Bar-Sagi, S. Marqusee and J. Kuriyan (2006). "A Ras-induced conformational switch in the Ras activator Son of sevenless." Proc Natl Acad Sci U S A **103**(45): 16692-16697.

Fukaya, M., A. Kamata, Y. Hara, H. Tamaki, O. Katsumata, N. Ito, S. Takeda, Y. Hata, T. Suzuki, M. Watanabe, R. J. Harvey and H. Sakagami (2011). "SynArfGEF is a guanine nucleotide exchange factor for Arf6 and localizes preferentially at post-synaptic specializations of inhibitory synapses." J Neurochem **116**(6): 1122-1137.

Fuss, B., T. Becker, I. Zinke and M. Hoch (2006). "The cytohesin Steppke is essential for insulin signalling in Drosophila." Nature **444**(7121): 945-948.

Garcia-Mata, R. and E. Sztul (2003). "The membrane-tethering protein p115 interacts with GBF1, an ARF guanine-nucleotide-exchange factor." EMBO Rep **4**(3): 320-325.

Geiger, C., W. Nagel, T. Boehm, Y. van Kooyk, C. G. Figdor, E. Kremmer, N. Hogg, L. Zeitlmann, H. Dierks, K. S. Weber and W. Kolanus (2000). "Cytohesin-1 regulates beta-2 integrin-mediated adhesion through both ARF-GEF function and interaction with LFA-1." EMBO J **19**(11): 2525-2536.

Gibbs, J. B., I. S. Sigal, M. Poe and E. M. Scolnick (1984). "Intrinsic GTPase activity distinguishes normal and oncogenic ras p21 molecules." Proc Natl Acad Sci U S A **81**(18): 5704-5708.

Gillingham, A. K. and S. Munro (2007). "The small G proteins of the Arf family and their regulators." Annu Rev Cell Dev Biol **23**: 579-611.

Godi, A., A. Di Campli, A. Konstantakopoulos, G. Di Tullio, D. R. Alessi, G. S. Kular, T. Daniele, P. Marra, J. M. Lucocq and M. A. De Matteis (2004). "FAPPs control Golgi-to-cell-surface membrane traffic by binding to ARF and PtdIns(4)P." Nat Cell Biol **6**(5): 393-404.

Goldberg, J. (1998). "Structural basis for activation of ARF GTPase: mechanisms of guanine nucleotide exchange and GTP-myristoyl switching." Cell **95**(2): 237-248.

Greasley, S. E., H. Jhoti, C. Teahan, R. Solari, A. Fensome, G. M. Thomas, S. Cockcroft and B. Bax (1995). "The structure of rat ADP-ribosylation factor-1 (ARF-1) complexed to GDP determined from two different crystal forms." Nat Struct Biol **2**(9): 797-806.

Guo, Y., T. C. Walther, M. Rao, N. Stuurman, G. Goshima, K. Terayama, J. S. Wong, R. D. Vale, P. Walter and R. V. Farese (2008). "Functional genomic screen reveals genes involved in lipid-droplet formation and utilization." Nature **453**(7195): 657-661.

Gureasko, J., W. J. Galush, S. Boykevisch, H. Sondermann, D. Bar-Sagi, J. T. Groves and J. Kuriyan (2008). "Membrane-dependent signal integration by the Ras activator Son of sevenless." Nat Struct Mol Biol **15**(5): 452-461.

Gureasko, J., O. Kuchment, D. L. Makino, H. Sondermann, D. Bar-Sagi and J. Kuriyan (2010). "Role of the histone domain in the autoinhibition and activation of the Ras activator Son of Sevenless." Proc Natl Acad Sci U S A **107**(8): 3430-3435.

Hafner, M., A. Schmitz, I. Grune, S. G. Srivatsan, B. Paul, W. Kolanus, T. Quast, E. Kremmer, I. Bauer and M. Famulok (2006). "Inhibition of cytohesins by SecinH3 leads to hepatic insulin resistance." Nature **444**(7121): 941-944.

Harvey, J. J. (1964). "An Unidentified Virus Which Causes the Rapid Production of Tumours in Mice." Nature **204**: 1104-1105.

Hashimoto, A., S. Hashimoto, R. Ando, K. Noda, E. Ogawa, H. Kotani, M. Hirose, T. Menju, M. Morishige, T. Manabe, Y. Toda, S. Ishida and H. Sabe (2011). "GEP100-Arf6-AMAP1-cortactin pathway frequently used in cancer invasion is activated by VEGFR2 to promote angiogenesis." PLoS One **6**(8): e23359.

Hattori, Y., S. Ohta, K. Hamada, H. Yamada-Okabe, Y. Kanemura, Y. Matsuzaki, H. Okano, Y. Kawakami and M. Toda (2007). "Identification of a neuron-specific human gene, KIAA1110, that is a guanine nucleotide exchange factor for ARF1." Biochem Biophys Res Commun **364**(4): 737-742.

He, J., J. L. Scott, A. Heroux, S. Roy, M. Lenoir, M. Overduin, R. V. Stahelin and T. G. Kutateladze (2011). "Molecular basis of phosphatidylinositol 4-phosphate and ARF1 GTPase recognition by the FAPP1 pleckstrin homology (PH) domain." J Biol Chem **286**(21): 18650-18657.

Hernandez-Deviez, D., A. Mackay-Sim and J. M. Wilson (2007). "A Role for ARF6 and ARNO in the regulation of endosomal dynamics in neurons." Traffic **8**(12): 1750-1764.

Hernandez-Deviez, D. J., J. E. Casanova and J. M. Wilson (2002). "Regulation of dendritic development by the ARF exchange factor ARNO." Nat Neurosci **5**(7): 623-624.

Hernandez-Deviez, D. J., M. G. Roth, J. E. Casanova and J. M. Wilson (2004). "ARNO and ARF6 regulate axonal elongation and branching through downstream activation of phosphatidylinositol 4-phosphate 5-kinase alpha." Mol Biol Cell **15**(1): 111-120.

Hernandez-Deviez, D. J. and J. M. Wilson (2005). "Functional assay of ARNO and ARF6 in neurite elongation and branching." Methods Enzymol **404**: 242-252.

Hillig, R. C., M. Hanzal-Bayer, M. Linari, J. Becker, A. Wittinghofer and L. Renault (2000). "Structural and biochemical properties show ARL3-GDP as a distinct GTP binding protein." Structure **8**(12): 1239-1245.

Hiroi, T., A. Someya, W. Thompson, J. Moss and M. Vaughan (2006). "GEP100/BRAG2: activator of ADP-ribosylation factor 6 for regulation of cell adhesion and actin

cytoskeleton via E-cadherin and alpha-catenin." Proc Natl Acad Sci U S A **103**(28): 10672-10677.

Hofmann, I., A. Thompson, C. M. Sanderson and S. Munro (2007). "The Arl4 family of small G proteins can recruit the cytohesin Arf6 exchange factors to the plasma membrane." Curr Biol **17**(8): 711-716.

Honda, A., M. Nogami, T. Yokozeki, M. Yamazaki, H. Nakamura, H. Watanabe, K. Kawamoto, K. Nakayama, A. J. Morris, M. A. Frohman and Y. Kanaho (1999). "Phosphatidylinositol 4-phosphate 5-kinase alpha is a downstream effector of the small G protein ARF6 in membrane ruffle formation." Cell **99**(5): 521-532.

Hu, Z., J. Du, L. Yang, Y. Zhu, Y. Yang, D. Zheng, A. Someya, L. Gu and X. Lu (2012). "GEP100/Arf6 Is Required for Epidermal Growth Factor-Induced ERK/Rac1 Signaling and Cell Migration in Human Hepatoma HepG2 Cells." PLoS One **7**(6): e38777.

Hurtado-Lorenzo, A., M. Skinner, J. El Annan, M. Futai, G. H. Sun-Wada, S. Bourgoin, J. Casanova, A. Wildeman, S. Bechoua, D. A. Ausiello, D. Brown and V. Marshansky (2006). "V-ATPase interacts with ARNO and Arf6 in early endosomes and regulates the protein degradative pathway." Nat Cell Biol **8**(2): 124-136.

Inaba, Y., Q. B. Tian, A. Okano, J. P. Zhang, H. Sakagami, S. Miyazawa, W. Li, A. Komiyama, K. Inokuchi, H. Kondo and T. Suzuki (2004). "Brain-specific potential guanine nucleotide exchange factor for Arf, synArfGEF (Po), is localized to postsynaptic density." J Neurochem **89**(6): 1347-1357.

Isabet, T., G. Montagnac, K. Regazzoni, B. Raynal, F. El Khadali, P. England, M. Franco, P. Chavrier, A. Houdusse and J. Menetrey (2009). "The structural basis of Arf effector specificity: the crystal structure of ARF6 in a complex with JIP4." EMBO J **28**(18): 2835-2845.

Itzstein, C., F. P. Coxon and M. J. Rogers (2011). "The regulation of osteoclast function and bone resorption by small GTPases." Small Gtpases **2**(3): 117-130.

Jian, X., J. M. Gruschus, E. Sztul and P. A. Randazzo (2012). "The PH domain of the Arf exchange factor Brag2 is an allosteric binding site." J Biol Chem.

Kagan, J. C. and C. R. Roy (2002). "Legionella phagosomes intercept vesicular traffic from endoplasmic reticulum exit sites." Nat Cell Biol **4**(12): 945-954.

Kahn, R. A., J. Cherfils, M. Elias, R. C. Lovering, S. Munro and A. Schurmann (2006). "Nomenclature for the human Arf family of GTP-binding proteins: ARF, ARL, and SAR proteins." J Cell Biol **172**(5): 645-650.

Kahn, R. A. and A. G. Gilman (1984). "Purification of a protein cofactor required for ADP-ribosylation of the stimulatory regulatory component of adenylate cyclase by cholera toxin." J Biol Chem **259**(10): 6228-6234.

Kahn, R. A. and A. G. Gilman (1986). "The protein cofactor necessary for ADP-ribosylation of Gs by cholera toxin is itself a GTP binding protein." J Biol Chem **261**(17): 7906-7911.

Katsumata, O., N. Ohara, H. Tamaki, T. Niimura, H. Naganuma, M. Watanabe and H. Sakagami (2009). "IQ-ArfGEF/BRAG1 is associated with synaptic ribbons in the mouse retina." Eur J Neurosci **30**(8): 1509-1516.

Kirsten, W. H. and L. A. Mayer (1967). "Morphologic responses to a murine erythroblastosis virus." J Natl Cancer Inst **39**(2): 311-335.

Klarlund, J. K., A. Guilherme, J. J. Holik, J. V. Virbasius, A. Chawla and M. P. Czech (1997). "Signaling by phosphoinositide-3,4,5-trisphosphate through proteins containing pleckstrin and Sec7 homology domains." Science **275**(5308): 1927-1930.

Klarlund, J. K., W. Tsiaras, J. J. Holik, A. Chawla and M. P. Czech (2000). "Distinct polyphosphoinositide binding selectivities for pleckstrin homology domains of GRP1-

like proteins based on diglycine versus triglycine motifs." J Biol Chem **275**(42): 32816-32821.
Klein, S., M. Partisani, M. Franco and F. Luton (2008). "EFA6 facilitates the assembly of the tight junction by coordinating an Arf6-dependent and -independent pathway." J Biol Chem **283**(44): 30129-30138.
Kolanus, W., W. Nagel, B. Schiller, L. Zeitlmann, S. Godar, H. Stockinger and B. Seed (1996). "Alpha L beta 2 integrin/LFA-1 binding to ICAM-1 induced by cytohesin-1, a cytoplasmic regulatory molecule." Cell **86**(2): 233-242.
Krauss, M., M. Kinuta, M. R. Wenk, P. De Camilli, K. Takei and V. Haucke (2003). "ARF6 stimulates clathrin/AP-2 recruitment to synaptic membranes by activating phosphatidylinositol phosphate kinase type Igamma." J Cell Biol **162**(1): 113-124.
Kumari, S. and S. Mayor (2008). "ARF1 is directly involved in dynamin-independent endocytosis." Nat Cell Biol **10**(1): 30-41.
Langille, S. E., V. Patki, J. K. Klarlund, J. M. Buxton, J. J. Holik, A. Chawla, S. Corvera and M. P. Czech (1999). "ADP-ribosylation factor 6 as a target of guanine nucleotide exchange factor GRP1." J Biol Chem **274**(38): 27099-27104.
Lemmon, M. A. (2008). "Membrane recognition by phospholipid-binding domains." Nat Rev Mol Cell Biol **9**(2): 99-111.
Li, C. C., T. C. Chiang, T. S. Wu, G. Pacheco-Rodriguez, J. Moss and F. J. Lee (2007). "ARL4D recruits cytohesin-2/ARNO to modulate actin remodeling." Mol Biol Cell **18**(11): 4420-4437.
Liu, L., H. Liao, A. Castle, J. Zhang, J. Casanova, G. Szabo and D. Castle (2005). "SCAMP2 interacts with Arf6 and phospholipase D1 and links their function to exocytotic fusion pore formation in PC12 cells." Mol Biol Cell **16**(10): 4463-4472.
Liu, Y., R. A. Kahn and J. H. Prestegard (2010). "Dynamic structure of membrane-anchored Arf*GTP." Nat Struct Mol Biol **17**(7): 876-881.
Luton, F., S. Klein, J. P. Chauvin, A. Le Bivic, S. Bourgoin, M. Franco and P. Chardin (2004). "EFA6, exchange factor for ARF6, regulates the actin cytoskeleton and associated tight junction in response to E-cadherin engagement." Mol Biol Cell **15**(3): 1134-1145.
Macia, E., M. Chabre and M. Franco (2001). "Specificities for the small G proteins ARF1 and ARF6 of the guanine nucleotide exchange factors ARNO and EFA6." J Biol Chem **276. 276**(27. 27): 24925-24930, 24925-24930.
Macia, E., M. Partisani, C. Favard, E. Mortier, P. Zimmermann, M. F. Carlier, P. Gounon, F. Luton and M. Franco (2008). "The pleckstrin homology domain of the Arf6-specific exchange factor EFA6 localizes to the plasma membrane by interacting with phosphatidylinositol 4,5-bisphosphate and F-actin." J Biol Chem **283**(28): 19836-19844.
Macia, E., M. Partisani, O. Paleotti, F. Luton, and M. Franco (2012). "Arf6 negatively controls the rapid recycling of the β2-AR." J Cell Sci [Epub ahead of print].
Madaule, P. and R. Axel (1985). "A novel ras-related gene family." Cell **41**(1): 31-40.
Margarit, S. M., H. Sondermann, B. E. Hall, B. Nagar, A. Hoelz, M. Pirruccello, D. Bar-Sagi and J. Kuriyan (2003). "Structural evidence for feedback activation by Ras.GTP of the Ras-specific nucleotide exchange factor SOS." Cell **112**(5): 685-695.
Matsuya, S., H. Sakagami, A. Tohgo, Y. Owada, H. W. Shin, H. Takeshima, K. Nakayama, S. Kokubun and H. Kondo (2005). "Cellular and subcellular localization of EFA6C, a third member of the EFA6 family, in adult mouse Purkinje cells." J Neurochem **93**(3): 674-685.
Mazaki, Y., Y. Nishimura and H. Sabe (2012). "GBF1 bears a novel phosphatidylinositol-phosphate binding module, BP3K, to link PI3Kgamma activity with Arf1 activation

involved in GPCR-mediated neutrophil chemotaxis and superoxide production." Mol Biol Cell.

Menetrey, J., E. Macia, S. Pasqualato, M. Franco and J. Cherfils (2000). "Structure of Arf6-GDP suggests a basis for guanine nucleotide exchange factors specificity." Nat Struct Biol **7. 7**(6. 6): 466-469, 466-469.

Menetrey, J., M. Perderiset, J. Cicolari, T. Dubois, N. Elkhatib, F. El Khadali, M. Franco, P. Chavrier and A. Houdusse (2007). "Structural basis for ARF1-mediated recruitment of ARHGAP21 to Golgi membranes." EMBO J **26**(7): 1953-1962.

Menju, T., S. Hashimoto, A. Hashimoto, Y. Otsuka, H. Handa, E. Ogawa, Y. Toda, H. Wada, H. Date and H. Sabe (2011). "Engagement of overexpressed Her2 with GEP100 induces autonomous invasive activities and provides a biomarker for metastases of lung adenocarcinoma." PLoS One **6**(9): e25301.

Milburn, M. V., L. Tong, A. M. deVos, A. Brunger, Z. Yamaizumi, S. Nishimura and S. H. Kim (1990). "Molecular switch for signal transduction: structural differences between active and inactive forms of protooncogenic ras proteins." Science **247**(4945): 939-945.

Misumi, Y., K. Miki, A. Takatsuki, G. Tamura and Y. Ikehara (1986). "Novel blockade by brefeldin A of intracellular transport of secretory proteins in cultured rat hepatocytes." J Biol Chem **261**(24): 11398-11403.

Moreau, K., B. Ravikumar, C. Puri and D. C. Rubinsztein (2012). "Arf6 promotes autophagosome formation via effects on phosphatidylinositol 4,5-bisphosphate and phospholipase D." J Cell Biol **196**(4): 483-496.

Morishige, M., S. Hashimoto, E. Ogawa, Y. Toda, H. Kotani, M. Hirose, S. Wei, A. Hashimoto, A. Yamada, H. Yano, Y. Mazaki, H. Kodama, Y. Nio, T. Manabe, H. Wada, H. Kobayashi and H. Sabe (2008). "GEP100 links epidermal growth factor receptor signalling to Arf6 activation to induce breast cancer invasion." Nat Cell Biol **10**(1): 85-92.

Mossessova, E., R. A. Corpina and J. Goldberg (2003). "Crystal structure of ARF1*Sec7 complexed with Brefeldin A and its implications for the guanine nucleotide exchange mechanism." Mol Cell **12**(6): 1403-1411.

Mossessova, E., J. M. Gulbis and J. Goldberg (1998). "Structure of the guanine nucleotide exchange factor Sec7 domain of human arno and analysis of the interaction with ARF GTPase." Cell **92. 92**(3. 3): 415-423, 415-423.

Mouratou, B., V. Biou, A. Joubert, J. Cohen, D. Shields, N. Geldner, G. Jurgens, P. Melancon and J. Cherfils (2005). "The domain architecture of large guanine nucleotide exchange factors for the small GTP-binding protein Arf." BMC Genomics **6**(1): 20.

Mukherjee, S., V. V. Gurevich, J. C. Jones, J. E. Casanova, S. R. Frank, E. T. Maizels, M. F. Bader, R. A. Kahn, K. Palczewski, K. Aktories and M. Hunzicker-Dunn (2000). "The ADP ribosylation factor nucleotide exchange factor ARNO promotes beta-arrestin release necessary for luteinizing hormone/choriogonadotropin receptor desensitization." Proc Natl Acad Sci U S A **97**(11): 5901-5906.

Murphy, J. A., O. N. Jensen and R. S. Walikonis (2006). "BRAG1, a Sec7 domain-containing protein, is a component of the postsynaptic density of excitatory synapses." Brain Res **1120**(1): 35-45.

Myers, K. R. and J. E. Casanova (2008). "Regulation of actin cytoskeleton dynamics by Arf-family GTPases." Trends Cell Biol **18**(4): 184-192.

Nagai, H., J. C. Kagan, X. Zhu, R. A. Kahn and C. R. Roy (2002). "A bacterial guanine nucleotide exchange factor activates ARF on Legionella phagosomes." Science **295**(5555): 679-682.

Nagel, W., P. Schilcher, L. Zeitlmann and W. Kolanus (1998). "The PH domain and the polybasic c domain of cytohesin-1 cooperate specifically in plasma membrane association and cellular function." Mol Biol Cell **9**(8): 1981-1994.

Ogasawara, M., S. C. Kim, R. Adamik, A. Togawa, V. J. Ferrans, K. Takeda, M. Kirby, J. Moss and M. Vaughan (2000). "Similarities in function and gene structure of cytohesin-4 and cytohesin-1, guanine nucleotide-exchange proteins for ADP-ribosylation factors." J Biol Chem **275**(5): 3221-3230.

Oh, S. J. and L. C. Santy (2012). "Phosphoinositide specificity determines which cytohesins regulate beta1 integrin recycling." J Cell Sci.

Orlichenko, L., D. B. Stolz, P. Noel, J. Behari, S. Liu and V. P. Singh (2012). "ADP-ribosylation factor 1 regulates trypsinogen activation via organellar trafficking of pro-cathepsin B and autophagic maturation in acute pancreatitis." J Biol Chem.

Pai, E. F., U. Krengel, G. A. Petsko, R. S. Goody, W. Kabsch and A. Wittinghofer (1990). "Refined crystal structure of the triphosphate conformation of H-ras p21 at 1.35 A resolution: implications for the mechanism of GTP hydrolysis." EMBO J **9**(8): 2351-2359.

Pajcini, K. V., J. H. Pomerantz, O. Alkan, R. Doyonnas and H. M. Blau (2008). "Myoblasts and macrophages share molecular components that contribute to cell-cell fusion." J Cell Biol **180**(5): 1005-1019.

Palacios, F., L. Price, J. Schweitzer, J. G. Collard and C. D'Souza-Schorey (2001). "An essential role for ARF6-regulated membrane traffic in adherens junction turnover and epithelial cell migration." EMBO J **20**(17): 4973-4986.

Pasqualato, S., J. Menetrey, M. Franco and J. Cherfils (2001). "The structural GDP/GTP cycle of human Arf6." EMBO Rep **2. 2**(3. 3): 234-238, 234-238.

Pasqualato, S., L. Renault and J. Cherfils (2002). "Arf, Arl, Arp and Sar proteins: a family of GTP-binding proteins with a structural device for 'front-back' communication." EMBO Rep **3**(11): 1035-1041.

Peyroche, A., B. Antonny, S. Robineau, J. Acker, J. Cherfils and C. L. Jackson (1999). "Brefeldin A acts to stabilize an abortive ARF-GDP-Sec7 domain protein complex: involvement of specific residues of the Sec7 domain." Mol Cell **3. 3**(3. 3): 275-285, 275-285.

Pommier, Y. and J. Cherfils (2005). "Interfacial inhibition of macromolecular interactions: nature's paradigm for drug discovery." Trends Pharmacol Sci **26**(3): 138-145.

Radhakrishna, H., R. D. Klausner and J. G. Donaldson (1996). "Aluminum fluoride stimulates surface protrusions in cells overexpressing the ARF6 GTPase." J Cell Biol **134**(4): 935-947.

Renault, L., B. Guibert and J. Cherfils (2003). "Structural snapshots of the mechanism and inhibition of a guanine nucleotide exchange factor." Nature **426**(6966): 525-530.

Riley, K. N., A. E. Maldonado, P. Tellier, C. D'Souza-Schorey and I. M. Herman (2003). "Betacap73-ARF6 interactions modulate cell shape and motility after injury in vitro." Mol Biol Cell **14**(10): 4155-4161.

Rojas, A. M., G. Fuentes, A. Rausell and A. Valencia (2012). "The Ras protein superfamily: evolutionary tree and role of conserved amino acids." J Cell Biol **196**(2): 189-201.

Sadakata, T., Y. Shinoda, Y. Sekine, C. Saruta, M. Itakura, M. Takahashi and T. Furuichi (2010). "Interaction of calcium-dependent activator protein for secretion 1 (CAPS1) with the class II ADP-ribosylation factor small GTPases is required for dense-core vesicle trafficking in the trans-Golgi network." J Biol Chem **285**(49): 38710-38719.

Saenz, J. B., W. J. Sun, J. W. Chang, J. Li, B. Bursulaya, N. S. Gray and D. B. Haslam (2009). "Golgicide A reveals essential roles for GBF1 in Golgi assembly and function." Nat Chem Biol **5**(3): 157-165.

Sakagami, H., M. Sanda, M. Fukaya, T. Miyazaki, J. Sukegawa, T. Yanagisawa, T. Suzuki, K. Fukunaga, M. Watanabe and H. Kondo (2008). "IQ-ArfGEF/BRAG1 is a guanine nucleotide exchange factor for Arf6 that interacts with PSD-95 at postsynaptic density of excitatory synapses." Neurosci Res **60**(2): 199-212.

Sakagami, H., H. Suzuki, A. Kamata, Y. Owada, K. Fukunaga, H. Mayanagi and H. Kondo (2006). "Distinct spatiotemporal expression of EFA6D, a guanine nucleotide exchange factor for ARF6, among the EFA6 family in mouse brain." Brain Res **1093**(1): 1-11.

Sakurai, A., X. Jian, C. J. Lee, Y. Manavski, E. Chavakis, J. Donaldson, P. A. Randazzo and J. S. Gutkind (2011). "Phosphatidylinositol-4-phosphate 5-kinase and GEP100/Brag2 protein mediate antiangiogenic signaling by semaphorin 3E-plexin-D1 through Arf6 protein." J Biol Chem **286**(39): 34335-34345.

Sanda, M., A. Kamata, O. Katsumata, K. Fukunaga, M. Watanabe, H. Kondo and H. Sakagami (2009). "The postsynaptic density protein, IQ-ArfGEF/BRAG1, can interact with IRSp53 through its proline-rich sequence." Brain Res **1251**: 7-15.

Santarius, M., C. H. Lee and R. A. Anderson (2006). "Supervised membrane swimming: small G-protein lifeguards regulate PIPK signalling and monitor intracellular PtdIns(4,5)P2 pools." Biochem J **398**(1): 1-13.

Santy, L. C. and J. E. Casanova (2001). "Activation of ARF6 by ARNO stimulates epithelial cell migration through downstream activation of both Rac1 and phospholipase D." J Cell Biol **154**(3): 599-610.

Santy, L. C., S. R. Frank, J. C. Hatfield and J. E. Casanova (1999). "Regulation of ARNO nucleotide exchange by a PH domain electrostatic switch." Curr Biol **9**(20): 1173-1176.

Schmitz, F., A. Konigstorfer and T. C. Sudhof (2000). "RIBEYE, a component of synaptic ribbons: a protein's journey through evolution provides insight into synaptic ribbon function." Neuron **28**(3): 857-872.

Scholz, R., S. Berberich, L. Rathgeber, A. Kolleker, G. Kohr and H. C. Kornau (2010). "AMPA receptor signaling through BRAG2 and Arf6 critical for long-term synaptic depression." Neuron **66**(5): 768-780.

Schultz, J., F. Milpetz, P. Bork and C. P. Ponting (1998). "SMART, a simple modular architecture research tool: identification of signaling domains." Proc Natl Acad Sci U S A **95**(11): 5857-5864.

Schweitzer, J. K. and C. D'Souza-Schorey (2005). "A requirement for ARF6 during the completion of cytokinesis." Exp Cell Res **311**(1): 74-83.

Scolnick, E. M., A. G. Papageorge and T. Y. Shih (1979). "Guanine nucleotide-binding activity as an assay for src protein of rat-derived murine sarcoma viruses." Proc Natl Acad Sci U S A **76**(10): 5355-5359.

Seabra, M. C. and C. Wasmeier (2004). "Controlling the location and activation of Rab GTPases." Curr Opin Cell Biol **16**(4): 451-457.

Shen, X., M.-S. Hong, J. Moss and M. Vaughan (2007). "BIG1, a brefeldin A-inhibited guanine nucleotide-exchange protein, is required for correct glycosylation and function of integrin beta1." PNAS **104**(4): 1230-1235.

Shen, X., V. Meza-Carmen, E. Puxeddu, G. Wang, J. Moss and M. Vaughan (2008). "Interaction of brefeldin A-inhibited guanine nucleotide-exchange protein (BIG) 1 and kinesin motor protein KIF21A." Proc Natl Acad Sci U S A **105**(48): 18788-18793.

Shen, X., K.-F. Xu, Q. Fan, G. Pacheco-Rodriguez, J. Moss and M. Vaughan (2006). "Association of brefeldin A-inhibited guanine nucleotide-exchange protein 2 (BIG2) with recycling endosomes during transferrin uptake." PNAS **103**(8): 2635-2640.

Shiba, T., M. Kawasaki, H. Takatsu, T. Nogi, N. Matsugaki, N. Igarashi, M. Suzuki, R. Kato, K. Nakayama and S. Wakatsuki (2003). "Molecular mechanism of membrane

recruitment of GGA by ARF in lysosomal protein transport." Nat Struct Biol **10**(5): 386-393.

Shih, T. Y., A. G. Papageorge, P. E. Stokes, M. O. Weeks and E. M. Scolnick (1980). "Guanine nucleotide-binding and autophosphorylating activities associated with the p21src protein of Harvey murine sarcoma virus." Nature **287**(5784): 686-691.

Shoubridge, C., P. S. Tarpey, F. Abidi, S. L. Ramsden, S. Rujirabanjerd, J. A. Murphy, J. Boyle, M. Shaw, A. Gardner, A. Proos, H. Puusepp, F. L. Raymond, C. E. Schwartz, R. E. Stevenson, G. Turner, M. Field, R. S. Walikonis, R. J. Harvey, A. Hackett, P. A. Futreal, M. R. Stratton and J. Gecz (2010). "Mutations in the guanine nucleotide exchange factor gene IQSEC2 cause nonsyndromic intellectual disability." Nat Genet **42**(6): 486-488.

Someya, A., J. Moss and I. Nagaoka (2006). "Involvement of a guanine nucleotide-exchange protein, ARF-GEP100/BRAG2a, in the apoptotic cell death of monocytic phagocytes." J Leukoc Biol **80**(4): 915-921.

Someya, A., J. Moss and I. Nagaoka (2010). "The guanine nucleotide exchange protein for ADP-ribosylation factor 6, ARF-GEP100/BRAG2, regulates phagocytosis of monocytic phagocytes in an ARF6-dependent process." J Biol Chem **285**(40): 30698-30707.

Someya, A., M. Sata, K. Takeda, G. Pacheco-Rodriguez, V. J. Ferrans, J. Moss and M. Vaughan (2001). "ARF-GEP(100), a guanine nucleotide-exchange protein for ADP-ribosylation factor 6." Proc Natl Acad Sci U S A **98**(5): 2413-2418.

Sondermann, H., S. M. Soisson, S. Boykevisch, S. S. Yang, D. Bar-Sagi and J. Kuriyan (2004). "Structural analysis of autoinhibition in the Ras activator Son of sevenless." Cell **119**(3): 393-405.

Soni, K. G., G. A. Mardones, R. Sougrat, E. Smirnova, C. L. Jackson and J. S. Bonifacino (2009). "Coatomer-dependent protein delivery to lipid droplets." J Cell Sci **122**(Pt 11): 1834-1841.

Spooner, R. A., P. Watson, D. C. Smith, F. Boal, M. Amessou, L. Johannes, G. J. Clarkson, J. M. Lord, D. J. Stephens and L. M. Roberts (2008). "The secretion inhibitor Exo2 perturbs trafficking of Shiga toxin between endosomes and the trans-Golgi network." Biochem J **414**(3): 471-484.

Stalder, D., H. Barelli, R. Gautier, E. Macia, C. L. Jackson and B. Antonny (2011). "Kinetic studies of the Arf activator Arno on model membranes in the presence of Arf effectors suggest control by a positive feedback loop." J Biol Chem **286**(5): 3873-3883.

Takai, Y., T. Sasaki and T. Matozaki (2001). "Small GTP-binding proteins." Physiol Rev **81**(1): 153-208.

Takashima, K., A. Saitoh, S. Hirose, W. Nakai, Y. Kondo, Y. Takasu, H. Kakeya, H. W. Shin and K. Nakayama (2011). "GBF1-Arf-COPI-ArfGAP-mediated Golgi-to-ER transport involved in regulation of lipid homeostasis." Cell Struct Funct **36**(2): 223-235.

Theard, D., F. Labarrade, M. Partisani, J. Milanini, H. Sakagami, E. A. Fon, S. A. Wood, M. Franco and F. Luton (2010). "USP9x-mediated deubiquitination of EFA6 regulates de novo tight junction assembly." EMBO J **29**(9): 1499-1509.

Tian, Q. B., K. Nakayama, A. Okano and T. Suzuki (1999). "Identification of mRNAs localizing in the postsynaptic region." Brain Res Mol Brain Res **72**(2): 147-157.

Torii, T., Y. Miyamoto, K. Nakamura, M. Maeda, J. Yamauchi and A. Tanoue (2012). "Arf6 guanine-nucleotide exchange factor, cytohesin-2, interacts with actinin-1 to regulate neurite extension." Cell Signal.

Uchida, Y., J. Hasegawa, D. Chinnapen, T. Inoue, S. Okazaki, R. Kato, S. Wakatsuki, R. Misaki, M. Koike, Y. Uchiyama, S. Iemura, T. Natsume, R. Kuwahara, T. Nakagawa, K. Nishikawa, K. Mukai, E. Miyoshi, N. Taniguchi, D. Sheff, W. I. Lencer, T.

Taguchi and H. Arai (2011). "Intracellular phosphatidylserine is essential for retrograde membrane traffic through endosomes." Proc Natl Acad Sci U S A **108**(38): 15846-15851.

Venkateswarlu, K. (2003). "Interaction Protein for Cytohesin Exchange Factors 1 (IPCEF1) Binds Cytohesin 2 and Modifies Its Activity." J. Biol. Chem. **278**(44): 43460-43469.

Vetter, I. R. and A. Wittinghofer (2001). "The guanine nucleotide-binding switch in three dimensions." Science **294**(5545): 1299-1304.

Viaud, J., M. Zeghouf, H. Barelli, J. C. Zeeh, A. Padilla, B. Guibert, P. Chardin, C. A. Royer, J. Cherfils and A. Chavanieu (2007). "Structure-based discovery of an inhibitor of Arf activation by Sec7 domains through targeting of protein-protein complexes." Proc Natl Acad Sci U S A **104**(25): 10370-10375.

Wennerberg, K., K. L. Rossman and C. J. Der (2005). "The Ras superfamily at a glance." J Cell Sci **118**(Pt 5): 843-846.

Wittinghofer, A. and I. R. Vetter (2011). "Structure-function relationships of the G domain, a canonical switch motif." Annu Rev Biochem **80**: 943-971.

Xie, C. G., S. M. Wei, J. M. Chen, X. F. Xu, J. T. Cai, Q. Y. Chen and L. T. Jia (2012). "Down-Regulation of GEP100 Causes Increase in E-Cadherin Levels and Inhibits Pancreatic Cancer Cell Invasion." PLoS One **7**(5): e37854.

Zeeh, J. C., M. Zeghouf, C. Grauffel, B. Guibert, E. Martin, A. Dejaegere and J. Cherfils (2006). "Dual specificity of the interfacial inhibitor brefeldin a for arf proteins and sec7 domains." J Biol Chem **281**(17): 11805-11814.

Zhang, Q., D. Cox, C. C. Tseng, J. G. Donaldson and S. Greenberg (1998). "A requirement for ARF6 in Fcgamma receptor-mediated phagocytosis in macrophages." J Biol Chem **273**(32): 19977-19981.

Zhao, X., A. Claude, J. Chun, D. J. Shields, J. F. Presley and P. Melancon (2006). "GBF1, a cis-Golgi and VTCs-localized ARF-GEF, is implicated in ER-to-Golgi protein traffic." J Cell Sci: jcs.03173.

ANNEXES

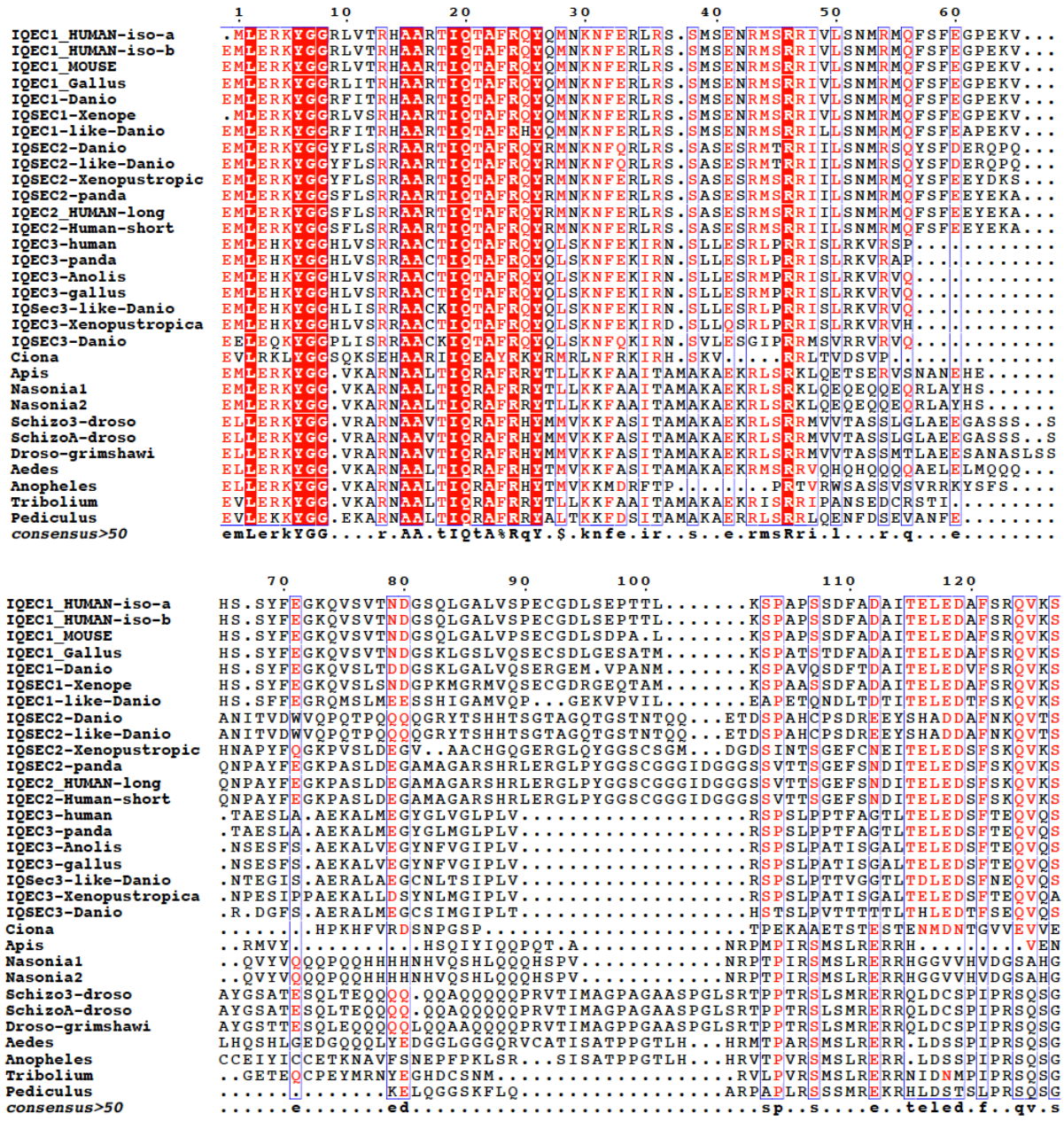
IQEC1_HUMAN-iso-a
IQEC1_HUMAN-iso-b
IQEC1_MOUSE
IQEC1_Gallus
IQEC1-Danio
IQSEC1-Xenope
IQEC1-like-Danio
IQSEC2-Danio
IQSEC2-like-Danio
IQSEC2-Xenopustropic
IQSEC2-panda
IQEC2_HUMAN-long
IQEC2-Human-short
IQEC3-human
IQEC3-panda
IQEC3-Anolis
IQEC3-gallus
IQSec3-like-Danio
IQEC3-Xenopustropica
IQSEC3-Danio
Ciona
Apis
Nasonia1
Nasonia2
Schizo3-droso
SchizoA-droso
Droso-grimshawi
Aedes
Anopheles
Tribolium
Pediculus
consensus>50

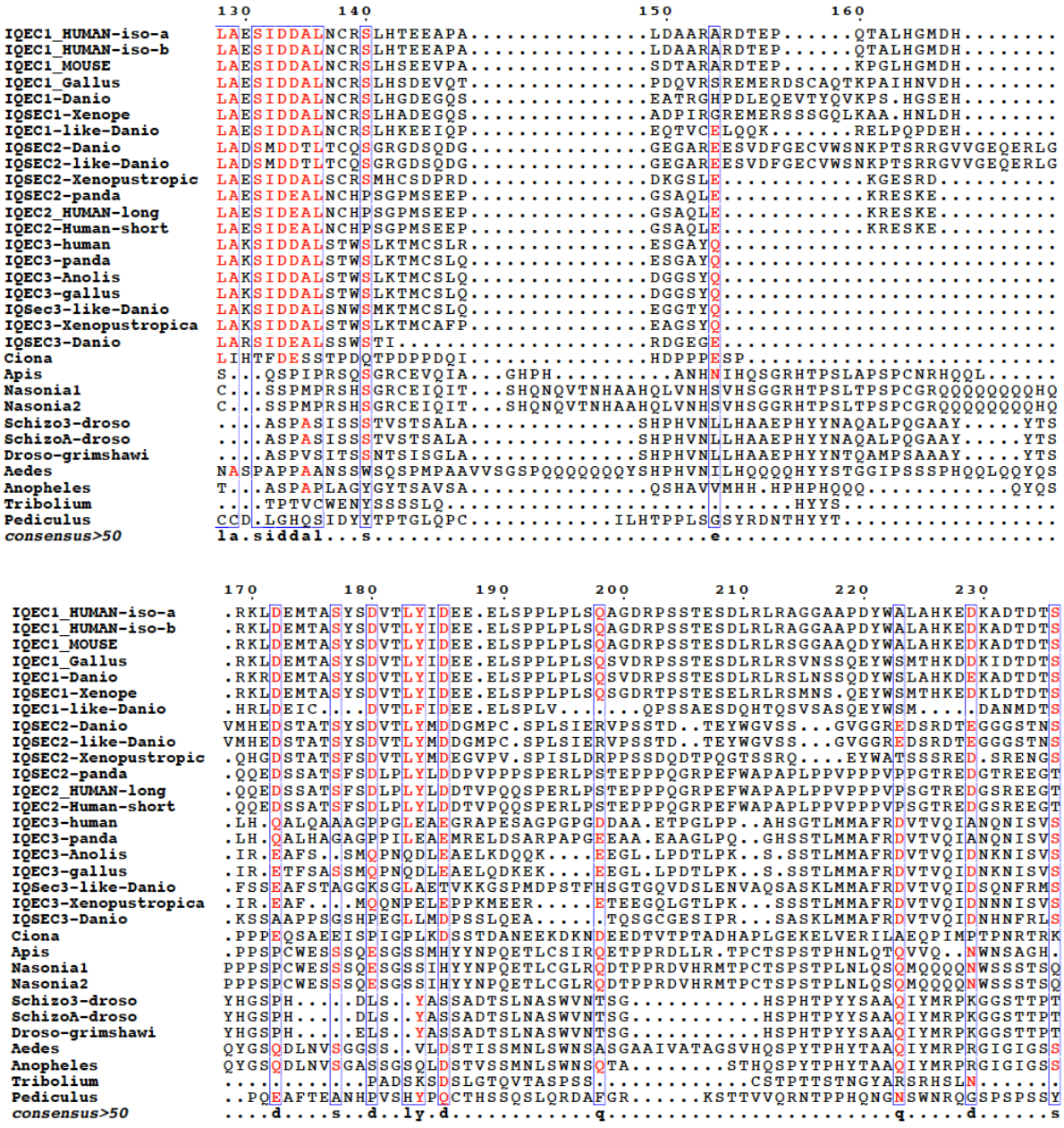
130 140 150 160
IQEC1_HUMAN-iso-a LAESIDDALNCRSLHTEEAPA.....LDAARARDTEP.....QTALHGMDH.....
IQEC1_HUMAN-iso-b LAESIDDALNCRSLHTEEAPA.....LDAARARDTEP.....QTALHGMDH.....
IQEC1_MOUSE LAESIDDALNCRSLHSEEVPA.....SDTARARDTEP.....KPGLHGMDH.....
IQEC1_Gallus LAESIDDALNCRSLHSDEVQT.....PDQVRSREMERDSCAQTKPAIHNVDH.....
IQEC1-Danio LAESIDDALNCRSLHGDEGQS.....EATRGHPDLEQEVTYQVKPS.HGSEH.....
IQSEC1-Xenope LAESIDDALNCRSLHADEGQS.....ADPIRGREMERSSSGQLKAA.HNLDH.....
IQEC1-like-Danio LAESIDDALNCRSLHKEEIQP.....EQTVCELQQK.....RELPQPDEH.....
IQSEC2-Danio LADSMDDTLTCQSGRGDSQDG.....GEGAREESVDFGECVWSNKPTSRRGVVGEQERLG
IQSEC2-like-Danio LADSMDDTLTCQSGRGDSQDG.....GEGARESVDFGECVWSNKPTSRRGVVGEQERLG
IQSEC2-Xenopustropic LAESIDDALSCRSMHCSDPRD.....DKGSLE.....KGESRD.....
IQSEC2-panda LAESIDEALNCHPSGPMSEEP.....GSAQLE.....KRESKE.....
IQEC2_HUMAN-long LAESIDEALNCHPSGPMSEEP.....GSAQLE.....KRESKE.....
IQEC2-Human-short LAESIDEALNCHPSGPMSEEP.....GSAQLE.....KRESKE.....
IQEC3-human LAKSIDDALSTWSLKTMCSLR.....ESGAYQ.....
IQEC3-panda LAKSIDDALSTWSLKTMCSLQ.....ESGAYQ.....
IQEC3-Anolis LAKSIDDALSTWSLKTMCSLQ.....DGGSYQ.....
IQEC3-gallus LAKSIDDALSTWSLKTMCSLQ.....DGGSYQ.....
IQSec3-like-Danio LAKSIDDALSNWSMKTMCSLQ.....EGGTYQ.....
IQEC3-Xenopustropica LAKSIDDALSTWSLKTMCAFP.....EAGSYQ.....
IQSEC3-Danio LARSIDEALSSWSTI.....RDGEGE.....
Ciona LIHTFDESSTPDQTPDPPDQI.....HDPPPESP.....
Apis S...QSPIPRSQSGRCEVQIA...GHPH.....ANHNIHQSGRHTPSLAPSPCNRHQQL.....
Nasonia1 C...SSPMPRSHSGRCEIQIT...SHQNQVTNHAAHQLVNHSVHSGGRHTPSLTPSPCGRQQQQQQQQQHQ
Nasonia2 C...SSPMPRSHSGRCEIQIT...SHQNQVTNHAAHQLVNHSVHSGGRHTPSLTPSPCGRQQQQQQQQQHQ
Schizo3-droso ....ASPASISSSTVSTSALA.....SHPHVNLLHAAEPHYYNAQALPQGAAY.....YTS
SchizoA-droso ....ASPASISSSTVSTSALA.....SHPHVNLLHAAEPHYYNAQALPQGAAY.....YTS
Droso-grimshawi ....ASPVSITSSNTSISGLA.....SHPHVNLLHAAEPHYYNTQAMPSAAAY.....YTS
Aedes NASPAPPAANSSWSQSPMPAAVVSGSPQQQQQQQYSHPHVNILHQQQQHYYSTGGIPSSSPHQQLQQYQS
Anopheles T...ASPAPLAGYGYTSAVSA.....QSHAVVMHH.HPHPHQQQ.....QYQS
Tribolium ....TPTVCWENYSSSSLQ.....HYYS.....
Pediculus CCD.LGHQSIDYYTPTGLQPC.....ILHTPPLSGSYRDNTHYYT.....
consensus>50 la.siddal...s.....e.....
170 180 190 200 210 220 230
IQEC1_HUMAN-iso-a .RKLDEMTASYSDVTLYIDEE.ELSPPLPLSQAGDRPSSTESDLRLRAGGAAPDYWALAHKEDKADTDTS
IQEC1_HUMAN-iso-b .RKLDEMTASYSDVTLYIDEE.ELSPPLPLSQAGDRPSSTESDLRLRAGGAAPDYWALAHKEDKADTDTS
IQEC1_MOUSE .RKLDEMTASYSDVTLYIDEE.ELSPPLPLSQAGDRPSSTESDLRLRSGGAAQDYWALAHKEDKADTDTS
IQEC1_Gallus .RKLDEMTASYSDVTLYIDEE.ELSPPLPLSQSVDRPSSTESDLRLRSVNSSQEYWSMTHKDDKIDTDTS
IQEC1-Danio .RKRDEMTASYSDVTLYIDEE.ELSPPLPLSQSVDRPSSTESDLRLRSLNSSQDYWSLAHKDEKADTDTS
IQSEC1-Xenope .RKLDEMTASYSDVTLYIDEE.ELSPPLPLSQSGDRTPSTESELRLRSMNS.QEYWSMTHKEDKLDTDTS
IQEC1-like-Danio .HRLDEIC....DVTLFIDEE.ELSPLV.....QPSSAESDQHTQSVSASQEYWSM.....DANMDTS
IQSEC2-Danio VMHEDSTATSYSDVTLYMDDGMPC.SPLSIERVPSSTD..TEYWGVSS...GVGGREDSRDTEGGGSTNS
IQSEC2-like-Danio VMHEDSTATSYSDVTLYMDDGMPC.SPLSIERVPSSTD..TEYWGVSS...GVGGREDSRDTEGGGSTNS
IQSEC2-Xenopustropic .QHGDSTATSFSDVTLYMDEGVPV.SPISLDRPPSSDQDTPQGTSSRQ....EYWATSSSRED.SRENGS
IQSEC2-panda .QQEDSSATSFSDLPLYLDDPVPPPSPERLPSTEPPPQGRPEFWAPAPLPPVPPPVPPGTREDGTREEGT
IQEC2_HUMAN-long .QQEDSSATSFSDLPLYLDDTVPQQSPERLPSTEPPPQGRPEFWAPAPLPPVPPPVPSGTREDGSREEGT
IQEC2-Human-short .QQEDSSATSFSDLPLYLDDTVPQQSPERLPSTEPPPQGRPEFWAPAPLPPVPPPVPSGTREDGSREEGT
IQEC3-human .LH.QALQAAAGPPGLEAEGRAPESAGPGPGDDAA.ETPGLPP..AHSGTLMMAFRDVTVQIANQNISVS
IQEC3-panda .LH.QALHAGAGPPILEAEMRELDSARPAPGEEAA.EAAGLPQ..GHSSTLMMAFRDVTVQIANQNISVS
IQEC3-Anolis .IR.EAFS..SMQPNQDLEAELKDQQK....EEGL.LPDTLPK..S.SSTLMMAFRDVTVQIDNKNISVS
IQEC3-gallus .IR.ETFSASSMQPNQDLEAELQDKEK....EEGL.LPDTLPK..S.SSTLMMAFRDVTVQIDNKNISVS
IQSec3-like-Danio .FSSEAFSTAGGKSGLAETVKKGSPMDPSTFHSGTGQVDSLENVAQSASKLMMAFRDVTVQIDSQNFRMS
IQEC3-Xenopustropica .IR.EAF....MQQNPELEPPKMEER.....ETEEGQLGTLPK...SSSTLMMAFRDVTVQIDNNNISVS
IQSEC3-Danio .KSSAAPPSGSHPEGLLMDPSSLQEA.....TQSGCGESIPR...SASKLMMAFRDVTVQIDNHNFRLS
Ciona .PPPEQSAEEISPIGPLKDSSTDANEEKDKNDEEDTVTPTADHAPLGEKELVERILAEQPIMPTPNRTRK
Apis .PPSPCWESSSQESGSSMHYYNPQETLCSIRQETPPRDLLR.TPCTSPSTPHNLQTQVVQ..NWNSAGH.
Nasonia1 PPPSPCWESSSQESGSSIHYYNPQETLCGLRQDTPPRDVHRMTPCTSPSTPLNLQSQMQQQQNWSSSTSQ
Nasonia2 PPPSPCWESSSQESGSSIHYYNPQETLCGLRQDTPPRDVHRMTPCTSPSTPLNLQSQMQQQQNWSSSTSQ
Schizo3-droso YHGSPH....DLS..YASSADTSLNASWVNTSG.....HSPHTPYYSAAQIYMRPKGGSTTPT
SchizoA-droso YHGSPH....DLS..YASSADTSLNASWVNTSG.....HSPHTPYYSAAQIYMRPKGGSTTPT
Droso-grimshawi YHGSPH....ELS..YASSADTSLNASWVNTSG.....HSPHTPYYSAAQIYMRPKGGSTTPT
Aedes QYGSQDLNVSGGSS..VLDSTISSMNLSWNSASGAAIVATAGSVHQSPYTPHYTAAQIYMRPRGIGIGSS
Anopheles QYGSQDLNVSGASSGSQLDSTVSSMNLSWNSQTA.....STHQSPYTPHYTAAQIYMRPRGIGIGSS
Tribolium ....PADSKSDSLGTQVTASPSS.....CSTPTTSTNGYARSRHSLN.....
Pediculus ..PQEAFTEANHPVSHYPQCTHSSQSLQRDAFGR.....KSTTVVQRNTPPHQNGNSWNRQGSPSPSSY
consensus>50 ....d....s..d..ly.d.....q.....q.....d.....s

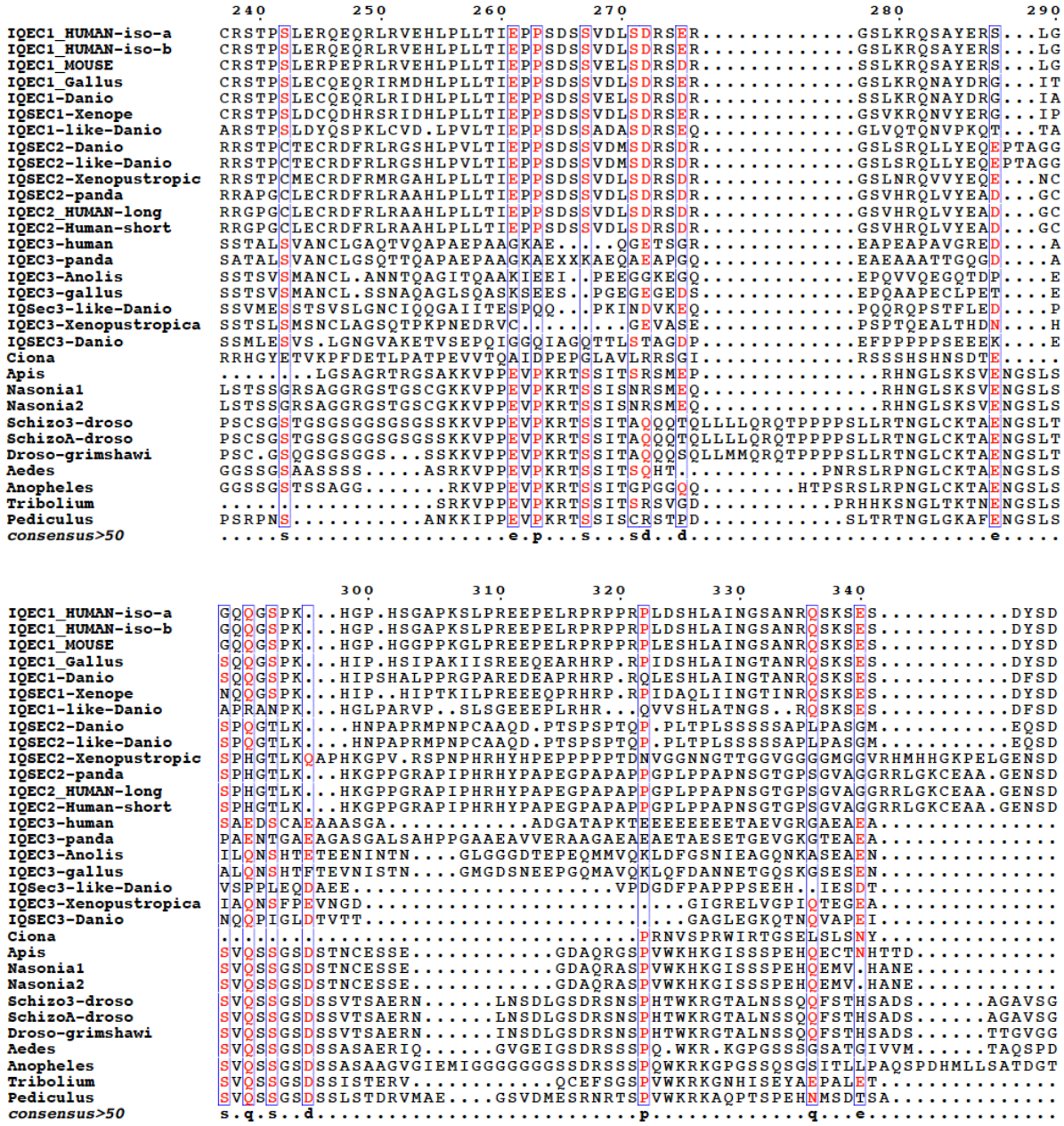
240 250 260 270 280 290
IQEC1_HUMAN-iso-a CRSTPSLERQEQRLRVEHLPLLTIEPPSDSSVDLSDRSER.....GSLKRQSAYERS...LG
IQEC1_HUMAN-iso-b CRSTPSLERQEQRLRVEHLPLLTIEPPSDSSVDLSDRSER.....GSLKRQSAYERS...LG
IQEC1_MOUSE CRSTPSLERPEPRLRVEHLPLLTIEPPSDSSVELSDRSDR.....SSLKRQSAYERS...LG
IQEC1_Gallus CRSTPSLECQEQRIRMDHLPLLTIEPPSDSSVDLSDRSER.....GSLKRQNAYDRG...IT
IQEC1-Danio CRSTPSLECQEQRLRIDHLPLLTIEPPSDSSVELSDRSDR.....SSLKRQNAYDRG...IA
IQSEC1-Xenope CRSTPSLDCQDHRSRIDHLPLLTIEPPSDSSVDLSDRSER.....GSVKRQNVYERG...IP
IQEC1-like-Danio ARSTPSLDYQSPKLCVD.LPVLTIEPPSDSSADASDRSEQ.....GLVQTQNVPKQT...TA
IQSEC2-Danio RRSTPCTECRDFRLRGSHLPVLTIEPPSDSSVDMSDRSDR.....GSLSRQLLYEQEPTAGG
IQSEC2-like-Danio RRSTPCTECRDFRLRGSHLPVLTIEPPSDSSVDMSDRSDR.....GSLSRQLLYEQEPTAGG
IQSEC2-Xenopustropic RRSTPCMECRDFRMRGAHLPLLTIEPPSDSSVDLSDRSDR.....GSLNRQVVYEQE...NC
IQSEC2-panda RRAPGCLECRDFRLRAAHLPLLTIEPPSDSSVDLSDRSDR.....GSVHRQLVYEAD...GC
IQEC2_HUMAN-long RRGPGCLECRDFRLRAAHLPLLTIEPPSDSSVDLSDRSDR.....GSVHRQLVYEAD...GC
IQEC2-Human-short RRGPGCLECRDFRLRAAHLPLLTIEPPSDSSVDLSDRSDR.....GSVHRQLVYEAD...GC
IQEC3-human SSTALSVANCLGAQTVQAPAEPAAGKAE.....QGETSGR.....EAPEAPAVGRED....A
IQEC3-panda SATALSVANCLGSQTTQAPAEPAAGKAEXXKAEQAEAPGQ.....EAEAAATTGQGD....A
IQEC3-Anolis SSTSVSMANCL.ANNTQAGITQAAKIEEI..PEEGGKEGQ.....EPQVVQEGQTDP....E
IQEC3-gallus SSTSVSMANCL.SSNAQAGLSQASKSEES..PGEGEGEDS.....EPQAAPECLPET....E
IQSec3-like-Danio SSVMESSTSVSLGNCIQQGAIITESPQQ...PKINDVKEQ.....PQQRQPSTFLED....P
IQEC3-Xenopustropica SSTSLSMSNCLAGSQTPKPNEDRVC.....GEVASE.....PSPTQEALTHDN....H
IQSEC3-Danio SSMLESVS.LGNGVAKETVSEPQIGGQIAGQTTLSTAGDP.....EFPPPPPSEEEK....E
Ciona RRHGYETVKPFDETLPATPEVVTQAIDPEPGLAVLRRSGI.....RSSSHSHNSDTE.....
Apis .....LGSAGRTRGSAKKVPPEVPKRTSSITSRSMEP.....RHNGLSKSVENGSLS
Nasonia1 LSTSSGRSAGGRGSTGSCGKKVPPEVPKRTSSISNRSMEQ.....RHNGLSKSVENGSLS
Nasonia2 LSTSSGRSAGGRGSTGSCGKKVPPEVPKRTSSISNRSMEQ.....RHNGLSKSVENGSLS
Schizo3-droso PSCSGSTGSGSGGSGSGSSKKVPPEVPKRTSSITAQQQTQLLLLQRQTPPPPSLLRTNGLCKTAENGSLT
SchizoA-droso PSCSGSTGSGSGGSGSGSSKKVPPEVPKRTSSITAQQQTQLLLLQRQTPPPPSLLRTNGLCKTAENGSLT
Droso-grimshawi PSC.GSQGSGSGGS...SSKKVPPEVPKRTSSITAQQQSQLLMMQRQTPPPPSLLRTNGLCKTAENGSLT
Aedes GGSSGSAASSSS.....ASRKVPPEVPKRTSSITSQHT.....PNRSLRPNGLCKTAENGSLS
Anopheles GGSSGSTSSAGG.....RKVPPEVPKRTSSITGPGGQQ.....HTPSRSLRPNGLCKTAENGSLS
Tribolium .....SRKVPPEVPKRTSSITSRSVGD.....PRHHKSNGLTKTNENGSLS
Pediculus PSRPNS.....ANKKIPPEVPKRTSSISCRSTPD.....SLTRTNGLGKAFENGSLS
consensus>50 .....s.....e.p...s...sd..d.....e.....
300 310 320 330 340
IQEC1_HUMAN-iso-a GQQGSPK...HGP.HSGAPKSLPREEPELRPRPPRPLDSHLAINGSANRQSKSES.....DYSD
IQEC1_HUMAN-iso-b GQQGSPK...HGP.HSGAPKSLPREEPELRPRPPRPLDSHLAINGSANRQSKSES.....DYSD
IQEC1_MOUSE GQQGSPK...HGP.HGGPPKGLPREEPELRPRPPRPLESHLAINGSANRQSKSES.....DYSD
IQEC1_Gallus SQQGSPK...HIP.HSIPAKIISREEQEARHRP.RPIDSHLAINGTANRQSKSES.....DYSD
IQEC1-Danio SQQGSPK...HIPSHALPPRGPAREDEAPRHRP.RQLESHLAINGTANRQSKSES.....DFSD
IQSEC1-Xenope NQQGSPK...HIP..HIPTKILPREEEQPRHRP.RPIDAQLIINGTINRQSKSES.....DYSD
IQEC1-like-Danio APRANPK...HGLPARVP..SLSGEEEPLRHR...QVVSHLATNGS..RQSKSES.....DFSD
IQSEC2-Danio SPQGTLK....HNPAPRMPNPCAAQD.PTSPSPTQP.PLTPLSSSSSAPLPASGM.....EQSD
IQSEC2-like-Danio SPQGTLK....HNPAPRMPNPCAAQD.PTSPSPTQP.PLTPLSSSSSAPLPASGM.....EQSD
IQSEC2-Xenopustropic SPHGTLKQAPHKGPV.RSPNPHRHYHPEPPPPPTDNVGGNNGTTGGVGGGGMGGVRHMHHGKPELGENSD
IQSEC2-panda SPHGTLK...HKGPPGRAPIPHRHYPAPEGPAPAPPGPLPPAPNSGTGPSGVAGGRRLGKCEAA.GENSD
IQEC2_HUMAN-long SPHGTLK...HKGPPGRAPIPHRHYPAPEGPAPAPPGPLPPAPNSGTGPSGVAGGRRLGKCEAA.GENSD
IQEC2-Human-short SPHGTLK...HKGPPGRAPIPHRHYPAPEGPAPAPPGPLPPAPNSGTGPSGVAGGRRLGKCEAA.GENSD
IQEC3-human SAEDSCAEAAASGA.....ADGATAPKTEEEEEEEETAEVGRGAEAEA.....
IQEC3-panda PAENTGAEAGASGALSAHPPGAAEAVVERAAGAEAEAETAESETGEVGKGTEAEA.....
IQEC3-Anolis ILQNSHTETEENINTN....GLGGGDTEPEQMMVQKLDFGSNIEAGQNKASEAEN.....
IQEC3-gallus ALQNSHTFTEVNISTN....GMGDSNEEPGQMAVQKLQFDANNETGQSKGSESEN.....
IQSec3-like-Danio VSPPLEQDAEE.....VPDGDFPAPPPSEEH..IESDT.....
IQEC3-Xenopustropica IAQNSFPEVNGD.....GIGRELVGPIQTEGEA.....
IQSEC3-Danio NQQPIGLDTVTT.....GAGLEGKQTNQVAPEI.....
Ciona .....PRNVSPRWIRTGSELSLSNY.....
Apis SVQSSGSDSTNCESSE.....GDAQRGSPVWKHKGISSSPEHQECTNHTTD.....
Nasonia1 SVQSSGSDSTNCESSE.....GDAQRASPVWKHKGISSSPEHQEMV.HANE.....
Nasonia2 SVQSSGSDSTNCESSE.....GDAQRASPVWKHKGISSSPEHQEMV.HANE.....
Schizo3-droso SVQSSGSDSSVTSAERN.....LNSDLGSDRSNSPHTWKRGTALNSSQQFSTHSADS.....AGAVSG
SchizoA-droso SVQSSGSDSSVTSAERN.....LNSDLGSDRSNSPHTWKRGTALNSSQQFSTHSADS.....AGAVSG
Droso-grimshawi SVQSSGSDSSVTSAERN.....INSDLGSDRSNSPHTWKRGTALNSSQQFSTHSADS.....TTGVGG
Aedes SVQSSGSDSSASAERIQ.....GVGEIGSDRSSSPQ.WKR.KGPGSSSGSATGIVVM.....TAQSPD
Anopheles SVQSSGSDSSASAAGVGIEMIGGGGGGGSSDRSSSPQWKRKGPGSSQSGSITLLPAQSPDHMLLSATDGT
Tribolium SVQSSGSDSSISTERV.....QCEFSGSPVWKRKGNHISEYAEPALET.....
Pediculus SVQSSGSDSSLSTDRVMAE....GSVDMESRNRTSPVWKRKAQPTSPEHNMSDTSA.....
consensus>50 s.q.s..d.....p.....q...e.....

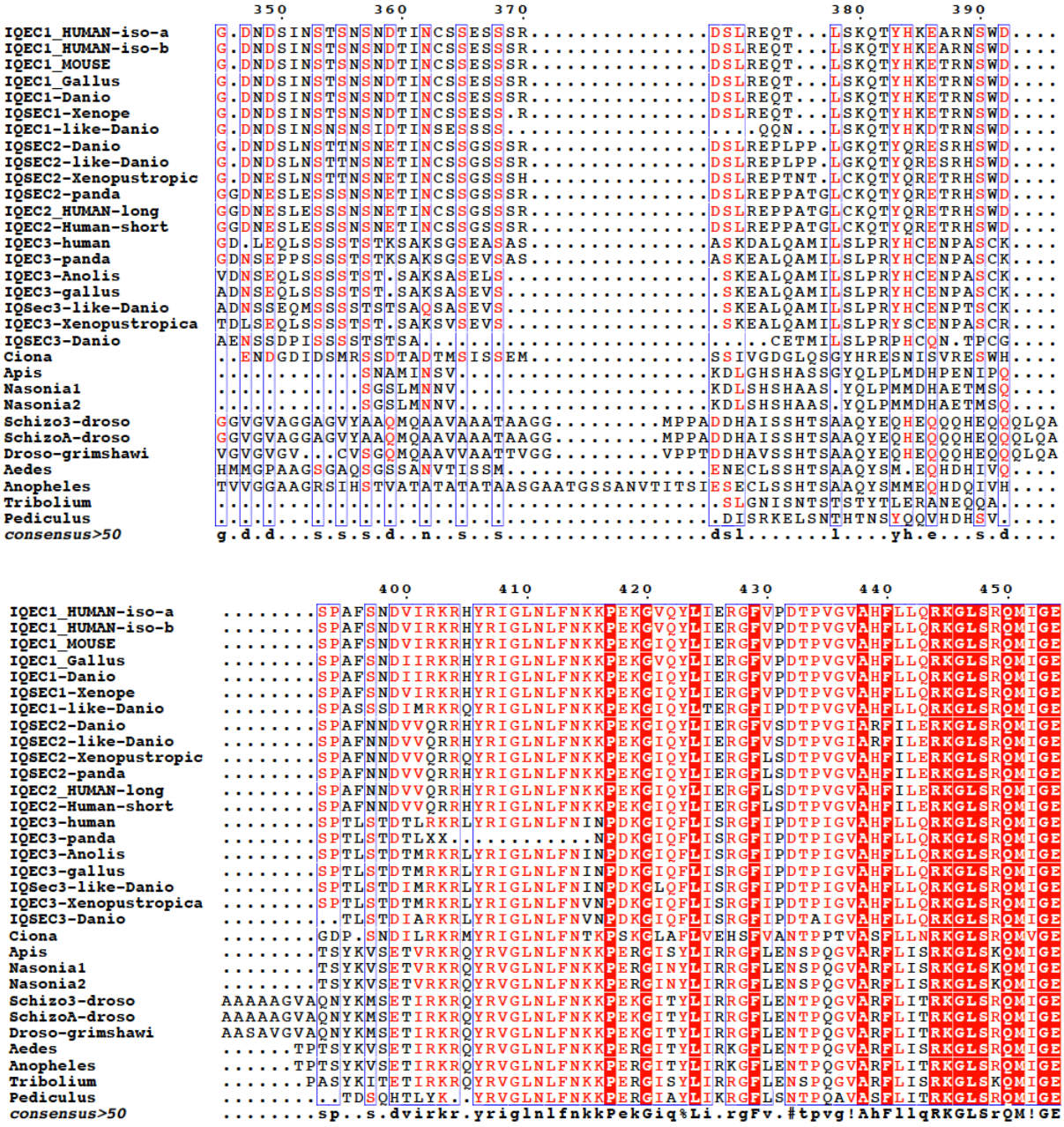
IQEC1_HUMAN-iso-a
IQEC1_HUMAN-iso-b
IQEC1_MOUSE
IQEC1_Gallus
IQEC1-Danio
IQSEC1-Xenope
IQEC1-like-Danio
IQSEC2-Danio
IQSEC2-like-Danio
IQSEC2-Xenopustropic
IQSEC2-panda
IQEC2_HUMAN-long
IQEC2-Human-short
IQEC3-human
IQEC3-panda
IQEC3-Anolis
IQEC3-gallus
IQSec3-like-Danio
IQSEC3-Xenopustropica
IQSEC3-Danio
Ciona
Apis
Nasonia1
Nasonia2
Schizo3-droso
SchizoA-droso
Droso-grimshawi
Aedes
Anopheles
Tribolium
Pediculus
consensus>50

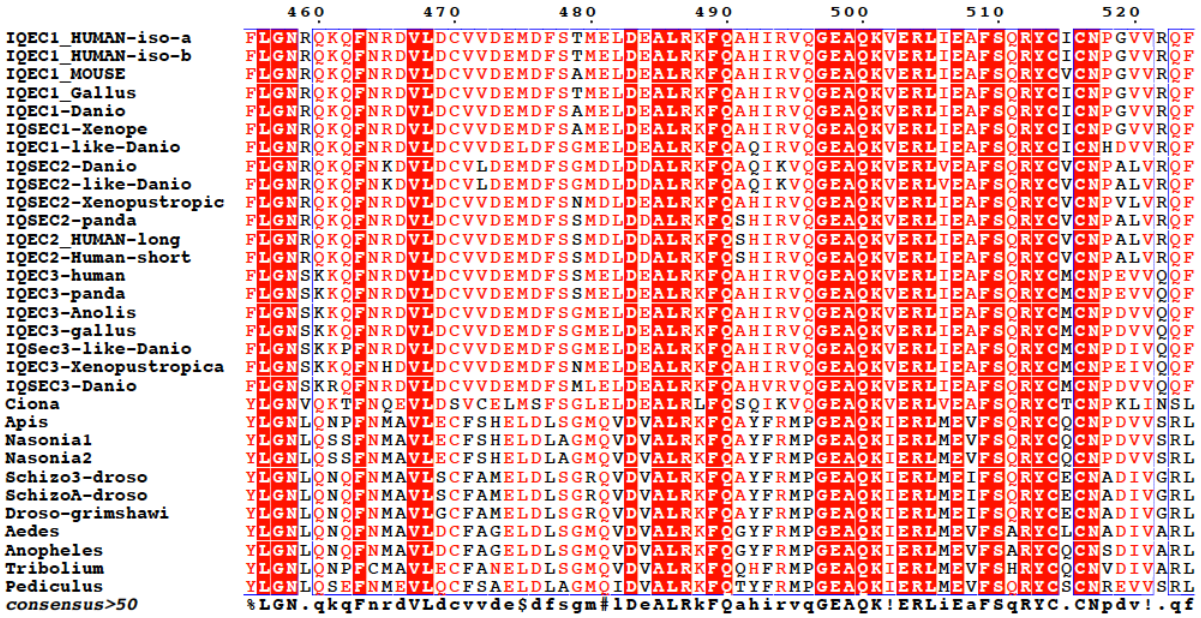
460 470 480 490 500 510 520
IQEC1_HUMAN-iso-a
IQEC1_HUMAN-iso-b
IQEC1_MOUSE
IQEC1_Gallus
IQEC1-Danio
IQSEC1-Xenope
IQEC1-like-Danio
IQSEC2-Danio
IQSEC2-like-Danio
IQSEC2-Xenopustropic
IQSEC2-panda
IQEC2_HUMAN-long
IQEC2-Human-short
IQEC3-human
IQEC3-panda
IQEC3-Anolis
IQEC3-gallus
IQSec3-like-Danio
IQEC3-Xenopustropica
IQSEC3-Danio
Ciona
Apis
Nasonia1
Nasonia2
Schizo3-droso
SchizoA-droso
Droso-grimshawi
Aedes
Anopheles
Tribolium
Pediculus
consensus>50

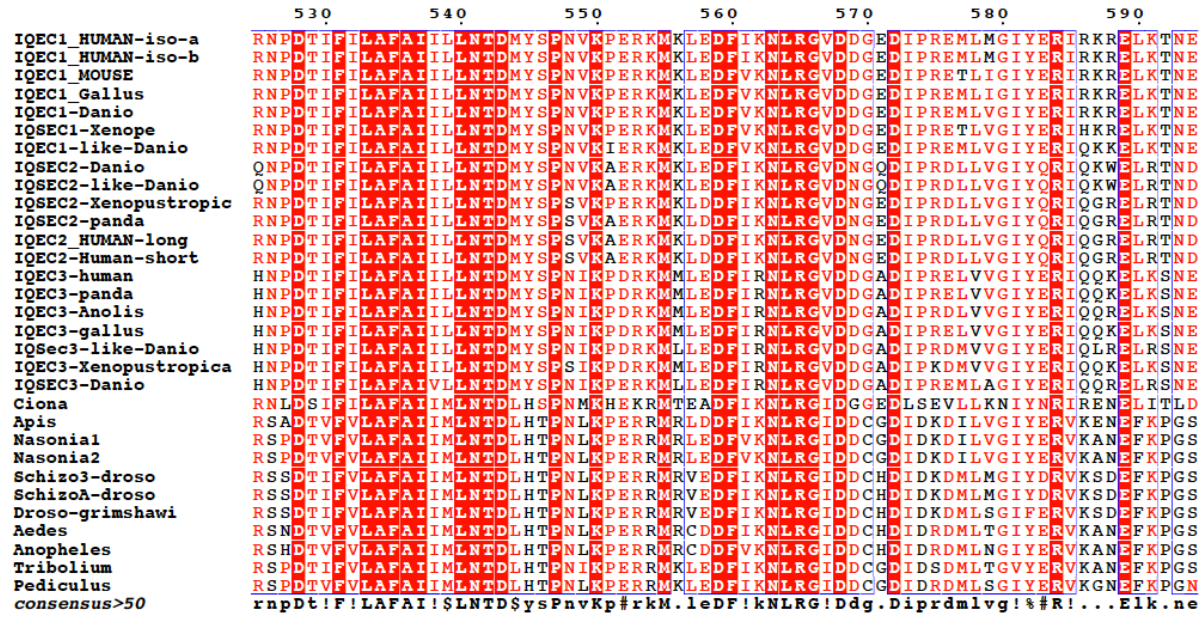
530 540 550 560 570 580 590
IQEC1_HUMAN-iso-a
IQEC1_HUMAN-iso-b
IQEC1_MOUSE
IQEC1_Gallus
IQEC1-Danio
IQSEC1-Xenope
IQEC1-like-Danio
IQSEC2-Danio
IQSEC2-like-Danio
IQSEC2-Xenopustropic
IQSEC2-panda
IQEC2_HUMAN-long
IQEC2-Human-short
IQEC3-human
IQEC3-panda
IQEC3-Anolis
IQEC3-gallus
IQSec3-like-Danio
IQEC3-Xenopustropica
IQSEC3-Danio
Ciona
Apis
Nasonia1
Nasonia2
Schizo3-droso
SchizoA-droso
Droso-grimshawi
Aedes
Anopheles
Tribolium
Pediculus
consensus>50

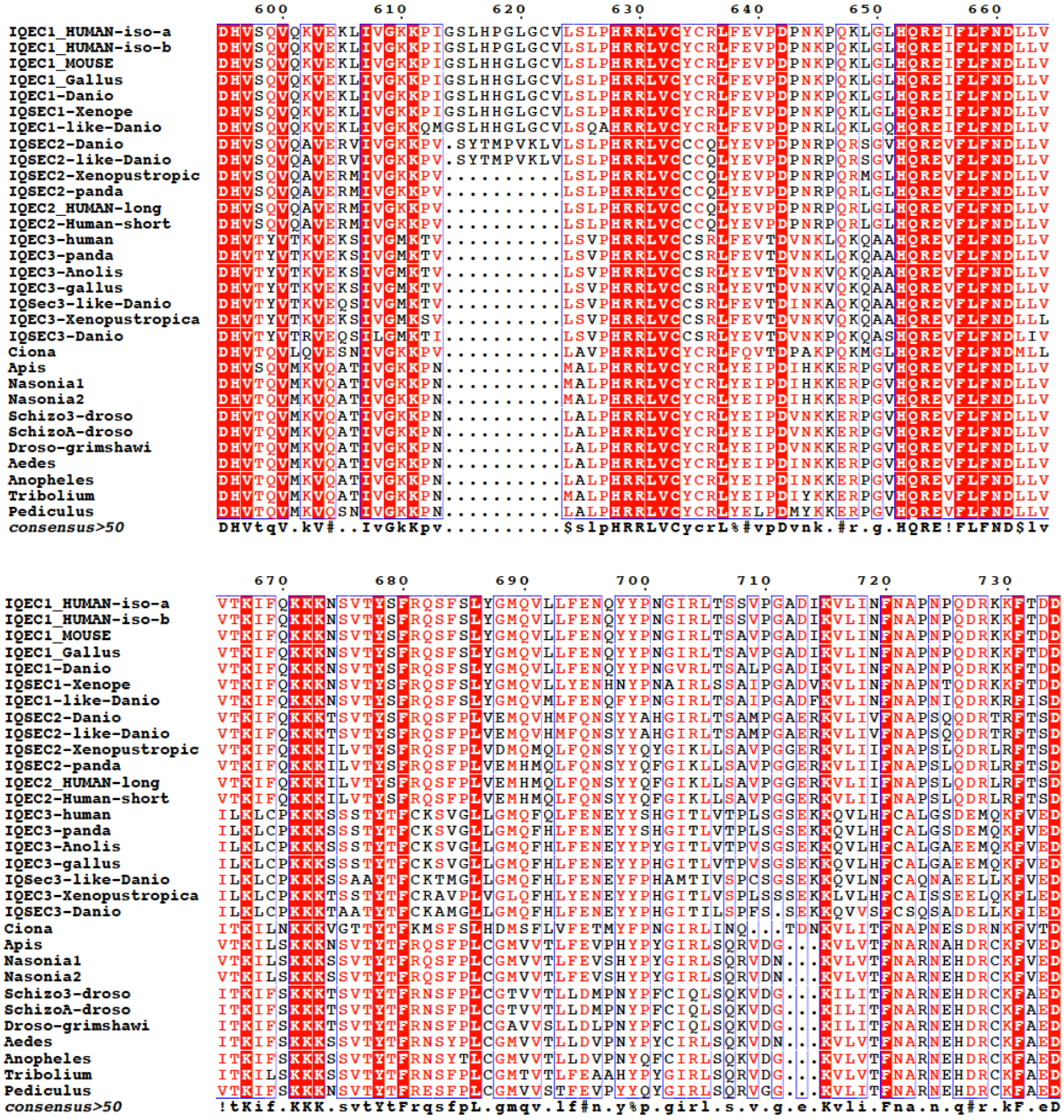
600 610 620 630 640 650 660
IQEC1_HUMAN-iso-a
IQEC1_HUMAN-iso-b
IQEC1_MOUSE
IQEC1_Gallus
IQEC1-Danio
IQSEC1-Xenope
IQEC1-like-Danio
IQSEC2-Danio
IQSEC2-like-Danio
IQSEC2-Xenopustropic
IQSEC2-panda
IQEC2_HUMAN-long
IQEC2-Human-short
IQEC3-human
IQEC3-panda
IQEC3-Anolis
IQEC3-gallus
IQSec3-like-Danio
IQEC3-Xenopustropica
IQSEC3-Danio
Ciona
Apis
Nasonia1
Nasonia2
Schizo3-droso
SchizoA-droso
Droso-grimshawi
Aedes
Anopheles
Tribolium
Pediculus
consensus>50
670 680 690 700 710 720 730
IQEC1_HUMAN-iso-a
IQEC1_HUMAN-iso-b
IQEC1_MOUSE
IQEC1_Gallus
IQEC1-Danio
IQSEC1-Xenope
IQEC1-like-Danio
IQSEC2-Danio
IQSEC2-like-Danio
IQSEC2-Xenopustropic
IQSEC2-panda
IQEC2_HUMAN-long
IQEC2-Human-short
IQEC3-human
IQEC3-panda
IQEC3-Anolis
IQEC3-gallus
IQSec3-like-Danio
IQEC3-Xenopustropica
IQSEC3-Danio
Ciona
Apis
Nasonia1
Nasonia2
Schizo3-droso
SchizoA-droso
Droso-grimshawi
Aedes
Anopheles
Tribolium
Pediculus
consensus>50

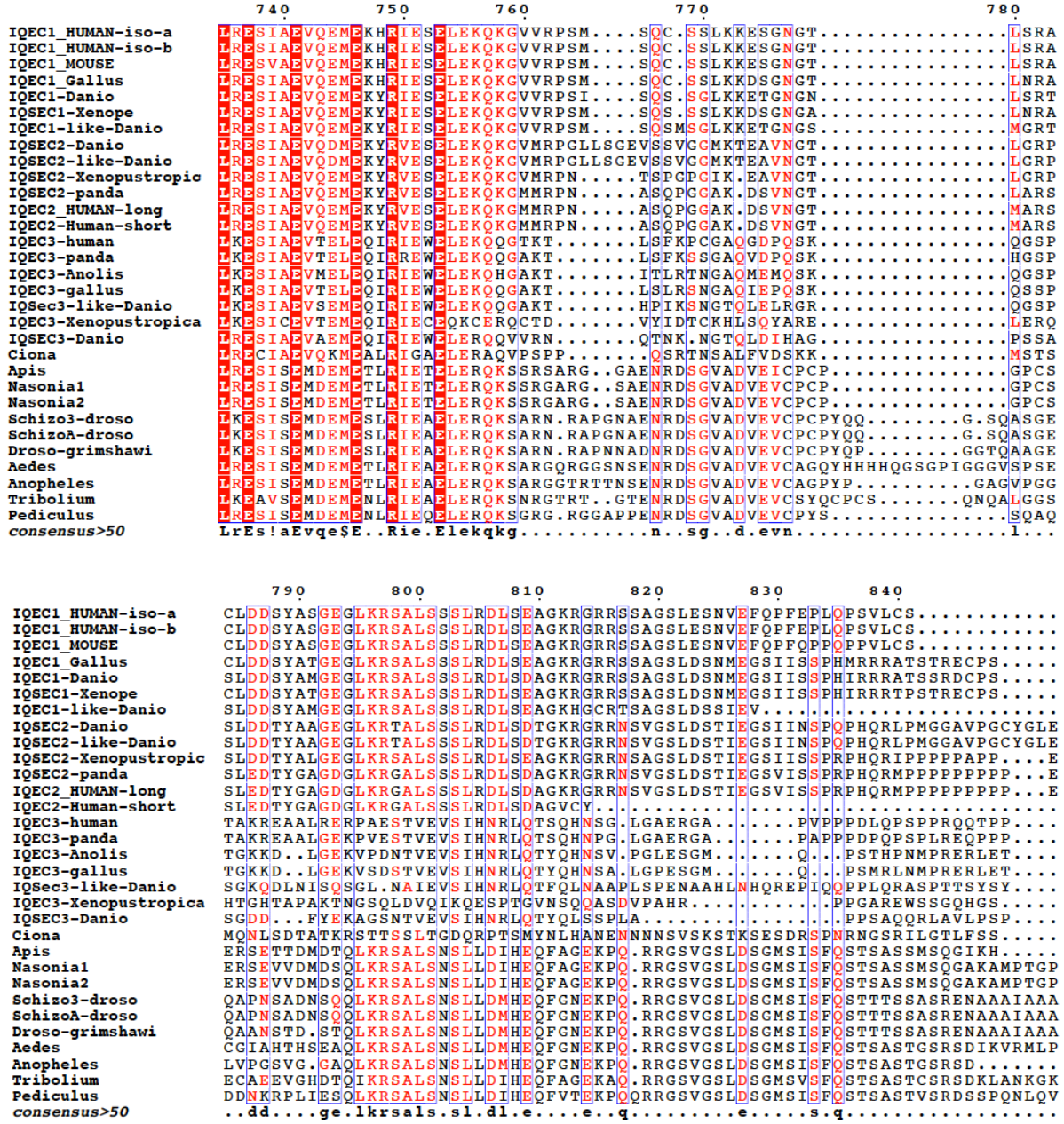

Annex 1: Multi-alignment of different species of members of the BRAG family. The sequence is from human BRAG2a (IQSEC1_human). The alignment was done with Multalin (http://multalin.toulouse.inra.fr/multalin/) and represented with ESPript 2.2 (http://espript.ibcp.fr/ESPript/ESPript/)

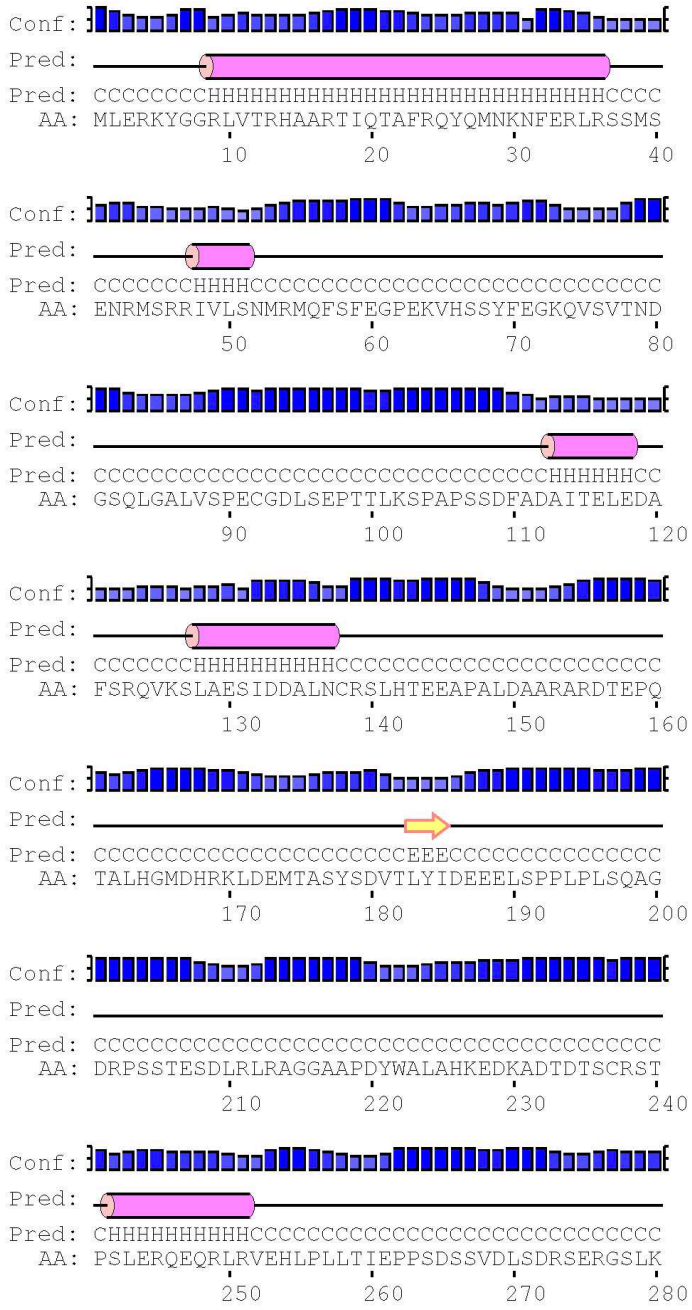
Conf:
Pred:
Pred: CCCCCCCCHHHHHHHHHHHHHHHHHHHHHHHHHHHHCCCC
AA: MLERKYGGRLVTRHAARTIQTAFRQYQMNKNFERLRSSMS
10 20 30 40
Conf:
Pred:
Pred: CCCCCCCHHHHCCCCCCCCCCCCCCCCCCCCCCCCCCCC
AA: ENRMSRRIVLSNMRMQFSFEGPEKVHSSYFEGKQVSVTND
50 60 70 80
Conf:
Pred:
Pred: CCCCCCCCCCCCCCCCCCCCCCCCCCCCCCCCHHHHHHCC
AA: GSQLGALVSPECGDLSEPTTLKSPAPSSDFADAITELEDA
90 100 110 120
Conf:
Pred:
Pred: CCCCCCCHHHHHHHHHHHCCCCCCCCCCCCCCCCCCCCCC
AA: FSRQVKSLAESIDDALNCRSLHTEEAPALDAARARDTEPQ
130 140 150 160
Conf:
Pred:
Pred: CCCCCCCCCCCCCCCCCCCCCCEEECCCCCCCCCCCCCCC
AA: TALHGMDHRKLDEMTASYSDVTLYIDEEELSPPLPLSQAG
170 180 190 200
Conf:
Pred:
Pred: CCCCCCCCCCCCCCCCCCCCCCCCCCCCCCCCCCCCCCC
AA: DRPSSTESDLRLRAGGAAPDYWALAHKEDKADTDTSCRST
210 220 230 240
Conf:
Pred:
Pred: CHHHHHHHHHHCCCCCCCCCCCCCCCCCCCCCCCCCCCC
AA: PSLERQEQRLRVEHLPLLTIEPPSDSSVDLSDRSERGSLK
250 260 270 280

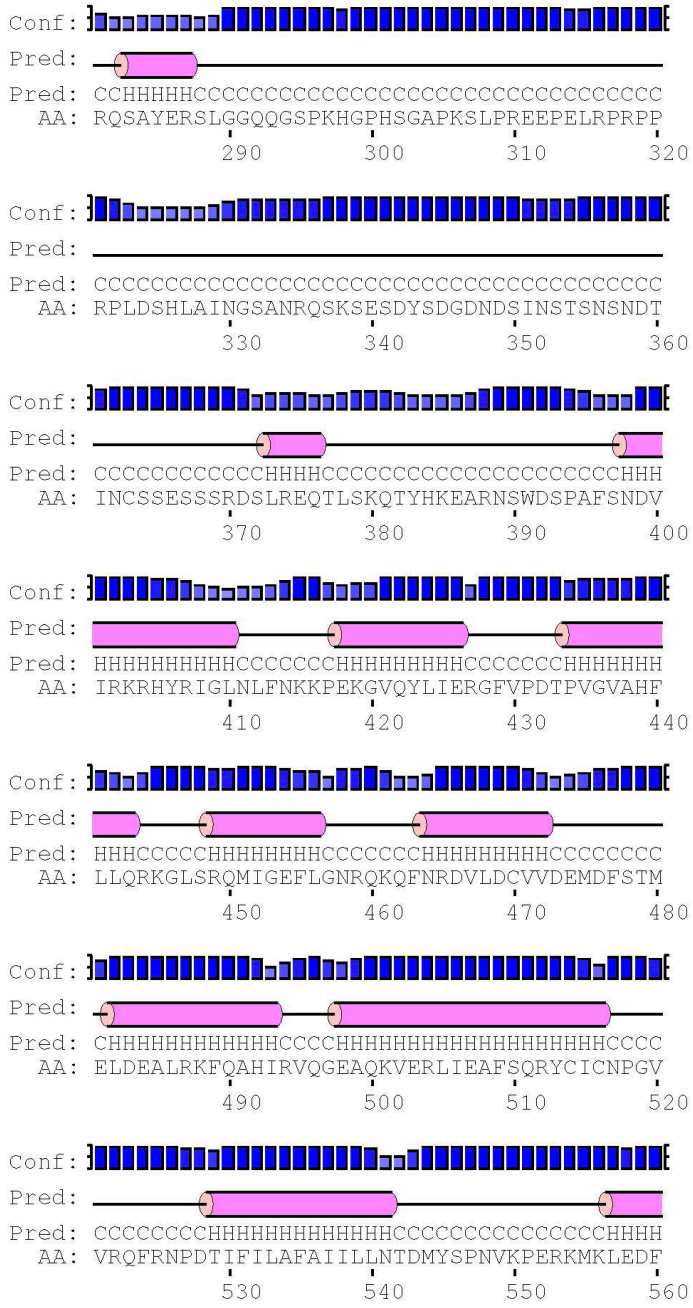
Conf:
Pred:
Pred: CCHHHHHCCCCCCCCCCCCCCCCCCCCCCCCCCCCCCCC
AA: RQSAYERSLGGQQQGSPKHGPHSGAPKSLPREEPELRPRPP
290 300 310 320
Conf:
Pred:
Pred: CCCCCCCCCCCCCCCCCCCCCCCCCCCCCCCCCCCCCCC
AA: RPLDSHLAINGSANRQSKSESDYSDGDNDSINSTSNSNDT
330 340 350 360
Conf:
Pred:
Pred: CCCCCCCCCCCCHHHHCCCCCCCCCCCCCCCCCCCCHHH
AA: INCSSESSSRDSLREQTLSKQTYHKEARNSWDSPAFSNDV
370 380 390 400
Conf:
Pred:
Pred: HHHHHHHHHHCCCCCCCCHHHHHHHHHCCCCCCCCHHHHHHH
AA: IRKRHYRIGLNLFNKKPEKGVQYLIERGFVPDTPVGVAHF
410 420 430 440
Conf:
Pred:
Pred: HHHCCCCCHHHHHHHHHCCCCCCCCHHHHHHHHHCCCCCCCC
AA: LLQRKGLSRQMIGEFLGNRQKQFNRDVLDCVVDEMDFSTM
450 460 470 480
Conf:
Pred:
Pred: CHHHHHHHHHHHHCCCCHHHHHHHHHHHHHHHHHHCCCC
AA: ELDEALRKFQAHIRVQGEAQKVERLIEAFSQRYCICNPGV
490 500 510 520
Conf:
Pred:
Pred: CCCCCCCCHHHHHHHHHHHHHCCCCCCCCCCCCCCCHHHH
AA: VRQFRNPDTIFILAFAIILLNTDMYSPNVKPERKMKLEDF
530 540 550 560

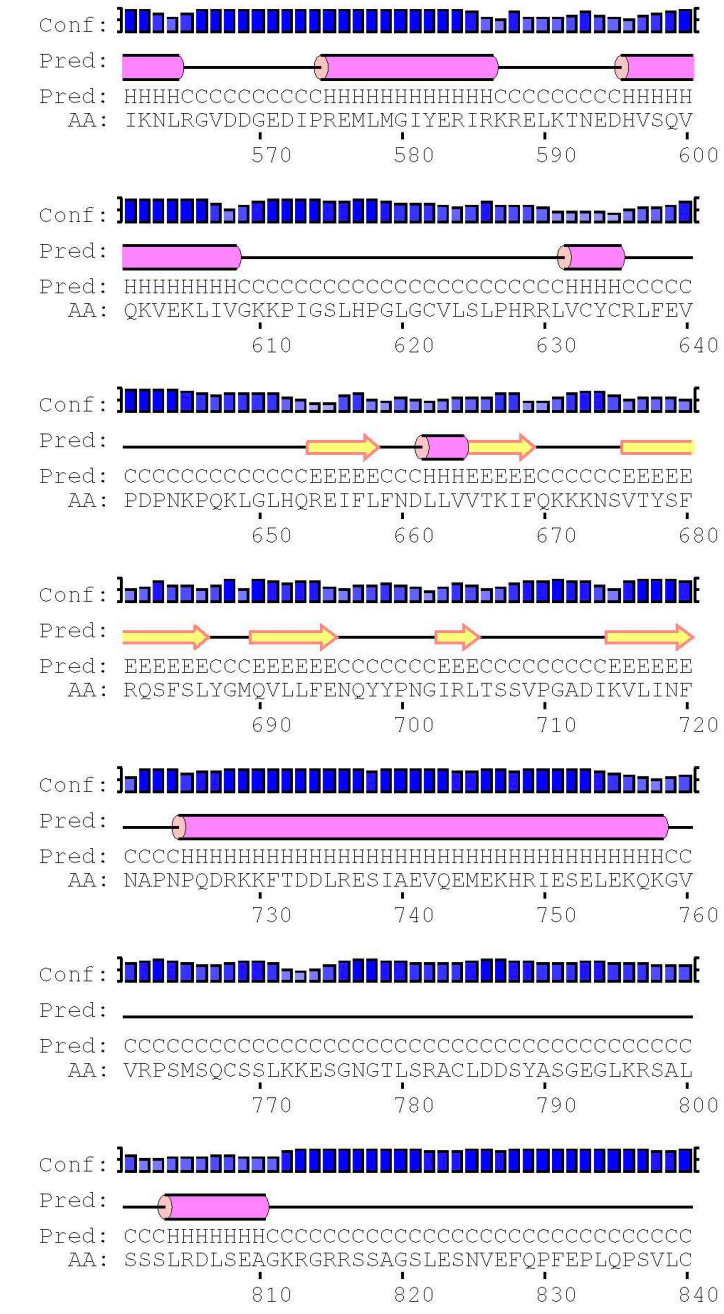

Annex 2: Secondary structure analysis of BRAG2 with PSIPRED (http://bioinf.cs.ucl.ac.uk/psipred/)

A.

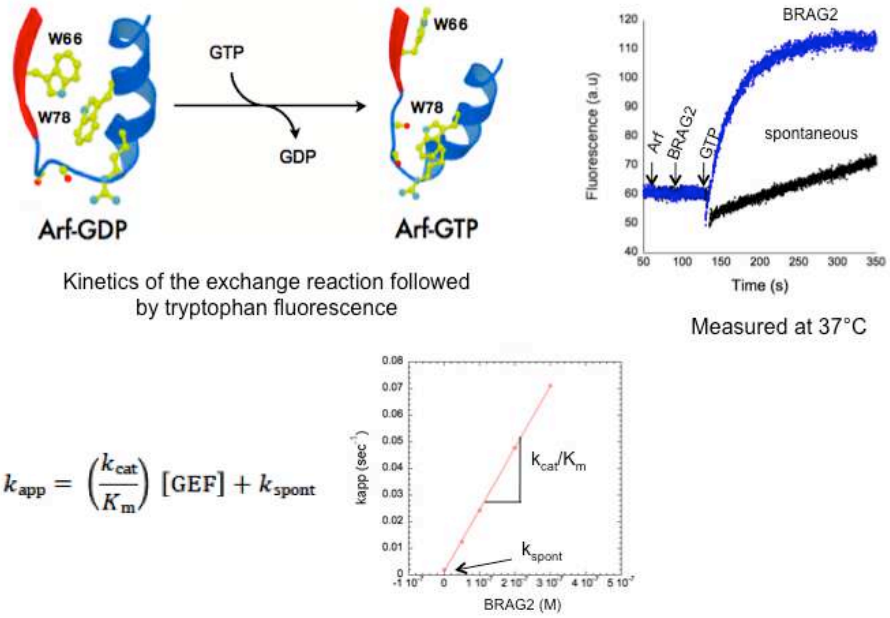

B.

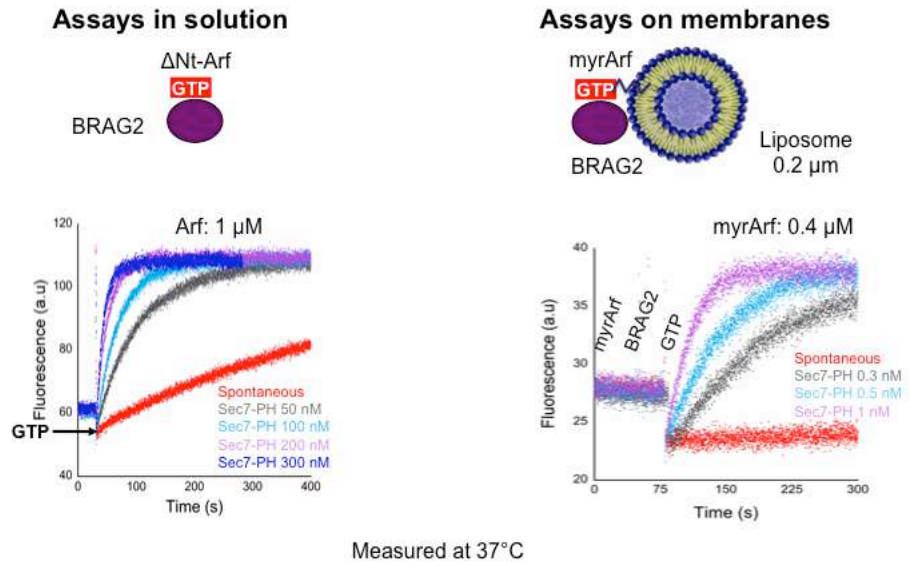

Annex 3: *In vitro* nucleotide exchange assays. A. Arf activation with or without BRAG2 was measured *in vitro* by following the tryptophan fluorescence of Arf in real time. In Arf-GDP tryptophans 66 and 78 are close to each other, which leads to a quench of their fluorescence. In Arf-GTP, these tryptophans are apart from each other, leading to an increase of their fluorescence. This is illustrated on the right, with the fluorescence change plotted as a function of time, for the spontaneous (in black) and in presence of BRAG2 (in blue). The apparent activation rate constant of Arf proteins (k_{app}) was determined by fitting the fluorescence change to a single exponential. Plotting this constant as a function of the GEF concentration allow us to determine the specific exchange constant kcat/Km, which according to the equation (bottom). B. Assays in solution were performed with ΔNt-Arfs at 1 µM and BRAG2 ranging from 0 to 300 nM (left). Assays on membranes were performed with myrArfs at 0.4 µM, BRAG2 ranging from to 0 to 1 nM and liposomes extruded at 0.2 µm (right). All the assays were performed at 37°C under continuous stirring.

◆ Résumé de la thèse

Les mécanismes de régulation d'un ArfGEF humain atypique, impliqué dans l'endocytose de récepteurs et associé à l'invasion tumorale des cellules cancéreuses ont été étudiés en utilisant la cristallographie et la reconstitution des activités ArfGEF sur des membranes artificielles. Les deux isoformes Arf1 et Arf6, qui diffèrent par leurs fonctions cellulaires et biochimiques sont étudiées par cristallographie, SAXS et RMN.

◆ Liste des mots clés relatifs au sujet de la thèse

ArfGEFs, GTPases, Arf1, Arf6, cancer, régulation par les membranes, cristallographie, SAXS
ArfGEFs, GTPases, Arf1, Arf6, cancer, regulation by membranes, X-ray cristallography, SAXS

◆ Nom du laboratoire de rattachement

Laboratoire d'Enzymologie et Biochimie Structurales
UPR3082-CNRS
Gif-sur-Yvette

PÔLE : INGENIERIE DES PROTEINES ET CIBLES THERAPEUTIQUES

UNIVERSITÉ PARIS-SUD 11
UFR «FACULTÉ DE PHARMACIE DE CHATENAY-MALABRY »
5, rue Jean Baptiste Clément
92296 CHÂTENAY-MALABRY Cedex